ALKALI ACTIVATED BINDERS VALORISED FROM TUNGSTEN MINING WASTE: MATERIALS DESIGN, PREPARATION, PROPERTIES AND APPLICATIONS

A thesis submitted for the degree of Doctor of Philosophy

by
Gediminas Kastiukas
College of Engineering, Design and Physical Sciences
Division of Civil Engineering
Brunel University London
August 2017

DECLARATION

This dissertation is the result of my own work and includes nothing, which is the outcome of work done in collaboration except where specifically indicated in the text. It has not been previously submitted, in part or whole, to any university or institution for any degree, diploma, or other qualification.

Signed: _____

Date: _____

Gediminas Kastiukas
Brunel University London

ABSTRACT

Alkali-activated binders (AABs) are the third-generation class of binders after lime and Portland cement. These binders have the potential to be made from a variety of industrial waste sources, many of which have remained largely unexplored. Significant drawbacks of AABs are the requirement of highly alkaline solutions for its production and the lack of available data regarding its implementation in the field.

To bridge this gap, this study aimed to research the recycling and valorization of tungsten mining waste (TMW) to produce AABs, using waste glass (WG) as a supplementary material for reducing the alkali activator demand. Finally, a connection was made between the fundamental research on AABs and a practical engineering application.

A detailed approach was undertaken to determine the most appropriate TMW-WG AAB preparation methods and curing conditions, an understudied area, with a strong emphasis on the microstructural development during hardening. The alkali activator appeared to be sensitive to prolonged stirring, which appeared to induce a stripping effect of the water molecules from the alkali metal ions, leading to a less intense attack on the silicon-oxygen bonds in precursor material. The effects of WG (dissolution and chemical reaction) were investigated to understand its contribution to the AAB system. WG was observed to provide an additional source reactive silica, contributing to the formation of a calcium-containing N-A-S-H gel, and significantly improve the mechanical strength.

PCM macro-encapsulated aggregates (ME-LWAs) were also researched and incorporated into the TMW-WG AAB for the development of an energy-saving building material. The ME-LWAs stood out to be leak proof, with excellent thermal stability and thermal conductivity, latent heat capacity and abrasion resistance. It was also found out it is feasible to produce foamed lightweight alkali-activated materials using tungsten mining waste (TMW-WG FAAB) and other precursor materials. FAAB can be used in several applications where low density and fire resistance is required. The TMW-WG FAAB was also designed to suit a wide range of densities and compressive strengths using chemical foaming, achieving very low thermal conductivity.

Finally, the TMW-WG AAB proved itself to be convenient to prepare on-site, demonstrating in service its ease of preparation, rapid hardening and durability as a novel road repair mortar.

ACKNOWLEDGEMENTS

This thesis could not have been realised without a great deal of guidance, and both mental and practical support. I would like to thank deeply those people who, during the doctoral program, provided me everything I needed.

First and foremost, I would like to express my deepest gratitude to my principle supervisor, Dr Xiangming Zhou for the continuous support of my doctoral program and research, for his patience, motivation, enthusiasm, and immense knowledge. His excellent guidance helped me in the investigation and writing of this thesis. I am also grateful for his encouragement to present my work at international scientific conferences, giving me the opportunity to broaden my horizons.

Special thanks go to Professor Castro-Gomes, who welcomed me at the University of Beira Interior to conduct a large part of my experimental work. Also from the University of Beira Interior, thanks go to Jorge Bento, who was very supportive of my experimental work and always prepared for new endeavours. I would like to extend my thanks to all the REMINE Project partners for their scientific inputs and support. Moreover, I greatly appreciate the support from the staff at Brunel University London the staff at the Experimental Techniques Centre (ETC) and the Wolfson Centre for sharing their discussions, experiences, and knowledge during the time of my study. The author is also very grateful to the Thomas Gerald Gray Charitable Trust for financial support in the form of grants and Doctoral scholarships.

Finally, I would also like to thank my father Saulyus and mother Regina, as well as my friends, for their continuing support and encouragement.

CONTENTS

LIST OF TABLES

LIST OF FIGURES

LIST OF ABBREVIATIONS AND ACRONYMS

Materials

AAB	Alkali-Activated Binder
C-A-S-H	Calcium Aluminium Silicate Hydrate
C-S-H	Calcium-Silicate-Hydrate
CH	Calcium Hydroxide
CF	Carbon Fibre
FAAB	Foamed Alkali-activated Binder
FCC	Fluid Catalytic Cracking
GGBS	Granulated Ground Blast-Furnace Slag
GS	Graphite Spray
HBCD	Hexabromocyclododecane
HPC	Hydroxypropyl Cellulose
IBA	Incineration Bottom Ash
L/FA	Liquid/Fly Ash ratio
LWA	Lightweight Aggregate
M	Muscovite
N-A-S-H	Sodium Aluminium Silicate Hydrate
PC	Portland Cement
PCM	Phase Change Material
POFA	Palm Oil Fuel Ash
RHA	Rice Husk Ash
SCM	Supplementary Cementitious Material
SH	Sodium Hydroxide (NaOH)
SS	Sodium silicate (Na2SiO3)
TMW	Tungsten Mining Waste
WG	Waste Glass

Techniques

BS EN	British standard-European norm
ATR	Attenuated Total Reflectance
ASTM	American Society of Testing Materials
CPR	Construction Products Regulations
DSC	Differential Scanning Calorimetry
EDX	Energy dispersive X-ray
EPS	Expanded polystyrene
FTIR	Fourier-Transforms Infra-red
MAS	Magic Angle Spinning
MIP	Mercury Intrusion Porosimetry
NMR	Nuclear Magnetic Resonance
SEM	Scanning Electron Microscope
XRD	X-Ray Diffraction
WD-XRF	Wavelength Dispersive X-Ray Diffraction

1 INTRODUCTION

This chapter introduces the research background, aims and objectives of the study and an outline of the thesis. The research question, research hypothesis and motivation are discussed and highlighted.

1.1 Research Background

Access to raw materials and resource efficiency are at the forefront of the EU political debate and recycling is the main part of the solution. Moreover, recycling offers significant investment, innovation and employment opportunities. Currently, the world's most widely used building material is Portland cement (PC) concrete. Energy consumption in the cement production process accounts for about 2% of global primary energy consumption, accounting for a global total industrial energy consumption of 5-6% (Potgieter, 2012). If the municipal infrastructure continues to grow for developing countries such as China and India and regions in the Middle East, the demand for cement will increase.

At present, all kinds of industrial production processes generate large quantities of industrial waste, many of which can be used as PC admixtures, blended with the raw material feed during the production of PC clinker or as a raw material for the direct production of other cementitious materials. It is the latter process that has caught the attention of many research groups and industries and will be at the core of this PhD thesis; that is alkali-activated cementitious materials.

Alkali-activated cementitious materials are based on a reactive solid substance that hardens under the influence of an alkaline activator and can be described as three-dimensionally networked amorphous to semi-crystalline aluminosilicate materials. In general, alkali-activated binders, commonly referred to as geopolymers, are low-calcium binding systems composed of an alkali-aluminosilicate gel as the primary phase, a small quantity of bound water and structure similar that of a zeolite (Provis, Lukey and Van Deventer, 2005a). A system containing a higher degree of calcium will result in a C-A-S-H gel primary phase. The secondary phases that may commonly

appear are largely the same as that for PC blends i.e. hydrotalcite, AFm phases and occasionally some zeolites (Li, Sun and Li, 2010). The structure of an alkali-activated binder tends to be more crosslinked and tends to bind less water than a PC system (Provis and Van Deventer, 2014). They possess excellent mechanical properties, fire resistance and chemical resistance, and this technology can be employed as cementitious binders, fireproof material and as a material for immobilising toxic metals.

The preferred or trusted precursor materials for alkali-activation are predominantly slags and fly ash. The cement and concrete industry has also made these latter industrial wastes the primary resources as supplementary cementitious materials (SCMs). In fact, some SCMs used by cement manufacturers can go up to 95% replacement of PC within the European Standards in the CEM III/C class (BSI Standards Publication, 2011). To mitigate future problems regarding insufficient pozzolanic materials for alkali-activation due to demands from the cement and concrete industry, it is essential to establish and secure new, non-conventional precursor materials for alkali-activation.

Mining and quarrying activities cause significant environmental, economic and social impacts. One of the consequences is the accumulation of mineral wastes in deposit fields. Apart from the risk of direct environmental pollution, it causes serious landscape impacts, affecting the quality of life for the local population. Mining and quarrying waste still represents 15% of total waste in Western Europe, 31% in Eastern Europe (Eurostat, 2016b) while the USA alone is estimated to produce between 1000-2000 Mt of mining waste annually (Szczepańska, 2004). The use of earth/ rock dams or lagoons to store the wastes seem to be a safer option. However, the collapse of such structures may also have serious impacts on the environment and human health and safe(Lucas, 2001; Galán, González and Fernández-Caliani, 2002)

Glass is a non-biodegradable waste material, which means depositing waste glass in landfill sites is not a favourable solution for the environment. Typically, most of the non-recyclable colour glass is from the bottling industry, where intricate cleaning of the waste glass and sorting is required before reuse. The procedure for recycling waste glass for the bottling industry is as follows; bottles are collected, sorted by colour then crushed ready for re-use as raw materials for new products, which is a costly process from collection to the laborious sorting of glass. In fact, based on EU statistics, the generation of glass waste was estimated to be 493 thousand tonnes, of which only 25% was recycled (Luiz A. Pereira-de-Oliveira, 2012).

The principle for the development of alkali-activated cementitious materials, should not, as far as possible, try to compete with the cement industries raw materials directly. Instead, it must be viewed as a new branch of cementitious binders with the advantage of being manufactured using industrial wastes to meet updated and higher criteria, such as better sustainability and longer durability. The chemistry of alkali-activated binders should be designed in a way which gives the behaviour, performance and characteristics that are desired to make the best use of the SCM as a primary material.

PCM’s are incorporated in many methods and aspects of construction, including active and passive energy storage systems. The use of this material may be applied as an additive substance to preferred building components. The macro-encapsulation containment method is also durable and simple for merging both PCMs and structural components. However, the phase change features may cause leakage issues due to the

simplicity of integration. Leakage is particularly unfavourable as surrounding materials might be affected by the leaching of the PCM. Solving the leakage issue and developing thermal energy storing macro-encapsulated aggregates incorporated into an alkali-activated binder would successfully create for the first time a novel composite material, opening a wide selection of applications for its inclusion e.g. surface cooling systems, construction materials such as wallboards and ceiling times, roads and pavements.

1.2 Aims and structure of this study

This PhD thesis aims to evaluate the performance and suitability of using non-conventional precursor materials to produce alkali-activated binders as an alternative to PC-based binders. The individual objectives are the following:

1. Studying the chemical activator preparation during prolonged mixing by monitoring changes in solution temperature under controlled conditions and the state of bonding in water molecules. Due to the requirements of a tailored curing process, the influence of the curing temperature and curing duration will be investigated with respect to mechanical strength. *(Chapter 3)*
2. Investigating the interaction of waste glass with tungsten mining waste and its effect on the reactivity of the blend. Also, the influence of waste glass on the reaction process and microstructure will be correlated to changes in the mechanical strength. *(Chapter 4)*
3. To reduce the high additions of strong alkaline activators needed in alkali-activated cementitious systems, optimisation of the mix design regarding reduced activator content in the mixture will be conducted. The activating solution itself was also varied regarding the quantities of sodium silicate and sodium hydroxide to determine their effect on reactant formation and mechanical strength. Optimum sodium silicate/sodium hydroxide, activator/precursor and water contents will be derived. *(Chapter 4)*
4. To enhance the alkali-activated binder technical performance, energy harvesting PCM encapsulated lightweight aggregates shall be investigated. A vacuum impregnation unit will be set up for the impregnation of PCM. A variety of coating materials and coating processes will be investigated to ensure leak-proof encapsulation. Also, the encapsulated PCM aggregates will be subjected to a series of thermal and mechanical performance tests; including exposure to elevated temperatures, thermal cycling, thermal conductivity, latent heat capacity, abrasion resistance and compatibility with the alkali-activated binder. *(Chapter 5)*
5. To explore the potential of the binder for foamed insulation material applications the tungsten mining waste and waste glass blend will be utilised to produce a foamed alkali-activated binder. Chemical foaming and pre-foamed foaming methods will be investigated using several formulations, and the performance will be measured regarding density, compressive strength and thermal conductivity. *(Chapter 6)*
6. To bridge the gap between the fundamental research on alkali-activated binders and its practical engineering application, the preliminary performance of the TMW-WG AAB developed in this study will be evaluated through a pilot test. The TMW-WG AAB will be evaluated regarding ease of preparation, hardening and long-term durability. *(Chapter 7)*

2 LITERATURE REVIEW

In this chapter, a comprehensive review and summary of the research status of alkali-activated binders, their development and shortcomings are presented. The focus is drawn to the utilisation of alternative industrial waste resources to produce cementitious binders and the potential of producing alkali-activated binders from tungsten mining waste. A review of phase change materials and their application in building materials is also outlined. Research ideas and methods presented in this study are based on the above analysis.

2.1 Issues and Challenges Facing the Cement Industry

The 20th century has seen a remarkable growth in the world population, rising from 1.5 billion to approximately 6 billion people. Forecasts predict a further growth, reaching around 9.6 billion by 2050. This global change has induced a paradigmatic societal shift whereby around 3 of the 6 billion inhabitants now live in and around cities. Large amounts of infrastructural and new city residential developments proceeded, consuming billion of tonnes of cement for concrete production. This comes with the negatives; since ordinary concrete contains 12% PC, 8% mixing water and 80% aggregates by mass, it is estimated that the concrete industry is not only consuming 1.5 billion tons of cement annually but also a vast amount of natural resources (9 billion and 1 billion tons of sand/gravel and water respectively). This brings to light the worrying issue that the concrete industry alone is responsible for consuming much of the world's natural resources with increasing demands respective to estimates that the current 11.5 billion tonnes a year for concrete will increase to 18 billion tonnes annually by the year 2050 (P.K. Mehta, 2014).

There are many different ways to calculate the embodied energy of concrete, and each method is dependent on assumptions, circumstances and varying processing stages (Dixit *et al.*, 2010). For example, it can be claimed that the embodied energy of concrete is quite low as it only contains around 15% PC (dry weight) and most of the remainder

is low energy aggregate (Prusinski, Marceau and VanGeem, 2004). While this may be true, the fact remains that carbon dioxide (CO_2) released from the production of cement represents a significant proportion of that derived from global human activity (Nature Materials, 2007; Allwood, Cullen and Milford, 2010). There are also claims that PC concretes have become less energy intensive. For example by, decreasing the clinker to cement ratio through substitution with pozzolanic materials such as fly ash (Huntzinger and Eatmon, 2009; O'Brien, Ménaché and O'Moore, 2009), higher efficiency kilns (Van Den Heede and De Belie, 2012) and by the use of alternative raw materials for fuel (Georgopoulos and Minson, 2014).

Leading global governments are taking initiatives to combat their greenhouse gas (GHG) emissions. Japan's cement (clinker production) sector has attained the world's highest level of energy efficiency by using waste heat power generation and introducing technology for using waste (e.g. waste plastic) as alternative thermal energy in the burning process (UNFCC, 2015). Even with the maximum production efficiency being reached in cement plant technology, high targets have been imposed on global governments to reduce greenhouse gas emissions (GHG) further. For example, Japan's Intended Nationally Determined Contribution (INDC) towards post-2020 GHG emission reductions has been set at a level of 26.0% by the year 2030. It is reported that that the majority of modern cement manufacturing plants have implemented the best energy-efficient technology for the production of cement, especially in the pyro-processing plant and fuels needed to heat the production process (Blockstein and Wiegman, 2009). The remaining and major GHG come from the necessary and unavoidable calcification process associated with baking the lime to make cement, and so the release of GHGs will continue if we do not focus more researching alternative raw materials. Fig. 2-1 shows diagrammatically, the typical emissions measured from existing EU kilns. It should be noted that the quantities of emissions are given as ranges since they depend on the cement plant technology, energy source, use of supplementary cementitious materials.

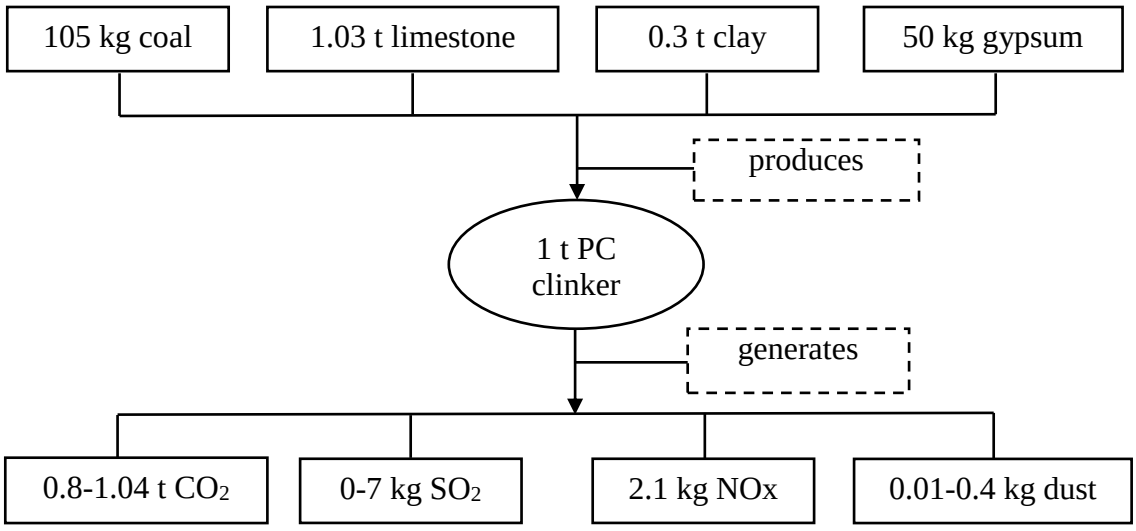

Fig. 2-1 Typical emissions measured from existing EU kilns (Schorcht *et al.*, 2013)

More than 600 Mt of clinker are being produced annually, costing 104 kWh/t of cement, consuming 3510 MJ/t of heat, and releasing a total gross of 546 Mt of CO_2 (WBCSD Cement Sustainability Initiative, 2013). Even though European cement production techniques are amongst the most energy efficient in the world, the EU

cement industry's energy bill still represents about 40% of total production costs (Dixit *et al.*, 2010). The world economy is prone to fluctuations, and a commodity such as fossil fuels is no exception. The world has been observing the significant fall in oil prices since mid-2014 (Economist, 2014), bringing benefits to oil-intensive manufacturing sectors as the price of their key input falls. The cement industry is one of the corporate winners, meaning cheaper energy bills for cement producers. However, these savings must be interpreted carefully and compared to the economic performance of individual countries and its impact on the cement industry. A recent example is a contraction of the construction market in Russia, whose construction output fell by 4.5% to US$81bn in 2014 (EuropaProperty, 2015). Also, countries such as China, which had experienced record-breaking economic growth in the last few decades, is showing signs of slowing down, which naturally means that their construction market may also suffer. Despite the economic and financial situation, global cement demand grew by approximately 3% in 2014 (Lafarge, 2014) and according to the PCA, is forecast to grow 5.7 % during 2017 (Rubenstone, 2016). China, which is already by far the largest market for cement in the world and accounting for about 60% of world production (WBCSD/CSI, 2015), will show the largest increase in total amount of cement sold due to continued national economic growth. Other developing parts of Eastern Europe (Statistia, 2016), as well as some nations in the Africa/Middle-East and Latin American regions, will also record above-average cement market gains. Vietnam, Thailand and Indonesia are also expected to record strong increases in percentage terms (World Cement, 2013). Such ever-increasing demands are placing a significant strain on the current energy infrastructure and damaging world environmental health by CO, CO_2, SO_2, NOx effluent gas emissions and global warming.

2.2 Outline of Alkali Activation of Cementitious Materials

The German chemist Kühl (Kühl, 1908) was the first to publish work related to alkali-activated binders back in 1908. The publication was for a patented process in which a basic blast furnace slag was blended with either sodium sulphate or carbonate, lime and water to produce a useful binder from slags which would otherwise hydrate only very slowly. However, only decades later did this type of material receive any significant attention, when in 1940 a detailed study by Purdon was published detailing the interaction of slags with different chemical activators (Purdon, 1940), later turning them into a commercial product under the name 'Purdocement'. Structures built in the 1950s using Purdocement still exist and have been surveyed in a recent publication by Buchwald et al. (Buchwald *et al.*, 2015), concluding that the structures were still fit for purpose for their respective service life. Nonetheless, the production of Purdocement never reached full economic viability, and in 1957, the company ceased operating.

The main research progress in the area of alkali-activated materials for the next several decades came from a Ukrainian research group initially led by Glukhovsky (Provis and Van Deventer, 2014), and later by Krivenko (Krivenko, 1994). Through their efforts, they developed alkali-activated mixes based on a wide range of precursor and activator chemistries, including both low and high calcium binder systems. The alkali-activated materials were adopted in a wide range of applications (Shi, Krivenko and Roy, 2006), including low and high rise residential blocks (Fig. 2-2) and provided very good performance in service over several decades (Palomo *et al.*, 2014). The impetus for conducting the research and commercialisation projects was due to the shortage of cement after the Second World War, but abundance of slag from the iron

and steel production that had gone through the Soviet system during the preceding years. Not a lot is known about these concretes, or how they perform largely due to the literature being in the Russian or Ukrainian languages and the fact that the mix designs have not been particularly well recorded.

By the 1970s, Davidovits was developing a series of binders based on the alkali activation of calcined clay, which in 1979 he named 'geopolymers' (Panagiotopoulou, Tsivilis and Kakali, 2015). This name has since been applied much more widely to various alkali-aluminosilicate binder systems and is now widely recognised as a generic term for alkali-activated binder systems. As previously mentioned in the detailed abstract part, and now in Table 2-1, alkali-activated binders have had various terminology assigned to them depending on the research group investigating them. A detailed explanation of the differences is given in Chapter *2.5.1 Microstructure and Mechanisms of Hardening.*

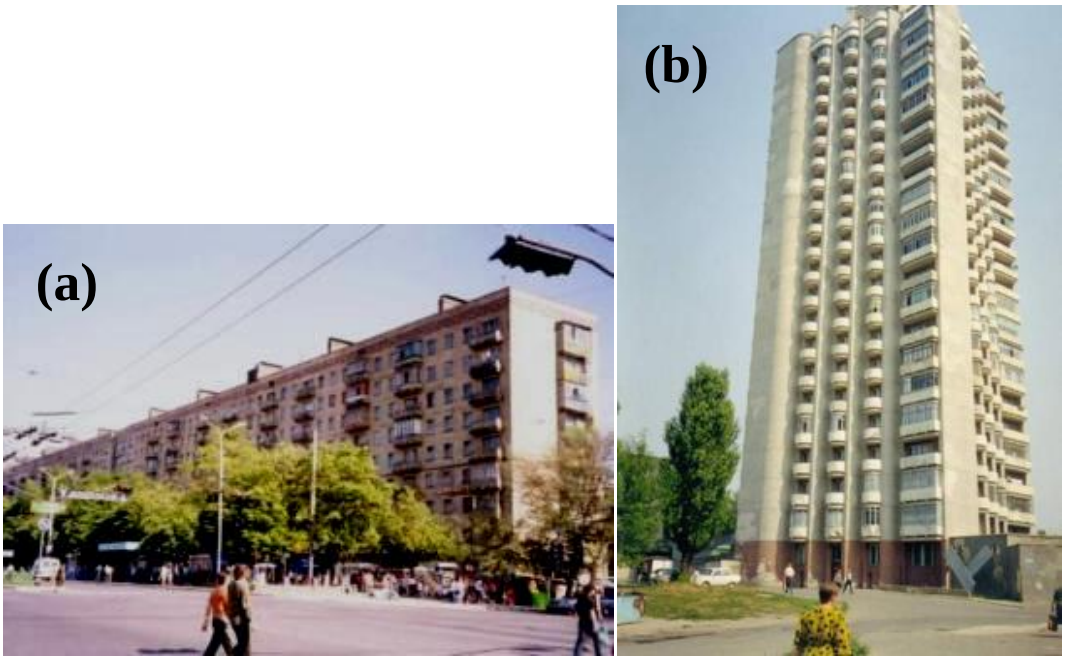

Fig. 2-2 (a) Low and (b) high rise residential blocks built from alkali-activated concrete in 1970's, Ukraine (Palomo *et al.*, 2014)

Table 2-1 Various terminology associated with chemically-activated cementitious materials

Terminology	Researcher
Soil Silicates	Glukhovsky (1957)
Geopolymers	Davidovits (1973)
Alkali-activated cement	Narang, Chopra (1983)
F-Cement	Forss
Gypsum-Free Portland Cement	Odler, Skalny, Brunauer (1983)
SKJ-Binder	Changgo (1991)
Geocements	Krivenko & Associates (1991)
Alkaline Cements	Krivenko (1994)

Research and development activities in the field of alkali activation began to expand during the 1980s and 1990s rapidly, and it is now a highly active area including efforts in scientific investigation, commercial deployment, and national and international standardisation (British Standards Institution, 2016). Table 2-2 summarises a historical timeline of important events in the development of alkali-activated materials. Furthermore, detailed reviews regarding the chemical, engineering and durability properties of alkali-activated materials can be found in a number of recent publications including (Van Deventer, Provis and Duxson, 2012; Bernal and Provis, 2014; Provis, 2014; Provis and Bernal, 2014; Provis and Van Deventer, 2014).

Table 2-2 The research process of chemically-activated cementitious materials (adapted from (Li, Sun and Li, 2010)**)**

Researchers	Year	Significance
Feret	1939	Slags used for cement
Purdon	1940	Alkali-slag combinations
Glukhovsky	1959	Theoretical basis and development of alkaline cements
Glukhovsky	1965	First proposed the term “alkaline cements”
Davidovits	1979	First proposed the term “Geopolymer”
Malinowski	1979	Ancient aqueducts characterised
Forss	1983	F-cement (slag-alkali-superplasticizer)
Langton and Roy	1984	Ancient building materials characterised
Davidovits and Sawyer	1985	Patent of “Pyrament” cement
Krivenko	1986	DSc thesis, $R_2O–RO–SiO_2–H_2O$
Malolepsy and Petri	1986	Activation of synthetic melilite slags
Malek et al.	1986	Slag cement-low level radioactive wastes forms
Davidovits	1987	Ancient and modern concretes compared
Deja and Malolepsy	1989	Resistance to chlorides shown
Kaushal et al.	1989	Adiabatic cured nuclear wastes forms from alkaline mixtures
Roy and Langton	1989	Ancient concretes analogs
Majundar et al.	1989	$C_{12}A_7$– slag activation
Talling and Brandstetr	1989	Alkali-activated slag
Wu et al.	1990	Activation of slag cement
Roy et al.	1991	Rapid setting alkali-activated cements
Roy and Silsbee	1992	Alkali-activated cements: an overview

Palomo and Glasser	1992	CBC with metakaolin
Roy and Malek	1993	Slag cement
Glukhovsky	1994	Ancient, modern and future concretes
Krivenko	1994	Alkaline cements
Wang and Scrivener	1995	Slag and alkali-activated microstructure
Fernández-Jimenez and Puertas	1997	Reaction of alkali-activated slag cement reaction kinetics
Katz	1998	Microstructure of alkali-activated fly ash
Davidovits	1999	Processes of mineral polymerisation
Gong and Yang	2000	Alkali-activated red mud-slag cement
Puertas	2000	Alkali activation of fly ash-slag cement
Bakharev	2001-2002	Alkali-activated slag concrete
Provis and Deventer	2005	Nano crystallinity in 'geopolymers'
Provis and Deventer	2009	Structure, preparation, properties and industrial applications of alkali-activated binders
Lothenbach et al.	2011	Influence of slag chemistry on the hydration of alkali-activated blast-furnace
Provis and Deventer	2014	Alkali-Activated Materials: State-of-the-Art Report
BSI	2016	First major performance specification for AACM

2.2.1 Physical and Chemical Differences Between PC and Alkali-activated Binders

Compared with calcium silicate-based cementitious materials e.g. PC, the hardening process of chemically activated cementitious material regarding the microscopic mechanisms have significant differences, mainly reflected in following points:

1) Chemical excitation of the cementitious materials hardening process needs to be under the influence of a chemical activator, the nature of which greatly impact the basic laws and characteristics of hardening. The employment of concentrations and dosages of chemical activator causes several changes in the chemistry of the reaction, affecting the quality and characteristics of the final compounds (Singh *et al.*, 2016).

2) In the excitation of cementitious materials by chemical activation, the role of water is different to that of a PC hydration system. Water takes part in the dissolution, hydrolysis and condensation reactions during chemically activated binder synthesis (Weng and Sagoe-Crentsil, 2007). It provides the medium for the dissolution of aluminosilicates and the transfer of various ions, hydrolysis of Al^{3+} and Si^{4+} compounds

and condensation of different aluminate- and silicate-hydroxyl species. As a result, water has a great effect on the binder formation and properties.

3) The type and chemical composition of the raw materials stimulate cementitious materials, leading to a chemical reaction and hardening process which is complex and difficult to understand using any macroscopic law.

4) The chemical activator does not only play the role of catalyst in the reaction process but also participates in the final composition of products, resulting in a very complex and different structure of reaction products. Hence, more advanced novel characterisation techniques must be employed to study the hardening kinetics and track changes. Nuclear Magnetic Resonance (NMR) spectroscopy, which is a common technique for determining the structure of organic compounds has been found to help elucidate many of the chemical changes in the early and late stages of activation (Singh, Bastow and Trigg, 2005). Table 2-3 provides further details of the differences between PC clinkers and chemically activated cementitious material from a compositional perspective, while Table 2-4 provides further details of the significant differences between PC and chemically activated cementitious from a chemical perspective. Note that in Table 2-3; R_2O is Na_2O, K_2O or Li_2O and RO is CaO.

Table 2-3 The main differences between PC clinkers and chemically activated cementitious material

Cement Type	PC	Alkaline PC	Alkaline blended PC	Slag alkaline cement	Ash alkaline cement	Geo-cement
Initial solid phase	PC clinker	PC Clinker + R_2O	PC clinker+ additive (slag, ash, red mud) +R_2O	Metallurgical Slag+R_2O	Fly ash of heat power stations+ R_2O	Clay+R_2O
Alkali content, R_2O, %	< 0.6	1-5	2-5	4-8	5-10	10-20
Hydration product	0% R_2O-Al_2O_3-SiO_2-H_2O → 100 %					
	100 % ← RO-SiO_2-H_2O					
	R_2O-CaO-$Al_2O_3SiO_2$-H_2O					
	High Ca-cements		Hybrid cements		Low Ca-cements	

Table 2-4 Differences between PC clinkers and chemically activated cementitious material from a chemical perspective

	Alkali-activated binder	PC binder
raw materials	Aluminosilicate materials + alkali activator	Calcium silicate/calcium aluminate system +water
reaction products	Aluminosilicate gel	CSH, CAH, CAFH, Ca(OH)2
calcium content		
XRD pattern	predominantly amorphous with small crystalline phase	amorphous CSH and crystalline phases such as Ca(OH)2
FTIR pattern	Si-O absorption peak intensity (970-1030 cm-1), Si-O-Si (Al) symmetric vibration absorption peak (720 cm-1), a cyclic silicate vibration absorption peak (590 cm-1)	Si-O strong absorption peak (970-1030 cm-1 trough), carbonates vibration absorption peak
27Al MAS-NMR pattern	57-58 ppm corresponds to AIQ4	64 ppm corresponds to tetrahedral Al in CSH, 12 ppm and 8 ppm correspond to octahedral Al in CaSO4 and CAH

2.2.2 Commercialisation of Alkali-activated Binders

The global business of alkali-activated materials is at an emerging stage at the moment and is expected to grow exponentially over the following years at a compound annual growth rate of 40% by 2020 (PRNewswire, 2015). By August 2013, 12,000 tonnes of alkali-activated concrete had been poured globally. Recent increased global acceptance of alkali-activated binders led the world's first building to use alkali-activated concrete for structural purposes successfully; a 4-story general public use building in Australia, comprised of 3 suspended alkali-activated concrete floors involving 33 precast panels (Geopolymer Institute, 2013). This project was swiftly followed by the completion of the Brisbane West Wellcamp airport in Australia in September 2014. During this project, 70,000 tonnes of alkali-activated concrete was used to build almost the entire airport, with the only exception being the main runway surface, which for Australian legal compliance purposes could only be constructed from Portland cement (Geopolymer Institute, 2014). There exists a wide variety of current and potential applications for alkali-activated binders. Some of the alkali-activated binder applications are still in development whereas others are already industrialised and commercialised. The greatest application in volume comes through alkali-activated cement, which has been commercialised in many countries, the foremost

being Australia with the product Earth Friendly Concrete (Wagners, 2016), but have also been manufactured and studied by several other international research institutes (Geopolymer Institute, 2011). Decorative architectural elements have also been manufactured using pre-cast methods in Brazil by a company called Wincret using geopolymer mortar in the replica of Solomon's Temple San Paulo, Brazil (base and chapiter of columns, upper and lower roof cornices and crowning), shown in Fig. 2-3.

Fig. 2-3 Alkali-activated (a) roof crowning and (b) base and chapiter of columns developed by Wincret (Pappalardo, Jalali and Silva, 2014)

In Europe, the Dutch company ASCEM have commercially been putting together pre-cast products, pipes using patented fly-ash reprocessing technology to produce the necessary precursors for their products (shown in Fig. 2-4). To prove that alkali-activated materials are not restricted to pre-cast applications, a major embankment retaining wall at Melbourne's Swan St Bridge was cast in-situ in 2010 (shown in Fig. 2-5) using an alkali-alkali-activated concrete derived from fly ash and blast furnace slag (ACM, 2009). Performance-based regulations like the ones implemented in Australia have proven to be very beneficial for the growth of alkali-activated binder research and industry. This is because the commercial implementation of alkali-activated material technology in Australia is being driven by multiple teams operating across the country, including the Centre for Sustainable Resource Processing, which has been making advances in this area over the past decade. On the other hand, national standards such as the European cement standard are more prescriptive in nature and explicitly limit concrete to a Portland cement based binder.

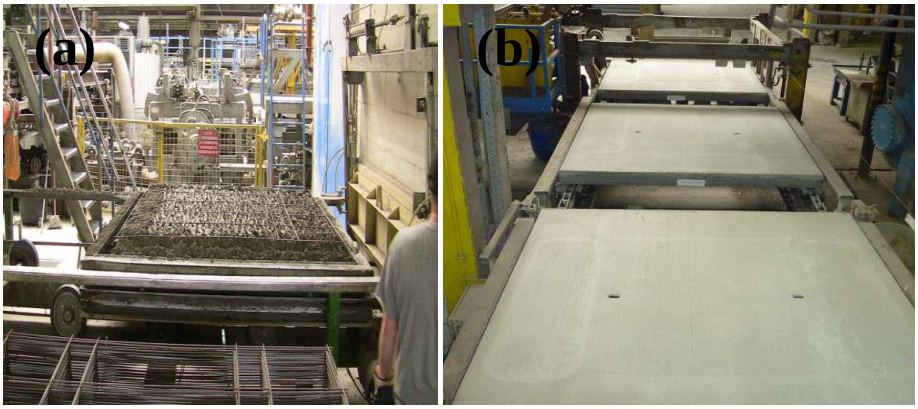

Fig. 2-4 Alkali-activated (a) fresh concrete and (b) final panel products developed by ASCEM (ASCEM B.V., 2015)

Fig. 2-5 In-situ casting of alkali-activated concrete (ACM, 2009)

2.3 Advances in Alkali-Activation of Non-Conventional Materials

A very wide range of largely low value or waste materials can be used for alkali-activation, the availability of which varies on a geographical scale. For instance, in the UK, fly ash, which is a by-product of burning coal in a power station furnace, is becoming scarce, while Australia and South African are producing more fly ash than cement. Various areas also have natural pozzolans; others have geological deposits of kaolin clay. Metakaolin is unique in that it is not the by-product of an industrial process nor is it entirely natural; it is derived from a naturally occurring mineral and is manufactured specially for cement applications. Metakaolin is usually produced by thermal treatment, i.e., calcination of kaolin clays within a definite temperature range (Ilić, Mitrović and Miličić, 2010). The raw materials such as metakaolin or low-calcium fly ashes have been the preferred choice of precursors for synthesising alkali-activated binders (Duxson et al. 2007). The primary reasons for this are the consistency of the latter materials regarding industrial output and chemical composition. However, the supply of fly ash in Europe is reducing due to the industry becoming increasingly less reliant on coal-fired power stations (Carroll, 2015) while the disposal of the 85% of host rock generated from kaolin clay mining is an increasingly critical issue (Murray, 2002).

More recently, however, researchers have become more innovative with the types of precursors materials used for alkali-activation and have demonstrated the potential of using more non-conventional materials, concentrating mainly on industrial wastes. Table 2-5 gives a summary of these materials, chemical composition, methods of activation and their availability. Some of the waste materials such as bottom ash need to be evaluated to make sure there are no chemo-toxicity in them and no leachable heavy metal components. The toxicity of these waste materials can present a significant caveat for their use but can nonetheless be overcome by ensuring the safe use of these materials e.g. by a simple dilution process e.g. mixing 15-20% of the waste material with fly ash or ground granulated blast furnace slag (GGBS).

Table 2-5 Summary of industrial waste materials available for chemical activation

Types of waste	Global availability	Chemical Composition (%)												Activators	References
		SiO_2	Al2O3	Fe_2O_3	Na_2O	MnO	CaO	TiO_2	K_2O	MgO	P_2O_5	SO_3	C		
silico-manganese (SiMn) slag	7.4 Mt/y	42.6	12.2	1.0	0.36	9.9	25.2	0.36	2.2	4.2	-	0.12	-	NaOH	(Kumar *et al.*, 2013)
Bayer Red Mud	100 Mt/y	20.38	24.50	9.48	11.46	-	12.86	2.92	0.88	1.00	-	1.00	-	NaOH and Na_2CO_3	(Ye *et al.*, 2016)
Palm Oil Fuel Ash	50 Mt/y	61.33	7.2	5.11	0.123	0.097	8.20	0.25	6.50	4.69	4,6	0.27	1	Na2SiO3 and NaOH	(Mijarsh, Megat Johari and Ahmad, 2014)
Incinerator bottom ash (IBA)	10^{12} t/y	32.75	8.57	10.02	2.87	0.15	29.06	1.57	1.24	1.75	4.77	3.01	-	NaOH	(Yamaguchi *et al.*, 2013)
Rice husk bark ash	110 Mt/y	81.36	0.4	0.12	-	-	3.23	-	-	-	-	0.85	-	Na2SiO3 and NaOH	(Nazari, Bagheri and Riahi, 2011)
Silica-rich vanadium tailing	1 ton of V_2O_5 generates 120–150 t of tailings	64.17	10.27	4.98	5.27	-	4.46	-	2.05	-	-	-	-	Na2O-1.5SiO2	(Jiao, Zhang and Chen, 2013)

Continued next page >>>

Ceramic waste	Red clay brick	3-7 wt.% of total production	50.95	16.92	6.68	0.55	-	9.92	-	4.33	5.62	/	3.37	-	Na2SiO3+NaOH	(Reig *et al.*, 2013)
	Porcelain stoneware		71.35	19.37	6.68	4.68	-	0.51	-	1.73	0.59	/	0.02	-		
Fluid catalytic cracking		14.2 M BPD	46.94	48.40	0.59	0.31	-	0.11	1.20	0.02	0.17	0.01	0.02	-	Na2O3Si+NaOH	(Rodriguez *et al.*, 2013)
Coal Gangue		2×10^{11} t/y	39.1	31.06	9.48	0.16	-	0.38	0.98	0.26	0.24	-	-	-	Na_2SiO_3	(Cao *et al.*, 2016)

2.3.1 Silicomanganese (SiMn) Slag

New slags are being produced by steel industries using electric arc furnace technology. Silicomanganese (SiMn) slag is a by-product generated during the production of the silicomanganese alloy by carbothermic reduction of raw materials from an electric arc furnace (Frias *et al.*, 2006; Kumar *et al.*, 2013). SiMn slag is characterised by its high manganese content, compared with traditional slag (blast furnace slag). The main constituents of SiMn slag are SiO_2, CaO and Al_2O_3 and comprise 80% of the total composition. Kumar et al. (2013) developed a binder paste from mechanically activated silico-manganese (SiMn), activated with sodium hydroxide, obtaining a compressive strength of up to 101 MPa after 28 days of sealed curing at 27 °C.

2.3.2 Bayer Red Mud

A one-part alkali-activated binder was synthesised from thermally activated Bayer red mud (Hind, Bhargava and Grocott, 1999; Gräfe, Power and Klauber, 2011; Ye *et al.*, 2016). Karl Josef Bayer developed and patented a process for refining bauxite to smelting grade alumina. The precursor, now called Bayer Process, has become the cornerstone of the aluminium production industry worldwide (Hind, Bhargava and Grocott, 1999). Bayer red mud is the residue of bauxite ores after digestion by caustic soda through the Bayer process to produce alumina. It is a highly alkaline waste with an average pH of 11.3 (Hind, Bhargava and Grocott, 1999; Gräfe, Power and Klauber, 2011; Ye *et al.*, 2016). Land disposal of red mud may cause serious environmental pollution if leaked into the surrounding environment, and cases of ecological disasters caused by the rupture of a red mud dam have occurred several times in the past (Hind, Bhargava and Grocott, 1999; Gelencsér *et al.*, 2011). Red mud alone has a poor reactivity and low SiO_2/Al_2O_3 molar ratio (< 2) (Dimas, Giannopoulou and Panias, 2009; Ye *et al.*, 2016) therefore research has been done on combining it with other precursor materials such as metakaolin. Hajjaji et al. (2013) used red mud and metakaolin with $NaOH/Na_2SiO_3$ activator solution, to produce a moderate 28-day compressive strength of 10.8 MPa.

2.3.3 Palm Oil Fuel Ash (POFA)

Palm oil is the most used vegetable oil in domestic cooking and food processing, in oleochemicals, cosmetic and also in fuel (Oosterveer, 2015). Mijarsh et al. (2014) ground palm oil fuel ash (POFA) in a ball mill to obtain particle sizes of about 10 µm. Grinding was followed by calcination at 500 °C for 1 h to remove the unburned carbon, then a second stage of grinding to form the treated palm oil fuel ash (TPOFA). The chemical compositions of TPOFA in their study are provided in Table 2-5. Ariffin et al. (2013) used untreated POFA in combination with pulverised fuel ash (PFA) and alkaline activator (NaOH and Na2SiO3) to produce a binder with a 28-day compressive strength of 30 MPa. According to the study of Khankhaje et al. (2016), it was concluded that the addition of POFA to concrete as partial replacement of cement could increase the compressive strength according to the low pozzolanic reactivity and higher water demand of POFA which reduces the workability and strength of POFA concrete.

2.3.4 Incineration Bottom Ash (IBA)

Municipal wastes, mostly consisting of urban refuses, are incinerated to prevent foul odour and to reduce its volume by up to one-twentieth. Consequently, millions of tonnes remain as ash which contains hazardous dioxin and heavy metals as well as chlorine. Although most modern incineration plants working at higher temperature have facilities to disintegrate the dioxin, chlorine contamination is unavoidable even by the more efficient electric smelting plants, since fly ash, consisting of volatiles and particulates of incineration ash is mixed with the main ash. Urban waste incineration slags have been applied as active fillers of alkali-activated binders. When cured at 80°C and 100%RH, flexural strength tests for pastes revealed a range of strength from 3-16 MPa for 24 h curing. The strength was not depending on the iron contents but instead on the degrees of foaming and swelling, i.e., bulk densities of the hardened bodies.

2.3.5 Rice Husk–Bark Ash (RHBA)

Rice husk–bark ash (RHBA) is a solid waste produced by burning a mixture of rice husk (65% by weight) and eucalyptus bark (35% by weight) as fuel by the fluidised bed combustion process in a biomass power plant. The major chemical constituent of RHBA is SiO2 (about 75%) (Sata, Jaturapitakkul and Kiattikomol, 2007; Sonebi and Cevik, 2009). The amorphous silica in rice husk (RHA) contained in the 65 % of RHBA can be used as a pozzolanic matter (Chindaprasirt et al. 2007).

2.3.6 Silica-Rich Vanadium Tailings

With the rapid development of vanadium extraction from stone coal, large amounts of tailing are produced, which occupy not only vast land but also cause secondary environmental pollution. Silica-rich vanadium tailings are converted into a thermostable alkali-activated binder. For its synthesis, the milled vanadium tailing is combined with fly ash and activated using sodium silicate. The results show that dry ball-milling could effectively enhance the reactivity of the vanadium tailing and samples calcined at 900°C could reach a compressive strength of approximately 55MPa. The application for such alkali-activated materials was suggested for synthesising fire-resistant alkali-activated products.

2.3.7 Ceramic Waste

Ceramic wastes are generated by the manufacturing and construction sectors and account for approximately 45% of construction and demolition. Different ceramic materials can be distinguished according to the source of raw materials e.g. structural ceramic products, ceramic tiles and stoneware (F. Pacheco-Torgal, C. Leonelli and Chindaprasirt, 2013). Reig et al. (2013) presented a study about the alkali-activation of two different ceramic waste materials, namely red clay brick and porcelain stoneware. For red clay brick powder, using an activating solution of NaOH, compressive strengths of 29-41 MPa were achieved, depending on the water/binder and activator/binder ratios. To produce alkali-activated mortars using porcelain stoneware, the addition of $Ca(OH)_2$ was necessary, resulting in a compressive strength of about 30 MPa after 7 days of curing at 65ºC.

2.3.8 Catalyst Residues

The fluid catalytic cracking catalyst residue (FCC) is obtained as a by-product from the petroleum industry. This material is classified as an aluminosilicate source in the production of alkali-activated binders. FCC catalyst obtained from the petroleum cracking process contains largely spherical or spheroidal shaped particles with diameters ranging from 100 to 20 μm (Payá, Monzó and Borrachero, 1999; Tashima *et al.*, 2013). In the study of Tashima et al. (2012), it was concluded that FCC could be successfully used as a precursor material for preparing alkali-activated binders when combined with $NaOH/Na_2SiO_3$ to produce a stable binder with a compressive strength ranging from 8.52–68.34 MPa.

2.3.9 Coal Gangue

Coal gangue is one of the major solid reject materials (Xiao and Liu, 2010) and poses many serious environmental problems (Cao *et al.*, 2016). It is produced during the excavation and washing of the coal mine and has a mineralogical composition consisting of illite, quartz and kaolinite. Its particles are flakes of scaly morphology with a partial wormlike structure, and the major chemical components are SiO_2 and Al_2O_3 (Wang *et al.*, 2015; Cao *et al.*, 2016). Calcined coal gangue possesses a high amorphous aluminosilicate content and can be used to prepare alkali-activated materials when combined with Na_2SiO_3 (Provis, Palomo and Shi, 2015). The compressive strength of calcined coal gangue paste could reach 42.5 MPa after 24 h of curing at 90 °C (Provis, Palomo and Shi, 2015).

2.4 The Panasqueira Tungsten Mine

The applications of tungsten are extremely varied, and the hardness of the mineral makes it valuable for shaping metals, plastics and ceramics. About two-thirds of tungsten is used for cemented carbide and other construction and chemical applications. However, it is also used for everyday purposes like the vibration alert in mobile phones, light bulb filaments, solar panels and window heating (Investing News, 2015a). China plays a dominant role in the tungsten industry, accounting for about 84.5% of the world's total output, and is a net importer of tungsten concentrates; as a result, it heavily influences the tungsten price (Investing News, 2015b). The Panasqueira mine is one of the largest operating tungsten mines in the Market Economy Countries and is considered a world-class Tungsten-Tin-Copper vein-type deposit, located in the Central Iberian Zone of the Palaeozoic Iberian Massif in Portugal, which is one of the most important metallogenic provinces of Europe (Franco, Vieira and Bunting, 2014). The tungsten concentrates produced have a WO_3 content of 74 – 75% which is one of the highest grades available in the market. The Panasqueira mine mines an iron rich tungstate termed ferberite. The production quantity of the WO_3 concentrate is variable but currently is in the range of 85,000 – 95,000 mtu (1 mtu – metric tonne unit – is equal to 10 kg) per year (Franco, Vieira and Bunting, 2014). In the process of producing the principle metal of tungsten and by-products of tin, copper and silver, the Panasqueira mine also generates a significant amount of wastes. These wastes are primarily (1) tin, copper, arsenic, and phosphorus contaminated water which is generated from the mining activities and from the hydro cyclone heavy media separation plant, (2) quartz and schist collected from the crushing of the ore and (3) tailings received from the water-treatment plant. The mining company have taken environmental preservation initiatives such as treating the wastewater which is generated on-site from the mining activities and plant operation by either re-using or

releasing it into the river. As for the coarse tailings, these are stockpiled and sold to local companies for re-use in road work. The Panasqueira mining company, however, have not been able to find any economically suitable way of re-using the fine tailings, and end up storing it in ponds. Fig. 2-6 is an aerial image of the principal waste disposal areas of the Panasqueira mine. In fact, the accumulation of these fine tailings has become increasingly large (more than 100 hectares) that an additional disposal pond is under construction. Fig. 2-7 shows at close range the existing fine tailings pond and the new pond under construction. The accumulation of these fine tailings for long periods of time can begin to contaminate soil, water and air in the surrounding areas, damaging flora and fauna and the health of local inhabitants. The accumulation of the tailings runs the risk of collapse which can cause severe metal accumulation in plants and animals, contamination of soil and loss of human/animal life. The effluent and dust emitted from the tailings combined are of alkali nature and contain dissolved metals such as sulphide, manganese and arsenic which are toxic to the environment.

Fig. 2-6 Satellite view of the disposal areas (Franco, Vieira and Bunting, 2014)

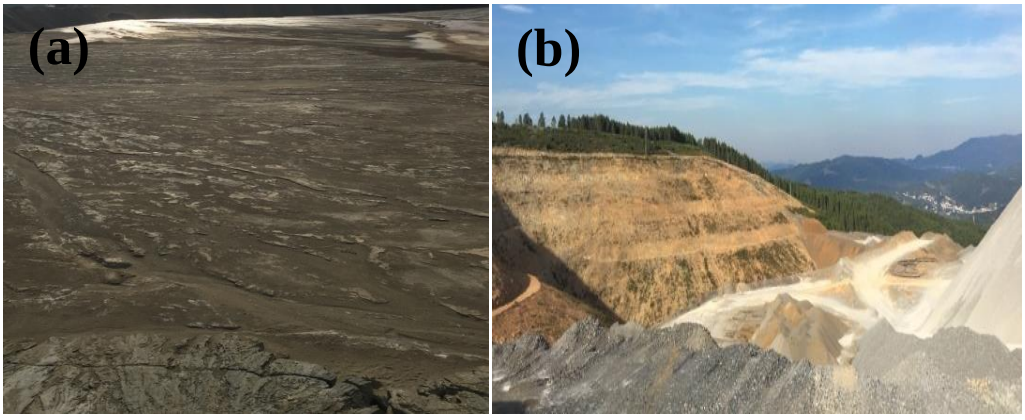

Fig. 2-7 (a) Existing fine tailings pond and (b) New pond under construction, Photo: Author (June 2016)

Some mining and quarrying wastes can be reused in earthworks and construction, particularly the coarser fractions. Typical applications include use in asphalt pavements (Akbulut and Gürer, 2007) and concrete (Yellishetty *et al.*, 2008; Hebhoub *et al.*, 2011). However, several aspects affects its potential for reuse on a national scale: they can

become raw material for industrial applications where the high value of the product does not prejudice its reuse due to transport costs, which includes, as an example, processing of calcium carbonate waste for Portland cement production in the specific case of marble industry (Raupp-Pereira *et al.*, 2008), or the reuse of fine tailings from abandoned mine in polyester mortars (Mun *et al.*, 2007). However, recent studies on the reuse of fine tailings as raw material for alkali-activated binders and applications have been conducted in EU and other countries and are considered to be most promising, from an environmental, technical and economic point of views (Pacheco-Torgal et al. 2008; F. Pacheco-Torgal et al. 2009). Initially, these studies aimed the development of a new alkali-activated binder by reusing mud waste from a tungsten mining exploration that presented very good re-activity with alkaline activators, after thermal treatment. This new binder was investigated first for its potential use as repair material of PC concrete. The results indicated such binder possesses very high bond strength even at early ages and that behaviour is not affected by low surface treatment roughness. As well, cost comparisons show this alkali-activated repair solution is by far the most cost efficient (Pacheco-Torgal, J. P. Castro-Gomes et al. 2008).

Later, alkali-activated artificial aggregates were produced from such mining waste mud (see Fig. 2-8), and their properties were studied as a potential substrate for fixed-film wastewater treatment processes (biofilm reactors). The results showed that the aggregates obtained have suitable resistance to acid attack and may be used as a substrate for fixed-film biological reactors for the treatment of acid wastewaters. Additionally, the appropriate porosity of the aggregates makes them suitable for providing good adhesion and development of a biofilm, essential for pollutant removal. Hence, the development of artificial aggregates through alkali-activation of mining waste mud for wastewater treatment by filtration, presents a viable technical solution to compete with other commonly adopted materials (e.g. crushed natural stone or expanded clay) (Silva, J. Castro-Gomes and Albuquerque, 2012; Silva, J. P. Castro-Gomes and Albuquerque, 2012a).

Fig. 2-8 Alkali-activated artificial aggregates produced from Panasqueira mining waste mud for wastewater treatment

Significant efforts have also been made in the design concept of a modular system for vegetated surfaces suitable for new or retrofitted buildings (see Fig. 2-9). The modular system consists of precast panels incorporating vegetation, where the base plate is made

with alkali-activated mortar using a blend of tungsten mining waste mud (from the Panasqueira mine), cork granules and other waste materials. So, the base plate final properties combine good water absorption, low density and good mechanical strength. The water absorption rate shows that the alkali-activated plate can absorb the water quickly and supply it to the plant substrate, minimising the irrigation needs (Manso *et al.*, 2013; Manso, Castro-Gomes and Silva, 2013).

Fig. 2-9 GEOGREEN modules, consisting of an alkali-activated base plate using tungsten mining waste mud and an insulation corkboard

Other innovative studies related to the alkali-activation of mining waste have been conducted at the University of Arizona, USA. A feasibility study of utilising copper mine tailings to produce of eco-friendly bricks based on the alkali-activation technology has been successfully carried on. Unlike the conventional method for producing bricks, the new procedure neither uses clay and shale nor requires high-temperature kiln firing, having significant environmental and ecological benefits. The results showed that copper mine tailings could be used to produce eco-friendly bricks based on the alkali-activation technology to meet the ASTM requirements (Ahmari and Zhang, 2012).

Moreover, an investigation on the utilisation of fly ash modified mine tailings as construction material through alkali-activation has also been carried out at the University of Arizona, USA. Considering the extremely high Si/Al ratio of the mine tailings, class F fly ash was used to modify the Si/Al ratio. The addition of fly ash to mine tailings resulted in the higher compressive strength of alkaline activated materials. The improving effect of adding fly ash to mine tailings was mainly due to the decrease of Si/Al ratio of the mix to reach the range of the optimum Si/Al ratio (Zhang, Ahmari and Zhang, 2011a).

2.5 Alkali-Activation of Cementitious Materials in Detail

2.5.1 Microstructure and Mechanisms of Hardening

The distinction between “alkali-activation” and “geopolymerisation” has been one of the main important subjects of discussion and debate during the last decades: considering the number of published research on this topic and the extensive nomenclature adopted by the authors, it is not easy to discern the differences between them. One of the most suitable key distinction has been presented by Provis and van Deventer (2009), stating that the alkaline activation generates a calcium silicate hydrate-based gel, with mainly one-

dimensional chains of silica, whereas the geopolymer gel is a 3-D alkali aluminosilicate framework structure, without calcium presence. Currently, a very wide variety of nomenclature exists for these materials, creating much confusion, especially about which terms refer to which precise compounds. Provis and Van Deventer (2009) consider a geopolymer as "a solid and stable aluminosilicate material formed by alkali hydroxide or alkali silicate activation of a precursor that is usually (but not always) supplied as a solid powder". According to Duxson et al. (Duxson *et al.*, 2007), this term is generally used to represent "the amorphous to crystalline reaction products from synthesis of alkali aluminosilicate from reaction with alkali hydroxide/alkali silicate solution". Although terms like "low-temperature aluminosilicate glass", "inorganic polymer glasses", "alkali-activated cement", "Geocements", "hydroceramic", "alkali-bonded ceramic", "inorganic polymer concrete", "alkali ash material" and a variety of other names are very commonly used in the academic literature, each of these terms represents a material synthesized using the same chemical processes. This chemical process can be summarized as "a complex system of coupled alkali mediated dissolution and precipitation reactions in an aqueous reaction substrate".

Thus, the term "geopolymer" appears to be broad and heterogeneous, also considering countless practical working definitions, which several authors have introduced in their works. As an example, Rees et al. (2007) defined their material as a "material formed by mixing an alkali metal source, a silica source, and an aluminium source in water at high pH, which transforms into a hardened solid capable of maintaining rigidity in water". Rees considers the stability in water as a distinctive factor of her material, differing from other working definitions, which include different parameters, such as strength development in ambient temperature, thermal stability at high temperature, Al-O and Si-O tetrahedral units in the structure and many others. Hence, the individuation of a unique definition of the geopolymer term seems to be a very hard task, considering the myriad of parameters and factors involved. Many authors, especially Davidovits (2016), have argued about the suitability of different nomenclatures that should be adopted, asserting that not all alkali-activated binders are real geopolymers and that the pozzolanic reaction is not a geopolymeric one.

2.5.2 Mechanisms of Alkali-Activation: A Conceptual Model

The exact mechanism of alkali-activation, although deeply explored and investigated, is not yet completely understood. The employment of different kinds of precursors and activators causes several changes in the chemistry of the reaction, affecting the quality and the characteristics of the final compounds. For this reason, it is possible to find many different types of research in the literature, in which many authors have tried to find out and explain the different phases of alkali-activation.

As already stated, Purdon was the first to propose a process of alkali-activation. By mixing sodium hydroxide with a variety of minerals and glasses, rich in silicon and/or aluminium, including blast furnace slag, he discovered that the involved mechanism takes place in two steps. First is the release of silica, alumina and lime; second is the formation of hydrated calcium silicates, aluminates as well as a regeneration of the alkali solution (Khale and Chaudhary, 2007). In other words, it was suggested that the hardening phase entails the dissolution of Si and Al in an alkali medium, provided by sodium hydroxide, followed by a precipitation of calcium silicate or aluminium hydrate, concluding that alkali

hydroxides act as catalysts during this process (Pacheco-Torgal, J. Castro-Gomes et al. 2008a).

Glukhovsky proposed a general model for the alkali activation of aluminosilicate materials, composed of three main stages: “destruction-coagulation”, “coagulation-condensation” and “condensation-crystallization”. The first disaggregation process is based on the decomposition of Si-O-Si and Al-O-Si covalent bonds contained in the starting material. The disaggregation takes place only if the ionic force is varied using the addition of electron donor ions, which happens when the pH of the medium solution increases. The second stage consists of an accumulation of disaggregated products which form a coagulated structure, leading to the polycondensation, thanks to OH^- ion which catalyses the reaction. Aluminates are also involved in this reaction; while they play the role of catalysers in the destruction phase, in the second and the third steps they are structural components. The last (third) stage leads to a generation of a condensed structure, during which the alkali-activated network structures are built up (Provis and Van Deventer, 2009). For a clearer understanding of the alkali-activation reaction, a summary of the alkali-activation process is shown in Fig. 2-10.

Aluminosilicate material is dissolved in an alkaline environment, the silicon-oxygen and aluminoxane bonds are broken, and the alkali-activation reaction commences: the dissolved aluminate monomer and the silicate salt are diffused from the surface of the solid particles to the interstices of the particles; the alkali silicates in the activator react with the aluminate monomer and silicate salt to form the gel phase. The gel phase gradually hardens, and the water produced in the polymerization reaction is discharged.

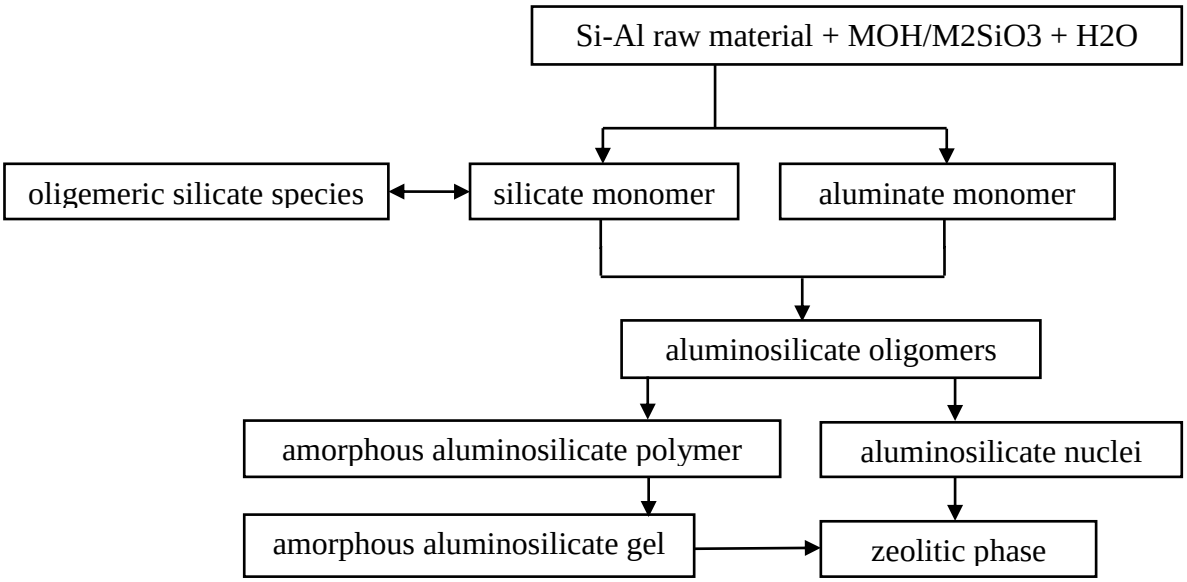

Fig. 2-10 Conceptual model of alkali-activation reaction process

Many of the authors have adopted this general three-stage mechanism, however, in the last years, it has been examined in depth, developed and expanded. Starting from the Glukhovsky theory, some researchers have improved the knowledge about each reaction process governing the alkali-activated synthesis, adding more specific descriptions and details about each phase. Also, the accumulated knowledge about zeolite synthesis has been used to clarify the alkali-activation, since their development is very similar. The main differences between these alike materials are in the composition of the initial mixture,

regarding the concentration of precursors, as well as the fact that zeolites are usually crystalline, while alkali-activated binders are amorphous to semi-crystalline. The latter grow in closed hydrothermal systems and crystallise from dilute aqueous solutions, whereas the former type can easily move and have enough time to orient and align themselves before turning into a crystal structure. Conversely, the setting of alkali-activated binders occurs quickly, preventing a proper crystallisation of the structure, even at ambient temperature and pressure (Khale and Chaudhary, 2007). A summary of the established differences between the syntheses of zeolites and the process of alkali-activation is presented Table 2-6.

Table 2-6 Differences between the synthesis of a zeolite and alkali-activation

	Synthesis of zeolite	Alkali-activation
Reactants	Al complexes solution + Si complexes solution	Al-Si solid source material + Alkaline solution + silicates (solid or liquid)
Early stage of reaction	Nucleation in solution	Leaching of Si-Al solid into paste
Later stage of reaction	Crystal growth in solution	Diffusion and condensation of leached Al and Si complexes in paste
Temperature	90-300°C	Ambient-80°C
pH	6-11	14
Product	Crystalline zeolite	Mixture of gel and Al-Si solid source material
Composition	Certain stoichiometric formula	No certain stoichiometric composition
Structure	Unique crystal	Mixture of amorphous to semi-crystalline gel phase and crystalline Al-Si source materials
Mechanical strength	Low	High

Despite these differences, Van Jaarsveld et al. (1997) proposed that the alkali-activation occur following the same processes of zeolites, with the initial dissolution, followed by the orientation of dissolved species and a final phase of hardening, in which an inorganic polymeric system is developed.

Duxson et al. (2006) provided a simplified reaction mechanism, suggesting the presence of two new stages which are also involved in zeolite synthesis: a nucleation phase, during which the formation of zeolite precursors, promoted by the dissolution of aluminosilicates in the alkaline medium takes place, followed by a stage of crystals development, as a result of the increase in the nuclei size. Fig. 2-11 shows this conceptual model discussed below. Although presented linearly, all the steps occur simultaneous, during a uniform process.

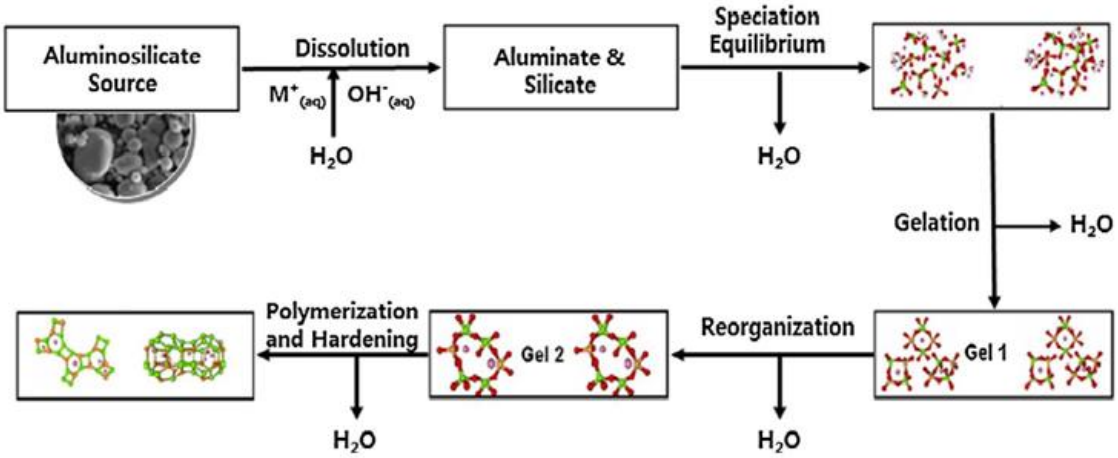

Fig. 2-11 Conceptual model of a simplified reaction mechanism for alkali-activation (Duxson, Lukey and van Deventer, 2006)

The solid aluminosilicate source, usually provided as a powder, is dissolved by alkaline hydrolysis, consuming water and releasing aluminates and silicates, probably as monomers. These small dissolved species interact between themselves, including the silicate, eventually provided by the activating solution, leading to the formation of aluminosilicate oligomers. When the saturation is reached, an aluminium-rich gel is formed (Gel 1 in Fig. 2-11.): Fernández-Jiménez and his collaborators (2006) provided an explanation for the formation of this gel, considered as an intermediate product, asserting that the copious presence of Al_3+ ions at the beginning of the process promotes its development since the dissolution of reactive aluminium is faster than that of silicon. While the first gelation carries on, Gel 2 (also shown in Fig 2-11) starts to be generated due to the increase of the silicon concentration in the alkaline medium (P. Duxson et al. 2006). These reorganisation processes are responsible for the features of the final binder, such as the microstructure and the porosity, influencing the physical properties. As confirmed by Duxson (2005), the activity of the silicate species inside the activating solution plays a crucial role, controlling the rate of structural reorganisation and densification. In fact, it was observed that the higher the activity, the more widespread the gel reorganisation and densification, leading to a microstructure characterised by dense gel particles and large intercommunicating pores. Conversely, a limited activity causes a less gel density and a distributed porosity. The time required for the complete set up of the final structure depends deeply on different factors, such as the mix design and the curing schedule. For some mixtures, this process can be almost instantaneous, while, for others, it can take several days.

According to Davidovits (2002 and 2015), the alkali-activation process exploits the hydroxylation and polycondensation of silico-aluminates, which are transformed in so-called “polysialates”, where sialate is an abbreviation for silicon-oxo-aluminate. The sialate network is composed of tetrahedral anions $[SiO_4]_4^-$ and $[AlO_4]_5^-$ linked alternately by all the oxygen, which need positive ions, like Na^+, K^+, Li^+, Ca^{2+}, Ba^{2+}, $NH3^+$, H_3O^+, to balance the negative electric charge of Al_3 in coordination IV. Polysialates are identified by the following:

Mn {– (SiO2)z –AlO2}n; wH2O (Eq. 1)

where M is a monovalent alkali cation, like sodium or potassium, n is the degree of polycondensation, w is the number of associated water molecules (hydration degree), z is 1, 2 or 3. Depending on its value, standard polysialate (z=1), polysialate-siloxo (z=2) and polysialate-disiloxo (z=3) can be distinguished, as shown in Fig. 2-12.

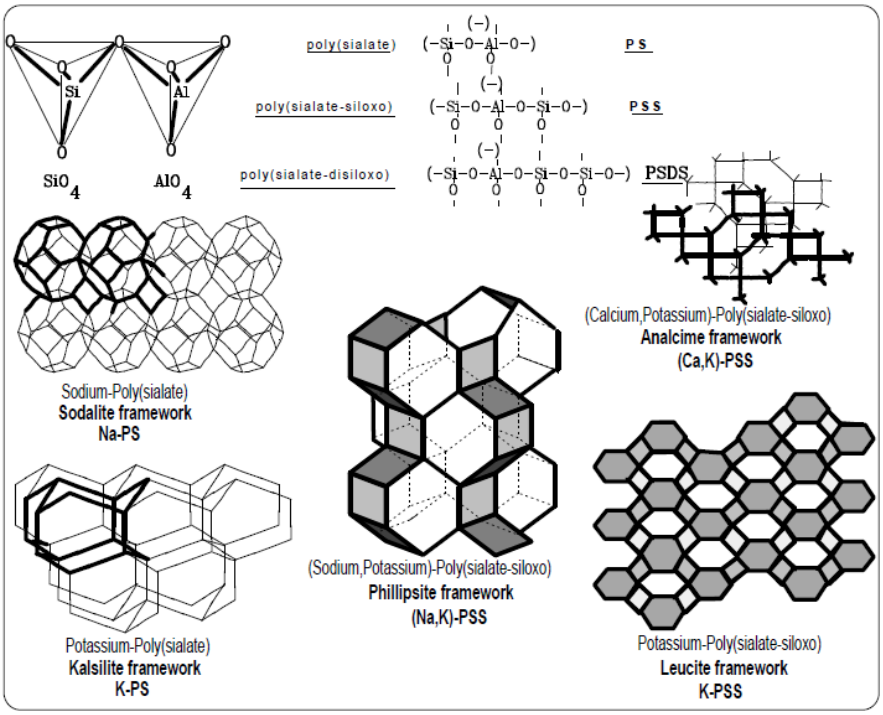

Fig. 2-12 Different types of polysialate formations (Davidovits, 1991)

Numerous authors have concentrated their efforts in studying and understanding the alkali-activation mechanisms of different kind of precursors, in particular, metakaolin (Rashad, 2013). For example, Granizo and Blanco (1998) investigated the reaction that occurs when metakaolin is mixed with NaOH solution. The result was an exothermic process which encompasses three different steps: a very fast dissolution phase, characterized by an intense heat release, followed by an induction period, in which the heat exchange rate decreases, and finally an exothermic step during which the precipitation of cementitious materials occurs . In another study, the same researchers discovered that the alkali-activation of metakaolin using a solution of sodium hydroxide and sodium silicate is different from that one with only sodium silicate. In the first case i.e. with sodium hydroxide and sodium silicate, the initial dissolution phase is immediately followed by a fast polycondensation reaction, producing materials with higher mechanical strength (Granizo, Blanco-Varela and Martínez-Ramírez, 2007).

Weng et al. (2007) have examined the activation of metakaolin in alkaline conditions with high and low Si/Al ratios, using the partial charge model to investigate the chemical reactivity of metal ions during the alkali-activation. They adopted a mechanism which comprehends dissolution, hydrolysis and condensation reactions. These first three steps are summarised in Eq. 2, Eq. 3 and Eq. 4:

$$Al_2O_3 + 3H_2O + 2OH^- \rightarrow 2[Al(OH)_4]^- \quad \text{(Eq. 2)}$$

$$SiO_2 + H_2O + OH^- \rightarrow [SiO(OH)_3]^- \quad \text{(Eq. 3)}$$

$SiO_2 + 2OH^- \rightarrow 2[SiO_2(OH)_2]^{2-}$ (Eq. 4)

The phase of condensation can occur in different ways, depending on the concentration of Si. When the Si/Al ratio is low, for example, equal to 1, the condensation takes place between silicates and aluminates species, creating polysialate structures. Otherwise, with higher Si/Al ratio (>1), the condensation process occurs in two stages; a very fast rate condensation between aluminates and silicates species followed by a slower one, which involves exclusively silicates themselves.

Xu and van Deventer (2000) proposed the following mechanism summarised in Eq. 5, Eq. 6 and Eq. 7 for the polycondensation that takes place during the alkali-activation of natural aluminosilicate minerals:

Al-Si material (s) + MOH (aq) + Na_2SiO_3 (s or aq) (Eq. 5)

Al-Si material (s) + [Mz (AlO_2)x $(SiO2)$y· nMOH · mH_2O] gel (Eq. 6)

Al-Si material (s) [Ma $((AlO_2)$a (SiO_2)b) nMOH · mH_2O] (Eq. 7)

The process begins with the dissolution of aluminosilicates material(s) in MOH alkaline solution (NaOH and KOH were used in this work), exploiting a hydrated reaction (Eq. 5). As shown in this equation, an addition of Na_2SiO_3, in liquid or solid form, is necessary, since several precursors used in this research cannot supply enough Si to give rise to the alkali-activation; the formation of [Mz (AlO_2)x (SiO_2)y· nMOH · mH_2O] gel is the next step (Eq. 6): alumino-silicates react with MOH solution and form a gel layer on their surfaces. This gel starts to spread into the interstitial pores, favouring the precipitation of the gel itself and a simultaneous dissolution of new solids. Finally, after a short setting time, the hardening phase occurs; the material increases its hardness, and the alumino-silicates particles are held together by the gel which acts as a binder (Eq. 7). As a final product, an alkali-activated binder with an amorphous structure is created.

2.5.3 Alkaline Activators

As already stated, the alkali activation process requires chemical activators, at least one, to initiate the reaction. In general, alkali hydroxides and silicates at high pH values, usually greater than 13, are needed for the initial dissolution phase. Sodium hydroxide (NaOH) and sodium silicate ($nSiO_2Na_2O$) are the most frequently used either individually or as a blend. However, potassium hydroxide (KOH) and potassium water glass ($nSiO_2K_2O$) are also fairly common (Vickers, Riessen and Rickard, 2015), as well as calcium hydroxide ($Ca(OH)_2$), also known as slaked lime (Granizo *et al.*, 2002).

Certainly, sodium hydroxide is the most employed activator in alkali-activated materials due to its wide availability and low viscosity. It is well known that its presence is essential for the beginning and the development of reactions, particularly for the formation of observable zeolitic structures. Increased contact between NaOH and the reactive solid particles results in a more profuse release of silicate and aluminate monomers during the dissolution step (Khale and Chaudhary, 2007). The concentration of NaOH is also a fundamental parameter since not only does it govern the amount of Si and Al leaching, but also influences the mechanical properties of alkali-activated binders (Vargas et al. 2006). Several authors have proved that a very low concentration of sodium hydroxide does not permit the onset of a strong chemical reaction, while too high a concentration results in an

untimely coagulation of Si, which, in both cases, lead to a weaker material (Ken, Ramli and Ban, 2015). The overuse of NaOH may cause the formation of white crystalline sodium carbonate, better known as efflorescence, which may be accompanied by further degradation of the alkali-activated binder. This common issue is due to the atmospheric carbon dioxide that reacts with the excess alkali, creating a white crystalline coating on the surface. This problem can be limited by the addition of alumina-rich compounds (Kani et al. 2012) or using potassium hydroxide (Szklorzová and Bílek, 2008).

KOH is sometimes used as an efficient alternative to sodium hydroxide. For instance, Barbosa and MacKenzie (2003) found that K-sialate alkali-activated binders possess extremely good thermal stability, showing a melting point of around 1400°C. The absence of free K^+ ions inside the pore solution has demonstrated that potassium is better assimilated into the solid phase than sodium. Also, it has been proved that larger cations, provided from KOH activator, allow for a stronger bond to be reached within the aluminosilicate gel framework, leading to a higher degree of connectivity (Duxson *et al.*, 2006). Despite this, the crystallisation of KOH-fly ash alkali-activated binders occurs slower than NaOH-fly ash systems (Fernández-Jiménez, A Palomo et al. 2006), as well as for metakaolin based alkali-activated binders.

Alkali metal silicates play an important role in the polymerization reaction, particularly when soluble silica is added to the activating solution. Sodium silicate, as a liquid compound, is surely the most used in alkali-activated binder production. It usually reacts with dissolved cations, such as Al^{3+}, forming insoluble silicates and, thus, silica gel (Vickers, Riessen and Rickard, 2015). Several types of research have demonstrated the benefits of this addition in the mixture. An increase of the structural stability of fly-ash alkali-activated binders has been proven by Lee and van Deventer (2002), who confirmed a remarkable enhancement of the aluminosilicate dissolution and an increase of the precipitation phase. Their findings are in agreement with the experience of Brough and Atkinson (2002), who, by analysing slag mortars activated with the addition of sodium silicate, obtained more amorphous products, with higher early strength and a lower level of porosity. The latter findings were later supported by Criado et al. (2005), who verified an improvement of mechanical strength when water glass was blended with NaOH. As shown in Fig. 2-13, the addition of soluble sodium silicates cause the gradual transition from mono silicate, chains and cyclic trimers to more complex structures and polymers, for instance with larger rings and a 3-D framework, generating an enhancement of the mechanical properties (Panias, Giannopoulou and Perraki, 2007).

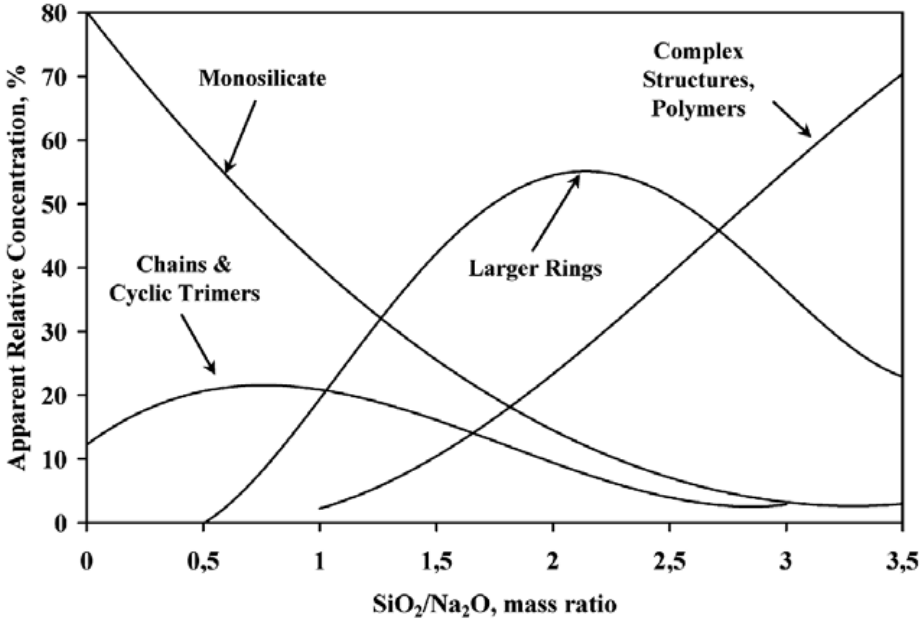

Fig. 2-13 Speciation diagram of Si in aqueous solution (Panias, Giannopoulou and Perraki, 2007)

Potassium silicate solutions show similar behaviour to sodium silicate ones, but also display some additional advantages, including a more favourable phase behaviour and rheology by providing delayed setting time (Yamaguchi and Ikeda, 2010). More prevalent precipitation of hydrated potassium silicates, higher solubility and compatibility with other additives, better refractoriness and the absence of efflorescence make the potassium silicate a very suitable material for alkali activation (Vickers, Riessen and Rickard, 2015). However, the high cost of these solutions has prevented its popularisation, especially in commercial production, limiting their use to laboratory studies only. When it is useful to have the lowest activator/binder ratio, the employment of potassium activators is recommended, thanks to their favourable rheology (Provis 2009).

2.6 Influence of Various Factors on the Properties of Alkali-Activated Materials

As extensively demonstrated in the literature, many factors, including specific mix composition and reaction conditions, may influence the mechanism of alkaline activation, affecting the formation and characteristics of alkali-activated products. The different nature and concentration of the chemical activators, as well as the curing conditions, in terms of time, temperature and water content, have a considerable effect on the properties of the materials (Ken, Ramli and Ban, 2015).

2.6.1 Precursors

After the 1970s, many materials, recycled as precursors, were subjected to accurate investigations to discover their adequacy to become alkali-activated binders. As well known, the synthesis of alkali-activated binders requires a remarkable presence of alkali-soluble aluminosilicates, usually provided through the addition of source powders. Theoretically, any material rich in silicon and aluminium could be suitable for alkali-activation, but source materials such as metakaolin, fly ashes, blast furnace slag, kaolinite clays, and red mud are commonly used in alkali-activated binder production. According to

Xu and Van Deventer (2003), it is appropriate to identify two different groups of precursor materials. To the first group belong the calcined materials, which include all the precursors that have undergone any treatments at high temperatures, such as metakaolin, fly ash, slags, pozzolanic waste. To the second group belong un-calcined materials, for instance, kaolinite and natural aluminosilicate minerals. Research studies have identified the effects of the employing calcined and uncalcined precursors on the final compounds, showing that the former usually display a higher reactivity than the latter. The calcination process modifies the structure of the materials, moving from the crystalline to the amorphous state, with a consequent build-up of extra energy (Komnitsas and Zaharaki, 2007). Thus, it has been proven that calcined source powders have a faster dissolution and gelation phases, providing a higher early compressive strength to the final alkali-activated binder.

Among all the precursors, metakaolin plays a fundamental role, since metakaolin based alkali-activated binders have often been used as a reference to understand and improve the knowledge of alkali-activated binders (Granizo and Blanco, 1998; Granizo *et al.*, 2002; Davidovits, 2015). It is produced by the dehydroxylation of the mineral clay kaolinite between 650 °C and 800 °C. The calcination treatment is an endothermic process responsible for breaking the crystal structure, during which silica and amorphous alumina in reactive form are released (Shvarzman *et al.*, 2003). Thanks to its chemical composition, an abundance of SiO_2 and Al_2O_3, and other qualities such as heat and fire resistance, metakaolin is one of the most widespread source materials in the field of alkali-activation. Before Palomo and Glasser in 1992, detailed studies were published about the activation of dehydroxylated clay in alkaline solution, leading to an amorphous/glassy aluminosilicate, called "low-temperature inorganic polymer glass" (Rahier, Mele and Wastiels, 1996; Rahier, Van Mele and Wastiels, 1996; Rahier *et al.* 1997). In these three papers, it was demonstrated that it is possible to obtain a "ceramic-like" material, starting from metakaolin and aqueous sodium silicate solution. Rahier's investigation was also concerned with the characterization of the binder with an exploration of the rheological transformations during low-temperature curing and the properties of the material when exposed to high temperatures. The latter research, along with that of Palomo and Davidovits, laid the groundwork for larger and deeper studies on such materials. Currently, metakaolin-based binders can be synthesised with predictable properties, although some factors, such as the specific surface or the composition and type of the initial kaolin, may have a significant influence (Granizo *et al.*, 2002). For instance, it is well known that the very high water demand, due to plate-like particle shape of the metakaolin powder, may affect not only the strength development but also the binder structure itself, owing to drying shrinkage and cracking. Additionally, the employment of a large amount of alkali solution facilitates efflorescence; an issue that is more common in metakaolin-based alkali-activated binders than in fly ash-based alkali-activated binders (Provis & Van Deventer 2009). Nonetheless, the great content of aluminium and the high surface area makes it suitable as a blending component with cement (Kinuthia *et al.*, 2000), slag (Buchwald, Hilbig and Kaps, 2007), and fly ash (Swanepoel and Strydom, 2002).

Fly ash is a by-product of the combustion formed during the electricity generation. It consists of the remnants of clays, sand and organic matter present in the coal, which is collected by electrostatic precipitators in the chimney of a furnace. Depending on the impurities present in the coal and the operating conditions of the combustion, the chemical composition and physical properties of this waste material can be different. The powder is composed of very fine spherical particles, with a broad particle size distribution, usually between 0.5 μm and 100 μm (Vickers, Riessen and Rickard, 2015). The main chemical

components of Class F-fly ash are silicon oxide, SiO_2, present in both amorphous and crystalline form, aluminium oxide, Al_2O_3, and iron oxide, Fe_2O_3. Also, a significant amount of calcium oxide, CaO, is present in Class C-fly ash (Blissett and Rowson, 2012). Concerning the Class F-fly ash, Fernández-Jiménez and Palomo (2003) have carried out an important investigation about different fly ashes to assess their capability for being alkali activated. They demonstrated that the most important reactivity parameters that led to a material with optimal binding properties are the reactive silica content between 40% and 50%, the high content of vitreous phase and the particle size distribution, with a percentage of particles finer than 45 μm between 80% and 90%. Also, the percentage of unburned residues less than 5%, the content of Fe_2O_3 not higher than 10% and a low content of calcium oxide (CaO) are other involved parameters to be monitored, since they may affect the mechanical strength of the binder. According to Duxson and Provis (2008), the final features and properties of alkali-activated binders are directly related to the availability of aluminium. While the silica deficiencies can be solved by direct addition, for instance using sodium silicate in alkaline dissolution media, the lack of aluminium is a more difficult problem to solve. It is known that the release rate of aluminium in fly ash is considerably slower than metakaolin, and the consequent deficit of this element affects not only the final strength but also the setting characteristics and the microstructure of alkali-activated binders (Van Jaarsveld, Van Deventer 1999; Duxson & Provis 2008). However, several investigations have been carried out during the last years which confirm that fly ash based alkali-activated binders remain one of the most widespread and used alkali activated materials, as affirmed by Fernández-Jiménez et al. (2003), as well as by (Feng *et al.*, 2005; Ryu *et al.*, 2013). Using fly-ash, it is possible to obtain a ceramic-like material, smooth, glassy and shiny, with a solid network structure which can reach high strength after a very short period of curing time.

Among many of the different types of slags that can be chemically activated, ground granulated blast furnace slags (GGBFS) are certainly the most common and employed not only in the field of chemical activation but also in the cement and concrete industries. This waste material is a by-product of iron and steel manufacture, generated in the blast furnace and rapidly cooled, and is characterised by appropriate amounts of SiO_2, Al_2O_3, CaO, MgO and Fe_2O_3. Its chemical composition and high reactivity make it a suitable material for alkali activation (Li, Sun and Li, 2010; Davidovits, 2011). Fernández-Jiménez et al. (1999) carried out a thorough investigation on alkali-activated slag mortars, demonstrating that the nature of alkaline activator, their concentration, curing temperature and specific surface of the source material are respectively the most significant factors that influence the development of mechanical strength.

Concerning un-calcined precursors, the study of Xu and Van Deventer (2000) plays a prominent role in the field of alkali-activation of cementitious materials. Extensive research was carried out on the alkali-activation of natural aluminosilicate minerals, during which sixteen different Al-Si minerals made of ring, chain, sheet and framework crystal structures, as well as the garnet, mica, clay, feldspar, were prepared, characterized and combined with NaOH and KOH solutions, to demonstrate that a wide range of natural minerals could be activated. It has been shown that, although the addition of the kaolinite is necessary for the formation of a gel, all of them, except hydroxy apophyllite, are suitable to produce acceptable matrices.

2.6.2 Nature and Concentration of Activators

As reported above, sodium hydroxide and water glass are commonly used for the activation of raw materials and the dissolution of silica and aluminium is directly dependent on the concentration of NaOH; higher concentrations of hydroxide ions improve the solubility of aluminosilicate (Khale and Chaudhary, 2007). Several authors have proved an enhancement of mechanical strength through an increase of the NaOH solution concentration. By analysing metakaolin-based alkali-activated binders, Wang et al. (2005) found that compressive strength, flexural strength and apparent density of the samples improved, increasing the NaOH concentration among 4 mol/l and 14 mol/l. Equally, Katz (1998) demonstrated the same trend for fly-ash specimens tested after 7 days, showing the significant enlargement of the compressive strength. This behaviour is due to a higher degree of silica and alumina leaching, which leads to a faster condensation of the monomer (Rashad, 2013). However, an excessive concentration of sodium hydroxide has the opposite effect on the mechanical features. Panias et al. (2007) verified that the compressive strength of fly ash alkali-activated binder is not a monotonous function of NaOH concentration, since a decrease in strength occurs going from 6.6 M to 10.25 M, while an increase has been found between 4.47 M and 6.6 M. Similar behaviour has been indicated by Somna et al. (2011), who discovered a substantial growth of compressive strength by increasing the NaOH concentration from 4.6 M to 16.5 M, followed by a decline beyond 16.5 M. This decrease compressive strength is mainly attributed to the highly rapid precipitation of gel, owing to the excessive presence of hydroxide ions, which leads to a formation of weaker alkali-activated binders.

The properties of the alkali-activated material may also be deeply influenced by the presence of sodium silicate in the activating solution, which provides an addition of soluble silica to the mixture. Several authors have supported the idea that the employment of sodium silicate, blended with NaOH, has a positive effect on the mechanical features of the produced materials. According to Granizo et al. (2007), metakaolin based alkali-activated binders experience a significant improvement of compressive and flexural strength with the silica supplement, compared with only NaOH activation. Fernández-Jiménez and Palomo (2005) noticed that the addition of water glass promotes the polymerization process, leading to an enhancement of compressive strength up to 65 MPa after 20 hours. The same effect has been tested by Hardjito et al. (2004), who reported a clear enhancement of 7-day compressive strength when the sodium silicate/NaOH liquids ratio are between 0.4 to 2.5.

However, the addition of water glass in the activating solution affects not only the mechanical properties but also the durability and the physical features of the final materials. For example, Duxson et al. (2005) stated that the concentration of soluble silica influences not only the compressive strength but also the distribution of the porosity. Low concentrations allow the formation of a dense gel, while too high a concentration results in reduced skeletal densities. Moving from Si/Al = 1.5 to Si/Al = 1.9, the specimens have shown a linear increase, approximately by 400%, of compressive strength, along with an improvement of Young's modulus. At the same time, alkali-activated binders with Si/Al ratio $\geq$ 1.65 were characterised to be more homogeneous, with very small and isolated pores, while samples with lower Si/Al ratio were categorised to have a microstructure with large and interconnected porosity. Similarly, Ridtirud et al. (2011) investigated the effect of NaOH concentration and sodium silicate/NaOH ratio (SS/SH) not only on the compressive strength but also on the drying shrinkage of fly ash-based mortars. SS/SH

ratio of 0.33, 0.67, 1.0, 1.5, 3.0 have led respectively to 25.0 MPa, 28.0 MPa, 42.0 MPa, 45.0 MPa and 23 MPa. The initial increasing trend is due to the growing presence of Na+ ions, as they support the alkali-activation, while an excessive amount of sodium silicate impedes the water evaporation and hampers a good formation of three-dimensional frameworks, weakening the final products. Also, they have found that the increase of SS/SH ratio generates lower values of shrinkage since the higher Si/Al ratio permits a quick reaction and condensation.

2.6.3 Precursor/Liquid Ratio

The ratio between the solid powder i.e. precursor and the liquid component i.e. chemical activator and water, play a fundamental role in the alkali activation, affecting the mechanical performance and physical properties significantly. The higher water content in the mixture is directly related to an increase of total porosity, as well as to a strength decrease. However, the adequate presence of liquid is required for a good outcome of the dissolution phase, since it plays the role of the medium through which dissolved aluminosilicates ions can move (Part, Ramli and Cheah, 2015). Also, depending on the type of source material, a specific amount of water is needed to reach a good level of workability for the fresh mixtures (Chindaprasirt et al. 2007).

Komljenovic et al. (2010) analysed several activators for fly ash-based mortars. Using NaOH, Na2SiO_3 and $Ca(OH)_2$, the compressive strength trend results were found to be inversely proportional to water/FA ratio. A similar behaviour was noted by Ridtirud et al. (2011); the mechanical strength of fly ash alkali-activated binders reduced with the increase of liquid/fly ash ratio from 0.4 to 0.7. The high content of water generated a high level of porosity and, thus, a decrease of the mechanical performance. At the same time, an increase of L/S ratio caused more pronounced shrinkage, affecting the final properties of the alkali-activated binders. Zhang et al. (2010) investigated the permeability of several specimens, prepared with different L/S ratios, using the Darcy method. As expected, the permeability coefficient increased with the increase of the liquid amount in the initial mixtures.

According to Panias et al. (2007), the water content should be minimised to affect all the stages of the alkali activation positively. However, the alkali-activated mixtures should contain enough moisture to retain their workability. This means the suitable L/S ratio depends directly on the kind of the source materials. Kong et al. (2007) have demonstrated that the fly ash alkali-activated binders need a lower amount of liquids comparing to metakaolin ones. The spherical shapes and fineness of fly ash particles allow specimens to reach a higher solid/liquid ratio, increasing the workability at the same water content. Sukmak et al. (2013a and 2013b) carried out different research in which they showed the relationship between compressive strength and liquid/fly ash ratio, keeping the fly ash/clay ratio fixed. The L/FA proportion that optimised the mechanical strength varied between 0.5 and 0.6 and showed a reduction with the increase of clay content in the mixture. Lin et al. (2012) activated a waste glass-metakaolin-based alkali-activated binder with different solid/liquid (S/L) ratios, ranging from 0.4 to 1.0, and different SiO_2/Na_2O ratios, investigating the compressive strength at 1, 7, 28 and 60 days. They discovered that the specimen with S/L=0.4 was the weakest at 1 day of curing as well as for 60 days. Instead, the sample with S/L=0.8 yielded the highest strength at 1 day, showing a continuous growth until 60 days. They also notice that S/L=1 led to a very similar mechanical performance to that of the material with a ratio of 0.6, proving that, when the percentage of

the solid part is so high, the mixture starts to be stiffer and less workable, affecting the compressive strength of the final products.

2.6.4 Curing Conditions: Time and Temperature

It is commonly known that curing conditions have a significant influence on the general properties of alkali-activated binders. Heat treatment is usually required to improve the mechanical performance significantly. Several authors have confirmed that an increase of reaction temperature is beneficial not only for the dissolution of precursors, in particular, alumina and silica species but also for the gelation phase, resulting in high early strength gain (Sindhunata *et al.*, 2006; Khater, 2012). However, the curing regime must be suitable for the aluminosilicate source involved. It is necessary to provide the ideal condition for the appropriate alkali-activation, since too long of heat treatment or an excessive temperature may undermine the features of the final products (Nazari, Bagheri and Riahi, 2011). Van Jaarsveld et al. (2002) investigated the curing time, showing an advantage in compressive strength until 48 hours of treatment. Beyond 48 hours, especially at high temperatures, the mechanical strength decreases, since the granular structure of the alkali-activated matrix starts to deteriorate. This damaging mechanism leads to dehydration and emphasises the shrinkage, preventing the reactive particles to complete the transformation to a semi-crystalline form (Khale and Chaudhary, 2007).

Mo et al. (2014) proved that the elevation of temperature increases the dissolution rate of metakaolin and the alkali-activated mechanism, improving the setting time of the slurries and mechanical and physical properties. Through heat treatments, the polycondensation and formation of hardened structures occur more rapidly, especially in the early stage (12 hours), by the increase of the polymerization rate and dehydration of water. At low curing temperatures (20 °C), the dissolution of metakaolin and, thus, the entire mechanism is slower, while the increase of heat up to 60 °C accelerates the hardening process and increases the mechanical strength. However, a curing temperature in the 80 -100 °C range can adversely affect not only the compressive strength but also the physical properties. Elevated temperatures ramp up the setting speed and prevent the formation of a compact and hard structure and, at the same time, lead to excessive dehydration and shrinkage, due to micro-cracking and contraction of the gel. A similar influence on setting and hardening of the metakaolin-based alkali-activated binder was noticed by Rovnaník (2010), who cured specimens at 10, 20, 40, 60 and 80 °C and measured compressive and flexural strength development. He discovered that the heat treatment at elevated temperatures improves the early-age compressive strength of the samples, with values close to 50 MPa being reached at only 1 day, but reduces the 28-day mechanical properties compared to the samples cured at ambient temperature. Also, porosimetry measurements showed that elevated temperatures cause an increase in pore size and an enhancement in cumulative pore volume, affecting both the mechanical and physical features of the final products. Concerning the compressive strength, an analogous trend has been described by Arellano-Aguilar et al. (2014), who demonstrated that a curing treatment at 75 °C for 24 hours permits the metakaolin mortars to reach a rapid strength gain at early stages, also remaining stable at later ages. However, curing at 20 °C shows the highest values of final strength, although a lower strength development during the early age.

Curing conditions also have a great influence on the physical properties, particularly the porosity, water content and shrinkage, which are directly connected to mechanical features

of alkali-activated binders. The effects of curing time and temperature on the apparent porosity have been studied by (Görhan and Kürklü, 2014). According to them, the increase of curing time leads to a reduction in porosity of fly ash-based mortars. The samples cured for 2 hours showed very high porosity since the short period of heat exposure had not allowed the reaction to progress, while in the specimens cured for 5 hours and 24 hours, pores had been filled with the gel formed during a more advanced process of alkali-activation. Also, the increase of the temperature from 65°C to 85°C favoured the water evaporation, enhancing the porosity of the specimens. Perera et al. (2007) carried out an intense study on the influence of curing schedule on the integrity of alkali-activated materials. They tested four different curing plans, varying both the temperature, between 20 °C and 80 °C and the humidity condition, moving from ambient to controlled relative humidity (RH). They concluded that, concerning the open porosity, the curing in the absence of tight sealing of the sample container, in an oven with RH held between 30-70%, does not produce any advantage over curing at ambient condition followed by mild heating (40 °C-60 °C). They also noticed that the water content in alkali-activated paste plays a fundamental role in obtaining a crack-free product. The evaporation, which gives rise to the formation of fissures, may be hindered by sealing the sample containers, preventing a rapid drying during the curing treatment. The behaviour of fly ash specimen's steam treated at 80°C for 16 hours under variable humidity conditions (40%, 60%, 80% and 100% RH) was investigated by (Feng *et al.*, 2005). A non-contracting material, with expansion and shrinkage levels very close to zero, was obtained, through the application of a curing treatment with 60 and 80% RH. Although an increase of bulk density is usually related to an enhancement of mechanical capabilities and, in this case, the highest value was reached under 100% RH; the maximum flexural strength was obtained by the specimens cured for 12 h under 40% RH. The authors explained by asserting that the drier condition, due to easier water evaporation, allows the polymer networks to develop unrestrictedly, improving the polycondensation of binder gels, despite the relatively lower bulk density.

2.7 Applications of Alkali-Activated Materials

Alkali-activated binders are a class of materials provided with high potential to be employed not only in the construction industry, essentially as an alternative to Portland Cement (PC), but also in other niche applications. As several researchers stated, this variety of uses derives directly from many beneficial features that these compounds can develop during and after the alkali-activation.

Environmental sustainability and the reduction of greenhouse gas emission from the building products industry are two of the most important reasons of alkali-activation technology research; the requirement to find a substitute for ordinary cement, with the same or even higher strength and durability, but with lower environmental footprint, has become more crucial. In recent researches (McLellan *et al.*, 2011; Turner and Collins, 2013), it has been stated that the CO_2 production due to PC industry is approximately 5-7% of global CO_2 emission, considering a range between 0.66 and 0.82 kg of CO_2 for every manufactured kilogramme of Portland cement. According to those studies, the comparison between PC and alkali-activated concrete manufacturing cycles, considering all the processes from the raw material supply to the final compounds, shows that the CO_2 impact of the latter is 9% less than the ordinary cement. However, the conclusions of the latter academic study must be interpreted with caution due to the bias coming from the inefficient mix design, heat curing and precursor supply being based on fly ash derived

from brown coal. The particular brown coal evaluated in the latter study is one originating from south-east Australia, contains a high ash content and a moisture content which ranges from 48-70 % rendering it an inefficient energy source (Minerals Council of Australia, 2014). Another issue when interpreting academic studies evaluating the energy saving of alkali-activated concretes is that very few studies refer to an application or take care to specify an appropriate reference concrete. The majority of studies are comparing to a CEM I concrete, which is an unrealistic benchmark in the modern use of concrete due to the majority of cement blends used in industry containing SCMs such as slag and fly ash (Thomas and Peethamparan, 2015).

Although a value of 9% may not seem to be not so high, from the ecological point of view, the recycling of waste material, particularly industrial scraps, with which most alkali-activated binders are made from, must be considered. As reported by Habert et al. (2011), industrial by-products, such as blast furnace slags and fly ashes do not require expensive storage facilities, nullifying the allocation impact. However, even if they require some treatment to be employed as precursors, the environmental footprint is lower than before. The latter points confirm that the utilisation of most standard types of alkali-activated concretes can reduce, even if only slightly, the strain that Portland cement production has on the environment.

The benefits of using alkali-activated binder can be further enhanced when they are used as a host matrix in waste encapsulation. Several features of these materials, such as a rapid setting and hardening, low shrinkage, high resistance to a range of acids and salt solution, the capability to incorporate toxic metal in their constitution have led to their employment in the immobilisation of toxic wastes, such as lead and chromium (Provis 2009). These binders have even been tested in the storage of nuclear waste, in particular for caesium and strontium (Fernandez-Jimenez *et al.*, 2005). Several authors have investigated the immobilisation efficiency mainly through leaching tests and other specific analyses to guarantee that physical properties remain stable. Van Jaarsveld et al. (1997; 1998) found very low concentrations of cations of many chemical elements in leachates from mine tailings and paint sludge, suggesting the opportunity to manufacture materials with enough compressive strengths and capability to immobilise heavy metals. In a more recent study, alkali-activated binders were confirmed to be suitable to be employed for nuclear waste storage since the lack of freeze-thaw problems, fire and leaching resistance make them better candidates than cement (Blackford *et al.*, 2007).

Fire and heat resistance are other properties not to be overlooked, as fire protection of structures is one of the most widespread applications for alkali-activated binders. Since 1970, several types of research have been focused on seeking inorganic-polymer technologies, which permit the creation of non-flammable and non-combustible plastic material. In one of the works, Kovalchuk and Krivenko (Provis & Van Deventer 2009) tested alkali-activated metakaolin and fly ash at very high temperature. They showed that metakaolin and fly ash is a remarkable base for many materials to be applied to more than 800°C, making them adequate for heat-resistant and fire-resistant concrete, high-temperature adhesive and ceramic applications.

In addition to the properties above, other advantages of alkali-activated binders have been identified in many types of research. The different material used as the precursor and different preparations factors, for example, curing time, temperature, chemical ratios, influence the final compounds and, thus, their features. Some of the characteristics are

listed below (Lee and Van Deventer, 2002; Duxson *et al.*, 2007; Duxson and Provis, 2008; Srinivasan and Sivakumar, 2013):

- Low shrinkage, controlled cracking and low thermal conductivity
- Rapid and controllable setting and hardening
- No emission of toxic fumes when heated
- High compressive strength, even higher than Portland cement
- Low-cost material (10-30% less than OPC)
- Good abrasion resistance
- High surface definition
- Good adhesion to fresh and old concrete surfaces, steel, glass, ceramics

All the above characteristics have made the realisation of many applications possible, proved by more than 30 patents that have been filed and issued in many countries (Davidovits, 2002). Davidovits, as well as other authors, have proposed a list of those applications, some of which are reported below:

- Fire resistant wood panels, insulated panels and walls
- Ceramic tiles
- Alkali-activated concrete and cement
- Structure and infrastructure repair, improvement and strengthening
- Encapsulation of toxic and radioactive waste
- Fireproof high-tech applications in aircraft, automobile
- Decorative stone artefact
- Refractory items, for example, thermal shock refractory
- Aluminium foundry application
- Restoration works

Concerning the storage and immobilisation of wastes, Van Jaarsveld (1997) also suggested some applications. He proposed the use of alkali-activated cement as surface capping and low permeability baseliners of waste dumps and landfill sites to prevent contact by rainwater and guarantee the minimum leakage of contaminants into the groundwater. In addition, the immobilization of toxic waste such as arsenic, mercury and lead and the inexpensive but durable encapsulation of hazardous waste was proposed, as already mentioned. Regarding the building sector, the production of bricks, ceramic tiles and cement have been suggested, along with the possibility to create structural surfaces like floors and pre-cast simple structure such as fences, as well as paving materials and low-cost pipes.

Although a niche application, the employment of alkali-activated binders in road field applications is becoming a valiant and efficient alternative to traditional materials. Malone et al. (Kirkpatrick and Pyrament, 1985) reported the use of alkali-activated binders in military operations, in particular for repair and construction of lines of communication, even for airfield restoration, exploiting the abilities of fast setting and development of high compressive and flexural strength, adaptability to a wide variety of substandard aggregates and to different climatic conditions and durability to trafficking. Tenn et al. (2015) studied different compounds of new alkali-activated binders to be mixed with road aggregates (diorite and granite). Investigating several parameters such as pH values, the nature of the

aggregates and the time evolution, they found some formulations that are promising to be used in addition to bitumen.

Several advantages and potential applications have been presented, but it is clear that the alkali-activation technology also has some disadvantages. The limited knowledge of involved mechanisms of alkali activation, complicated by a wide variety of chemical and mineralogical compositions of the components, the use of alkaline solutions, which are harmful to the health, the employment of silicates, in particular sodium silicate, which have a high environmental impact, are just some of drawbacks that do not facilitate the diffusion and commercialization of alkali-activated binders (Habert, d'Espinose de Lacaillerie and Roussel, 2011; Nazari *et al.*, 2017).

2.8 Phase Change Materials and Encapsulation

The subject of the fossil fuel and electricity consumption can be considered an expensive element within the utilised raw materials/resources in construction. From a financial point of view, the capital costs of a project will be vastly affected by the consumption of these materials. It is highly favourable to preserve the resources of solar thermal, or thermal energy in the construction industry, as this indulges efficiency and is useful to projects. The reduction of these controlled variables can be arranged through the mechanism of phase change materials (PCMs).

PCM technology has been on-going for almost 30 years and is an important topic in building physics (Zalba *et al.*, 2003). PCM's have been applied to such areas were the thermal energy storage (TES), or thermal energy release (TER) maintains highly considerable efficiency energy levels while being sustainable. Energy can be stored in certain forms and therefore can acquire a different source of outcome used.

The PCM can store or release a large amount of energy by a simple temperature change, to trigger the action force. PCMs can be classified into three components of material substances being organic, inorganic or eutectics (Pereira da Cunha and Eames, 2016). Each single type of PCM has special characteristics regarding the melting temperature point and latent heat of fusion. Therefore, for certain design types, the PCMs specified will be unique to its properties regarding the desirability in thermal storage. Also, the suitability of the different characteristics will also depend on the availability of substance.

Main property factors of PCM include thermo-physical, kinetic and chemical considerations. Hence, ensuring a conventional PCM for utilisation may rely on the thermal properties such as adaptability to heat transfer, appropriate phase-transition temperatures and excessive levels of latent heat transitions. Regarding physical characteristics, these factors will be extremely vital in the structural design aspect. One factor includes the PCM having a minimum volume change, phase stability (to maintain heat storage) and lastly to adopt low vapour changes (Sharma *et al.*, 2009).

In the classification of the PCM, the paraffin and non-paraffin compounds make up the organic group. Primarily focusing on paraffin compound materials, the recommended thermo-physical properties of the low volume and vapour changes are present within paraffin. Also, this material is essentially safe to use as the chemical mixture is fairly stable below 500°C (Sharma *et al.*, 2009). Any temperature increase above the specified limit could induce flammability hazards of all sorts. Paraffin tends to change phases from a

liquid to a solid, and vice-versa, with the almost negligible amount of sub-cooling. One of the most known significant facts about paraffin is that not only it easily dissolves in water, but also it acts a hydrophobic, thus preventing any possible reactions with other chemical components. The straight chains of n-alkanes in paraffin have a specific formula of CH_3–(CH_2)–CH_3. The CH_3 chain produces a large amount of latent heat, thus the longer the chain length, the higher latent heat infusion and melting point (Sharma *et al.*, 2009). However, looking at the non-paraffin compounds, it could be argued that properties within the region do vary from one type to another. These organic non-paraffin's can be made up of various materials such as fatty acids, acetic acids, alcohols and glycols (Abhat, 1983). On the other hand, inorganic PCM's are usually formed from either two components, being metallic or salt hydrates.

When evaluating organic and inorganic PCMs, the latent heat per unit mass and the melting point is interpreted to be roughly the same values for both variables. However, when introducing the volumetric unit, the inorganic PCM's are noticeably higher in latent heat per unit volume value (Wahid *et al.*, 2017). The reason behind this theory is due to the density being higher than organic compounds.

Lastly, eutectics, also known as ionic liquids are another separate type of PCM used for compositions that mostly specialise in minimum melting features. The density of these materials tends to be higher than all other PCMs. Since the research on eutectics is rather recent and minimum, some values and data have been incorporated to predict missing values (Pereira da Cunha and Eames, 2016).

2.8.1 Paraffin as a Phase Change Material

Petroleum materials have been playing a major role in the worldwide industry and economy. Within this specific industry, paraffin is a very well acknowledged and historical substance utilised in most of the daily production and elements. Crude oil is the main source of a refinery for paraffin wax and is produced from its degradation. Previously, the degradation of paraffin was highly expensive however cheaper alternative methods have been introduced, resulting in significantly lower costs. The process method of extracting paraffin is performed through many stages of the refining scheme. These include the lubricating oil fractionation, de-waxing and de-oiling (crystallisation) (shown in Fig. 2-14).

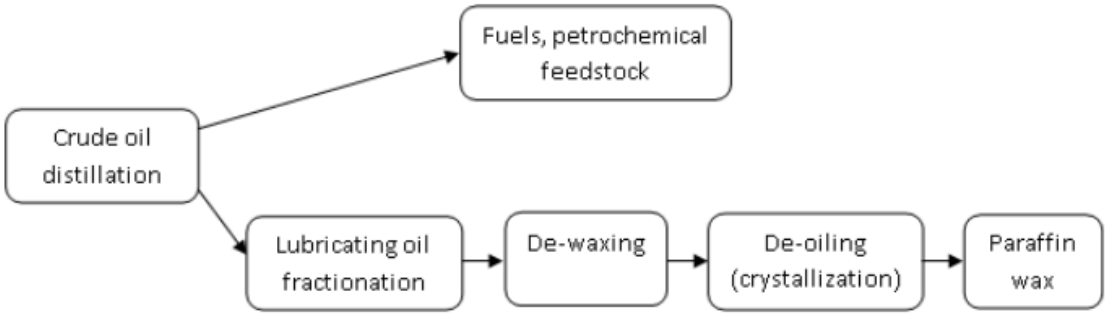

Figure 2-14 Degradation process of paraffin wax (Akeiber *et al.*, 2016)

The theoretical performance of paraffin's behaviour is described differently in various condition states. The paraffin maintains solidity (paraffin wax) at certain temperatures, and then essentially may start turning into free-flowing liquids (liquid paraffin oil) at slightly higher melting points. The chemical composition of paraffin is complicated having

saturated hydrogen carbons included. However as mentioned previously, the alkanes are always present in high portions, to make up the structural chain lengths.

The main objectives of paraffin impregnation in a building application are to store or release thermal energy under certain weather conditions. One of the strong benefits of paraffin usage is the negative temperature control, where this building function method of heating and cooling were first introduced by Telkas in 1975 (Ronc and Bollon, 1982). Largely, there are many different systems adopted in the generation of thermal energy performances for cool, heat or even balancing temperature fluctuation system. For example, when the weather becomes extremely cold, the material would activate the thermal storage features. Vice versa, in hot weather conditions, the thermal heat will be unfavourable, and therefore energy is released, in comparison to the cold environments.

Many individuals such as Lorsch and Kauffman (Ronc and Bollon, 1982) describe the different methods in which paraffin could be used for its general purposes. The used technique is known as the multilayer storage system, with water and TES materials integrated together (shown in Fig. 2-15).

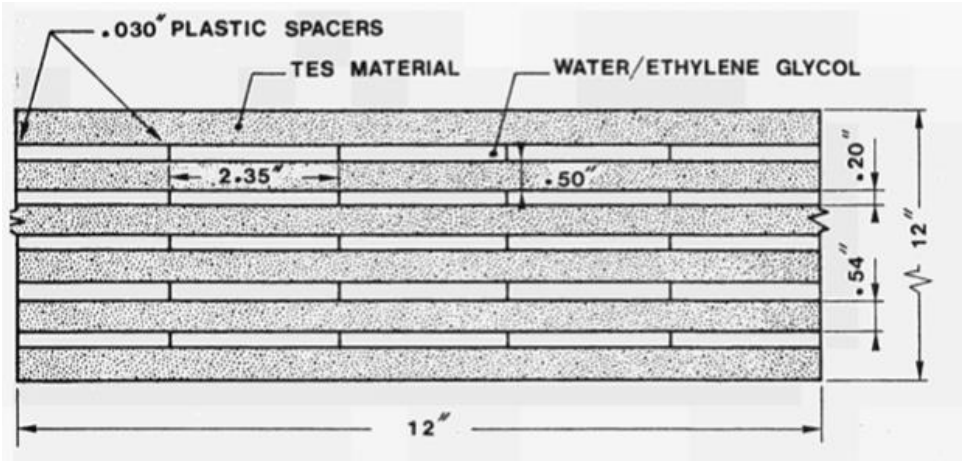

Figure 2-15 Multilayer storage system by Lorsch and Kauffman (Ronc and Bollon, 1982)

Other beneficial effects of the concrete usage can be through the prevention of freezing or thawing of concrete in extreme weather conditions. The aspect of storing energy and avoiding the build-up of frozen concrete will avoid any possible future failings. These defects include the cracking and dislocating of concrete structures. Volume changes proportionally with temperature and therefore the expansion and reduction in volume cause major defects. Hence the outcome is observed to be the cracking of concrete since this material is not essentially elastic. These listed advantages can have a positive effect on the cost of projects in the short and long term run.

However, there are current setbacks and pitfalls that could be based on safety hazards such as the materials responsiveness to fire ignition. Paraffin is known to be a highly flammable subject; this could add a higher chance of fire being uncontrolled. Though an article by Slayer (2001) had suggested a method in which fire-retardant additives could be used in improving the flammability reaction. These additives are found to be organic halogenous compounds as they generate a flame redundancy, while utilised in paraffin (Zalba *et al.*, 2003). Also, although paraffin is a very efficient and economic substance when being produced and manufactured, the application of building integrations at larger

scales could be highly expensive. When this substance is used in many areas of building construction, the cost of paraffin value may outweigh other raw materials in projects, such as cement, aggregates or sand. Lastly, the impurities within paraffin concentration can play a vital role in heat capacity. Thus a pure state of paraffin must be used at all time when adapting this technology.

2.8.2 Thermal Energy Storage/Release

The method of using PCMs for thermal energy storage and release became an essential aspect of energy management. Particularly, when the energy crisis occurred in 1973-1974 (Pielichowska and Pielichowski, 2014), a higher awareness on the consumption of energy had risen. Today, TES/TER has enhanced major issues with utilising efficient energy rates and the need for conserving energy for the future. Also, the application of PCMs for energy storage improves the phenomenon of supply and demand for current and later energy commitments.

PCM's have both abilities and features in a way that it can absorb energy to produce heat, and release energy to supply cooling phases. While operating TES and TER systems in building application, there are two main methods in which it can be used. Heat can be stored or released in different approaches, either through Sensible Heat Storage or Latent Heat Storage. Both types have different approaches to the conservation of certain temperatures.

2.8.2.1 Sensible Heat Storage (SHS):

This technique has a principal necessity on suitably adjusting temperatures within a solid or a liquid, to store thermal energy. The primary principle of SHS is recognised through the heat capacity and the general temperature of the material. When heat is required, the temperature of this material will rise thus storing heat as a function. However, cooling takes place because lowering the temperature. Hence the heat capacity causes a freezing action to provide cold/cooling environments. A related example can be water in its heating and freezing system. High specific heat capacity and suitable adjusting molecular phases illustrate water as an appropriate SHS material.

2.8.2.2 Latent Heat Storage (LHS):

The most efficient method of TES/TER is through the PCM's change of state conditions from either solid-to-solid, solid-to-liquid, or liquid-to-gas, or vice versa in their transformation (Pielichowska and Pielichowski, 2014). The LHS method has unique benefits of offering high storage densities, which is a valuable factor in the building applications. As discussed previously in this paper research, paraffin being an organic PCM is considered a suitable example that obliges to the characteristics of the LHS system.

Energy storage systems can be incorporated in building applications for heat or cooling features. There are two main types of energy storage systems that provide these features, either being passive or active in their storage process.

Passive storage systems are developed with the added technology of sustaining temperature through temperature controlling's without any active devices or machines. The system relies on zero or low external energy, and therefore it is greatly an efficient process

method. Passive methods have been studied in different areas of the world including Japan, United States and Germany since the 1980's (Pielichowska and Pielichowski, 2014).

On the other hand, active storage systems are henceforth active in motion throughout off peaks of thermal energy storage. This system relies on the consumption of energy that is previously stored during peak loads and thus shifted to off-peak timings during night time, as colder temperatures initiate. This is due to its vulnerability of producing heat from the operation of the active storage systems. The main integrated systems that are currently being used include floor heating and photovoltaic devices (Tyagi and Buddhi, 2007).

2.8.3 Aggregate Encapsulation

2.8.3.1 Microencapsulation Technology

In microencapsulation, micro-size materials are wrapped or coated with a slender sealing high molecular weight polymeric film. The seal generates an outer and inner surface within the particle, consisting an organic PCM as a core and a polymer or inorganic material as a solid structural shell (shown in Fig. 2-16). This specific structural component when encapsulated (also known as microparticle or microcapsule) prevents the main issue of PCM leakage as it also aids retaining the shape of a particle. Usual size diameters of these capsules range between 1 μm to 1000 μm (Khadiran *et al.*, 2015). It is vital to ensure that the compatibility of the combination between the shell and the PCM is being adopted successfully, as the composition may fail in application. Such containment methods include spray drying, coacervation, condensation, emulsion or polymerization (Pendyala, 2012; Wahid *et al.*, 2017).

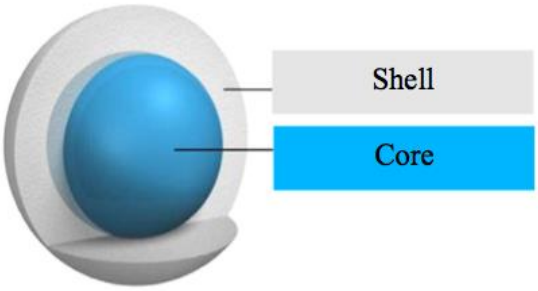

Figure 2-16 Micro-Capsule layer structure (Khadiran *et al.*, 2015)

On the advantages, micro-encapsulation has high comprehensive properties that include a reduction in the reactions of the outer environment with internal materials. Whereby the heat transfer is superior due to the microcapsules tolerating high surface-volume ratios. Moreover, the hard shell containment provides the ability to withstand numerous repeated volume changes during a phase-changing liquid/solid state (Jayalath *et al.*, 2011; Huang *et al.*, 2016). Nonetheless, the main topic of cost-effectiveness is considered as a huge drawback. The integration of micro-particles in construction building is considered relatively low (Rao, Jha and Misra, 2007), whereas the investment of micro-encapsulation is highly expensive thus infeasible for commercial use (Huang *et al.*, 2016). Lastly, to establish an adequate cycle stability through numerous phase changing cycles, the encapsulation must remain impermeable (Jayalath *et al.*, 2011).

2.8.3.2 Macro-encapsulation Technology

When utilising PCMs in any material for any application purpose, encapsulation must be done to ensure the adaptability and efficiency of this technique. This encapsulation is explained through having the PCM confined into the porous modes, where the macroscopic containment prevents any interaction with external environments. In return, the phase changes of PCM could apply to transit forms from liquid-solid, and vice versa. The change of phases is a key factor for maintaining thermal energy storage or release in required areas within construction. Macro-encapsulation can be formed in many ready shapes or sizes (usually from 1 millimetre and upward). These self-assembled structures include a wide range of steel and plastic materials with tubes, spheres, bottles and pouches. All of this work can be incorporated in many building elements such as pipes and wallboards, though heavy integrated work must be done on building structures (Jayalath *et al.*, 2011).

Mechanical properties are mentioned in works by Wahid et al. (2017), which note that improvements in structure stability are developed, especially in areas where the container material is strong. Other than the disadvantage of handling the PCM of paraffin from leakage, the main drawbacks of this practice may be about the redundancy of the thermal heat conductivity (Wahid *et al.*, 2017). If paraffin leakage has not been resolved properly, the flammability risks will increase, due to the escape of PCM during phase condition changes. However, the main advantage of using macro encapsulation is recognised through the cost effectiveness and time consumption, as it is considerably low in both cases (Huang *et al.*, 2016).

2.8.3.3 Vacuum Impregnation

A common method of macroencapsulation is processed through set pressure conditions in a well-sealed desiccator. This complete equipment set-up includes the pipes attached to a PCM container tank and a vacuum pump (as shown in Fig. 2-17). The main ideology of this macroencapsulation technique is to prevent any possible air contact with the PCM impregnation. Maintaining a constant pressure during impregnation has important benefits by retaining air from the porous media of the aggregate.

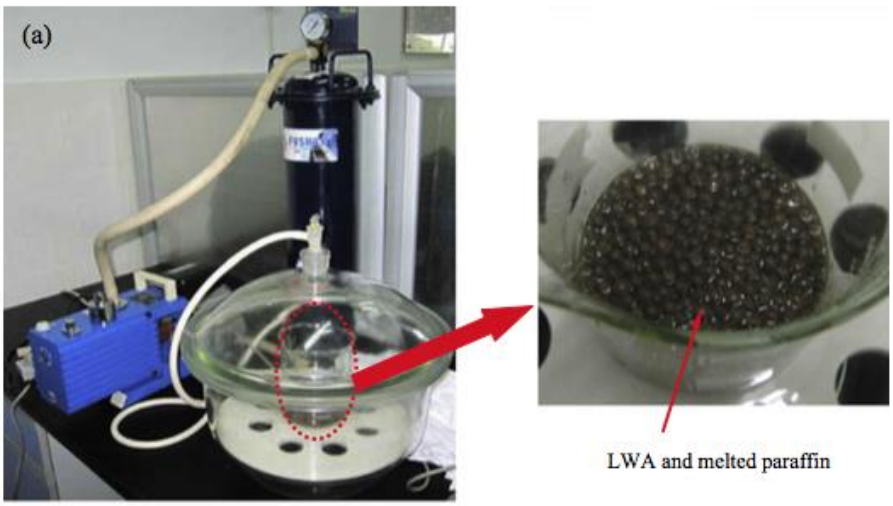

Figure 2-17 Vacuum impregnation unit for LWAC (Memon *et al.*, 2015)

2.9 Summary

As outlined in this chapter, alkali-activated binders as new "green" engineering materials have the potential to exceed PC-based materials regarding technical and environmental performance. The following conclusions can be made:

- Alkali-activated binders have been identified as being significantly different from Portland cement based systems, not only in chemical formation but also in the manufacturing process; this has been the primary obstacle in understanding, harnessing and commercialising this technology.
- The research and development history of chemically-activated binders is still in the infancy; there has been a significant leap in determining fundamental concepts related to its hardening process and microstructure.
- Research has also begun evaluating several types of key waste precursor materials suitable for chemical activation and has begun unravelling the important factors influencing the properties of chemically-activated binders. Nonetheless, due to the lack standardisation and limited control over precursor materials, the knowledge gathered for one type of chemically-activated binder is not always transferrable to another.
- There remain many fundamental steps to be completed for the realisation of the alkali-activated binder industry, particularly its long-term durability performance.

3 PREPARATION OF ALKALI-ACTIVATED CEMENTITIOUS MATERIALS

This section firstly summarises the issues associated with the production and application of Portland cement. This is followed by a discussion of how supplementary cementitious materials can in some respects replace Portland cement and help to solve these problems. The focus is then drawn to the alkali-activation of blended tungsten mining waste and waste glass, particularly focusing on the preparation of raw materials, sample curing time and duration and their effect on the binder mechanical properties. The results demonstrate that the activator solution preparation regarding mixing time can significantly influence final binder mechanical properties. Also, preparation conditions such as curing temperature and duration are also factors determining the mechanical strength properties influence.

3.1 Introduction

Although the development of Portland cement (PC) research and its application has considerably matured in last few decades, it is still facing challenges due to its impact on the environment. The production of cement is one of the industry's most energy intensive processes next only to steel and aluminium (Napp *et al.*, 2014). In 2011, the European states accounted for 7.6% of total global cement production (European Cement Association, 2014). The manufacture of PC can consume approximately 3.2-6.3 GJ of energy (thermal and electrical) per tonne of clinker product (Rahman *et al.*, 2016) with almost half of this being used for the fine grinding of clinker to make the cement. The main

raw material used in cement production has traditionally been the abundantly available limestone which, by its inevitable transformation into lime, is responsible for over 60% of the cement industry's CO_2 emissions (Mikulčić *et al.*, 2012). For every kg of PC clinker produced, about 0.87 kg of CO_2 is released (Telesca *et al.*, 2017). Therefore, the main challenge of the cement industry is focused on the CO_2 emission reduction to 1.55 Gt per year (about 45% of the current value) by 2050 (Telesca *et al.*, 2017).

To reduce the carbon footprint and conveniently dispose of the variety of waste material available from multiple industries, composite cement, also known as blended cement, containing reactive inorganic materials that contribute significantly to the hydration products formed, have been significantly researched and commercially applied in industry. The additional reactive material may be described as a supplementary cementitious material (SCM) and can be interground with cement clinker or blended at a later stage, typically at the concrete plant or on site. The most common examples of SCMs are fly ash, blast furnace slag and limestone. The environmental benefits of using these materials have become increasingly important since often, as with fly ash and slag, they are by-products from other processes that would otherwise go to landfill. The use of composite cement can bring technical benefits regarding improved mechanical and durability properties. Some types of SCMs are known as 'latently hydraulic' meaning they are slightly reactive in water but are most reactive when activated by an alkaline material such as lime or cement. The most commonly-used SCM of this type is slag. Other SCMs are pozzolanic; these do not react with water alone but do react with water and lime or cement. They are deficient in lime and so need the addition of lime to form calcium silicate hydrate (C-S-H). Examples of pozzolanic materials are fly ash, micro-silica, metakaolin and volcanic glass. The addition of SCMs increase the total amount of C-S-H in the hydration product; since it is the C-S-H that is mainly responsible for the increase in strength if the proportion of C-S-H can be increased, it is likely that strengths will also increase, other factors being equal. The basic mechanism behind the strength gain is the following: Inclusion of any of the SCMs mentioned above in cement increases the amount of silica available for the formation of hydration products. The additional silica combines with calcium hydroxide (CH) in the paste, producing more C-S-H and with a higher Si/Ca ratio.

The above principle has been adopted and enhanced for the production of alkali-activated binders which have been at the centre of academic curiosity as environmentally favourable alternatives to PC (Bădănoiu et al. 2015; Barbosa et. al. 1999; Singh et al. 2016; Choi et al. 2009; Dong et al. 2014). Instead of using cement as the source of alkalinity for the activation of SCM's, researchers have instead been able to activate aluminosilicate rich materials using highly alkaline chemicals to produce three-dimensional polymer like network materials, free of cement. As already discussed in Chapter *2.7 Applications of Alkali-Activated Materials*, these special binders yield high strength with a rapid setting, good durability and high resistance to chemical attack (Hardjito *et al.*, 2009; Ariffin *et al.*, 2013; Thomas and Peethamparan, 2015). By manufacturing alkali-activated binders through the substantial re-use of industrial waste, there is the possibility to achieve a significantly lower CO_2 emission per tonne in comparison with PC. With optimised dosages of activator, this could produce a binder with the same advantages of PC but with a potentially lower cost, a larger reduction in CO_2 emissions and encourage the recycling of industrial waste into new raw materials.

The raw materials for synthesising alkali-activated binders are typically calcined clays or low-calcium fly ashes (Duxson et al. 2007). However, the supply of fly ash in Europe is

reducing due to the industry becoming increasingly less reliant on coal-fired power stations (Carroll, 2015) while the disposal of the 85% of host rock generated from kaolin mining is an increasingly critical issue (Murray, 2002). On the other hand, mining and quarrying waste still represent 15% of total waste in Western Europe, 31% in Eastern Europe (Eurostat, 2016b) while the USA alone is estimated to produce between 1000-2000 Mt of mining waste annually (Szczepańska, 2004). The favourable mineralogical composition of mining waste for alkali activation (Jiao, Zhang and Chen, 2013; Ye, Zhang and Shi, 2014; Zhang, 2014) combined with its continuously large production make it an attractive and environmentally friendly feedstock for AABs.

Some mining and quarrying wastes can be reused in earthworks and construction, particularly the coarser fractions. Typical applications include use in asphalt pavements (Akbulut and Gürer, 2007) and concrete (Yellishetty *et al.*, 2008; Hebhoub *et al.*, 2011). However, recent studies on the reuse of fine tailings as raw material for AABs are most promising; from an environmental, technical and economic point of views. For this study, the wastes of interest are fine tailings derived from tungsten mining. Preliminary research has been conducted on the transformation of this type of waste into AABs and has shown promising results. Pacheco-Torgal et al. (2007) first highlighted the potential of using calcined tungsten mining waste mud blended with calcium hydroxide for the development of a high early strength geopolymeric binder. Tungsten mining waste also identified to be very effective for stabilizing/solidifying heavy metals, particularly when used in conjunction with blast-furnace slag (Choi *et al.*, 2009) and overall, suggested that mortar with acceptable properties can be developed using up to 10% by mass tungsten mining waste. Later, alkali-activated artificial aggregates were produced from such mining waste mud, and their properties were studied as a potential substrate for fixed-film wastewater treatment processes (biofilm reactors). The results showed that the aggregates obtained have suitable resistance to acid attack and may be used as a substrate for fixed-film biological reactors for the treatment of acid wastewaters (Silva, J. Castro-Gomes and Albuquerque, 2012). Also, mine tailings blended with other industrial by-products such as fly ash have resulted in the production of an AAB with high compressive strength, mainly due to the Si/Al ratio of the raw material blend falling within the optimum Si/Al ratio for alkali-activation (Zhang, Ahmari and Zhang, 2011b; Ahmari and Zhang, 2012).

Despite the research conducted so far, it remains that tungsten mining waste possesses a low degree of reactivity due to it crystalline phases. Thermal treatments have previously been studied to improve the amorphicity of tungsten mining waste, and satisfactory strengths have been achieved (F. Pacheco-Torgal, Castro-Gomes and Jalali, 2009a), nonetheless at the expense of the high amount of energy. A more sustainable method would be to blend the tungsten mining waste with a material that would increase not only its level of amorphicity but also maintain its environmental appeal. In this case, the waste glass would be the ideal candidate since it is a very common construction and household waste material with a highly amorphous structure. It is estimated that out of 18 million tonnes of glass wastes accumulated in 2012 in the EU, only 35% of this was recycled (Glass for Europe, 2013). The feasibility of using ground waste glass to improve mechanical performance has already been achieved with PC concrete (Shao *et al.*, 2000a) and initiated with metakaolin based AABs (Christiansen and Sutter, 2013).

Also when assessing novel binder materials, it is of as much importance to study the preparation/manufacturing techniques as it is the final material properties (Van Jaarsveld, Van Deventer and Schwartzman, 1999). The preparation/manufacturing techniques are a

domain which currently remains understudied for AABs in general, let alone those based on tungsten mining waste. Thus, the primary objective of this study is to determine the fundamental aspects of AAB synthesis using tungsten mining waste as the principal raw material with the added feasibility of its partial replacement by the waste glass. Particular focus will be on (1) the influence of waste glass on tungsten mining waste reactivity; (2) alkali activator solution preparation and kinetics; (3) AAB curing temperature and curing duration.

3.2 Materials and Methods

3.2.1 Materials

The raw materials used in this investigation consisted of tungsten mining waste (TMW), waste glass (WG), 98% pure sodium hydroxide (NaOH) (SH) (Fisher Scientific, Germany), and sodium silicate (Na_2SiO_3) (SS) (Solvay SA, Portugal). The TMW was derived in powder form from the Panasqueira mine in Castelo Branco, Portugal, and the WG was received from the local municipality of Covilhã, Portugal. The micro-morphology of the TMW and WG was observed using a scanning electron microscope (SEM) (Supra 35VP, Carl Zeiss, Germany) as shown in Fig. 3-1. A Sequential benchtop Wavelength Dispersive X-ray Florescence (WD-XRF) spectrometer (Supermini200, Rigaku, Japan) mounted with LiF(200) and PET crystals, was used to obtain the chemical composition of the TMW and WG, of which the main oxides are presented in Tables 3-1. The mineralogical compositions of the TMW and WG were obtained by powder X-ray diffraction (XRD) (D8 Advance, Bruker, Germany) diffractometer with an automatic slit, monochromated CuKα radiation (λ=1.5405 Å), 5-80° 2θ range, with steps of 0.02°/2θ and 0.5 s/step. Peak shapes were studied using the program DIFFRACT.SUITE (Bruker, Germany) and the results are shown in Fig. 3-2. The TMW was determined to consist mainly of crystalline phases of silica, muscovite, albite and pyrite, while the WG consists of silica, most of it being amorphous.

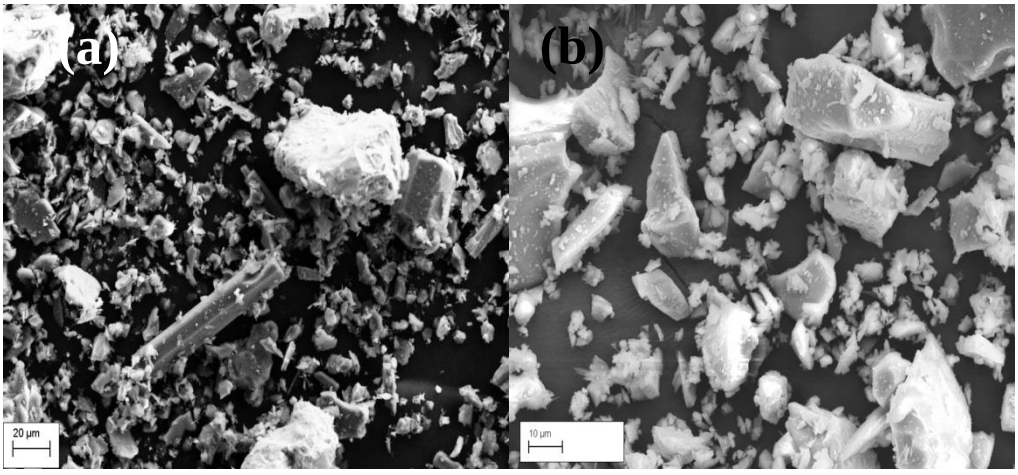

Fig. 3-1 SEM image of (a) TMW and (b) WG

Table 3-1 Chemical composition of TMW by WD-XRF

Component	TMW Result (%)	WG Result (%)
Na_2O	0.51	12.44
MgO	2.16	1.76
Al_2O_3	14.89	2.12
SiO_2	49.17	68.71
SO_3	8.98	0.33
K_2O	2.92	0.77
Fe_2O_3	13.69	1.48
CaO	0.58	10.04
P_2O_5	0.32	0.00
TiO_2	0.5	0.00
ZnO	1.25	0.00
CuO	0.32	0.00
As_2O_3	4.26	0.00

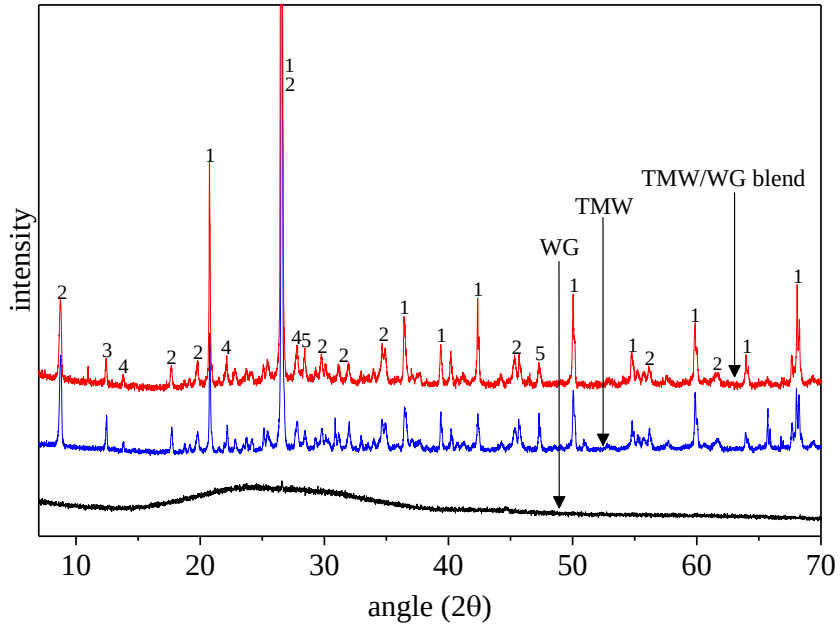

Fig. 3-2 XRD patterns of TMW, WG and blended TMW/WG (1- silica, 2- muscovite, 3- sodium aluminosilicate, 4- albite, 5- pyrite)

Attenuated Total Reflectance Fourier Transforms Infra-Red (ATR-FTIR) spectroscopy tests were carried out to determine these products and their relative intensities according to the measured absorbance. The recorded spectra of raw TMW, WG and an 80%/20% blend by weight of TMW and WG respectively, are shown in Fig. 3-3. For the spectra of WG, the highest absorption coefficient is associated with the Si-O bending vibration near 453 cm^{-1}. A weaker band due to the bending mode near 1000 cm^{-1} is accompanied by the still weaker feature near 775 cm^{-1}. For the TMW, the highest absorption coefficient is associated with the bending vibration of the Si-O between 465 and 424 cm^{-1}. Weaker features are associated with the bending vibration of Si-O at 984 cm^{-1} and its symmetric stretching vibration between 797 and 694 cm^{-1}. The weakest bands at 827cm^{-1} and 1163 cm^{-1} can be associated with the bending of the Si-O bond of the raw TMW. The absorbance spectrum of the TMW/WG blend displays the same spectral bands as the raw TMW, only at lower intensities, obviously due to the combination of different intensities.

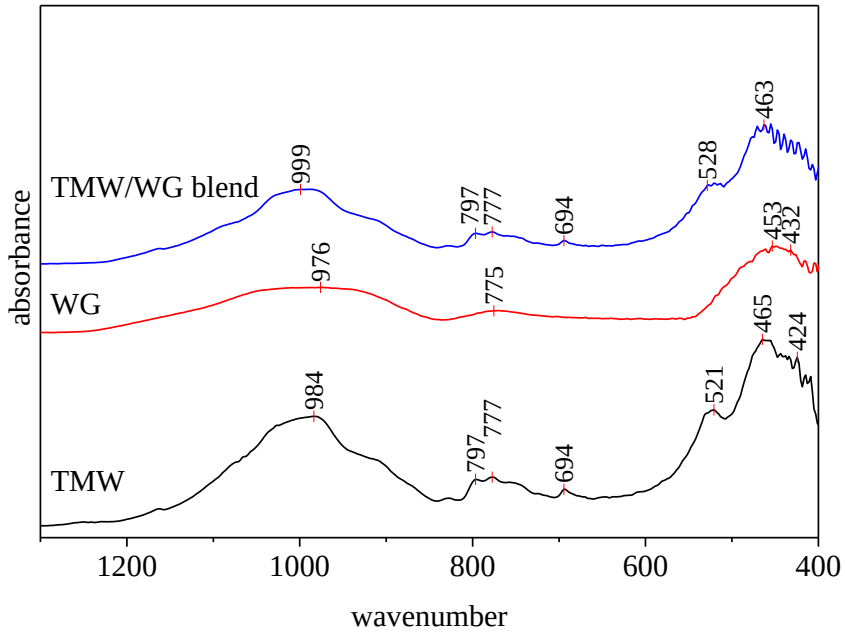

Figure 3-3 ATR-FTIR absorbance spectra of the as received raw TMW, WG, and TMW/WG blend (80 and 20% mass fractions, respectively)

The position of TMW regarding its oxide composition on a wt. based ternary CaO-SiO_2-Al_2O_3 diagram can be seen in Fig. 3-4, represented by the black circle. With respect to other common precursor materials which also appear in the diagram, the TMW falls between the chemical composition of fly ash and blast furnace slag.

Particle size distribution analysis (Fig. 3-5) was performed for the precursor materials after mechanical sieving by laser diffraction according to BS ISO 13320:2009 using a Horiba LA-920 in water dispersion with ultrasound. Water dispersion was determined adequate due to the non-hydraulic nature of the TMW and WG. The TMW was determined to have a mean particle size of 26 μm while the waste glass had a mean particle size of 39 μm. The WG was intentionally used with a larger mean particle size to reduce the energy consumption during the milling process. The bulk powder densities of TMW and WG were determined using a gas displacement pycnometer (AccuPyc II 1340, Micromeritics, U.S.A) and were 3.08 and 2.53 g/cm^3, respectively. A 10M sodium hydroxide solution was prepared by dissolving sodium hydroxide pellets in de-ionized water and allowed to cool before use. Sodium silicate had a SiO_2/Na_2O = 3.23 (8.60 wt.% Na_2O, 27.79 wt.% SiO_2, 63.19wt.% H_2O, 0.4wt.% Al_2O_3). The selection of the activator components was based on a literature survey followed by a previous screening test regarding setting times.

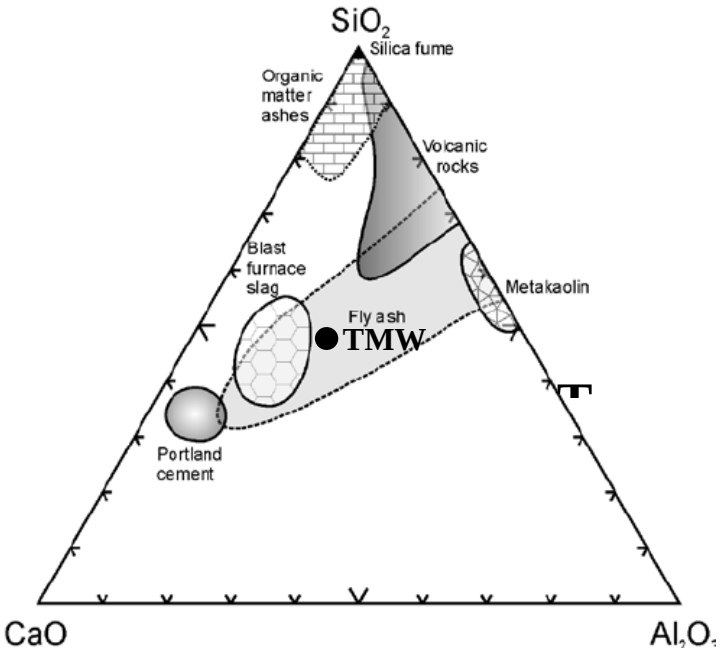

Fig. 3-4 Wt. based ternary CaO-SiO_2-Al_2O_3 diagram (modified after Snellings et al. 2012)

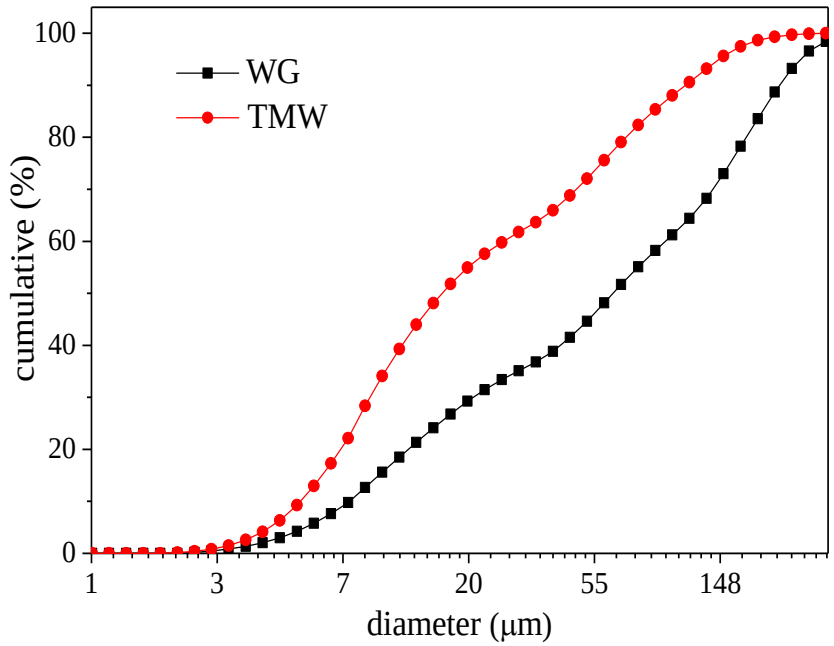

Fig. 3-5 Particle size analysis of TMW and WG

3.2.2 Synthesis of Samples

All mixing operations were carried out at 20°C. Based on the research on alkali-activation available in the literature concerning mechanical strength and efflorescence formation potential in AABs combined with the experience gained from previous studies (Pacheco-Torgal, J.P. Castro-Gomes and Jalali, 2008; Silva, J. P. Castro-Gomes and Albuquerque, 2012b; Kastiukas, Zhou and Castro-Gomes, 2016), the following ranges were selected for the constituents of the AABs:

- Molarity of SH = 10M
- Weight ratio of SS/SH = 4
- Weight ratio of precursor/activator = 3.6
- 80% by mass of TMW and 20% by mass of WG

The following ratios produced an AAB with a flowability of 130 ± 5mm determined using the method proposed by EN 1015-3:1999 (2006) and initial and final setting times of 90 and 110 minutes determined EN 196-3 ((CEN) European Committee for Standardization, 2005a). In the precursor/activator ratio, the precursor is the TMW and WG, and the activator is the solution containing the alkali, the silicate and the water.

To produce the TMW-WG AAB, the TMW, and WG were mixed in the dry state for five minutes with a dispersing mixer (IKA Ultra-Turrax T50, Germany) at 360 rpm, forming the precursor materials. The sodium hydroxide and sodium silicate solutions were mixed for a period ranging from 2.5 to 20 mins at 700rpm, depending on the type of condition being tested, forming the alkali activator. The alkali-activator solution was slowly added to the precursor materials, and the resulting paste was stirred for 2.5 minutes at 200 rpm, followed by 2.5 minutes at 400 rpm. The resulting AAB was then placed in prismatic 40x40x160 mm Styrofoam moulds. The mould was filled with the AAB in three stages and manually vibrated after each successive filling stage to release trapped air bubbles, and sealed with a film to prevent moisture loss from the surface. The specimens were placed immediately after moulding (which on average was 15 minutes after the activator and precursor made contact) in a temperature and humidity controlled environmental chamber at 50% RH for curing between 20 and 80°C for 4-36h, depending on the type of condition being tested. After curing, prisms were de-moulded and left in a laboratory condition of 20°C for curing until the test age. The specimens cured at 20°C were de-moulded after 48 h due to a slow setting. Fig. 3-6 shows the TMW-WG AAB preparation process, and Table 3-3 summarises synthesis conditions tested in this study i.e. activator solution mixing, curing temperature, curing time and exposure conditions during curing.

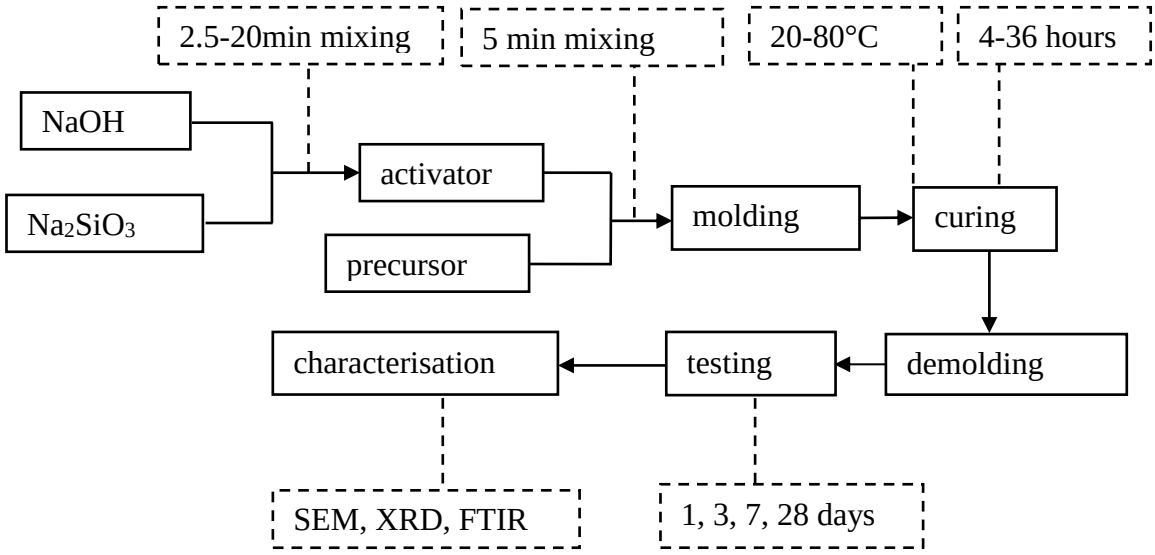

Fig. 3-6 Process flow diagram of TMW-WG AAB production

Table 3-2 Summary of preparation and curing regimes for the variables studied

Sample	Activator mixing (mins)	Curing temperature (°C)	Oven curing duration (hours)
M2.5	2.5	60	24
M5	5		
M10	10		
M15	15		
M20	20		
T20	5	20	24
T40		40	
T60		60	
T80		80	
D4	5	80	4
D12			12
D24			24
D36			36

To observe for chemical changes in the activator solution during mixing, the first it was decided to isolate the activating solution and monitor its temperature during the mixing process. The temperature evolution of the activator solution was measured using the setup shown in Fig. 3-7. The activator solution was prepared at the same SS/SH solution ratio as that used to make the TMW-WG ABB i.e. 4.0. A polystyrene enclosure was used to contain the activator solution and provided a thermodynamically stable environment. Two K-type thermocouples with the tips wrapped in temperature sensitive copper tape were connected to a multi-channel data logger and used to measure the temperature of the activator solution and enclosure's interior, respectively. Once the activator temperature was deemed constant, mixing was started and continued for 20 minutes at 700 rpm.

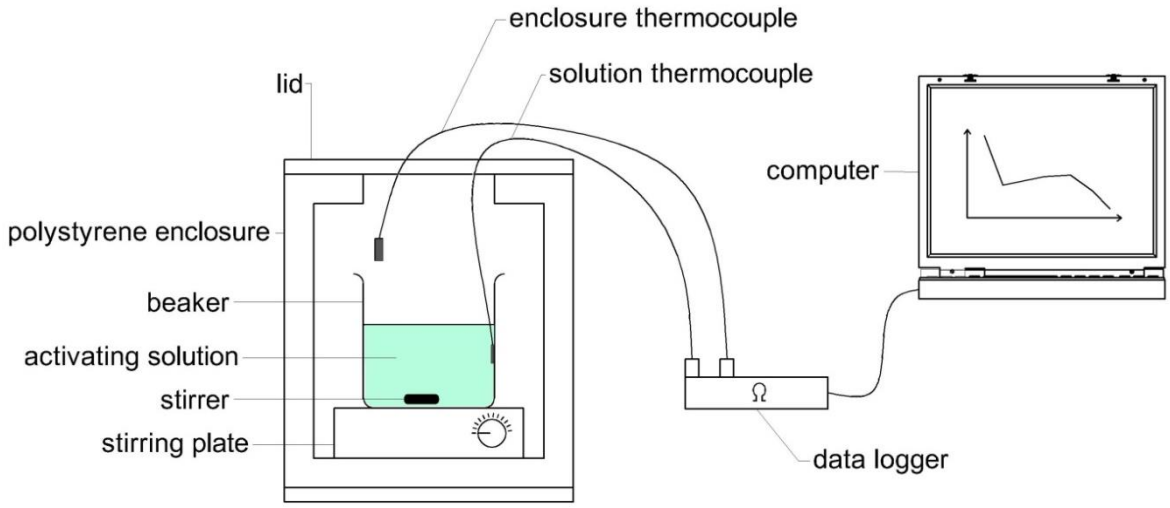

Fig. 3-7 Na_2SiO_3/NaOH activator solution temperature measurement set up

3.2.3 Compressive Strength

The demolded samples were left to rest at 20°C and a relative humidity of 75 % until the specific age of testing. The compressive strength of the prismatic sample fractured counterparts was tested after 1, 3, 7, 28 days in accordance with EN 196-1 using a universal testing machine (Instron 5960, United Kingdom) at a constant loading rate of 144 kN/min. The compressive strength value was the average of values obtained from three specimens.

3.2.4 X-ray Diffraction Analyses

To characterize the precursor material phase compositions, identify newly formed phases, define the degree to which starting materials have reacted and assess the level of amorphicity of the final products, a Bruker X-ray diffractometer (D8 Advance) in the 2°-80° range, 0.600 s count time, Cu radiation, 40kV and 40mA was used.

3.2.5 Fourier Transform Infra-Red Analyses

Fourier Transform Infra-Red (FTIR) spectra were recorded from 400 to 4000 cm^{-1} with a 2-cm^{-1} resolution, 5 kHz scanning speed and a 25-scan count (Shimadzu IRAffinity-1, Japan) fitted with a attenuated total reflectance (ATR) accessory (Specac Quest, United Kingdom).

3.2.6 Scanning Electron Microscopy

Microstructural studies were performed using SEM (Supra 35VP, Carl Zeiss, Germany)) equipped with EDS analyser (EDAX, U.S.A). Backscattered and Secondary electron images were collected from polished specimens to overcome the main limitation of fracture surfaces. To prepare the polished specimens, 5-mm-thick slices were cut using a low-speed saw. The samples were first impregnated with ultra-low viscosity resin and then polished.

3.2.7 Stopping the Activation Process

Both the XRD and FTIR samples were tested in a state where the alkali activation process was stopped using the combined water and solvent extraction protocol developed by Chen et al. (2014). Around 0.8 g of the specimen was stirred with 50 mL deionized water and the liquid removed by centrifuging (which required about 5 min). Soluble silicate species could be observed in the liquid layer upon addition of methanol (using a volume twice that of the collected liquid) because the alcohol reduces the solubility of silicate species and causes their precipitation. Water extraction of the AAB sample was repeated until no precipitation was observed in the collected liquid upon addition of methanol and then once more. Specimens were then ground to micron-sized particles using a mortar and pestle. The solvent was added, a 50/50 (vol) methanol/acetone mixture, and the resulting suspension, around 0.8 g specimen and 80 mL solvent, was further ground with the pestle so that all particles would contact the solvent. After 5 min, the solvent was removed using vacuum filtration, and the new solvent was added. This procedure was repeated for five times (i.e., totally 400 mL of solvent was used).

3.3 Results and Discussion

3.3.1 Alkali Activator Preparation Conditions

To prepare the TMW-WG AAB, it is necessary that the alkali activator is in a homogeneous state upon mixing with the powder precursors. Fig. 3-8 shows the effect of activator mixing time on the 80TMW20WG AAB compressive strength. The 28-day strength increases when using the activator which has been mixed between 2 and 5 minutes only (i.e. M2.5 and M5), reaching the maximum 28-day strength of 17 MPa at an activator mixing time of 5 minutes (i.e. M5). As the activator mixing time is extended, an immediate drop in compressive strength is observed. The activator solution mixing time has a strong impact on the 28-day strength, as a 26% drop in compressive strength is recorded for the TMW-WG AAB when prepared using an activator solution stirred for 20 minutes i.e. M20.

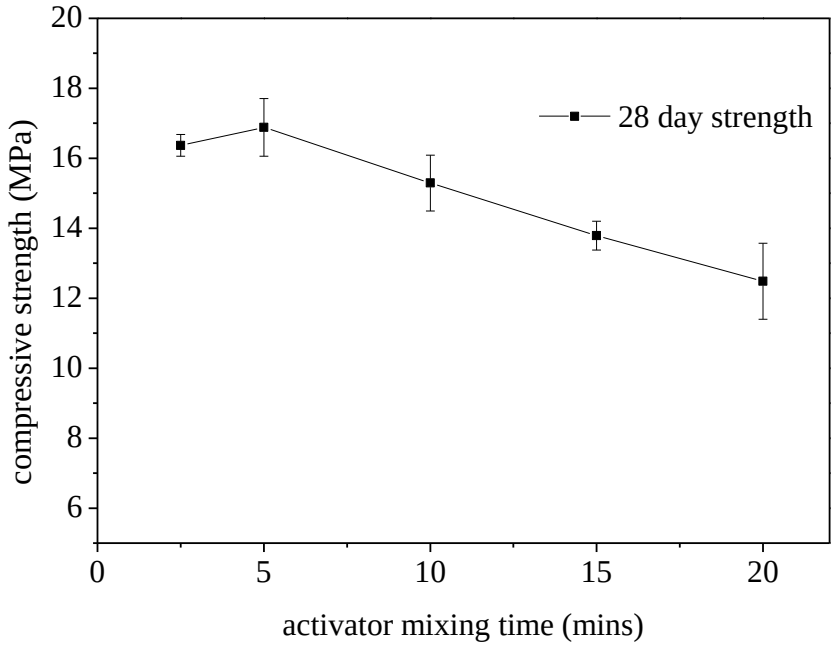

Fig. 3-8 Effect of Na_2SiO_3/NaOH activator solution mixing time on 28-day compressive strength of 80TMW20WG ABB cured at 60ºC for 24 hours

Fig. 3-9 presents the results of the activator solution temperature during mixing. The black and red curves represent the activator and enclosure air temperature, respectively. Over the course of 20 minutes of mixing, an average reduction of 3.13°C in activator temperature was recorded from three identical tests, while the enclosure temperature was recorded to remain stable at 23°C±0.1°C. This drop activator solution temperature is an endothermic process resulting from the reorientation of the water molecules, leading to a disruption of the hydration shells surrounding the ions. The positive metal ions, in this case, Na^+, are particularly at risk since they inherently possess weaker attractions to the negative oxygen end of the water molecule. The prolonged mixing can be thought to cause a net stripping effect of the water molecules from the ions. The latter would impact the dissolution and subsequent mobility of the siliceous material present in TMW and WG, leading to a less intense attack on the silicon-oxygen bonds and thus a reduction in mechanical performance, as verified by the results in Fig. 3-8.

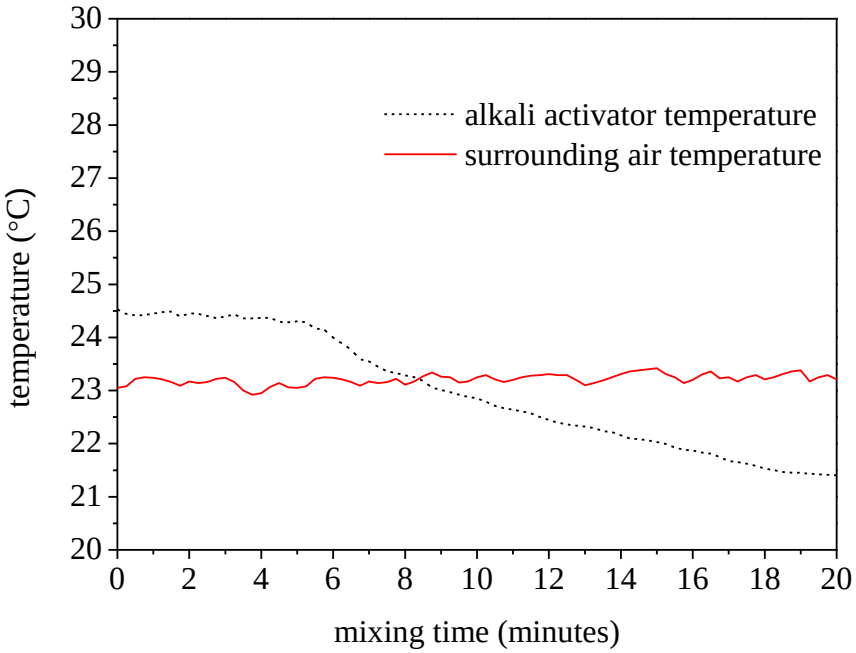

Fig. 3-9 Na_2SiO_3/NaOH activator solution temperature due to prolonged mixing

Further interpretation of this is shown by the ATR-FTIR spectra of the activator mixed for 5 and 20 minutes in Fig. 3-10. The 3270cm^{-1} band (which is a sensitive and well-defined band corresponding to the O-H vibrations in water) is revealed to increase in intensity by 21.4%, which based on literature concerning FTIR spectra of water at different temperature (Praprotnik, Janezic and Mavri, 2004), may be considered as a significant amount. It is an indication that the activator solution mixed for 20 minutes possesses a higher unbound water content with fewer solvated ions and more available as free molecules. Also, visually observed after 20 minutes of mixing was the partial gelation of the soluble silicate anions detected by the loss of uniform fluid flow and the adherence of solid gel to the glass wall. Polymerization of silicates commonly occurs at pH close to neutral, but can also be triggered by an increased water content (Hu, Chung and

Mackenzie, 1993). Gelation would also contribute to reducing the effectiveness of the activator to balance the charge of the aluminate groups in the phyllosilicate, resulting in a negative effect on the kinetics of the reaction and therefore the development of mechanical strength. From a practical outlook, it must be emphasised that the preparation of the alkali activator be independent of the mixing of the final binder. Therefore, the alkali-activators dependence on mixing time should not be considered to interfere with the upscaling potential of AABs.

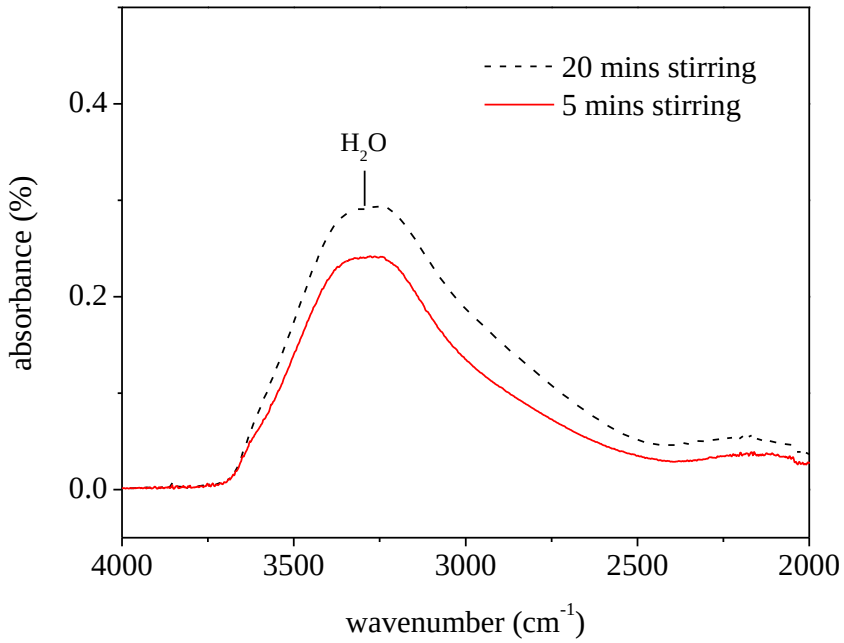

Fig. 3-10 ATR-FTIR spectra of Na_2SiO_3/NaOH activator solution with varying mixing time

3.3.2 Curing Temperature

It has been reported previously that for metakaolin (Assaedi, Shaikh and Low, 2015) and fly ash (Palomo, Grutzeck and Blanco, 1999) based AAB systems the temperature at which samples are cured greatly affects their final compressive strength. Samples T20 through to T80 in Table 3-3 were made so that the effect of different curing temperatures on compressive strength of TMW-WG AAB could be studied. The prisms cast were cured under sealed conditions at 20, 40, 60 and 80°C for 24h, then tested for compressive strength after 1, 3, 7 and 28 days. The compression strength results in Fig. 3-11 present details on the role of temperature on the properties of TMW-WG AAB. The compressive strength of all the samples at all ages increased with increasing curing temperature. Samples cured at 20°C (i.e. T20) did not develop appreciable compressive strength for the first 7 days of curing and were only able to attain 2.6 MPa after 28 days. The highest compressive strengths were obtained by curing at 80°C (i.e. T80), allowing the TMW-WG ABB to attain 22MPa at 28 days. From this, it can be concluded that the reaction that took place was a temperature-driven process. Van Jaarsveld et al. (2002) and Bakharev (2005) reported comparable compressive strength results for fly ash based AABs. Curing the samples above 80°C was not attempted due to the sufficient strength gained from curing at 80°C. Higher temperatures would also require a greater energy input; a factor this study wanted to avoid by keeping the production of the binder as less energy intensive as practically possible.

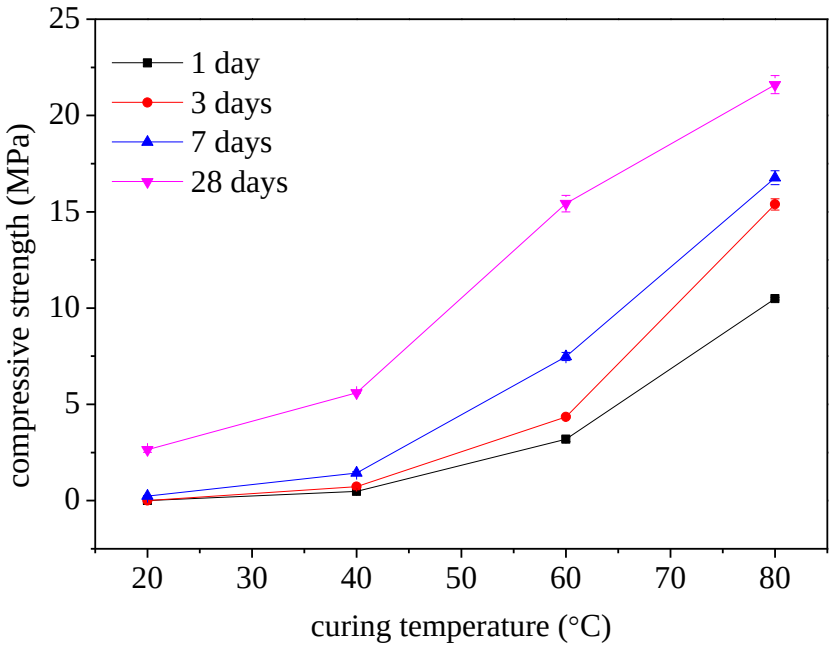

Fig. 3-11 Effect of curing temperature on compressive strength (1-28d), for 80TMW20WG samples cured at 20, 40, 60 and 80ºC for 24 hours

Fig. 3-12 shows the FTIR spectra of the TMW/WG blend of raw materials and the TMW-WG AAB cured at different temperatures (i.e. T20-T80). The TMW-WG AAB cured at 20°C (i.e. T20), as expected, displays the highest absorbance, which can be inferred as reduced hardening activity and thus slow strength development. The spectra of samples cured at 40 and 60°C (i.e. T40 and T60) match each other closely indicating similar molecular structures are present in both samples when curing at the respective temperatures. However, the change in absorbance for the sample cured at 80°C (i.e. T80) is more evident. The latter spectrum shows a great reduction in absorbance and broadening between 850 and 1100 cm^{-1} associated with the Si–O-Si symmetric stretching vibrations for the gel product and is an indication of increased activation. A similar feature can be observed at 775 and 694 cm^{-1}, the region of the spectrum also representing symmetric stretching vibration of the raw material Si-O bonds. The development of a more amorphous gel phase with the increase in curing temperature can be inferred from the spectrum of the TMW-WG AAB sample at 80°C matching that of the raw WG, which is confirmed to be inherently amorphous from the XRD results (refer to Fig. 3-2). Nonetheless, the presence of asymmetric stretching vibration (Si–O–Si) related to non-solubilised particles at ~1000 cm^{-1} and ~450 cm^{-1} in the TMW-WG AAB indicates that unreacted precursor materials are still present, supporting the same result found in the XRD analysis. Milling the precursor materials to a fine particle size has been shown to improve reactivity and dissolution in an alkali activator solution. In the case of fly ash, Temuujin et al. (2009) showed that vibration milling could reduce the median particle size by more than 50% and improve the compressive strength by 80%. This method of mechanical activation could potentially be used to improve the dissolution properties of TMW further, if the additional energy input did not compromise the low energy potential of the TMW-WG AAB.

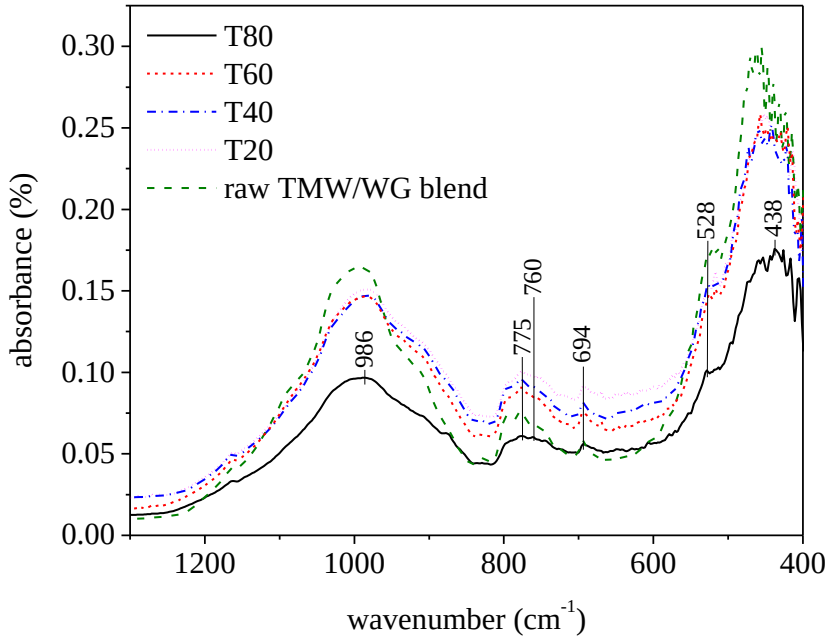

Fig. 3-12 ATR-FTIR absorbance spectra of as received raw TMW/WG and 80TMW20WG at 28 days allowed to cure at 40, 60 and 80°C

3.3.3 Curing Time

Just as important as curing temperature is the AAB heat curing duration. Samples D4 through to D36 in Table 3-3 were prepared to study the effect of curing time on the compressive strength of TMW-WG AAB. Samples were cured in sealed conditions for 4, 12, 24 and 36h at 80°C and tested for compressive strength after 1, 3, 7 and 28 days. In Fig. 3-13, it is shown that the compressive strength improves with an increase in curing time from 4 to 24h. The improvement in compressive strength continues at an even higher rate when the curing time increases from 12 to 24h. However, after 36h of curing a depreciation of the compressive strength at 36h (identified by the yellow marker in Fig. 3-13), 3 days and 7 days is observed, leaving the 28-day strength unchanged. Thus, it can be concluded that the activation reaction that took place was time-dependent. Fig. 3-14 shows the SEM images of TMW-WG AAB samples cured at 80°C for 24 and 36h. The microstructure of the sample cured for 24h consists of close-packed quasi-unreacted WG particles embedded in a continuous matrix of gel products while the sample cured for 36h exhibits visible contraction, particularly around the WG particles. Although samples were kept in sealed conditions during curing, it was observed during de-molding that some water was still able to evaporate into the surrounding air within the curing bag. Previous work by Mo et al. (2014) suggested that the contraction of AAB samples cured under sealed conditions at 80°C occurs after 7days. However, the results of this study suggest that contraction can initiate as early as 36h. It is possible that prolonged exposure to the elevated temperature may have led to the water evaporation rate being greater than that of re-saturation, thus triggering the accumulation of internal stresses and subsequent contraction of the AAB matrix.

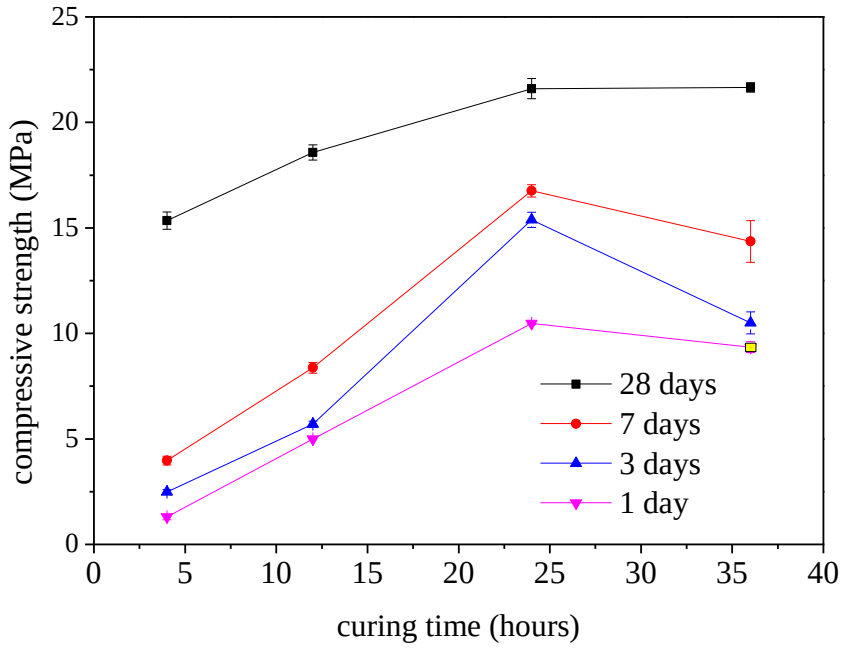

Fig. 3-13 Effect of curing time on compressive strength (1-28d), for 80TMW20WG samples cured at 80ºC

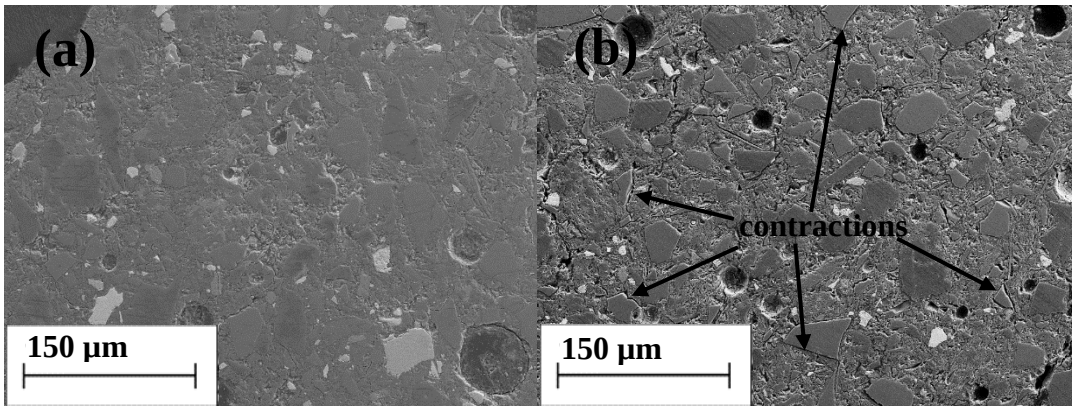

Fig. 3-14 TMW-WG ABB sample cured at 80°C for (a) 36h and (b) 24h

The absorbance spectra for the raw TMW/WG blend and TMW-WG AAB, cured for varying periods of time (i.e. D4-D36) are shown in Fig. 3-15. A reduction in the absorption intensity of the main bands at ~1000, ~775 and ~446 cm^{-1} indicates that longer curing times led to the further dissolution of Si-O from the raw materials. Also, the position of Si-O bending vibration peaks shifted from 999 and 463 cm^{-1} in the raw TMW/WG to 989 and 446 cm^{-1} respectively for the TMW-WG AAB specimen cured for 24h, a type of shift associated with a greater extent of polymerization in alumino-silicates (Sarkar, Dana and Das, 2015). Also, it is important to observe that the absorbance spectrum for the TMW-WG AAB sample cured for 24h (i.e. D24) displays lower absorbance intensities than the TMW-WG AAB sample cured for 36h. It can be inferred from this latter result that curing times above 24h can lead a reduction in Si-O dissolution and complements the mechanical strength results in Fig. 3-13 which show reductions in compressive strength for samples cured for 36h. Previous research regarding the curing time of AAB's made from fly ash (Li, Wang and Jiao, 2013) and metakaolin (Heah *et al.*, 2011) have shown similar results. Also, the broadening of the characteristic bands between 1100-850 cm^{-1} and 800-750 cm^{-1}

implies the overlap of more bands with a higher intensity which in this case is attributed to the asymmetric stretching vibrations of T-O-Si (where T= Si or Al) (Khater, 2013).

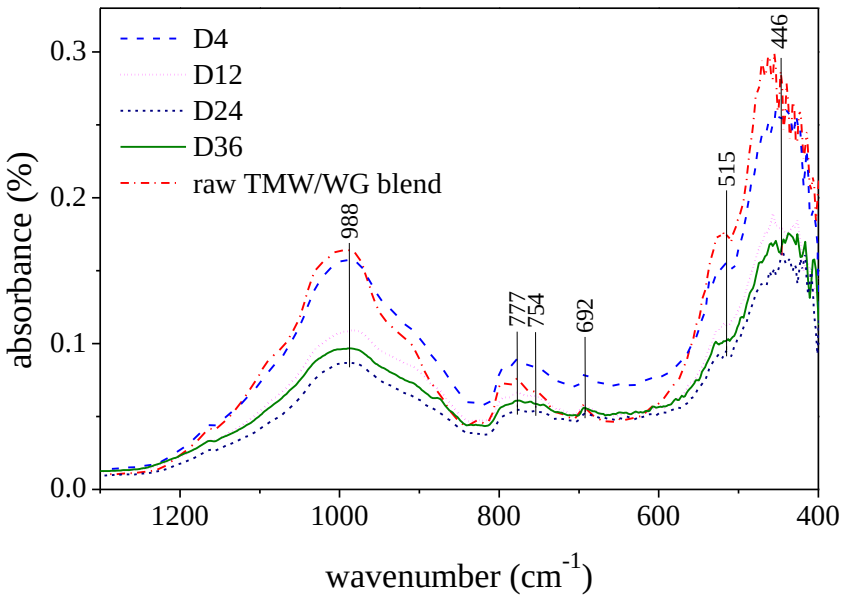

Fig. 3-15 ATR-FTIR absorbance spectra of as received raw TMW/WG and TMW-WG AAB at 28 days that has been allowed to cure at 4, 12, 24 and 36 hours.

Fig. 3-16 shows the XRD patterns of TMW-WG AAB at different curing ages of 1, 3, 7 and 28 days. After a curing period of 28 days, the peaks for the TMW-WG AAB (i.e. mix D24) reduce in intensity at 8°, 21°, 37° and 50° and adopt a broader shape in comparison with XRD pattern of the raw TMW/WG blend, demonstrating that those mineral phases were partially dissolved in the activator solution leading to the production of more amorphous reaction products. The presence of the characteristic peaks from the TMW in the hardened material indicates that the precursor material is not fully broken down by the activator solution. Nonetheless, it can also be seen that no new crystalline peaks can be detected in any of the XRD patterns recorded, inferring that gel phases, which cannot be detected by XRD, formed during the activation of the TMW/WG. From the chemical analysis presented in Table 3-1, the TMW contains an appreciable level of iron which may have positively contributed to the hardening process, since according to literature (Duxson *et al.*, 2007), iron precipitates under alkaline conditions and enhances the setting time and mechanical strength of AAB's.

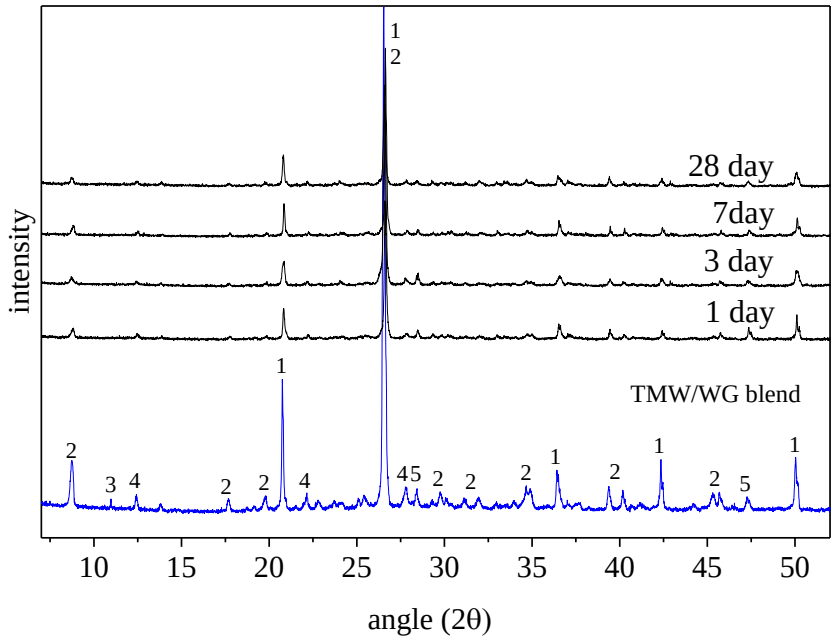

Fig. 3-16 XRD patterns of raw TMW and TMW-WG AAB (D24) at 1, 3, 7 and 28 days (1- silica, 2- muscovite, 3- sodium aluminosilicate, 4- albite, 5- pyrite)

3.4 Summary

The effects of synthesis conditions on the mechanical properties of TMW-WG AAB were investigated. The results demonstrate that the activator solution preparation along with reaction conditions such as curing temperature can significantly influence the formation and properties of TMW-WG AABs, leading to the following discoveries:

- Prolonged activator mixing can reduce the dissolution of the aluminosilicate precursor due to fewer available alkali metal ions in solution. The initiation of silicate gelation due to prolonged stirring would also contribute to reducing the activator effectiveness. The correct preparation of the activator solution is imperative and would be expected to extend to other classes of alkali activated cementitious systems.
- The optimum conditions for obtaining the most significant dissolution of the aluminosilicate oxides were curing for 80°C for 24h. When the curing time is greater than 24h i.e. 36h as investigated in this study, it can lead to a reduction in compressive strength and contraction of the AAB matrix, even under sealed conditions.

4 EFFECTS OF WASTE GLASS ON TUNGSTEN MINING WASTE ALKALI-ACTIVATED BINDERS

The theme of this section is on the recycling of waste materials with the highest technical and economic interest for the promotion of reducing the quantity of the high alkali solution required for the activation of the tungsten mining waste. The focus is on varying the waste glass content and the activating solution itself regarding the quantities of sodium silicate and sodium hydroxide to determine the effect on reactant formation and mechanical strength. The effect of mixing water on the binder workability and subsequent mechanical strength is also investigated. The results show that waste glass can effectively act as an additional source of reactive silica, allowing for the quantity of sodium silicate to be reduced.

4.1 Introduction

High additions of strong alkaline activators are needed in alkali-activated cementitious systems, which may pose health risks, especially when such binders are used in dry mix mortar formulations (e.g. tile adhesives), where the workers get into contact with the highly alkaline material. The cost of manufacture and associated health risks make highly alkaline conditions unreasonable and one of the principle drawbacks of AAB systems. The use of different such “mild” activators including alkali carbonates and sulfates (Donatello et al. 2013; Garcia-Lodeiro et al. 2013; Garcia-Lodeiro et al. 2013; Shi & Day 1995) and organic activators with carboxylate groups such as lactates or citrates (Alahrache *et al.*, 2016) has been reported previously. Alternatively, activation using phosphoric acid has

also shown promising results regarding durability with excellent resistance to elevated temperatures (Liu *et al.*, 2012). The presence of soluble silica is also known to improve the mechanical properties of the resulting AABs (Fernández-Jiménez, Palomo and López-Hombrados, 2006) at early ages. Palomo et al. found that after curing at 85°C for 24 h, different types of fly ash activated with 8–12 M NaOH yielded a material with mechanical strength ranging from 35 to 40 MPa, and up to 90 MPa when water glass was added to the NaOH solution (SiO2/Na2O = 1.23) (Fernández-Jiménez and Palomo, 2005). Nonetheless, there is a lack of detailed studies of using waste materials to supplement the chemical activation. Previous research has established that SiO_2 is highly soluble in alkaline solutions making the SiO_2/Na_2O molar ratio an important parameter of AABs (Cheng *et al.*, 2015) while the composition and dosage of the activating solution also plays a critical role in controlling the gelation process (Joshi and Kadu, 2012). In this contribution, a study of the interaction of the tungsten mining waste with varying proportions of siliceous waste glass is discussed. The first stage of the study is a report on the effects of increased replacement of TMW with WG. In the second stage of the paper, a systematic study of the effects of the individual NaOH and Na_2SiO_3 components of a multi-compound alkali activator is reported. Scanning electron microscopy (SEM) is used to characterise the hardening process and structural composition of the final products, respectively while crushing tests at specific ages are made to determine the mechanical strength.

4.2 Materials and Methods

4.2.1 Materials

Tungsten mining waste (TMW) obtained from the Panasqueira mine, Portugal and a siliceous waste glass (WG) obtained from the Covilhã local authority were used as the raw materials. Their chemical composition and particle size distributions are given in Table 3-1 and Fig. 3-5, respectively. 10M sodium hydroxide and liquid sodium silicate (8.60% by mass Na_2O, 27.79% by mass SiO_2) were used to produce the chemical activator.

4.2.2 Synthesis of Samples

The first stage of the study involved testing the effect of TMW replacement with WG. Three combinations were considered with the first containing 20wt.% WG (80TMW20WG), the second 30wt.% (70TMW30WG) and the third 40wt.% (60TMW40WG). An AAB using TMW only was also prepared for comparison purposes. For the first stage of the study, a preliminary mix ratio with satisfactory workability was obtained using activator/precursor (a/p) and sodium silicate/sodium hydroxide (SS/SH) ratios of 0.3 and 4.0, respectively, based on previous screening tests. During the second stage of the study, the TMW AAB with a WG replacement that provided the highest compressive strength at 28 days from the first stage of the study was used to investigate the effect of the a/p ratios, as shown in Table 4-1 and Table 4-2, respectively. The samples names were chosen based on whether the NaOH/Precursor ratio or the Na_2SiO_3/Precursor was varied. For example, sample SH-P_002 has a NaOH/Precursor of 0.02, and sample SS-P_022 has a Na_2SiO_3/Precursor ratio of 0.22.

Table 4-1 Composition of TMW-WG AAB synthesised with a varying NaOH/precursor ratio

Sample	a/p	SS/SH	NaOH/precursor	H_2O/precursor	%Na_2O	Ms
	g/g		g/g	g/g	%	g/mol
SH-P_002	0.24	11.10	0.02	0.156	2.5	2.51
SH-P_004	0.26	5.55	0.04	0.171	3.1	2.00
SH-P_006	0.28	3.70	0.06	0.186	3.7	1.69
SH-P_008	0.3	2.77	0.08	0.201	4.4	1.45
SH-P_01	0.32	2.22	0.1	0.217	5	1.27
SH-P_012	0.34	1.85	0.12	0.232	5.6	1.13

Table 4-2 Composition of TMW-WG AAB synthesised with a varying sodium silicate/precursor ratio

Sample	a/p	SS/SH	Na_2SiO_3/Precursor	H_2O/Precursor	%Na_2O	Ms
	g/g	g/g	g/g	g/g	%	g/mol
SS-P_016	0.22	2.88	0.16	0.143	3.1	1.48
SS-P_019	0.25	3.50	0.19	0.162	3.4	1.62
SS-P_022	0.28	3.96	0.22	0.181	3.6	1.75
SS-P_025	0.31	4.50	0.25	0.2	3.8	1.85
SS-P_028	0.34	5.00	0.28	0.219	4.1	1.94

All sample preparation was carried out at 20°C. Alkali-activated TMW pastes containing up to 40% by mass replacement of WG were blended in a dry state with an IKA Ultra-Turrax T50 mixer at 360 rpm for 60 seconds. Separately, the NaOH and Na_2SiO_3 solutions were combined in the ratios defined in Table 4-1and Table 4-2 and stirred magnetically for 5 minutes at 700rpm. After stirring of the activating solution was complete, it was added to the TMW/WG precursor blend. Stirring of the resulting paste was conducted for 2.5 minutes at 200 rpm, followed by a 30-second pause to scrape material adhered to the sides of the mixing bowl and then finally for a further 2 minutes at 400 rpm. Prismatic 40x40x160 mm Styrofoam molds were filled with the AAB and sealed in plastic bags to prevent moisture loss during curing. The specimens were placed in a temperature and humidity controlled environmental chamber for curing at 80°C. Samples

were removed from the environmental chamber after 24 hours, demolded and left in a laboratory condition of approximately 20°C and 50 % R.H for curing until the test age.

4.2.3 Compressive Strength

The compressive strength of the samples was determined in accordance with EN 196-1 using a universal testing machine (Instron 5960) at a constant loading rate of 144 kN/min. Prismatic sample fractured counterparts were tested after 1, 3, 7, 28 days. The reported compressive strength result was the average of values obtained from three specimens with the error reported as average deviation from the mean; the deviation of results fluctuated between 0.22% and 1.4%.

4.2.4 Setting Time and Flow Testing

The setting time of the TMW-WG AAB was measured according to EN 196-3 (British Standards Institution 2005). The samples were kept in the curing chamber at 80°C during the measurements and setting was measured from the time the precursor materials contacted the activating solution until the penetration of a 2-mm diameter needle was less than 10 mm. The reported setting time results were the average of two specimens. The flow test cone with an internal diameter of 100 mm was used to evaluate the fluidity of TMW-WG AAB as described by EFNARC (2002). Before the test, the frustum mold was placed on a clean metal plate, and the freshly prepared TMW-WG AAB mixture was poured into the cone without any compaction. Once the cone was fully filled with the mortar, the cone was lifted vertically, and the spread diameters of the freshly prepared mortar in two perpendicular directions were measured. All flow test measurements were conducted 7 minutes after mixing and the occurrence of bleeding, if any, was visually observed and noted during the mini-slump flow test.

4.2.5 Activator Bleeding Test

This procedure was conducted according to the reference standard EN 480-4:2005 (CEN (European Commitee for Standardization), 2005). It involved filling a cylindrical vessel with an inside diameter and height of 250 mm and 280 mm, respectively with fresh TMW-WG AAB binder and subsequently drawing activator solution from the surface of the test specimen every 30 minutes. The activator bleeding is expressed as a percentage of the total activator content.

4.2.6 Scanning Electron Microscopy

Electron microscopy was performed using a Zeiss Supra 35VP using backscattered electron (BSE) mode combined with energy-dispersive X-ray spectroscopy (EDS) to analyse the sample morphology and microstructure. Samples were impregnated in low viscosity epoxy resin and polished using consecutively finer media. The polished sample surfaces were coated using a gold sputter coater to eliminate effects of charging during micrograph collection.

4.2.7 Stopping the Activation Process

SEM samples were tested in a state where the alkali activation process has been stopped using a combined water and solvent extraction protocol. A summary can be found in

Chapter 3.2.7 *Stopping the Activation Process*, and the detailed procedure can be found in the literature by Chen et al. (Chen, Meawad and Struble, 2014).

4.3 Results and Discussion

4.3.1 Influence of Waste Glass on Tungsten Mining Waste Reactivity

Results of the XRD analyses shown in Fig. 4-1 reveal that the TMW precursor material predominantly consists of muscovite and quartz with traces of albite and pyrite and is similar to the TMW chemical composition identified by Pacheco-Torgal et al. (2009). The WG is revealed to consist of quartz, lime and sodium oxide with traces of potassium and iron oxide. Using a general non-linear least squares system software (TOPAS V5), the TMW and WG were determined to be 97% and 15% crystalline, respectively. Compared to other materials commonly used as AAB precursors such as fly ash (Van Jaarsveld and Van Deventer, 1999) and metakaolin (Provis, Lukey and Van Deventer, 2005b), the TMW is of a far less amorphous nature. In this study, a sustainable approach was chosen to increase the amorphicity of the TMW through the addition of WG. The addition of 40 wt.% WG led to an increase in the amorphicity, qualitatively indicated by the more intense amorphous background from 15° to 45° in the TMW/WG blend XRD spectrum and also by a 21% calculated reduction in crystallinity.

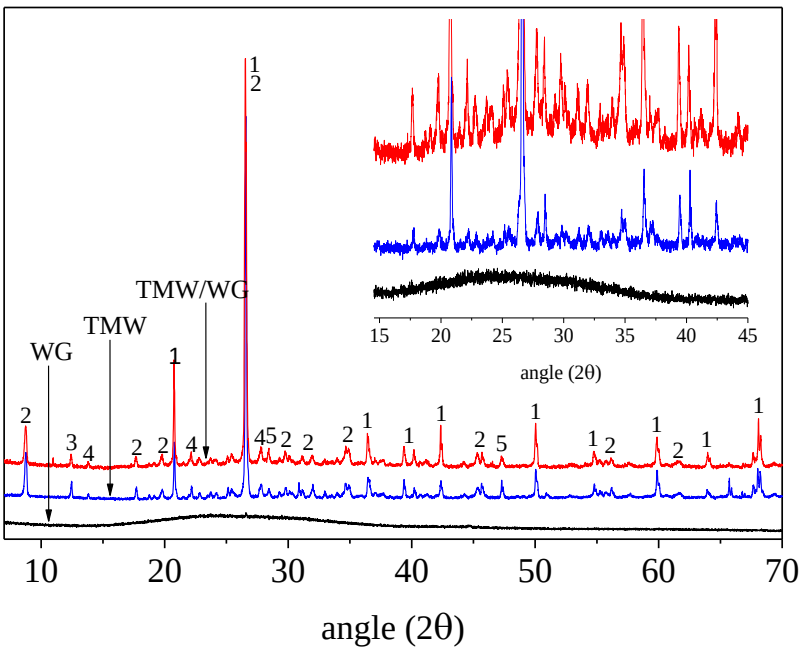

Figure 4-1 XRD pattern of raw WG, TMW and TMW/WG blend (1- silica, 2- muscovite, 3- sodium aluminosilicate, 4- albite, 5- pyrite)

The compressive strength of TMW-WG AAB was used to evaluate the strength contribution potential as a function of the degree of amorphicity. Thus Fig. 4-2 shows the evolution of compressive strength in TMW-WG AAB with 20, 30 and 40 wt.% WG replacement over 28 days. The results obtained for pure TMW AAB are also included. Each reported result corresponds to the average measurement in three specimens per each WG replacement value and age; the deviation of results fluctuated between 0.22 and 1.4%. In Fig. 4-2 it can be observed the compressive strength increased with an increase in the

WG content at all ages. The highest 28-day strength was obtained by the 60TMW40WG sample at 41MPa, which is 127% higher than the control sample 100TMW. The compressive strength would be influenced primarily by the additional release of reactive silica. However, it also expected that the CaO content in the WG would contribute to the strengthening of the reaction products, most likely in the form of a (C, N)-A-S-H gel.

The compressive strength results with the highest replacement level of WG i.e. 40wt.% is consistent with the compressive strength results previously obtained by Pacheco-Torgal et al. (2009b), specifically 39.6 MPa at 28 days, for mortar prepared with TMW. However, this was achieved only after an energy intensive calcination treatment of the TMW at 950°C for 2 hours.

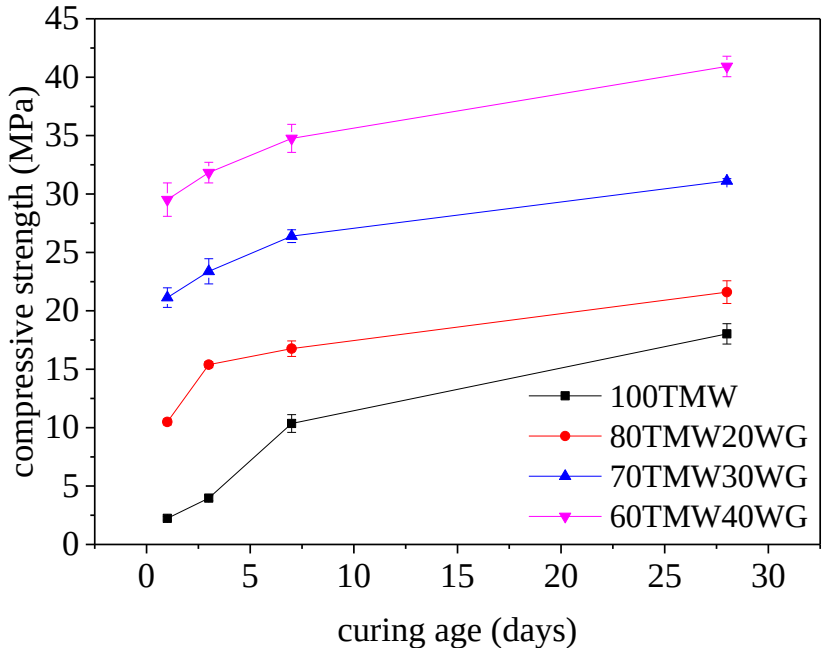

Figure 4-2 Effects of WG substitution on compressive strength

Finally, the reactive silica-containing WG combined with the highly alkaline activator solution may create the potential for the deleterious process of alkali-silica reaction (ASR) and required validation. TMW-WG AAB with the highest replacement of WG i.e. 40 wt.% was stored at a RH of 80% at 38°C to accelerate the ASR reaction; a thin section of this sample shown in Fig. 4-3. Observation of the section, which is representative of the WG, revealed that there were no signs of ASR gel formation around the WG particles or in the open voids. Data reported in the literature established that if the waste glass is ground under 75 μm, the ASR effect does not occur, and binder durability is guaranteed (Shao *et al.*, 2000b). Water is also a necessary condition for ASR; considering the TMW-WG AAB only required a water/precursor demand of 0.179, this may also be the reason for the absence of ASR.

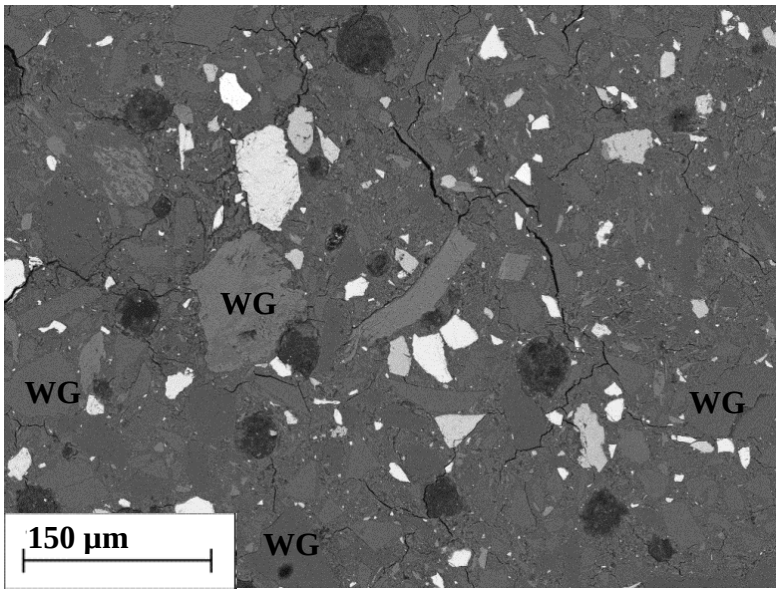

Figure 4-3 Polished thin section of TMW-WG AAB with 40 wt.% WG at 28-days

4.3.2 Influence of Waste Glass on Tungsten Mining Waste Mechanical Performance

Results from the SEM imaging show the early age product formation in the 100TMW sample (Fig. 4-4). Sites of N-A-S-H alkalinisation products (P1) with different cation and anion substitution of Fe, Mg and K are amorphous in structure and show branch-like formations bridging the reaction products together (shown in Fig. 4-4a). The same reaction products in Fig. 4-4b can also be seen merging with the quartz particles from the TMW. The muscovite detected according to the XRD analysis (Fig. 4-1) was the hydrous layer silicate minerals muscovite-2M, indicating that it had not reached a state of dehydroxylation. The muscovite crystals usually have a flake-like appearance, separated from each other, providing a highly-striated structure most likely the result of thermal decomposition (thermal shock treatment) during the mining process. The rapid heating of raw muscovite crystals results in the transformation of the interlayer water into steam, which under pressure forces the silicate layers to separate forming packets, which are several orders thicker than the fundamental layer to produce “accordion” type morphology. Fig. 4-4c shows a muscovite crystal (M) regaining its laminated structure during alkali activation. Using EDX microanalyses, the Al/Si ratio for unreacted muscovite was determined as 1.0, while measurements made after 1 day of reacting with the alkali activator saw the latter value drop to 0.65 due to leaching of the aluminium and potassium cations.

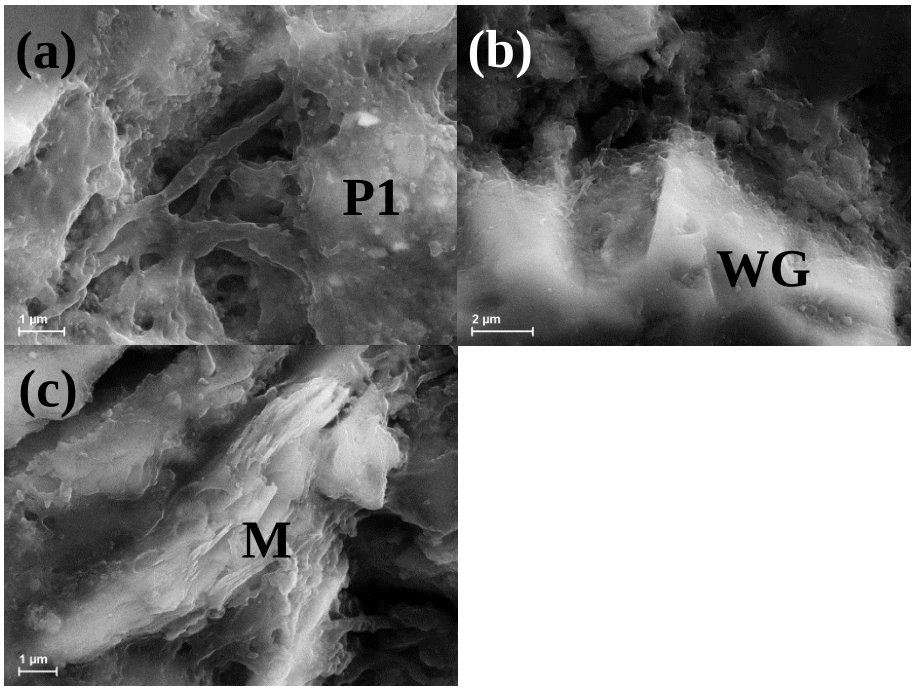

Fig. 4-4 TMW AAB showing (a) branch-like product formations; (b) reaction product and quartz; and (c) muscovite crystal

Fig. 3-2 clearly shows that the TMW-AAB obtained improved compressive strength with an increase of WG. In fact, a 20 wt.% increase in WG from a 20 to 40 wt.% replacement level raised the 28-day compressive strength by 90% to 41MPa. Fig. 4-5 shows how the TMW particles in the 1-day 60TMW40WG sample (Fig. 4-5a) exhibited more regions of the muscovite crystal regaining its laminated structure (identified by its lighter regions) which can be inferred as in increase in the level of Al and Si leaching. On the other hand, the muscovite particle in the 1-day 100TMW sample (Fig. 4-5b) remained relatively unchanged. The 60TMW40WG sample structure appears to contain fewer voids while the reaction products appear denser and have more continuity i.e. are not comprised of isolated regions like in the 100TMW sample. Dense amorphous gel-like formations were also observed also in the 60TMW40WG (Fig. 4-5c). The latter figure also shows how particles of WG are partially transforming into amorphous reaction products supporting the idea that an increased replacement of WG provides a means of increasing reactive silica and thus increasing the Si/Al ratio without resorting to using the more expensive and less sustainable soluble silica found in the Na_2SiO_3 solution. By the age of 28 days, many large particles of SiO_2 chemical composition were found embedded in the AAB matrix (shown in Fig. 4-5d); however, it was difficult to establish the quantity that came from the TMW and WG. Nonetheless, it can be inferred that the increased WG content not only supplied reactive silica to the mix but may have also contributed to strengthening the AAB as an inert filler.

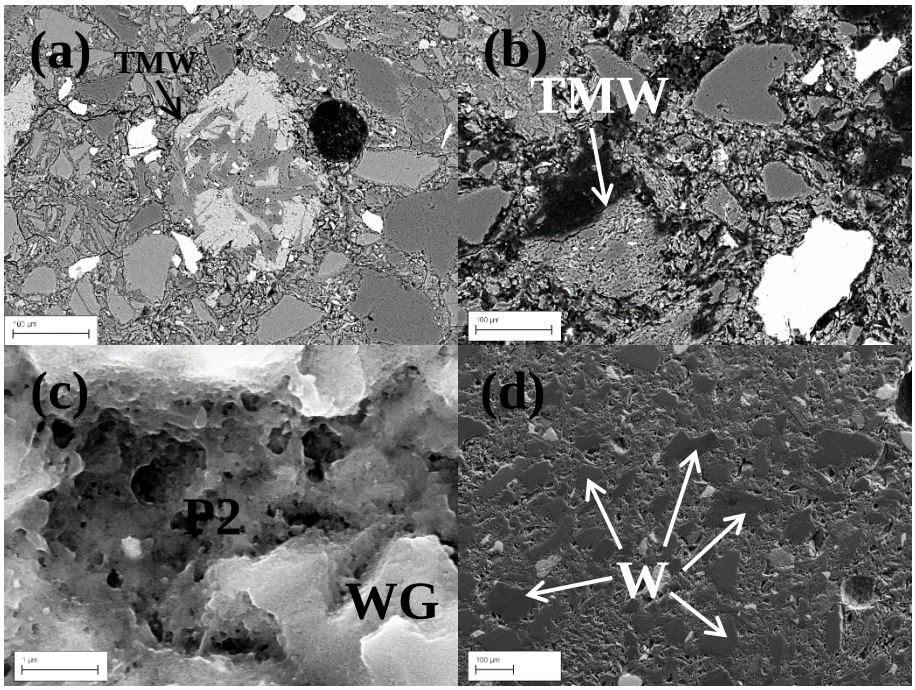

Fig. 4-5(a) 60TMW40WG (b) 100TMW (c) amorphous reaction products in 60TMW40WG

Fig. 4-6 shows the Energy Dispersive X-ray (EDX) spectra for the 1-day reaction products in the 100TMW sample (P1) and the 60TMW40WG sample (P2). The distinction between the spectra is firstly the increased intensity of the main silicon peak at 1.7keV (4.5K for P1and 14.4K for P2) which is due to the contribution of amorphous silica from the WG. The Si/Al molar ratio for the reaction product P1 in the 100TMW sample was measured to be 1.08, while Si/Al molar ratio of the reaction products P2 for the sample containing a 40% mass fraction of WG increased to 3.0. Secondly, the identification of (C,N)-A-S-H gel formation is also believed to contribute to the increased mechanical strength of the 60TMW40WG sample due to the presence of calcium compounds from the WG, which in another study has also been shown to improve the mechanical properties of AABs (Temuujin, van Riessen and Williams, 2009)

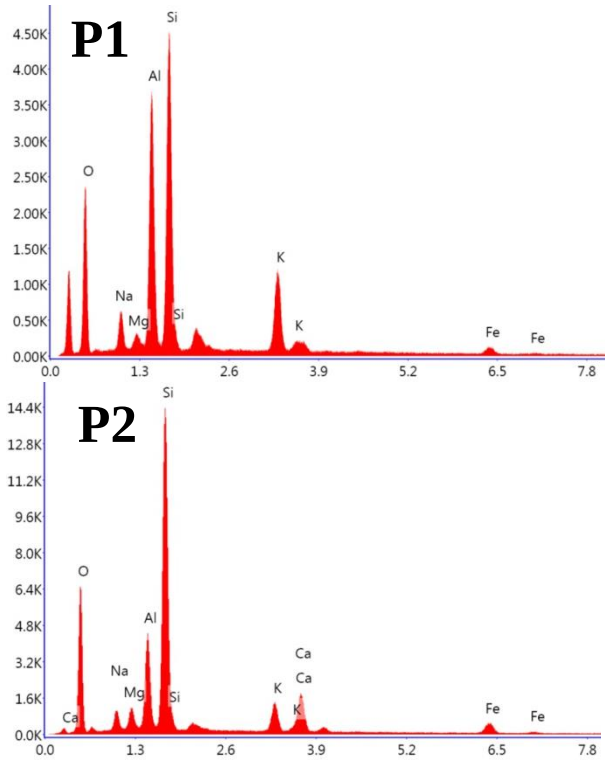

Fig. 4-6 SEM-EDX of (P1) 100TMW and (P2) 60TMW40WG

4.3.3 Influence of Alkali-Activator Composition

The results from the first stage revealed that the TMW-AAB with the highest replacement by WG i.e. 40 wt.% led to the highest compressive strength. Thus, it was the latter AAB composition which was chosen for further investigation in the second stage of this study. Fig. 4-7 presents the results of the 60TMW40WG AAB compressive strength with varying values of Ms i.e. SiO_2/Na_2O. Fig. 4-7a shows the effect of an increased Ms due to SH while maintaining a constant quantity of SS, while in Fig. 4-7b, it is vice versa. The results reveal that the values of Ms show more variation and thus impact on the AAB strength development due to changes in the SH component of the alkali activator rather than SS. For the TMW-WG AAB samples presented in Fig. 4-7a, made with a constant SS/precursor ratio of 0.22 and varying SH/precursor ratio from 0.02 to 0.12, the increase in Ms over the 1.13 to 2.0 range results in an increase in compressive strength across all ages. However, a further increase in Ms over the 2.0 to 2.51 range resulted in an immediate reduction in the 28-day compressive strength. The latter result can be related to the reduction in $\%Na_2O$ content (mass ratio of total Na_2O in the activator solution to precursor). The increase in compressive strength from 29 to 46 MPa is for a reduction of $\%Na_2O$ from 5.6 % to 3.1% while the reduction in compressive strength from 46 to 42 MPa occurs when the $\%Na_2O$ falls from 3.1% to 2.5%. The charge distribution of Na alkali metal ions surrounding the Al and Si ions defines the ionic atmosphere and depends on the concentration of the Na ions. The ionic atmosphere can be thought of as a measure of the ion-ion interaction (Juška *et al.*, 2000), in the sense that when it is much larger that the Si or Al ionic radius, the ions can be considered as point charges with reduced interaction, while if it is in the same range with the ionic radius then this can allow for stronger ion-ion interactions. Thus, the initial reduction in the alkalinity from 5.6% to 3.1 % would, in turn, reduce the Na ionic atmosphere and improve the Al and Si interaction, allowing less interference in the creation of bonds within the aluminosilicate gel framework and

increasing the degree of connectivity. The latter would also reduce the setting time, an aspect of the TMW-WG AAB discussed further on in this study.

On the other hand, the samples which are presented in Fig. 4-7b were made with a constant SH/precursor ratio of 0.06 and an SS/precursor ratio ranging from 0.16 to 0.28. The increase in $\%Na_2O$ for these samples was over a smaller range (3.1% to 4.1%) and thus impacted the compressive strength to a lower degree. Sample SS-P_016, which had a $\% Na_2O$ content of 3.1, developed the highest 28-day compressive of 61MPa. Increasing the content of SS resulted in immediate reductions in compressive strength. Starting at a Ms value of 1.48 and a corresponding $\%Na_2O$ content of 3.1%, the 28-day compressive strength depreciated by 23% when a Ms value of 1.94 and corresponding $\%Na_2O$ content of 4.1% was reached. From both series of samples, a clear correlation can be observed; the highest compressive strengths were attained at a Ms value between 1.27 and 1.48, while significant reductions in compressive strength were found at Ms values above 1.48, corresponding to a $\%Na_2O$ content of 3.1% and above. Although the best performing samples regarding compressive strength i.e. SH-P_004 and SS-P_016 had the same $\%Na_2O$ contents i.e. 3.1%, the (a/p) ratio for SS-P_016 was only 0.22, meaning it contained 27% less activator than SH-P_004. The latter is apparent since, at the higher a/p ratio range i.e. 0.34, the compressive strength achieved was significantly reduced regardless of whether the SS/SH ratio was high as in the case of SS-P_028 (SS/SH = 5.0) or low as in the case of SH-P_012 (SS/SH = 1.85). Furthermore, when compared to the 100TMW control sample investigated in the first stage, SS-P_016 was calculated to contain 22.5% less SS. This is based on the reduction in the a/p ratio from 0.28 to 0.22 and the SS/SH ratio from 4.0 to 2.88. The latter observations lead to the following relationships: (i) samples made with low a/p ratios i.e. below 0.28 can achieve superior compressive strength when made with an alkali activator consisting of a SS/SH ratio between 3.7 and 5.0 (ii) WG can effectively reduce the SS component in AAB systems.

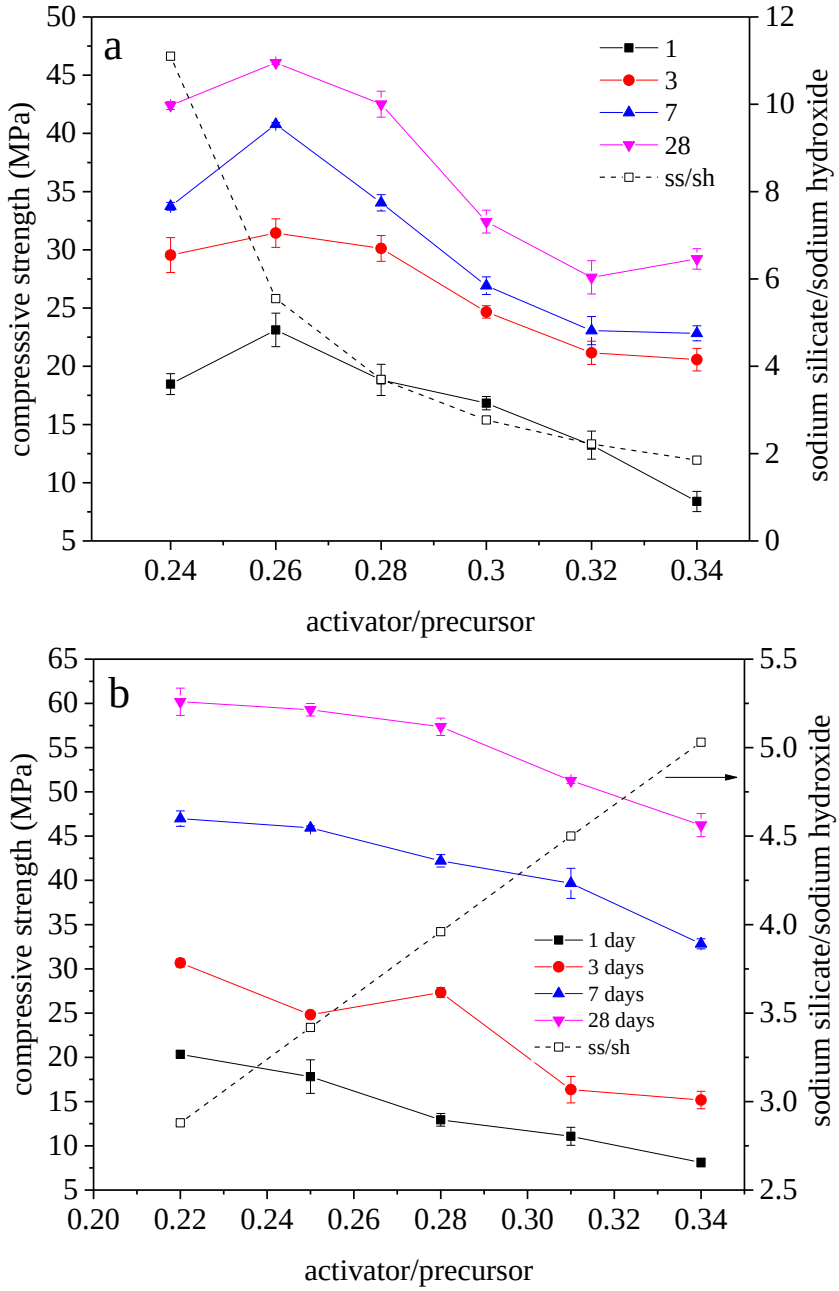

Fig. 4-7 Effect of varying (a) NaOH and (b) Na_2SiO_3 in the activator/precursor ratio

In both series, however, samples prepared with the lowest a/p ratios did suffer from a 'balling' effect (Kay, 2003) which caused the precursor materials to agglomerate into spheres due to the low water/solid ratio, shown in Fig. 4-8a. Nonetheless, SEM analyses revealed a highly compact paste microstructure (Fig. 4-8b) which may partly explain the high compressive strength attained by these samples. The increase in water/solid content has previously been shown to contribute to the reduction of fly ash-based AAB compressive strength due to crystallisation of the otherwise amorphous reaction products (Bakharev, 2005). However, in the samples prepared in this study, no products of crystalline nature were observed for the highest water/precursor ratio of 0.23. Instead, at high a/p ratios, the activating solution was observed to bleed, covering the sample surface and mold (Fig. 4-8c). The activator bleeding measured for SS-P_028 and was determined as 21% of the total activator in the AAB. The latter value of bleeding is significantly large and means only 79% of activator participated in the reaction. Unlike in concrete where the

excess bleed water can evaporate without affecting the mechanical strength, the loss of activating solution in AABs is detrimental to the hardening and thus contributes to the lower mechanical strength observed in this study. SEM analyses of samples with a high a/p ratio support the latter claim by revealing the channel-like paths that formed around particles (Fig. 4-8d) through which the activator solution could escape.

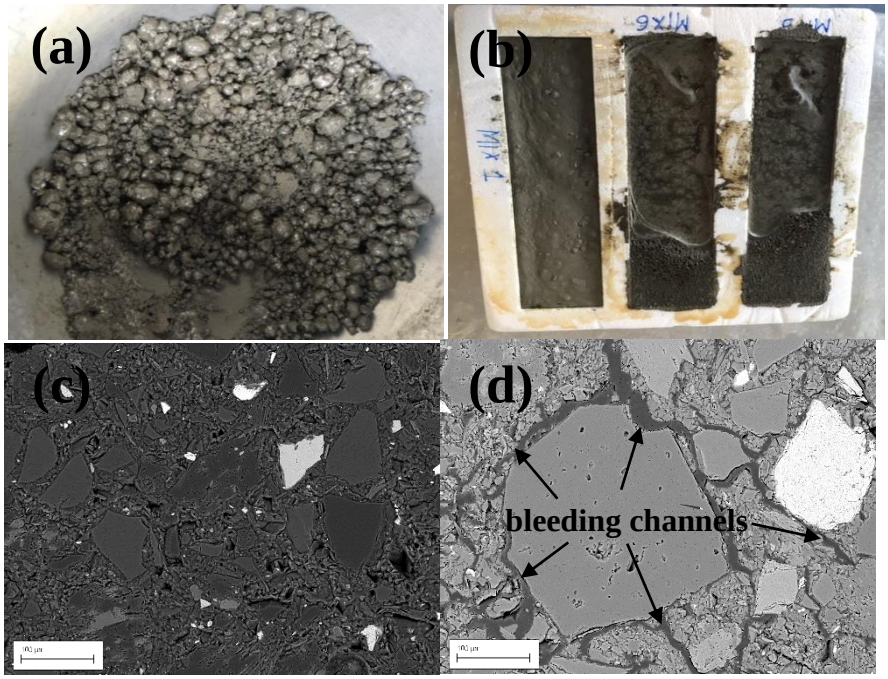

Fig. 4-8 Images of (a) 'Balling' effect of a low a/p ratio mix (b) Activator bleeding in a high a/p ratio mix (c) Microstructure of a low a/p ratio mix (d) Bleeding channels in a high a/p ratio mix

The reduced water content of the low a/p ratio samples was counteracted by the addition of extra mixing water by weight of precursor. In this case, 6 wt.%, 7 wt.% and 8 wt.% of water was chosen to be added to SS-P_016, initially consisting of a water/precursor ratio of 0.14 and SS/SH and a/p ratio of 2.88 and 0.22, respectively. It can be seen from Fig. 4-9 that the initial introduction of mixing water led to a slight reduction in the 28-day compressive strength. However, the further increase in the mixing water content contributed to restoring the compressive strength, and ultimately at 8 wt.% extra mixing water, the compressive strength reached the same value as the control sample (SS-P_016). The total liquid present in the system originates from the water contained in the activator solution (63.2% H_2O from the SS and 69% H_2O from the SH) and from the extra mixing water. Thus, the total water/precursor ratio of the optimised sample containing extra 8 wt.% mixing water was calculated as 0.21. The flow of the pastes with 6 wt.%, 7 wt.%, and 8 wt.% extra mixing water was 101 ± 5 mm, 116 ± 5 mm and 136 ± 5 mm, respectively. The coarser nature and reduced water absorption properties of the WG particles led to the AAB requiring such a low water demand. No bleeding was detected for any of the TMW-WG AAB mixtures. Improvements in compressive strength with an increase in mixing water content at a constant a/p and SS/SH ratio confirm that the observed reductions in compressive strength shown in Fig. 4-7 are in fact due to the increased content of $\%Na_2O$ from the activator solution, and not the increase in the water content.

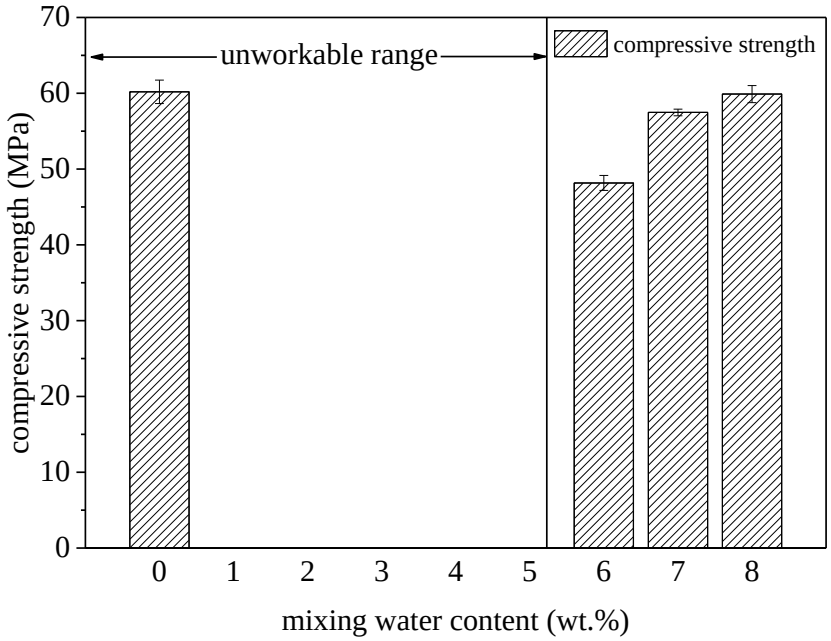

Fig. 4-9 TMW-WG AAB 28-day compressive strength with varying quantities of mixing water

Fig. 4-10 presents the initial and final setting times of all the samples evaluated in the second stage of this study. The SH-P samples were made with activating solutions of varying SH quantity and a constant SS/precursor ratio while samples SS-P were made with activating solutions of varying SS quantity and a constant SH/precursor ratio; a horizontal dashed line is included in Fig. 4-10 to distinguish the two sets. A distinct reduction in initial and final setting time can be observed when the activators SH content increases from 0.02 to 0.06. Further increasing the SH after that leads to an immediate increase in initial setting time while leaving the final setting time largely unaffected, as shown by SH-P_008 and SH-P_01. SH-P_012 which contained the highest SH content evaluated in this set of samples and consequently the highest a/p ratio of 0.34 leads to the slowest initial setting of 2.12 h.

The initial and final setting times of the SS-P range of samples were far lower than those of the SH-P range. The SS/SH ratio for the samples SS-P_016 to SS-P_028 was increasing with an increase in the a/p ratio however for the samples SH-P_002 to SH-P_012, it was the inverse i.e. the SS/SH ratio was increasing with a decrease of the a/p ratio. The common trend which can be observed in both sets of samples is the fact that the initial setting time increased when the a/p ratio was greater than 0.28, indicating that the total activator content was the most dominant factor in controlling the AAB setting time. The setting time also appeared to be affected by the SS/SH ratio, however to a lesser extent, and predominately in the samples for which the amount of SH was varied i.e. samples SH-P_002 to SH-P_012. As an example, SH-P_008 which was produced with a SS/SH ratio of 2.77 at an a/p ratio of 0.3 attained a 28-day compressive strength of 32.5 MPa whereas SS-P_016 which was produced with an almost identical SS/SH ratio of 2.88 but instead with a lower a/p ratio of 0.22, attained 61MPa at 28 days. SS-P_016 yielded the initial and final setting times of 42 minutes and 52 minutes, respectively. With the addition of 8 wt.% mixing water, the initial and final setting times slightly increased to 54 minutes and 66 minutes, complying with EN 196-3:2016 which specifies that the initial setting time should not be less than 45 minutes while the final setting time should not be more than 10 hours. The short time interval between the initial and final setting, but with appropriate

initial setting time would make it an ideal candidate for pre-cast fabrication and rapid road repair, an application which is explored in Chapter 7 *applications* of alkali-activated binders for road repair . It must be noted, however, that these results are valid within the specified range of the process parameters along with their chosen levels and for the specific tungsten mining waste.

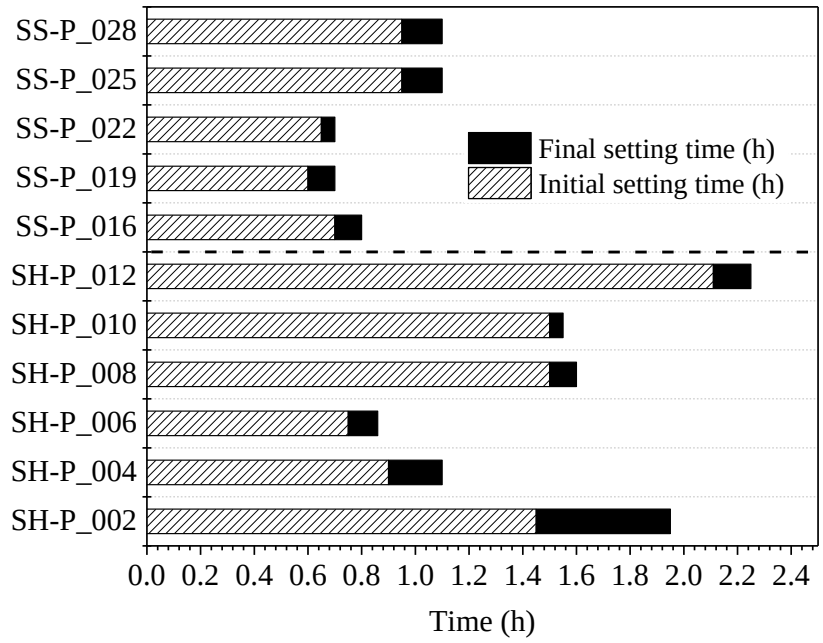

Fig. 4-10 Initial and final setting times of samples SH-P_002 to SH-P_012 and SS-P_016 to SS-P_028

4.4 Summary

The influence of the waste glass and alkali activator composition were examined regarding mechanical strength and workability for TMW-WG AAB. Balance was required between sufficient stimulation of precursor dissolution and avoidance of using highly alkaline conditions due to the associated health risks. Based on these conditions and the results obtained, the following conclusions can be drawn:

- The condition for achieving the highest strength was achieved with a WG replacement by 40 wt.%. In combination with the calcium component, the reactive silica led to the formation of (C, N)-A-S-H gel products whilst also providing a 22.5% reduction in the SS content. Thus, WG can be considered to impart high strengths with a potential for lower alkali solution demands.
- The TMW/WG blend was successfully cured primarily at room temperature and evaluated to have a low activating solution demand and produced 28-day compressive strength above 42MPa when an activator/precursor ratio was maintained <0.28.
- The values of Ms for an activator/precursor ratio <0.28 were calculated to be in the 1.48-2.0 range. The lower end of the range i.e. 1.48 proved to be the most economical since it represents the lowest quantity of alkali activator, and achieved the highest compressive strength i.e. 61 MPa.

- The properties of TMW-WG AAB systems can be drastically affected by minor changes in the alkali activator Na2O concentrations, values of which should not surpass 3.6% when controlling the SS/SH ratio.
- A water/precursor ratio of 0.21 for TMW-WG AABs resulted in the optimal compressive strength and most satisfactory workability and setting time.

5 EXPERIMENTAL STUDY OF TMW-WG AAB WITH ENERGY EFFICIENT AGGREGATES

This section studies macro-encapsulated aggregates (ME-LWAs) consisting of expanded clay lightweight aggregates (LWAs) impregnated with a paraffin wax phase change material (PCM). To fully exploit the thermal energy retaining properties of PCM, a polyester resin was developed to retain the PCM. In addition, granite powder was used for the separation of aggregates during the resin coating process. Thermal resistance and cycling tests were performed to determine coating performance and PCM thermally stability, respectively. The ME-LWAs showed improved thermal conductivity for increased heat exchange and possessed an excellent latent heat capacity. Finally, the ME-LWAs showed excellent durability when exposed to a combined wet and abrasive environment.

5.1 Introduction

In our current time, large proportions of energy are still supplied from the exploitation of fossil fuels which are finite natural resources. Exploitation and usage of fossil fuels bring a negative impact to the environment. In response to this, different techniques have been studied related to space cooling and heating in buildings to improve their energy efficiency using ‘active methods’ (Zhang *et al.*, 2004; Cabeza *et al.*, 2007; Tyagi and Buddhi, 2007). It is also evident that more focus should be placed on the use of renewable energy sources that reduce environmental pollution and, at the same time, improve our

quality of life (Kanagaraj and Mahalingam, 2011). According to the European Commission, buildings account for 40% of EU final energy demand, and the Horizon 2020 EU Framework Programme for Research and Innovation has made it a priority to deliver innovative, affordable and applicable technologies for energy efficiency for building envelopes(Programme and Portal, 2015). The initiative aims to reduce the total primary energy consumption of a building by at least a factor of 2, with great emphasis being placed on the development of prefabricated components with the re-use of recycled and residue materials from the construction and industrial sectors. By the end of 2020, all new buildings should meet the Energy Performance of Buildings Directive obligations and thus reach 'nearly zero-energy' performance levels using innovative, cost-efficient solutions while also integrating renewable energy sources.

One of the most effective 'active methods' to reduce a building's energy consumption is to incorporate a phase change material (PCM) as an additive into the desired building component. The building components used for the incorporation of PCM have ranged from actual cement powder (Memon, Lo, Cui et al. 2013), mortar (Shadnia, Zhang and Li, 2015) concrete (Eddhahak-Ouni *et al.*, 2014), plastering mortar (Kheradmand *et al.*, 2014) and many others (Feldman, Banu and Hawes, 1995) (Dincer and Rosen, 2010). PCM's have high latent heat storage densities and can, therefore, absorb thermal energy when transforming from solid to liquid or release it when turning back to solid (Pomianowski *et al.*, 2014). This property allows the PCM to function as a heating and cooling system for a building since, during the daytime, the PCM in a building component absorbs surplus thermal energy by melting and at cooler temperatures during the night, will solidify and release thermal energy back into the environment. Incorporation of PCM's into building components can be achieved primarily in three different ways: The first method is direct incorporation at the time of mixing. The second method is the immersion of the building component in liquid PCM. The third method is micro/macro encapsulation of the PCM (Khudhair and Farid, 2004). The method of encapsulation is considered to be the most advanced and popular because it allows for better dispersion, reduces the external volume changes and reduces the possibility of PCMs leaching into the surrounding material by eliminating the direct interaction between PCM and host material (Hunger *et al.*, 2009; Cabeza *et al.*, 2011). There is a host of production methods for microencapsulation; physical processes include through spray cooling, spray drying, and fluidised bed processes; chemical processes include in-situ polymerization, complex coacervation, sol-gel method, and solvent extraction/evaporation. Although PCM microcapsules are produced on an industrial scale, the production process is very expensive and is limited to only a few companies worldwide (Kosny, Shukla and Fallahi, 2013). In the case of macro-encapsulation, PCM is forced into the pores of the host material under vacuum, proving to be very efficient with highly porous materials such as expanded clay lightweight aggregates (LWAs) (Kastiukas, Zhou and Castro-Gomes, 2016).

Previous studies have investigated different types of PCM for obtaining the optimum energy performance (Cabeza *et al.*, 2011). Other references have discussed methods of encapsulation to prevent PCM leakage (Jacob and Bruno, 2015; Dong *et al.*, 2016), while others have even investigated the most appropriate sequence of microcapsule addition (Castellón *et al.*, 2010). Macroencapsulation using fine and lightweight aggregates (LWAs) has been studied recently, however very little research focus has been concentrated on ensuring the PCM, once impregnated, does not leak out during its phase change, which may cause contamination of the host material. Researchers who have impregnated lightweight aggregates with PCM have either incorporated the aggregates into

building materials without applying any protective coating (Nepomuceno and Silva, 2014) or have applied a coating without establishing its effectiveness at preserving the PCM (Memon *et al.*, 2015) thoroughly. The coating is an integral part of impregnated LWA's as it is the boundary between the PCM and host building material and must, therefore, be made as leak proof as possible. This study aimed to uncover the effectiveness of different types of coating materials, fine tune their composition and means of application.

Paraffin PCM has an inherently low thermal conductivity so for it to take advantage of its capabilities to absorb and release large amounts of thermal energy, its ability to exchange heat with the surroundings must be enhanced. Carbon based fillers have been used to successfully improve the thermal performance of the PCM itself (Cui *et al.*, 2011) and of resins (Fu *et al.*, 2014). Results show that with the addition of 7% wt. of carbon fibres to PCM, the thermal conductivity can be quadruplicated (Frusteri *et al.*, 2005) while the addition of 71.7% wt. of silicon carbide to epoxy can improve its thermal conductivity by 20 times (Zhou *et al.*, 2013).

In this research, the impregnated aggregates with the best performing coating were incorporated into square panels made from an AAB to establish their thermal performance. An AAB was chosen because the authors felt that using coated lightweight PCM impregnated aggregates as an addition to an AAB is a unique combination and has not yet been explored. Another reason was to promote the use of AABs as an alternative to cement-based binders and initiate innovative uses for it such as the development of sustainable and energy-saving concrete, mortar plaster and facade panels.

5.2 Materials and Methods

5.2.1 Materials and Preparation of Coated PCM-LWA

To produce the coated PCM-LWA, commercially available expanded clay LWAs conforming to EN 13055-1 supplied by Argex S.A were used. Table 5-1 shows physical properties, and chemical composition of the LWA and Fig. 5-1 shows the microscopic images of the LWA. The numerous small and large pores can be clearly seen. The LWA was sieved to reduce it to the maximum dimensions of 8mm. This limit was chosen considering the increase in radius after the coating and ensuring the radius of aggregates would not be above 10mm after coating. They were also blow dried with compressed air to remove surface dust before impregnation. Technical grade paraffin was chosen as the PCM with the following thermo-physical properties according to the producer: phase change temperature in the range of 22-26°C, thermal energy storage capacity of 230 kJ/kg, specific heat capacity of 2 kJ/kg K, density 0.77 kg/L at 40°C, thermal conductivity of 0.2W/m K and a maximum operation temperature of 60°C. Three different materials were investigated for the coating of PCM-LWA: a commercial synthetic rubber emulsion (Sika Latex) provided by Sika S.A., chosen due to it being used in a previous study to coat granular PCM composites (Zhang *et al.*, 2005); a commercial liquid membrane used for waterproofing roofs (Weber Dry-Lastic, Saint Gobain-Weber S.A) also previously used to coat PCM impregnated LWAs (Kheradmand *et al.*, 2015); a polyester resin adhesive (Palatal P 4-01) due to its good surface hardness and stiffness, good compressive, tensile and shear strength, withstanding relatively well high and low temperatures. The mixing ratio was determined after preparing trial mixes. The adhesive:harder:catalyser ratio which provided the most manageable working time, in this case, 15 minutes, was determined to

be 1:0.02:0.03 by mass. Moreover, the milled carbon fibre powder was supplied by SLG Group and has a mean fibre length of 80 microns. Finally, three powders were investigated for the separation of the PCM-LWA after coating with polyester resin: granite, quartz and waste glass powder.

Table 5-1 Physics properties and chemical composition of LWA

Bulk particle density	555 kg/m^3
Bulk particle SSD density	689 kg/m^3
Apparent density	1800 kg/m^3
Bulk (tap) density	327kg/m^3
Porosity (MIP)	61.55%
Water absorbing capacity by immersion (24h)	26.45%
PCM absorbing capacity by immersion (1h)	9.5%
PCM absorption capacity by vacuum impregnation (1h)	100%

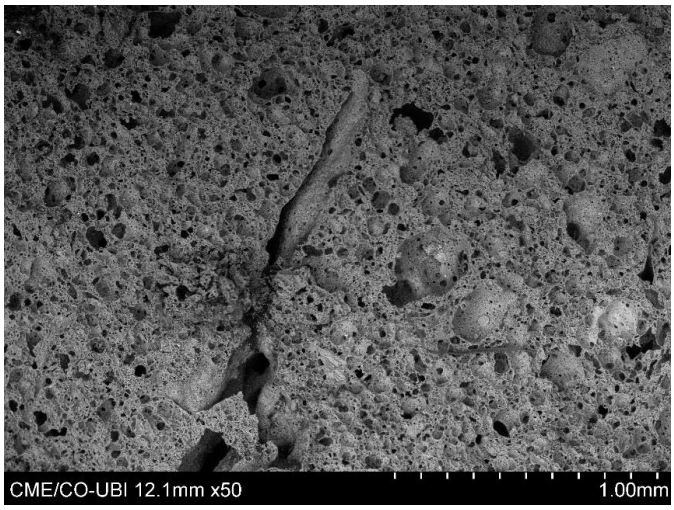

Fig. 5-1 x50 magnification SEM image of the LWA pore structure

PCM was introduced into the pores of the LWA using an in-house vacuum impregnation system (Fig. 5-2). Weighed samples of LWA was placed into vacuum chambers and sealed using vacuum gel. Air entrapped within the pores of the LWA were removed under a vacuum pressure of -860mbar for 30 minutes. Liquid paraffin was then allowed to enter the chambers and completely submerge the LWA. The air was then allowed to enter the chambers to help force the paraffin into the pores. After this, the sample was left to rest for a further 30 minutes. An attempt was made to keep the sample at 50°C during the rest stage to improve the PCM absorption as suggested by other researchers (Zhang *et al.*, 2005). However, an insignificant 1.3% gain in absorption was made, so it was decided not to include this in the final impregnation process. Upon completion of the impregnation process, the PCM-LWAs were surface dried using absorbent towels to remove excess paraffin and immediately placed in an environmental chamber maintained at a temperature below phase change temperature to allow the PCM to solidify. The absorption capacity of the LWA was determined by calculating the mass change of the PCM impregnated LWA and using the PCM density of 0.77 g/mL and an average LWA intrusion volume of 0.82 mL/g. For comparison, normal immersion of the LWA into PCM was also evaluated. The absorption capacity of normally immersed LWAs

was a tenth of that reached using vacuum impregnation (Table 5-1). Table 5-2 shows the measured PCM-LWA physical properties, including the apparent particle volume, which is defined as the total volume of the particle, excluding open pores, but including closed pores.

Fig. 5-2 LWA vacuum impregnation system

Table 5-2 PCM-LWA physical properties

Apparent density	1328 kg/m^3
Bulk SSD density	1326 kg/m^3
Bulk density	1318 kg/m^3
Bulk (tap) density	838kg/m^3
Water absorbing capacity (24h)	0.055%

The PCM-LWA were either immersed for 5 minutes or sprayed with the Sikalatex and Weber Dry-Lastic coating materials and then subjected to curing regimes of drying in a revolving mechanical drum, laid flat on a metal net in ambient air or in the environmental chamber. In the case of the polyester resin coating, it was poured over the PCM-LWA and mixed with a plastic spatula for 3 minutes. All the combinations of coating and drying regimes investigated in this research can be seen in Table 5-3.

To improve the heat exchange of the encapsulated PCM-LWA with the surrounding AAB, the polyester resin-granite powder coating was further modified with carbon-based nanomaterials. One type of modification was by incorporation of milled carbon fibres (CF) into the coating during the mixing of resin. The CF was incorporated at 10% wt. of resin. Before the filler material could be effectively used, its surface had to be treated with silane to improve the dispersion and bonding to the resin. 3 wt.% of CF of hexamethyldisilazane silane (Sigma-Aldrich) was used due to its advantage of improving solubility and enhanced product stability. The second type of modification was done by spraying the resin coatings with a conductive pure and fine graphite powder (GS) (Kontakt-Chemie), which was chosen for its good adhesion on plastics.

Table 5-3 Coating combinations and drying regimes

	Coating material	LWA coating method	Number of coatings	Drying regime
1	Sikalatex	Immersion	1	Net
2	Sikalatex	Immersion	1	Drum
3	Sikalatex	Spray	1	Net
4	Sikalatex	immersion	2	1st coating - net 2nd coating - drum
5	Sikalatex	immersion	1	Fridge
6	Weber Dry-Lastic	Immersion	1	Net
7	Weber Dry-Lastic	Immersion	1	Drum
8	Weber Dry-Lastic	Immersion	2	Net
9	Weber Dry-Lastic	Spray	1	Net
10	Weber Dry-Lastic	Immersion	1	Fridge
11	polyester resin	Immersion	1	Net
12	polyester resin	Immersion	1	Drum
13	polyester resin-powder	immersion	1	Drum
14	polyester resin-powder	Immersion	2	Drum

5.2.2 Materials and Preparation of Panels

For the synthesis of the AAB, the principal solid reactant used to produce the TMW-WG panel i.e. sodium hydroxide and sodium silicate alkali solutions, TMW and WG precursors were the same quality and composition as described in Chapter 2.2.1 *Materials*. 20% wt. of the TMW was replaced with WG to increase the overall SiO_2 content. The SEM images of the TMW and WG and chemical composition are given in Fig. 3-1 and Table 3-1, respectively. The size distribution of waste mud is provided in Fig. 3-5. The TMW and WG were used in the dry and sieved state dried. A combination of sodium hydroxide solution and sodium silicate solution was used to produce the chemical activator. A total of 5 mixes were designed for this study (see Table 5-4). Sample AAB is a TMW-WG AAB without any ME-LWA, and all the remaining samples are TMW/WG AABs containing 20% wt. resin-granite powder coated PCM-LWA (ME-LWA), coated using method 14 from Table 5-3. Sample AAB ME-LWA contains ME-LWA without any modification; sample AAB ME-LWA-CF contains carbon fibre nanofiller and sample AAB ME-LWA-GS contains ME-LWA coated by a graphite spray. All samples were made with a constant by mass SS/SH and precursor/activator ratio of 4 and 3 respectively.

Table 5-4 Mix design formulation for cement mortar and TMW-WG AAB

	PC	AAB	AAB-ME-LWA	AAB-ME-LWA-CF	AAB-ME-LWA-GS
Cement (kg/m^3)	364.3	0	0	0	0
Sand (kg/m^3)	979	0	0	0	0
Water (kg/m^3)	165.3	0	0	0	0
TMW (kg/m^3)	0	1583	1266	1266	1266
WG (kg/m^3)	0	395	316	316	316
SS (kg/m^3)	0	527	422	422	422
SH (kg/m^3)	0	131	105	105	105
ME-LWA (kg/m^3)	0	0	201	211	203
Water/cement	0.45	0	0	0	
SS/SH mass ratio	0	4.0	4.0	4.0	4.0
Precursor/activator mass ratio	0	3.0	3.0	3.0	3.0

The TMW and WG were firstly mixed in a dry state for 1 min. The alkali activator was made by combining the sodium silicate and sodium hydroxide and mixed for 5 minutes at 700RPM. The precursor blend (i.e. TMW and WG) and activator solution were then combined and mixed using a bench at 200 rpm for 2.5 minutes and for another 2.5 minutes at 400 rpm. Finally, the ME-LWAs were added as the last component and mixed by hand to avoid damaging them during the mixing process. The binder was poured into 150x150x30mm panel molds and vibrated for 30 seconds. The samples were sealed to prevent moisture loss and placed in the oven at 80°C for 24h for curing. After curing in the oven, the samples were demolded and left to cure in laboratory conditions at 20°C until testing of the thermal conductivity at 7 days. For the synthesis of the sample PC, cement (CEM I), natural river sand and water were combined and mixed for 5 minutes in benchtop mixer. The mortar was molded into 150x150x30mm panels and left to cure in RH> 90% for 7 days to produce a mortar as a reference binder for comparing the thermal conductivity with the AAB binder with macro-encapsulated lightweight aggregates (ME-LWAs).

5.3 Characterisation Techniques

5.3.1 Pore Structure

Mercury Intrusion Porosimetry (MIP) technique was used to determine the pore structure and porosity of the raw materials and LWA with an AutoPore IV 9500 (Micrometrics Instrument Corporation). The intrusion accuracy of the AutoPore IV 9500 was ±1% of full-scale intrusion volume.

5.3.2 Phase Change behaviour

Differential scanning calorimetry (DSC) analysis was used to evaluate phase changing behaviour i.e. phase change temperature and thermal energy storage. The ME-LWA was crushed to a coarse powder, which was used to conduct the DSC test on a Q2000 (TA Instruments). The DSC samples weight was approximately 10mg.

5.3.3 Thermal Conductivity

The thermal conductivity of cement mortar and alkali-activated paste with and without ME-LWA was measured on 150x150x30mm samples at 7days. The apparatus used was a Netzsch HFM 436 Lambda (Netzsch Gerätebau GmbH, Germany) heat flow meter with a hot plate and cold plate set at 35 and 15°C respectively. The mean temperature of the sample was 25°C so measurement could be made at the PCMs phase change temperature. The surface of the samples was not completely plane therefore thin felt strips were placed around the border of the samples to create a better seal between the testing plates.

5.3.4 Microstructure Analysis

For the characterization and analysis of the surface morphology and microstructure of ME-LWA and TMW-WG AAB, a scanning electron microscope (Zeiss Supra 35VP) was used. Specimens were pre-coated with a 12nm layer of gold and then analysed by SEM.

5.3.5 Strength Testing

The prisms were demolded after 1 day and cured subsequently at 20°C and a relative humidity of 75 % until the specific age of testing. The compressive strength of the prismatic sample fractured counterparts for TMW-WG AAB with and without ME-LWA was tested after 1, 3, 7, 28 days in accordance with EN 196-1 using a 300kN universal testing machine (Instron 5960) at a constant loading rate of 144 kN/min. The compressive strength value was the average of values obtained from three specimens.

5.4 Results and Discussion

5.4.1 Coating Material and Methods

5.4.1.1 Sikalatex Coating

In its natural state, the Sikaltex coating was very liquid hence all its layers were very thin (Fig. 5-3 a-c). Even with the application of two layers, the coating could still be easily removed under small pressure. In previous research conducted by Zhang et al. (2005), the Sikalatex coating material was used in a thickened form to coat LWA. However, in this study, thickening could not be replicated since the details of how it was accomplished were not stated in the study. All efforts were made to separate the coated PCM-LWA while drying on the net. However, a large proportion would remain stuck together. After the coating had dried, particles which were stuck together had to be pulled apart causing a portion of the coating to be removed, allowing the PCM-LWA to leak (Fig. 5-3 c). When placed dry in the drum, the problem of the particles sticking together during drying was eliminated, however, led to the particles reducing in size. The size reduction was due to the

constant particle collisions which slowly chipped away pieces of the LWA which mixed with the leaked PCM to form the dark coating around the LWA, as shown in Fig. 5-3 d.

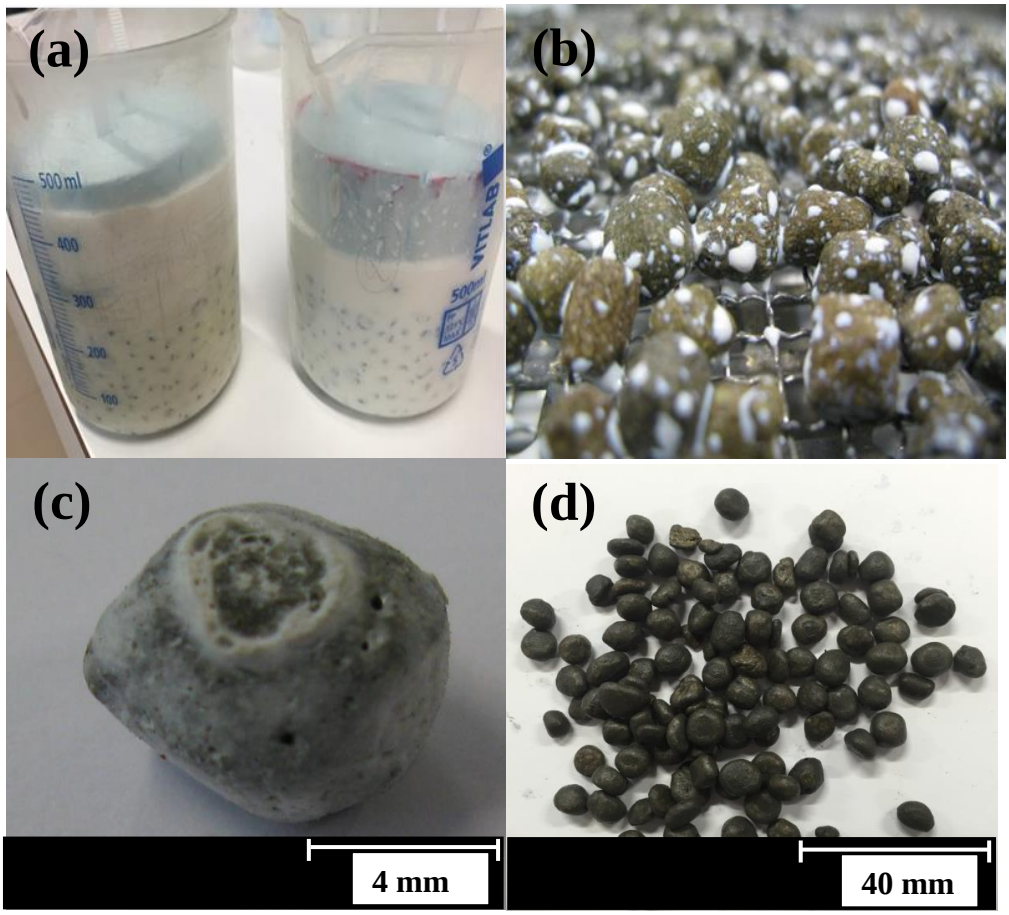

Fig. 5-3 PCM-LWA (a) Sikalatex immersion process (b) Coated using Sikalatex drying on net (c) Separated after coating using Sikalatex (d) Coated using Sikaltex after drying in the drum

5.4.1.2 Weber Dry-Lastic Coating

The application of this coating material enabled a thicker layer of coating to be applied however the problem of particles sticking together while drying on a net could not be eliminated (see Fig. 5-4a). The drying of this material in the drum resulted in the aggregates not only sticking to each other but also to the wall of the drum (see Fig. 5-4b). Finally, this coating material could not be applied as a spray since it was of a very thick consistency and diluting it was not an option due to its incompatibility with water.

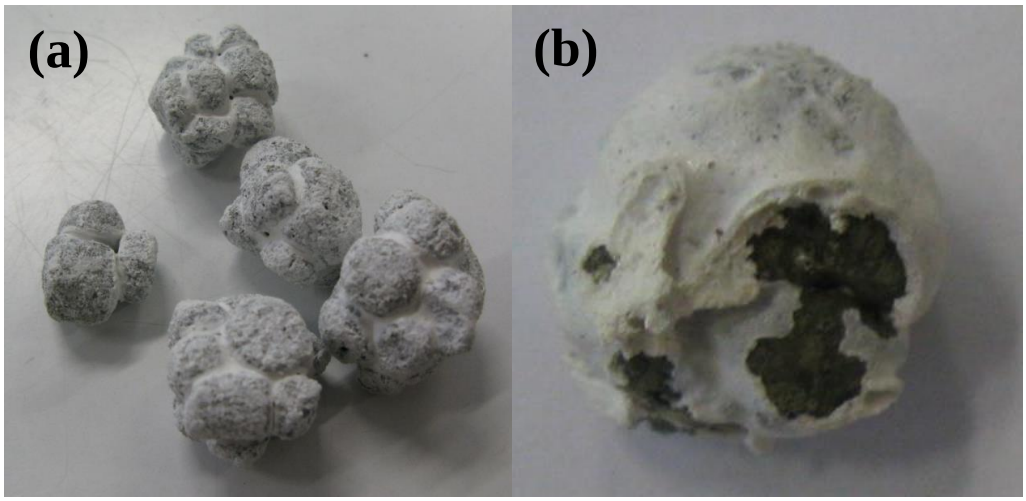

Fig. 5-4 PCM-LWA (a) agglomeration after coating using Weber Dry-Lastic (b) separated after coating using Weber Dry-Lastic

5.4.1.3 Polyester Resin Coating

This polyester resin coating produced a smooth and hard layer around the PCM-LWA. The curing speed was only 15 minutes making it the quickest out of the three coating materials tested. When drying on the net, particles tended to stick together and separating them after curing caused a brittle fracture of the aggregates (See Fig. 5-5).

Fig. 5-5 PCM-LWA coated with resin

5.4.1.4 Polyester Resin-Powder Coating

In order to separate the particles during curing, the granite, quartz and glass powders were chosen to be sprinkled over the PCM-LWA immediately after coating with resin and shaken manually in a drum. The powder that provided the best separation and most uniform coating were the granite powder. Quartz powder tended to clump together and was easy to dislodge (see Fig.5-6a) while the glass powder a rough textured surface (see Fig.5-6b). Using granite powder under 500 microns for the first layer and granite powder under 250 microns only for the second layer produced a coating with the best appearance, shown in Fig. 5-6c, and PCM retention capacity explained in *Chapter 5.4.2 Impregnation and PCM Retention*.

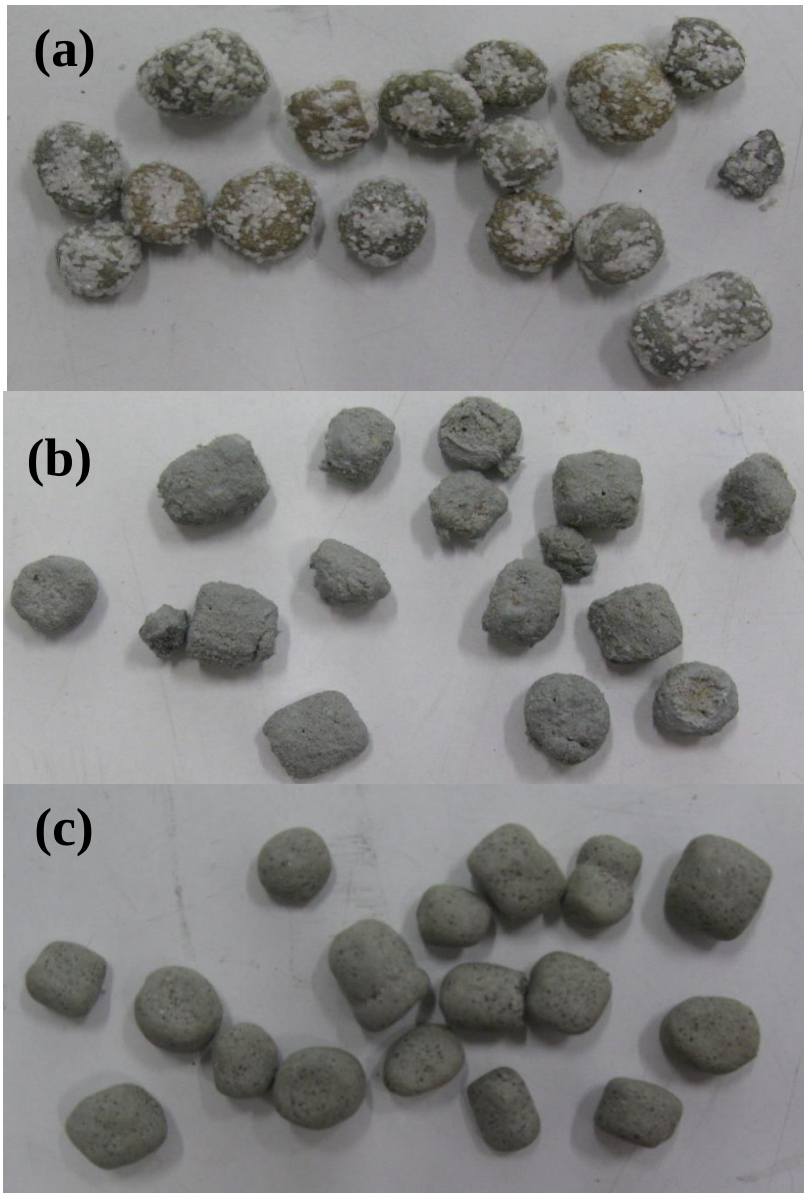

Fig. 5-6 Powders used to separate the ME-LWA (a) quartz powder (b) glass powder (c) granite powder

The polyester resin-powder coating process provided the most satisfactory results with respect to ease of coating and speed of curing therefore only this coating was investigated further for its PCM retention capacity, chemical stability, thermal conductivity and compatibility in an AAB, all of which are described in the following sections. The impregnation and coating process can be seen in Fig. 5-7. Fig. 5-7a shows the LWA being sieved and Fig. 5-7b shows the sieved LWA being loaded into the vacuum chambers. Fig. 5-7c and Fig. 5-7d show the LWA submerged in the PCM after impregnation and subsequent drying of the surface, respectively. Fig. 5-7e and Fig. 5-7f show the coating of the LWA and finally Fig. 5-7g and Fig. 5-7h show the drum used for agitating and separating the aggregates in granite powder and the final ME-LWAs, respectfully.

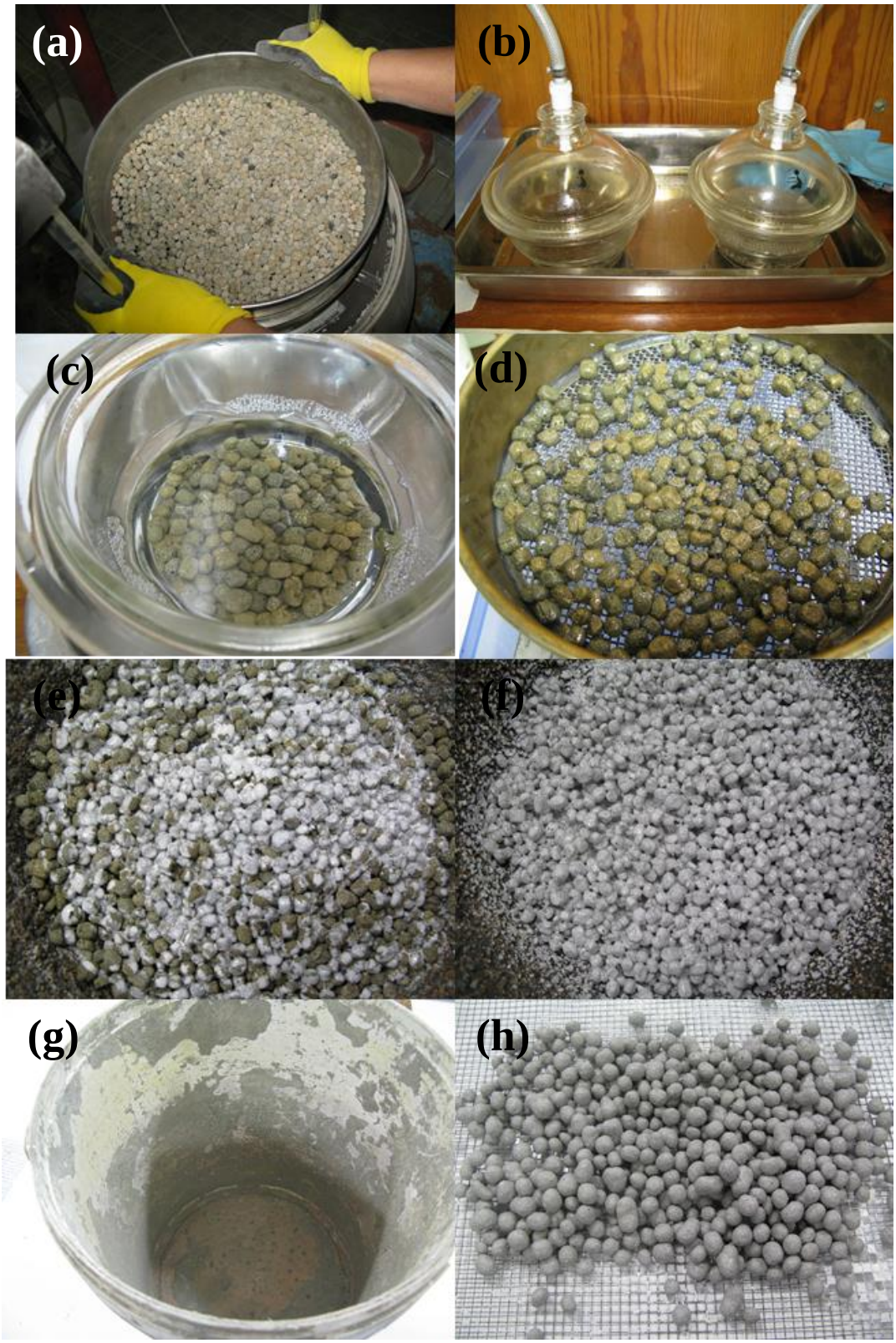

Fig. 5-7 Impregnation and coating process of ME-LWA showing (a) LWA sieving (b) vacuum chambers (c) LWAs soaking in PCM after impregnation (d) drying of PCM-LWAs (e) coating the PCM-LWAs with resin (f) resin coated PCM-LWAs (g) drum used for separation of the resin coated PCM-LWAs (h) final product of ME-LWA

5.4.2 Impregnation and PCM Retention

To determine the encapsulation efficiency, which is a measure of how well the ME-LWA prevent the loss of PCM, the ME-LWA were heated at 50°C for 500 hours. The recorded mass loss after heating was only 2.99% by weight of sample shown in Fig. 5-8. However, it is not expected that the ME-LWA would be exposed to such elevated temperatures since the phase change temperature and the maximum operating temperature of this PCM is 25°C and 65°C, respectively. Therefore, when left in more realistic ambient laboratory conditions (approx. 21°C) the mass loss of the ME-LWA was only 1.11% as shown in Fig. 5-9. The principal reason for the loss in mass can be due to small connected pores which formed during the coating process. It can be seen in the electron mapping image of the polyester resin and granite powder coating in Fig. 5-10 the resin which is represented in red does not form a continuous seal around the aggregate and small interconnected channels exist, allowing for a small percentage (<3%) of the PCM to leak out. A part of this mass loss can also be attributed to the loss of the powder coating during the transfer between containers during mass measurement which was observed visually.

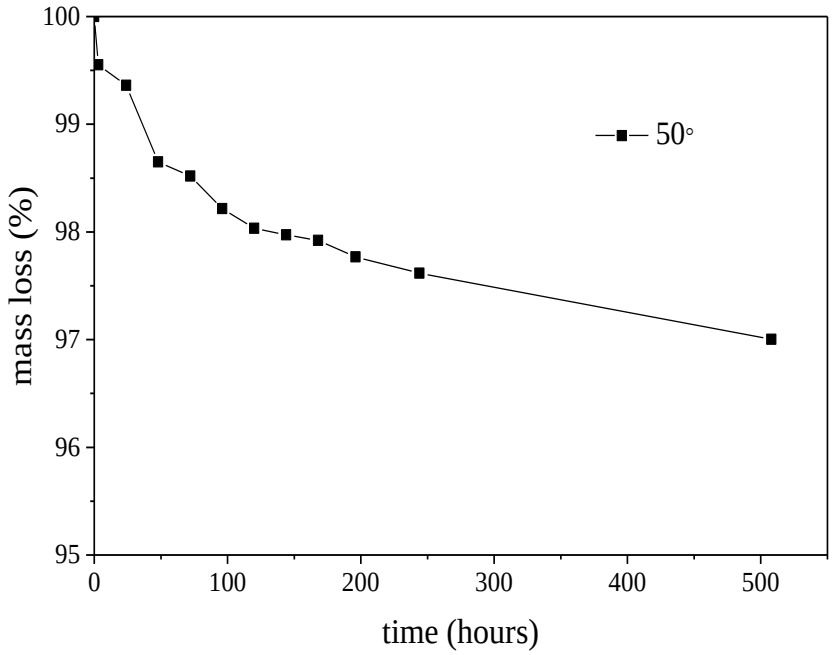

Fig. 5-8 PCM mass loss curve at 50°C

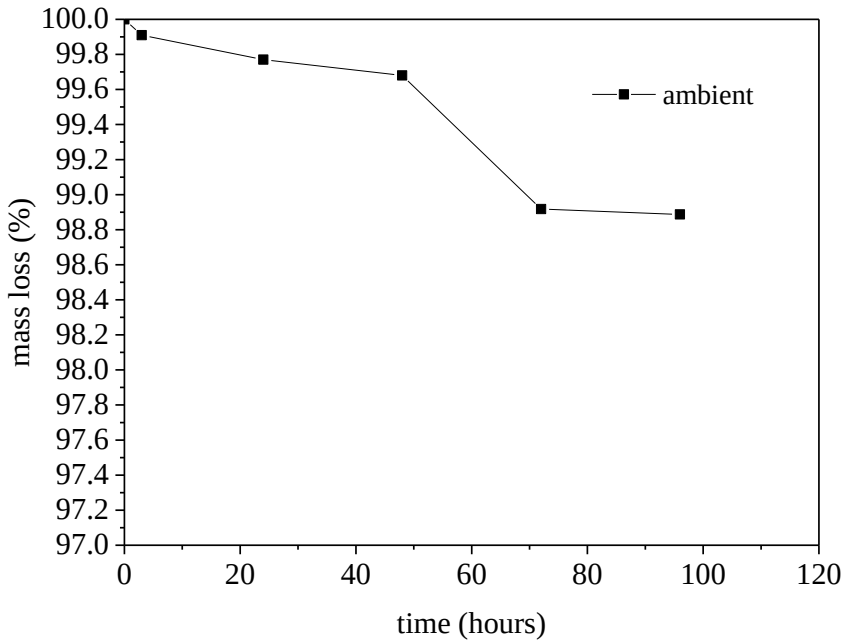

Fig. 5-9 PCM mass loss curve at ambient temperature (~21°C)

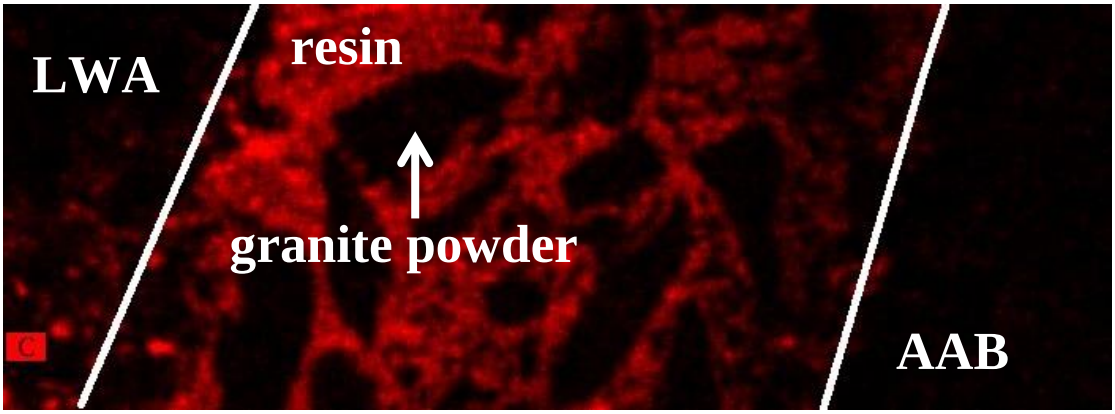

Fig. 5-10 SEM image of the ME-LWA coating using electron mapping

5.4.3 SEM Analysis

Fig. 5-10 shows more clearly the resin and granite powder distribution through the electron mapping function in EDX. From Figs. 4-11 and 4-12 it can also be seen that the distribution of granite grains in the resin coating are in two layers. The combined large and small granite crystals which were used during the first coating process can be observed closer to the inner circumference of the coating, and smaller crystals used only during the second coating process appear at the outer circumference. The intention was to fill the interstitial space between the larger crystals with smaller crystals to create a more effective barrier against PCM leakage, which according to the mass loss curves, has been achieved

The SEM micrograph of the ME-LWA is shown in Fig. 5-11. The contact or bond between the impregnated LWA and layer of coating is well-developed in the composite mortar. The granite powder used to separate the aggregates during coating was also intended to increase the roughness of the surface, helping the ME-LWA interlock with the alkali-activated matrix during hardening and provides better aggregate-paste bond strength. However, it can be seen from Fig. 5-12 that some voids exist between the ME-LWA and

AAB matrix. The average thickness of the coating was determined by taking measurements during the SEM analysis (Fig. 5-12). The average coating thickness achieved using the procedure described in Chapter *5.4.1.4 Polyester Resin-Powder Coating* was 0.8 mm.

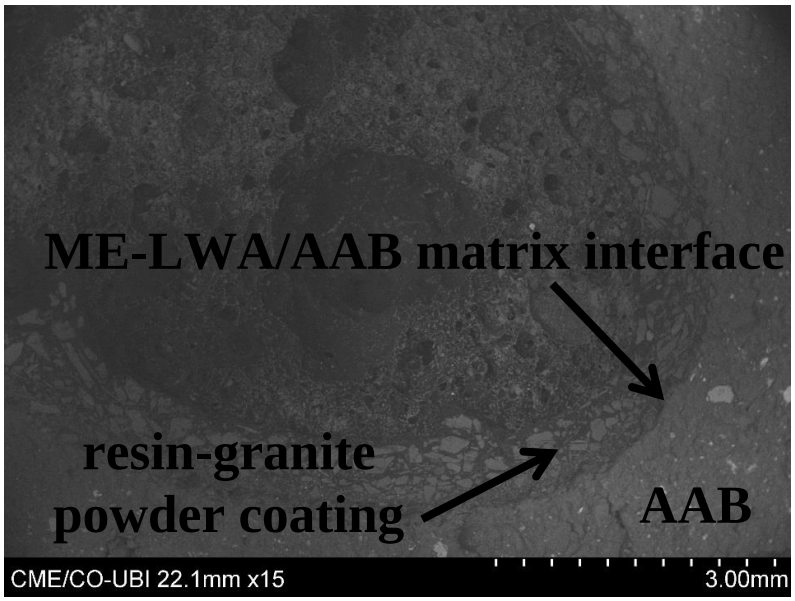

Fig. 5-11 SEM image of ME-LWA embedded in TMW-WG AAB

Fig. 5-12 SEM image of the ME-LWA resin-granite powder coating

Fig. 5-13 reveals some flaws at the PCM-LWA and resin-granite powder coating interface. Fig. 5-13a shows a pore within the resin and Fig. 5-13b shows a fissure leading from PCM-LWA across the resin coating. These flaws may be responsible for the small loss of PCM from the ME-LWA discussed in *5.4.2 Impregnation and PCM Retention*.

.

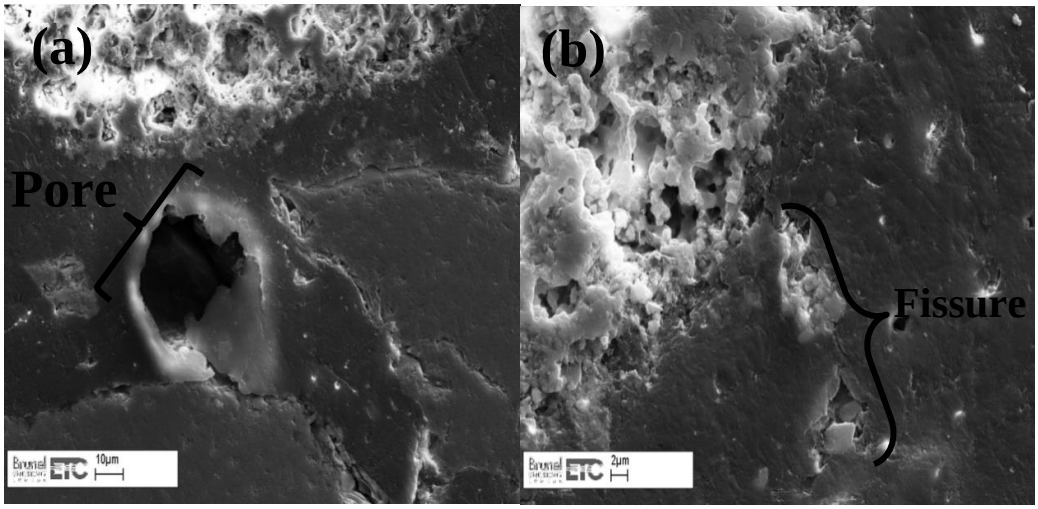

Fig. 5-13 SEM images showing (a) pores (b) fissures in the PCM-LWA and resin-granite powder coating interface

5.4.4 DSC of ME-LWA

The phase change temperature can be viewed as having three main stages i.e. onset, offset and peak temperature. The starting and ending temperatures are found by intersecting the baseline and taking the tangent to the left and right respectively of the DSC curve, while the peak temperature represents the peak point of the DSC curve. From Fig. 5-14, the starting, ending and peak temperatures were found to be 24.49°C, 21.16°C and 25.41°C for RT25, which is the same value given in the manufacturer's data sheet. For ME-LWA the values were 24.76°C, 23.80°C and 25.76°C respectively. In a previous study by Zhang et al. (2005) a significant increase in the phase change ending temperature was found between the pure PCM and an expanded clay lightweight aggregate impregnated with the PCM, however in this study, such a relationship was not identified – the phase change melting temperature for the ME-LWA was only 0.65°C lower than that of pure RT25 PCM while the crystallisation temperatures of both are almost the same.

The latent heat of melting (H_m) is calculated automatically by the DSC software by integrating the area between the baseline and the DSC curve. The H_m for the RT25 PCM in its pure state is 130.5 J/g while for this PCM impregnated in the ME-LWA, it is 57.93 J/g. The lower thermal conductivity and intricate pore structure of the ME-LWA affect the heat transfer efficiency to the PCM inside the pore space during melting, decreasing the energy storage density of the system to pure PCM. Nonetheless, the performance of this ME-LWA stands out when compared to other PCM composite materials developed by other researchers. For example, a form-stable PCM composite material made by incorporating dodecyl alcohol into ground granulated blast furnace slag also through vacuum impregnation only achieved 22.51 J/g (Memon, Lo, Barbhuiya, *et al.*, 2013), while the specific latent heat of melting achieved for a Paraffin-Kaolin composite was only 27.88 J/g (Memon *et al.*, 2015). Finally, the overall heat storage capacity achieved by commercial microencapsulated PCM is approximately 51 J/g when used in surface cooling systems and 55 J/g for the stabilisation of indoor temperature in the comfort zone (BASF, 2009). These values are very close to the PCM-LWA composite developed in this research, further supporting its potential to be used in heat storage applications.

The heat flow curve for the ME-LWA randomly extracted from a tested AAB panel sample very closely matches that of an unused ME-LWA indicating that the thermal properties of the ME-LWA are not chemically altered when added to the AAB matrix. This can also allow us to assume qualitatively the ME-LWA remain damage free and the resin-granite powder coating has an adequate impact resistance to stop the PCM from leaking out.

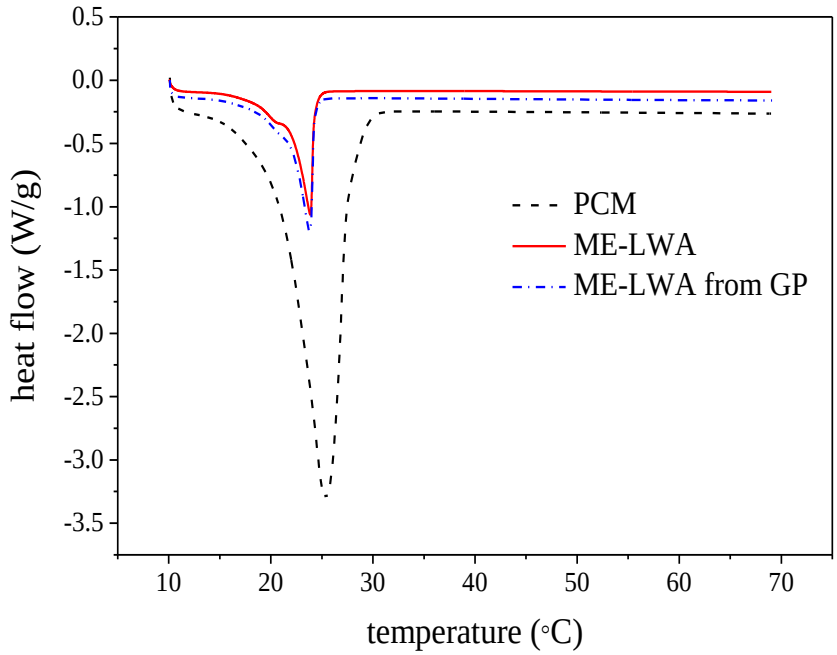

Fig. 5-14 DSC curves of PCM, ME-LWA and ME-LWA extracted from TMW-WG AAB

5.4.5 ME-LWA Thermal Stability

To ensure a reliable and consistent performance by the ME-PCM, the PCM encapsulated within the pores of the host material, in this case, lightweight aggregate (LWA) should be thermally reliable over many melting and freezing cycles. According to S. Memon et al. (2013), the encapsulated PCM should show little or no change in thermal properties after a long period of service. Therefore, the PCM ME-LWA aggregates were subjected to 70 melting/solidifying cycles in a temperature and humidity controlled environmental chamber to detect if there is any change in the phase change behaviour of the PCM and further verify the encapsulation efficiency. Fig. 5-15 shows the typical two-day, time vs. temperature cycle environment for 5 weeks. The thermal properties i.e. phase change temperature and latent heat of the PCM after repeated thermal cycling were investigated by DSC. The DSC curve of the PCM before and after thermal cycling is shown in Fig. 5-16. When comparing the melting temperature of the PCM in the LWA-PCM before and after thermal cycling, the melting temperature changes only by 0.56 °C while the latent heat storage capacity at melting changes by 12.56 kJ/kg. The change in mass of the 200g sample of ME-LWA was only 0.9g. The changes observed in the thermal characteristics of the PCM contained in the LWA are very small, and it can, therefore, be concluded that the prepared LWA-PCM is thermally reliable.

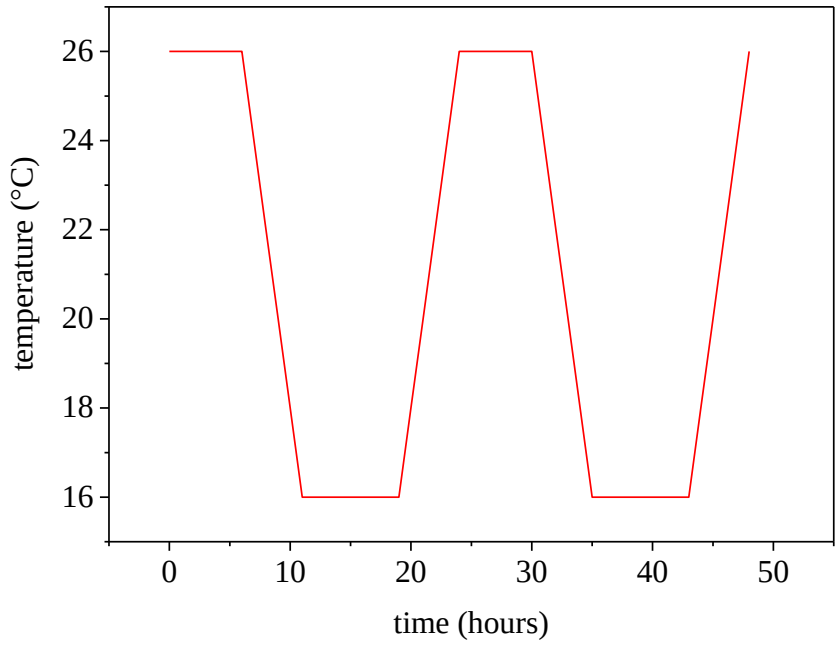

Fig. 5-15 typical 48-hour heating and cooling cycle

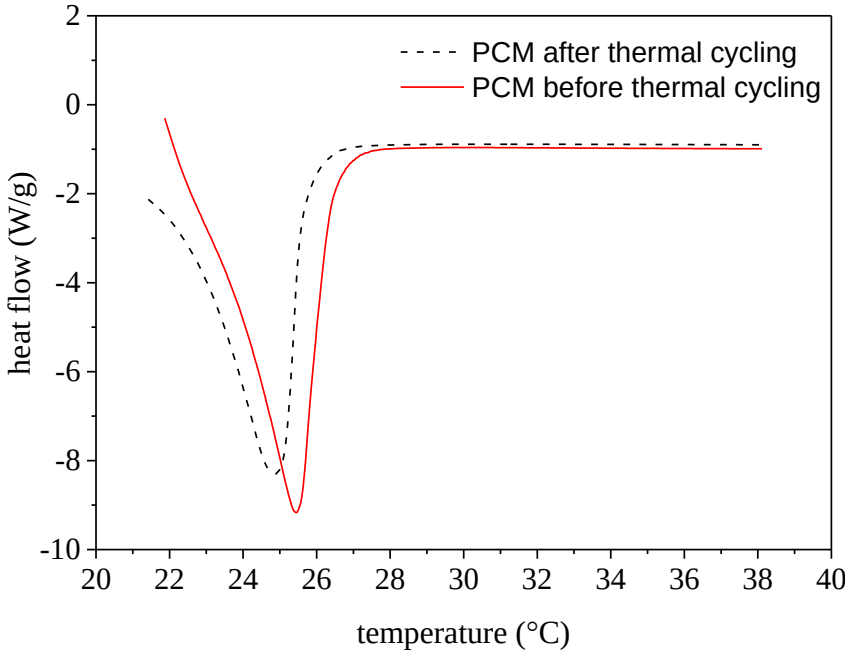

Fig. 5-16 DSC curves of ME-LWA before and after thermal cycling

5.4.6 ME-LWA Thermal Conductivity

The thermal conductivity of modified and non-modified ME-LWA is shown in Table 5-5. The effect of the different ME-LWA on thermal conductivity of TMW-WG is shown in Table 5-6. Compared to the LWA, the thermal conductivity of ME-LWA shows an improved of almost 42%. The modification of the coating layer with CF did not show any improvement in thermal conductivity as using 10% by weight of the resin was not enough to create a conductive link with the PCM. Fig. 5-17 shows a few of the CF's embedded in the coating. However, the number of CF's viewed using the SEM was low. CF's effectiveness in improving the thermal conductivity of resin has been proved in loadings of

40% and above (Heiser and King, 2004). Using a quantity larger than 10% could not be achieved due to the increased CF filler aggregation as well as dramatically increased viscosity, making the resin unworkable for its application to the LWA. In the case of GS, a small reduction in thermal conductivity was measured. Its ineffectiveness in creating heat conductive chains could be due to the spray nature of its application and graphene particles rubbing off during the AAB-ME-LWA mixing process.

The other important observation is the reduction in thermal conductivity of TMW-WG AAB when ME-LWAs are included. Compared to the reference PC binder, the TMW-WG AAB displays a 25% reduction in thermal conductivity and with the inclusion of ME-LWAs, a 45% reduction. The latter reduction could be due to the diverse composition of the ME-LWAs. Although the granite powder used in the coating of LWA has a high thermal conductivity of 3.1 W/m K, it is balanced by the low thermal conductivity of the LWA and PCM, 0.0974 and 0.2 W/m K respectively. The size of the ME-LWA used in the TMW-WG AAB panel preparation is in the 2-10mm range while sand used in the PC panel is 0-2mm which is also a contributing factor in the reduction of the thermal conductivity of AAB. The increased thermal conductivity of the ME-LWAs combined with the reduced thermal conductivity of the TMW-WG AAB accumulates an improved heat transfer capacity and beneficial effect on improving the thermal isolation performance of buildings, respectively.

Table 5-5 values of thermal conductivity of coated aggregates with and without modification

Sample	Thermal conductivity (W/m K)
LWA	0.0974
ME-LWA	0.1382
ME-LWA-CF	0.1382
ME-LWA-GS	0.1337

Table 5-6 values of thermal conductivity at 7 days of mixes from Table 5-4

Sample	Thermal conductivity (W/m K)
PC	0.388
AAB	0.288
AAB-ME-LWA	0.211
AAB-ME-LWA-CF	0.225
AAB-ME-LWA-GS	0.203

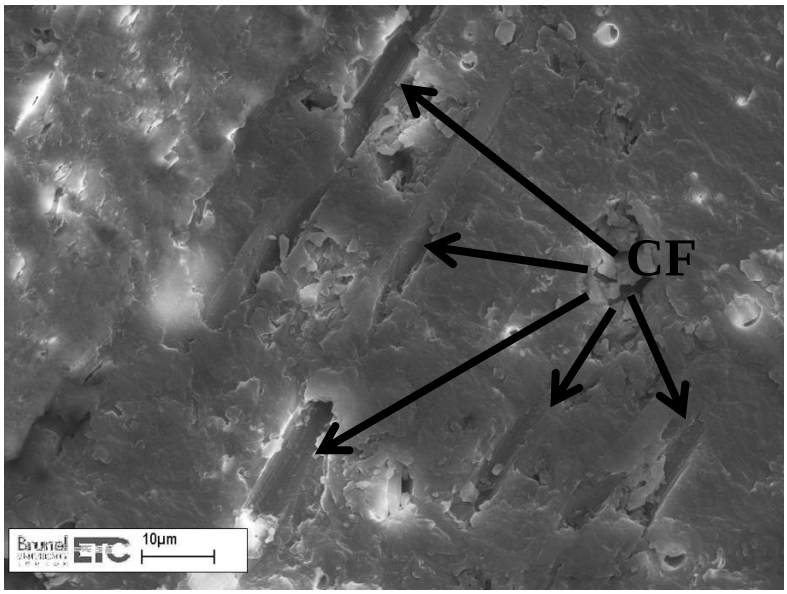

Fig. 5-17 CF embedded in the resin-granite powder coating

5.4.7 ME-LWA Durability

The Micro-Deval abrasion test is a test of aggregate to determine the resistance to fragmentation in the presence of water and an abrasive charge. Many aggregates are more susceptible to abrasion when wet than dry (Richard and Scarlett, 1997). The Micro-Deval test incorporates the use of water in contrast to some other tests, which are conducted on dry aggregate and is the reason why this type of test was chosen. The test results are helpful in evaluating the toughness/abrasion resistance of coarse aggregate subject to abrasion. This test is usually used for detecting changes in properties of aggregate produced from an aggregate source as part of a quality control or quality assurance process. In the EN 1097-2 standard of the Micro-Deval test, a micro-Deval coefficient which is the percentage of the original sample reduced to a size smaller than 1,6 mm during abrasion is determined (CEN (European Commitee for Standardization), 2011). However, in this study, the factor to be determined was the percentage of original sample which did not incur any damage during the test. Hence the procedure adopted in this study can be considered a variation of the EN 1097-1 standard. In terms of sample preparation, a sample of ME-LWA was weight to the nearest gram and recorded as *A*. Fig. 5-18 shows visually the steps involved in this abrasion resistance test. The sample was first soaked in 2-L of pure water for 1 hour (Fig. 5-8a), after which the sample was transferred to the Micro-Deval container (Fig. 5-8b) with the steel charges which themselves had a total mass of 953±5g (Fig. 5-8c and Fig.5-8d). The machine was run for 120 minutes at 80 RPM, resulting in a total of 9,600 revolutions. After the test was complete, the sample and the steel balls were carefully poured over a 125-micron sieve (Fig. 5-8e and Fig.5-8f). The sample was washed with water until the washings were clear and all material smaller than the 125-micron sieve has passed. The steel charge was removed manually, and the ME-LWA was then air dried. Damaged ME-LWAs were determined visually and subsequently removed, and the mass of the undamaged ME-LWAs was recorded as *B*. Some typical types of damage can be seen in Fig. 5-19. The ME-LWAs suffered a varying degree of damage, ranging from small to large pits in the coating (Fig. 5-19a and Fig. 5-19b respectively) and then to complete fracture with significant loss of coating (Fig. 5-19c and Fig. 5-19d). The percentage mass of ME-LWA which was left undamaged from the Micro-Deval abrasion test was calculated to the nearest 0.1% using the following equation:

$$\%\mathbf{ME-LWA\ damaged} = \frac{\mathbf{A-B}}{\mathbf{A}} \times \mathbf{100} \qquad \textbf{(Eq. 8)}$$

The mass of sample which did not incur any damage was determined as 600g hence if *A*=1000g and *B*=600g then *% ME-LWA damaged* = 40%. The interpretation of this result is straightforward and indicates that under the most severe conditions of wet abrasion; only 40% of the ME-LWAs suffered some form of damage which could lead to the leaking of PCM. Under more realistic conditions e.g. during mixing of a cementitious binder, the ME-LWAs would not undergo such severe conditions.

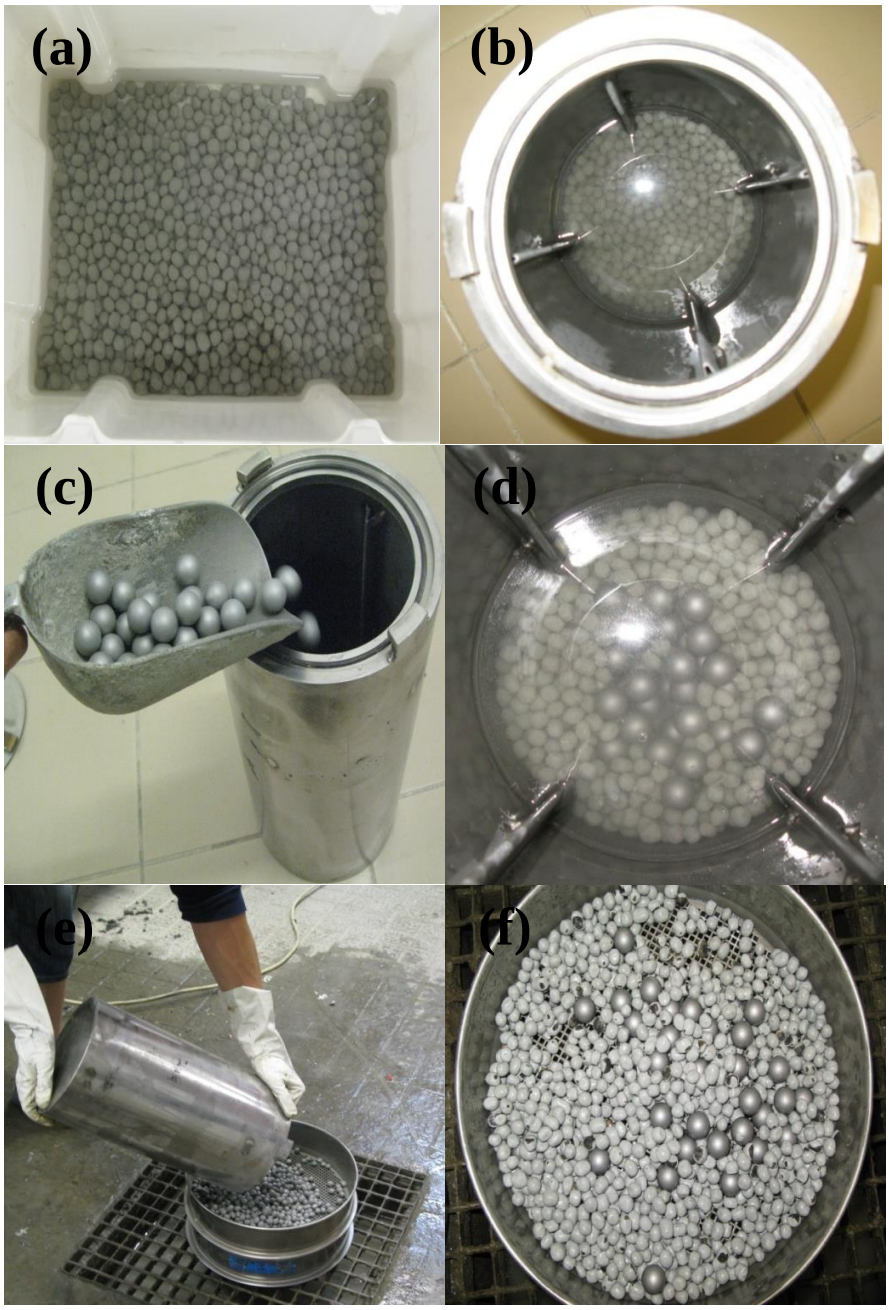

Fig. 5-18 test procedure to determine the ME-LWA durability showing (a) soaking the ME-LWAs (b) ME-LWAs in the drum (c) addition of the steel charge (d) ME-LWAs with steel charge in the drum submerged in water (e) removal of ME-LWAs after the test (f) separation of the ME-LWA from the steel charge

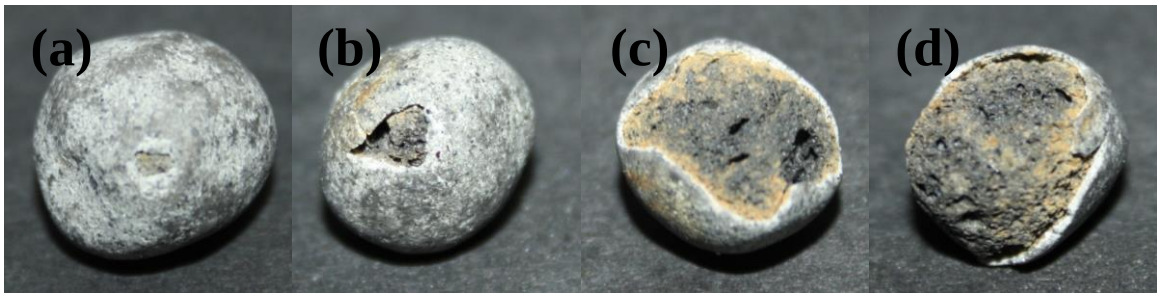

Fig. 5-19 ME-LWA after the abrasion resistance test showing (a) small pit (b) large pit (c) small fracture (d) large fracture

5.4.8 AAB Compressive Strength with ME-LWA

The compressive strength of TMW-WG AAB with and without ME-LWA was obtained through the cube crushing test performed in accordance with BS EN 197. Three 40x40x40 mm cubes were tested for both mixes at four different curing ages (i.e. 3-day, 7-day, 14-day and 28-day). It is evident from the results summarised in Fig. 5-20 that, at a given age, compressive strengths of TMW-WG AAB reduced with the inclusion of ME-LWA. Only at 3-day strength did the AAB ME-LWA mix exceed TMW-WG AAB in compressive strength. Visual observations of the fractured samples showed that the fracture occurred through the TMW-WG AAB and not through the ME-LWA indicating that the TMW-WG AAB is the weaker constituent of the ME-LWA and TMW-WG AAB composite.

The decrease in compressive strengths observed for TMW-WG AAB with ME-LWA can be attributed firstly to the porous nature of the LWA, making them inherently weaker in compression than the normal weight coarse aggregate. Secondly, the AAB ME-LWA mix contained ME-LWA in the 2-10mm particle size range without any fines to improve the packing efficiency of the aggregates also possibly contributing to the reduced strength. Thirdly, some voids appear at the interface between the AAB matrix and ME-LWA as seen in Fig. 5-13, indicating a potential zone of weakness. A reduction in compressive strength has also been reported in Portland cement mortars containing PCM impregnated expanded clay aggregates (Sakulich and Bentz, 2012). This research also indicated that the compressive strength depends not only on the type of LWA that is used but also on the type of PCM.

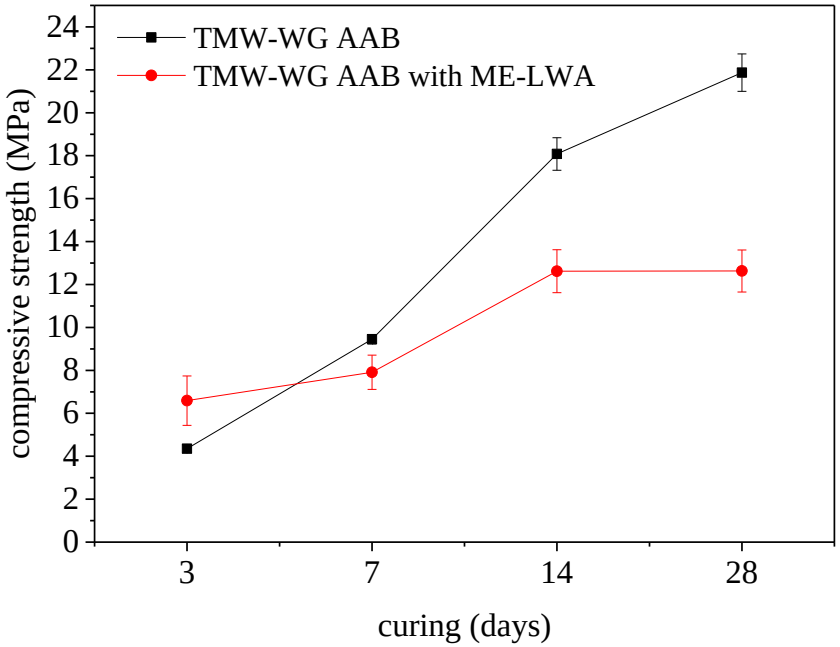

Fig. 5-20 Compressive Strength of TMW-WG AAB with and without ME-LWA

5.5 Summary

Fabrication method and performance of macro encapsulated PCM made from organic paraffin and expanded lightweight clay aggregates, along with their compatibility in an AAB are presented in this research, from which the following conclusions can be made:

- Paraffin, an organic PCM with an approximate melting temperature of 25°C has been evaluated to be compatible for the use in impregnation of expanded clay lightweight aggregate in the 2-8mm size range. The low cost, abundance and wide availability of technical grade paraffin are also very beneficial.
- Vacuum impregnation and coating procedures benefit from easy preparation and can be performed for desirable aggregate dimensions.
- Polyester resin was determined to be the most suitable choice of coating material for the PCM impregnated lightweight aggregates. In addition, granite powder under 500 microns was determined to be the most suitable powder for the separation of aggregates during the resin coating process. The macroencapsulated lightweight aggregate sealing performance was evaluated at elevated temperatures for over 500 hours with the minor mass loss, rendering it practically leak proof.
- The phase change melting and solidification temperatures of PCM are not affected due to impregnation. The final macro encapsulated phase changing composite has shown to have a heat storage capacity like that of commercialised PCM impregnated products.
- The resin and granite powder-coated aggregates showed a 42% higher thermal conductivity than that of the aggregates in their raw state. Modification of the resin coating with milled carbon fibres and graphene spray did not lead to an improvement in thermal conductivity.
- The resin and granite powder-coated aggregates generally reduced the compressive strength of the AAB. The physical interaction between the aggregate and AAB should be further studied.

- The thermal energy storing macro-encapsulated aggregates were for the first time successfully incorporated into an AAB, creating a novel composite material, opening a wide selection of applications for its inclusion e.g. surface cooling systems, construction materials such as wallboards and ceiling tiles, roads and pavements.

6 APPLICATION FOR LIGHTWEIGHT ALKALI-ACTIVATED INSULATION MATERIALS

To reduce the problem of high energy consumption in buildings, it is urgent to study energy efficient cementitious materials. Alkali-activated binders have the potential of high compressive strengths with low cost and can be transformed into a foamed material with low density and thermal conductivity. As the thermal insulation material, the combined tungsten mining waste and waste glass alkali-activated binder was used as the base materials; aluminium powder, hydrogen peroxide and non-ionic surfactant as the foaming agents; manganese dioxide as a foaming catalyst and starch and hydroxypropyl cellulose as foam stabiliser to prepare the lightweight insulation material. The main performance criteria were satisfied and showed superior performance than the existing cement-based insulation materials.

6.1 Introduction

The EU is targeting for a move towards a 20 % increase in energy efficiency. In absolute terms, this means that by 2020, EU energy consumption should not exceed 1483 MTOE of primary energy or 1086 MTOE of final energy By 2030 (Eurostat 2016). The urban human population is estimated to almost double from approximately 3.4 billion recorded in 2009 to 6.4 billion in 2050 (World Health Organization, 2014) which will naturally be accompanied by a dramatic increase in electricity demand. To reach the 2006 IEA World Energy Outlook for “Alternative Policy Scenario for CO_2 reduction”, 40% of

all final energy savings should be produced by the buildings sector. The ageing building stock across Europe is consuming an ever-increasing amount of energy, while deep renovation and shifting the energy requirements of the buildings closer to zero is often out of reach for economic and technical reasons. A substantial share of the building stock in Europe is older than 50 years with many buildings in use today that are hundreds of years old. More than 40% of residential buildings have been constructed before the 1960s when energy building regulations were very limited. Countries with the largest components of older buildings include the UK, Denmark, Sweden, France, Czech Republic and Bulgaria. The 2020 and 2050 objectives recognise the need for efficient, affordable and deep refurbishment especially in the residential sector that comprises 34% of the building stock. With the development of a resource-saving society and the requirements of the national energy policy to lower building energy consumption, energy-efficient building materials are bound to become the future direction of development.

Energy efficiency is the most cost-effective and long-term strategy to reduce emissions. The Energy Road Map 2050 (European Commission, 2012) confirmed that higher energy efficiency in new and existing buildings is key to the transformation of the EU's energy system. The new addition to the recently updated European Energy Performance of Buildings Directive (EPBD), 2010/31/EU is the ambitious agenda on the reduction of the energy consumption through the introduction of the concept of near zero-energy buildings (Torgal, 2013). The use of thermal insulation materials constitutes the most effective way of reducing heat losses in buildings thus reducing heat energy demands. The thermal insulation market is predicted to grow at a rate of 2.8% year-on-year to 2019 which would forecast the total demand for thermal insulation products in Europe to reach a total of 269.3 million m^3 by 2019 (IAL Consultants, 2015). With the exception of organic insulation materials, which are based on a renewable and completely recyclable material, fossil organic insulation materials have negative impacts associated in terms of toxicity (Remberger et al. 2004; Doroudiani & Omidian 2010). Although glass wool and stone wool combined, represent 58% of the European thermal insulation market, organic polymer foam materials such as polystyrene and polyethylene remain very popular materials for external wall insulation. Styrene, which is the basic building block of polystyrene, is classified as a possible human carcinogen by the EPA and by the International Agency for Research on Cancer (IARC). The pentane gas blowing agent used to produce Expanded Polystyrene Foam (EPS) is classified ozone safe but has a global warming potential (GWP) 7 times greater than carbon dioxide. There is also enough evidence to prove that the commonly used flame retardant hexabromocyclododecane (HBCD) used in EPS is hazardous to both human health and the environment; something that European agencies are moving to restrict the use of. Besides, the recently approved EU Regulation (EU) 305/2011 related to Construction Products Regulations (CPR) highlighted the specific needs for information on the content of dangerous substances in construction products (EU Commission, 2014).

As already mentioned in the Chapter *2.7 Applications of Alkali-Activated Materials*, AABs have been shown to possess a high-temperature resistance, good abrasion resistance, high compressive strength evolution and a low thermal conductivity and therefore ideal candidates for the development of a low-density insulation material. The use of foamed cementitious binders has in the past decade grown very rapidly and is the leading technology in the "special" concrete category. The two main ways of producing foamed cementitious binders are by introducing mechanically pre-formed foam into the binder or by using a chemical foaming technique. While foamed products based on PC are well

established and commercialised (Narayanan and Ramamurthy, 2000), alkali-activated foamed materials remain in the early stages of development.

Recently, alkali-activated materials have been foamed to achieve satisfactory thermal conductivity and low density for the application a new type of thermal insulation material (Zhang *et al.*, 2014). The methods used to make alkali-activated foam materials have been the same as for traditional aerated concrete i.e. pre-foaming or mixed-foaming (Henon *et al.*, 2013; Hlaváček *et al.*, 2015). Nonetheless, the porosity and the thermal insulation properties of alkali-activated foam materials prepared by the mixed-foaming method have not surpassed those of traditional porous materials such as glass foam or autoclaved aerated concrete. Currently, these are the issues limiting the use of alkali-activated foam as alternative thermal insulation materials to compete with traditional porous inorganic materials.

In this study, it is proposed to utilise the large market availability of tungsten mining waste to produce a foamed alkali-activated binder (FAAB) for use as an insulation panel. This research would contribute well with a contribution to achieving the objectives of the European Innovation Partnership on Raw Materials, in particular to the relevant impacts of recycling raw materials. Therefore, this chapter will investigate the compatibility of AABs based on tungsten mining waste and waste glass with three different foaming agents, namely hydrogen peroxide, aluminium powder and a sodium dodecyl benzene sulfonate anionic surfactant. Also, the addition of three additives, namely manganese dioxide (MnO_2), starch $(C_6H_{10}O_5)_n$ and hydroxypropyl cellulose (HPC) was investigated. In the case of MnO_2, which is a naturally occurring catalyst and can be used to increase the rate of decomposition of the H_2O_2 to H_2O and O_2, was used to increase the AAB foaming action. The starch has been successfully used as a low cost and sustainable alternative to commercial stabilisers to stabilise dairy food products which are whipped to add air bubbles into the products. HPC is a derivative of cellulose, one of the most common occurring polysaccharides. It is non-toxic and widely used in food, drug and cosmetics areas (Heitfeld *et al.*, 2008) for their ability to form viscous solutions and stabilise foams. Both latter additives were used to attempt to improve the FAAB foam stability.

6.2 Materials and Methods

6.2.1 Materials

The raw materials used to produce the FAAB in this investigation consisted of the same precursor i.e. tungsten mine tailings (TMW), waste glass (WG), and activator solution i.e. sodium hydroxide (NaOH) and sodium silicate (Na_2SiO_3) as in all the previous tests. The TMW was derived from the Panasqueira mine in Castelo Branco, Portugal, and the WG was received from the local municipality of Covilhã, Portugal. For the chemical composition and grain size distribution of the precursor materials, reference should be made to Table 3-1 and Fig. 3-5.

From the three foaming agents investigated in this study, hydrogen peroxide (H_2O_2) and aluminium powder were both used to produce foam via the chemical foaming technique whilst the sodium dodecyl benzene sulfonate surfactant was used to produce foam via the mechanical pre-foaming technique. The hydrogen peroxide used was a 35 wt.% water solution with a density of 1.13 g/cm^3 at 25°C. The aluminium powder used was 99 % pure

and had an average particle size of 75 microns and molar mass of 26.98 g/mol. The anionic surfactant used was a sodium dodecyl benzenesulfonate powder with a molecular weight of 348.48g/mol. All three foaming agents are of analytical or technical grade and were obtained from Sigma-Aldrich.

The manganese dioxide (MnO_2) additive had a particle size less than 10 microns and a molecular weight of 86.94 g/mol. The starch is a naturally high-polymeric carbohydrate derived from potato. The hydroxypropyl cellulose (HPC) had a specific gravity of 1.0 (3% solution at 20°C), pH of 4.33 (3 % solution at 20°C) and a viscosity of 4000 mPa s (3 % solution at 20°C, Brookfield RVT). All the additives were obtained from Sigma-Aldrich and used as received.

6.2.2 Synthesis of Samples

The mix parameters analysed in this part of the study were FAAB curing temperature (40°C, 60°C, 80°C), SS/SH mass ratio (2.88, 2.45, 2.0), chemical foaming agent type (hydrogen peroxide, aluminium powder, hydroxypropyl cellulose (HPC) and foaming agent mass ratio content (1%, 2%, 3%).

All experiments were carried out at 20°C. For the preparation of the TMW-WG FAAB, the optimal synthesis conditions for achieving the highest strength and satisfactory workability of TMW-WG AAB were adopted based on the results obtained in this study. This resulted in using a 10M concentration of sodium hydroxide solution, an activator/precursor mass ratio of 0.22, an SS/SH mass ratio of 2.88, 8 % mass fraction of mixing water and a 40% mass fraction substitution of TMW with WG. Solutions of sodium hydroxide and sodium silicate along with the water were mixed for a period of 5 minutes at 700 rpm, forming the activator solution.

6.2.2.1 Foaming with aluminium powder

The principle of foaming with aluminium powder is the following: when the aluminium and NaOH react, H_2 is produced, initiating the expansion of the system according to the following chemical reaction formula:

$$2Al + 2NaOH + 2H_20 = 2NaAlO_2 + 3H_2 \quad \text{(Eq. 9)}$$

Determining the fundamental production conditions such as curing temperature, SS/SH ratio and mixing water content for FAABs was considered a pre-requisite and the first step in this investigation.

When the aluminium powder was used as the foaming agent, the TMW, WG and aluminium powder at selected proportions were dry-blended in a commercial mixer at 300 rpm for five minutes, forming the precursor materials. The activator solution was slowly added to the precursor materials and then stirred for 2.5 minutes on a slow speed (200rpm), followed by 2.5 minutes on a fast speed (500rpm) to form the FAAB paste. Plastic molds 4x4x16 cm^3 in size were filled with the FAAB in three stages and manually vibrated after each successive filling stage to release trapped air bubbles. The TMW-WG FAAB was allowed to rest until the foaming process was complete. This rest period depended on the quantity of aluminium powder and the SS/SH ratio since different combinations produced different rates of expansion.

6.2.2.2 Foaming with H_2O_2

When the foaming agent is hydrogen peroxide, a decomposition reaction occurs between the NaOH and H_2O_2 to produce O_2 gas which enables the system expansion, according to the following chemical reaction:

$$2H_2O_2 = 2H_2O + O_2 \quad \text{(Eq. 10)}$$

When hydrogen peroxide solution was used as the foaming agent, the procedure to combine the materials required a different sequence. Firstly, the precursor materials and activator solution were mixed stirred for 2.5 minutes on a slow speed (200rpm), followed by 2.5 minutes on a fast speed (500rpm) to form the AAB paste. This was followed by the addition of the H_2O_2 and a further 20s of mixing. The resulting FAAB was filled into the same size molds and in the same manner. A rest period followed to allow the TMW-WG FAAB finish expanding. For the preparation of the gelling agent, mass fractions of 3, 6 or 9 % HPC based on the total binder water content were added at the beginning of the mixing FAAB mixing process.

6.2.2.3 Foaming with Surfactant

Since foaming with the surfactant followed the pre-formed foaming technique, another different mixing procedure was adopted. TMW, WG at selected proportions were dry-blended in a commercial mixer at 300 rpm for five minutes, forming the precursor materials. The activator solution, however, was firstly combined with the surfactant and stirred for 5 minutes at 1200 rpm, to produce what could be called “activator foam”. The “activator foam” was then combined with the precursors and mixed for 2.5 minutes on a slow speed (200rpm), followed by 2.5 minutes on a fast speed (500rpm). A beater attachment was used for the mixing to allow more air to be entrapped into the FAAB.

6.2.3 Heat Curing

The specimens were placed in a temperature and humidity controlled environmental chamber at temperatures ranging 40 to 100°C, depending on the type of temperature condition being tested. After 24 hours of curing, the FAAB samples were demolded and cut into regular shapes. Electronic weighing scales determined the performance density according to the ASTM C 373-78 and were the average of values obtained from three specimens.

6.2.4 Thermal Conductivity

The thermal conductivity was measured with a thermal conductivity meter (Fox 200, TA Instruments, U.S.A). The steady state heat flux through the rectangular block sample was measured for a temperature gradient of 10°C between the upper and the lower face of the sample. The geometry of the samples was 30x30 mm^2 and 25 mm thick. Two identical samples of the same material were measured for evaluation of the thermal conductivity of the material. To eliminate the contact resistance between the sample and the plate sensors, the samples were cut precisely to ensure the entire surface made complete contact with the plate sensors. Before measurement, the samples were left 24 h at 60°C and placed 30 min in a dry chamber for cooling without moisture absorption.

6.2.5 Compressive Strength

The TMW-WG FAAB prisms were demolded after 1 day and cured subsequently at 20°C and a relative humidity of 75 % until the specific age of testing. The compressive strength of the TMW-WG FAAB prismatic sample fractured counterparts was tested after 1, 3, 7, 28 days in accordance with EN 196-1 using a 50kN universal testing machine (Instron 5960, United Kingdom) at a constant loading rate of 3 kN/min. The compressive strength value was the average of values obtained from three specimens.

6.3 Results and Discussion

6.3.1 Aluminium Foaming Agent

1. Effect of heat curing in aluminium powder FAAB

Fig. 6-1 shows the effect of curing temperature on the 7-day compressive strength and density of the foamed sample using 0.4 wt.% of aluminium powder, an SS/SH ratio of 2.88 and additional 8 wt.% mixing water. The compressive strength of the sample increases with curing temperature, while the density remains in practical terms unchanged within the range of 0.97 and 1.01 g/cm^3. As expected, the lowest compressive strength was attained by the sample cured at the lowest temperature i.e. 40°C, reaching 3.15 MPa. Likewise, the compressive strength increased with curing temperature for the same reasons as for unfoamed AAB i.e. a higher curing temperature increases the reaction activation rate between the liquid and solid material and thus accelerates the ion diffusion rate to produce a denser colloidal structure. SEM images of the aluminium powder FAAB pore structure support the latter result, revealing that the average pore size distribution was similar at all the tested curing temperatures, ranging between small 120 μm pores to large voids 1.46 mm in size (shown in Fig. 6-2). The FAAB sample cured at the highest temperature i.e. 100°C was 5.45 MPa. The ultimate compressive strength and density of the sample were not found to be interactive, and thus the optimal curing temperature of the FAAB can be based on a compromise based on the compressive strength. In this case, since the difference in compressive strength is only 10% of the samples cured at 80°C and 100°C, based on the principle of using less energy in the production of the AAB product, curing at 80°C was chosen to be the curing temperature used for all subsequent samples.

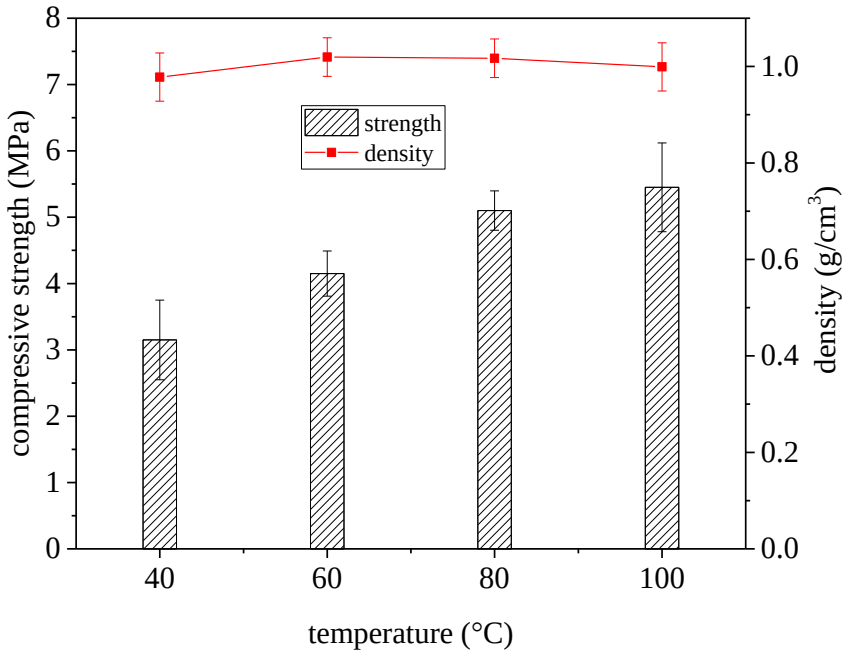

Fig. 6-1 effect of curing temperature on compressive strength and density of aluminium powder FAAB

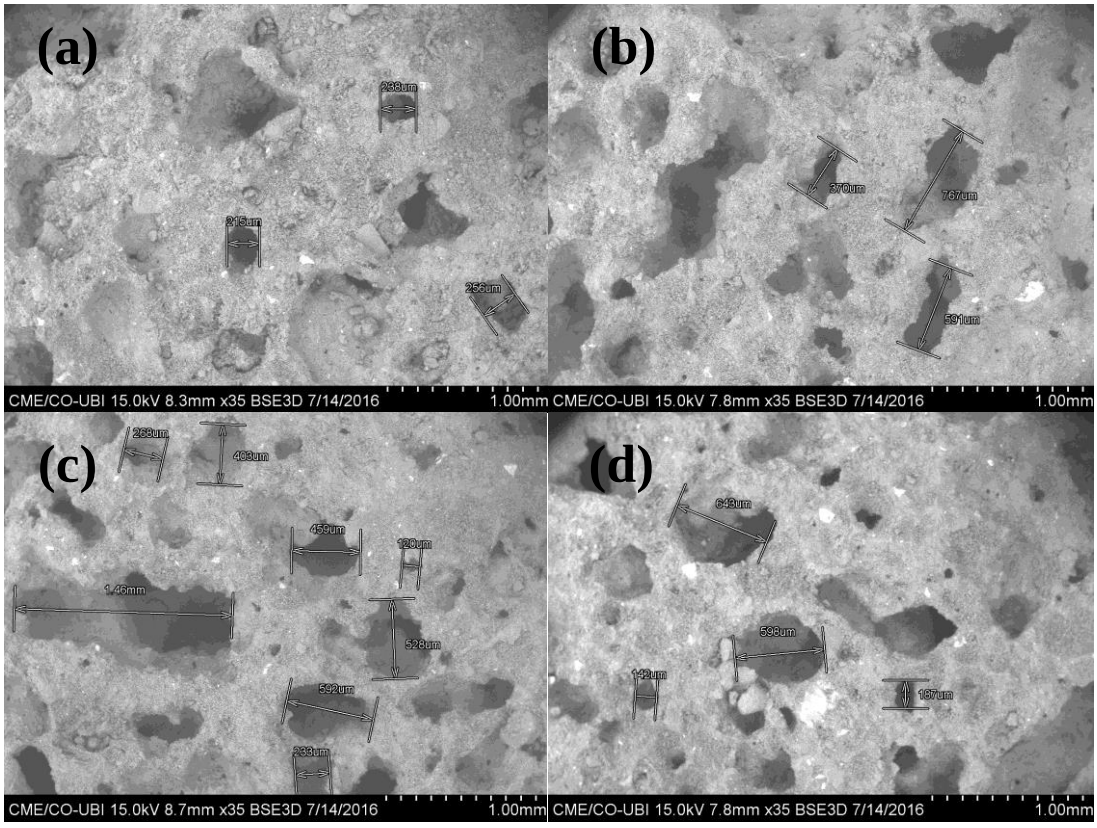

Fig. 6-2 effect of curing temperature on porosity of aluminium powder FAAB

2. Effect of SS/SH ratio

Under normal circumstances, aluminium does not react with water, as an impermeable protective layer composed of aluminium hydroxide forms within seconds. With the addition of sodium hydroxide, the formation of a protective layer is prevented. With the production of aluminates ($Al(OH)_4^-$), the amphoteric aluminium hydroxide $Al(OH)_3$ goes into solution, and the layer of aluminium oxide previously formed by passive corrosion is dissolved by the addition of sodium hydroxide. For this reason, the reaction takes place at the beginning relatively slowly. Fig. 6-3 clearly shows how the density of the aluminium powder FAAB reduces with reduction of the SS/SH ratio since the formation of hydrogen leads to a foaming effect which will be enhanced with the increase of sodium hydroxide. Reducing the SS/SH ratio from 2.88 to 2.0 reduced the density by 49 % from 1.34 to 0.67 g/cm^3. The increased foaming will increase the porosity and reduce the density, but will naturally be followed by a reduction in the compressive strength of the FAAB. In this case, the compressive strength reduced from 11.36 MPa to 3.3 MPa.

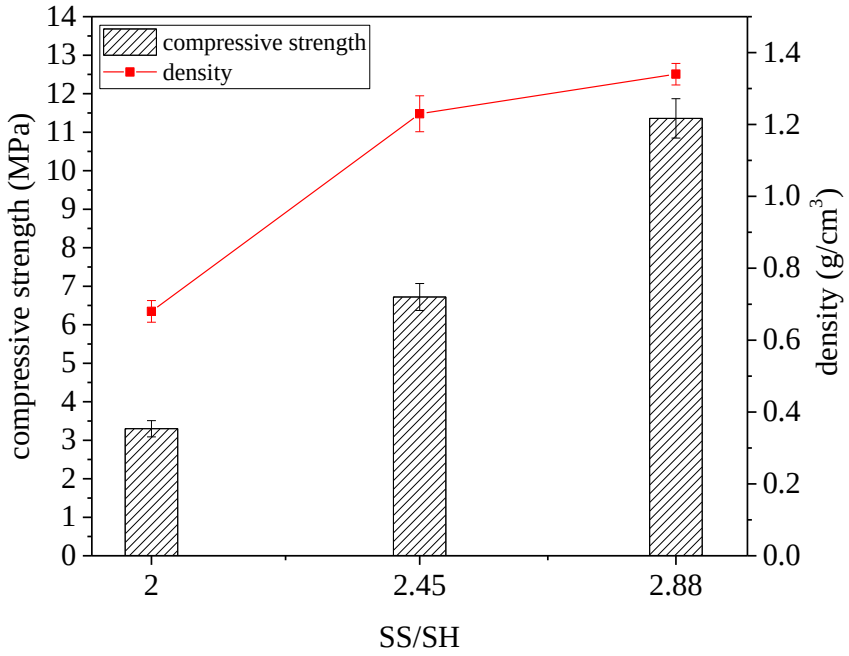

Fig. 6-3 effect of SS/SH ratio on compressive strength and density of aluminium powder FAAB

3. Effect of additional mixing water in aluminium powder FAAB

Fig. 6-4 shows the effect of extra mixing water on the compressive strength and density in samples A6, A2 and A7 containing 7, 8 and 9 wt.% of extra mixing water, respectively. At the two extremes, i.e. 7 and 9 wt.% of extra mixing water, the compressive strength remains practically the same at 18.4 MPa and 17.3 MPa, respectively and so does the density of 1.59 and 1.63 g/cm^3, respectively. With increased water content, the consistency of the raw material mixture slurry is decreased, and the sample density decreases. Due to the fineness of the aluminium powder (75μm), particles may be carried away with the excess water, reducing the amount of aluminium powder that actively participates in the reaction with the NaOH, thus leading to less foaming, and hence increased density and compressive strength. The amplitude of the decline in the compressive strength of sample

A2 follows the decline in density with 8 wt.% of additional mixing water, hence why this amount was chosen to produce all subsequent aluminium powder FAAB samples.

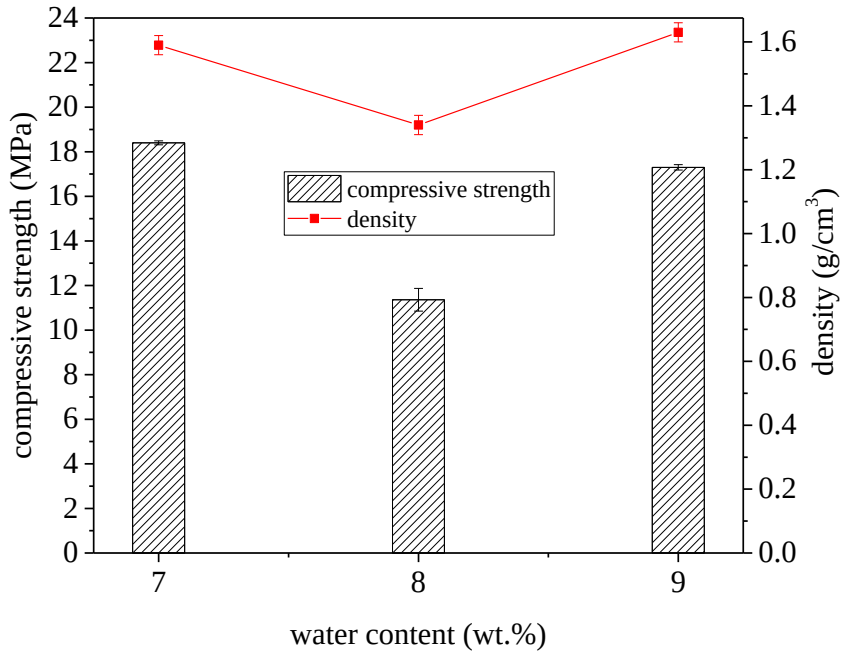

Fig. 6-4 effect of mixing water on compressive strength and density of aluminium powder FAAB

To determine the relationship between the various factors and indicators, in Fig. 6-5 to Fig. 5-7 the horizontal x-axis presents the variables i.e. aluminium powder, extra mixing water, manganese dioxide and starch content, respectively while the vertical y-axis' present the average of the assessment indicators i.e. compressive strength and density. Table 6-1 lists the varying aluminium FAAB samples produced with varying quantities of starch and manganese dioxide.

Table 6-1 composition of TMW-WG samples foamed using aluminium powder

	Aluminium powder content (wt.%)	Starch content (wt.%)	MnO_2 content (wt.%)
A1	0.2	0.0	0.0
A2	0.4	0.0	0.0
A3	0.6	0.0	0.0
A4	0.6	0.0	0.2
A5	0.6	0.0	0.4
A6	0.6	0.0	0.6
A7	0.6	2.0	0.0
A8	0.6	4.0	0.0
A9	0.6	6.0	0.0

4. Effect of aluminium powder foaming agent content on FAAB

Fig. 6-5 shows the effect of the amount of aluminium powder on the compressive strength and density of the sample. The sample density decreased from 1.52 g/cm^3 to 1.34 through to 1.2g/cm^3, resulting in a final reduction in density by 21%. However, the compressive strength of the sample decreased from 17 MPa to 8.7 MPa, a decrease of 48%, indicating that an increase of aluminium foaming agent has an adverse effect on the samples mechanical properties. Based on the latter result which shows that sample A3 containing 0.6 wt.% aluminium powder achieved the lowest density and satisfactory compressive strength, it will be used as the benchmark sample for evaluating the effects of manganese dioxide and starch addition.

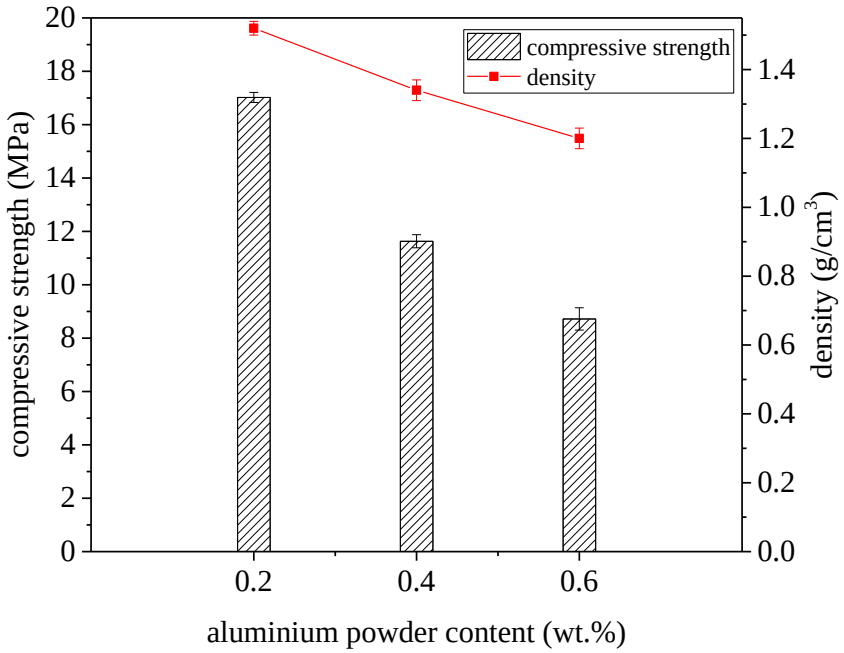

Fig. 6-5 effect of aluminium powder on compressive strength and density of aluminium powder FAAB

5. Effect of Manganese Dioxide content in aluminium powder FAAB

Fig. 6-6 shows the effect of manganese dioxide content of aluminium powder FAAB. With the increase of manganese dioxide from 0.2 to 0.4 wt.% and finally to 0.6 wt.%, there appears to be a clear relationship in that both the density and strength reduce in a steady manner because of the thermite reaction between the manganese dioxide and the aluminium powder foam. With a content of 0.40%, the foaming action became too severe and unstable, resulting in excessive bubble size and their subsequent rupture. With the increase of manganese dioxide content from 0.40 to 0.60 wt.%, both the density and compressive strength are reduced.

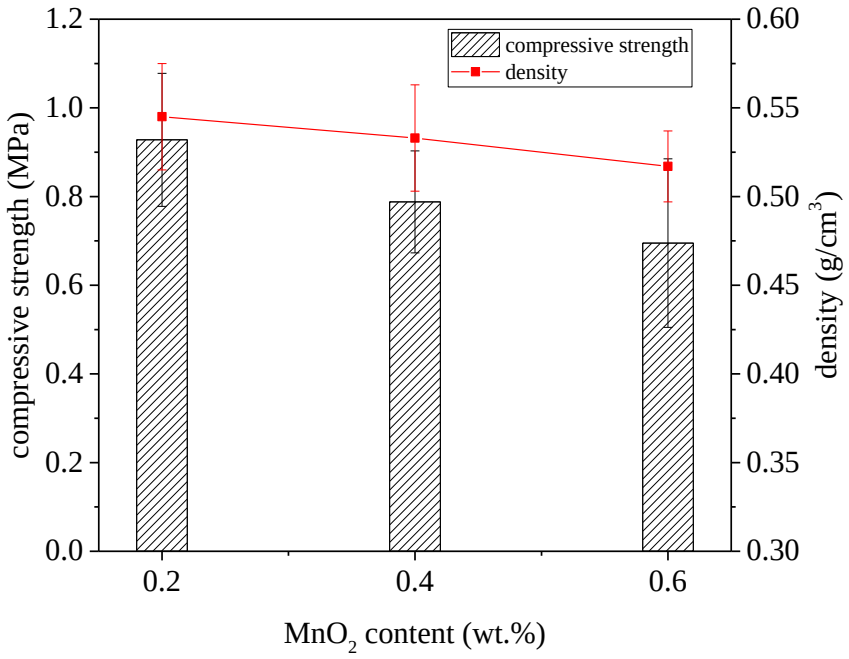

Fig. 6-6 effect of manganese dioxide on compressive strength and density of aluminium powder FAAB

6. Effect of starch content in aluminium powder FAAB

Fig. 6-7 shows the effect of starch on the density and compressive strength of aluminium powder FAAB. After adding 2 wt.% starch, the density was reduced from 0.68 g/cm^3 to 0.6 g/cm^3, indicating that starch can significantly improve the effectiveness of aluminium powder foaming agent. However, when the starch concentration increased to 4 wt.% and followed by 6 wt.%, the foaming capacity significantly decreased, represented by the increase in the density. The addition of starch above 2 wt.% increased the relative concentration of particles in the system thus increasing the reaction time and subsequent formation of reaction products. The loss of compressive strength can be explained by the reduced liquid-solid ratio due to the low molecular weight of starch, resulting in a prolonged coagulation time and reduced paste fluidity. The reduced fluidity due to the increased starch content also caused the gas released from the reaction between the aluminium powder and sodium hydroxide to be blocked during the expansion process. Therefore, the appropriate amount of starch should not exceed 2 wt.%.

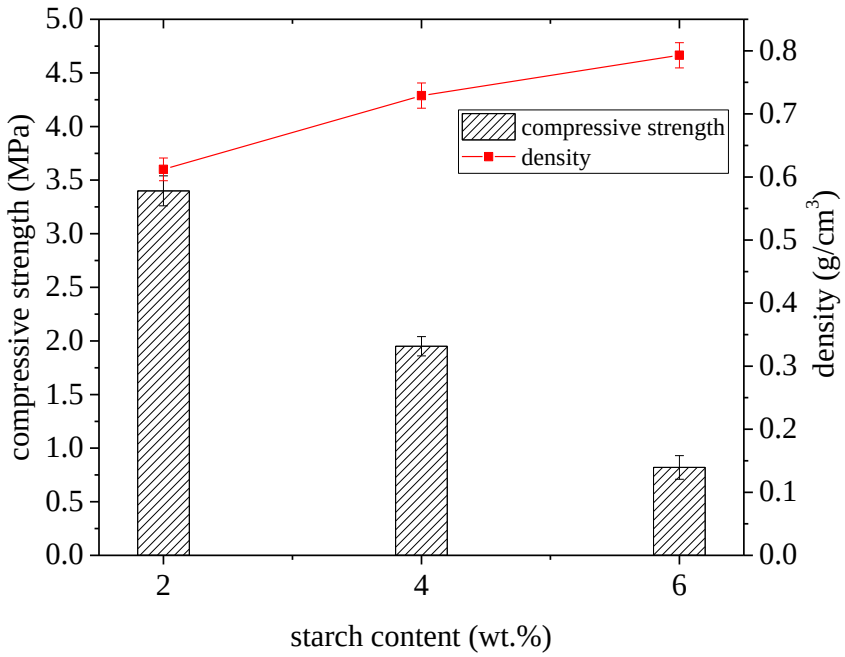

Fig. 6-7 effect of starch on compressive strength and density of aluminium powder FAAB

6.3.2 Hydrogen Peroxide as a Foaming Agent

1. Effect of water content in hydrogen peroxide FAAB

With the increase of hydrogen peroxide content, the amount of water introduced also increased; thus, this was taken into consideration and the extra mixing water added to all the mixes was adjusted by considering the 65% water content of the H_2O_2 solution. Fig. 6-8 shows the effect of water on the compressive strength and density of the samples H4, H5 and H6 containing 7, 8 and 9 wt.% of extra mixing water, respectively. The compressive strength of the respective samples increased with the increase of extra mixing water content, whilst the density of the samples decreased slightly, indicating that the compressive strength of the samples decreased mainly due to the compressive strength of the matrix.

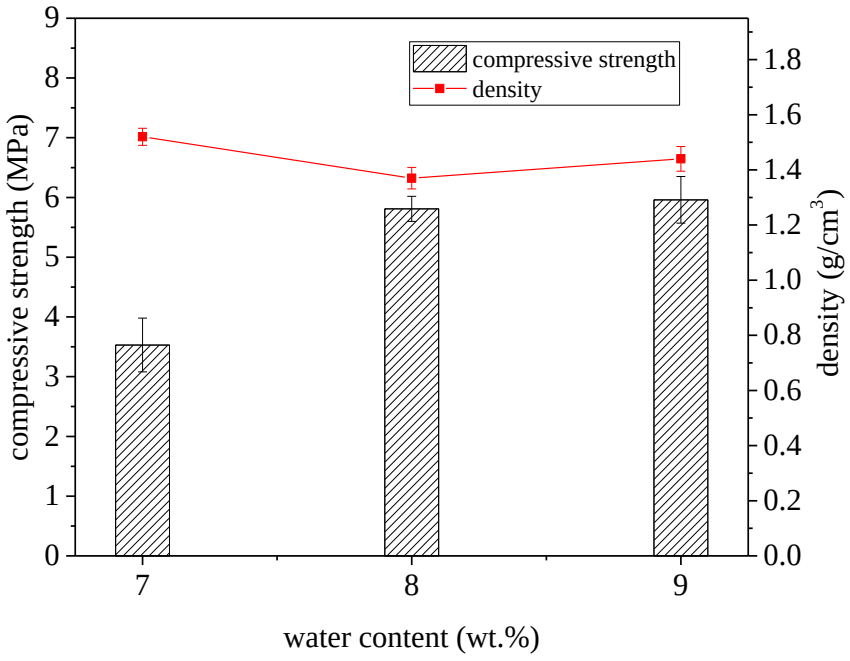

Fig. 6-8 compositions of TMW-WG AAB samples foamed using hydrogen peroxide

	H_2O_2 content (wt.%)	MnO_2 content (wt.%)	HPC content (wt.%)
H1	0.5	0	0
H2	1.0	0	0
H3	1.5	0	0
H4	1.5	0.2	0
H5	1.5	0.4	0
H6	1.5	0.6	0
H7	1.5	0	3
H8	1.5	0	6
H9	1.5	0	9

To draw the relationship between the various factors and indicators, from Fig. 6-9 to Fig. 6-11, the horizontal x-axis presents the variables i.e. contents of hydrogen peroxide, mixing water, manganese dioxide and HPC, respectively while the vertical y-axis' present the average of the assessment indicators i.e. compressive strength and density.

2. Effect of hydrogen peroxide content in hydrogen peroxide FAAB

Fig. 6-9 shows the effect of the content of hydrogen peroxide on the compressive strength and density of the sample. The density of the sample decreased linearly with the increase of the amount of hydrogen peroxide, and the compressive strength also decreased in the same manner, mainly due to the increase of the gas released. The increase of the porosity in the sample resulted in the decrease of density and compressive strength. Sample H1, containing the least hydrogen peroxide i.e. 0.5 wt.%, attained a density of 1.83 g/cm^3 and a compressive strength of 15.1 MPa whilst the sample H3, containing 1.5 wt.% of hydrogen peroxide, attained a far lower density of 0.84 g/cm^3 but also a significantly reduced 28-day compressive strength of 4.77 MPa. Based on the latter result which shows that sample H3 containing 1.5 wt.% hydrogen peroxide achieved the lowest density and

satisfactory compressive strength, it will be used as the benchmark sample for evaluating the effects of manganese dioxide and HPC addition.

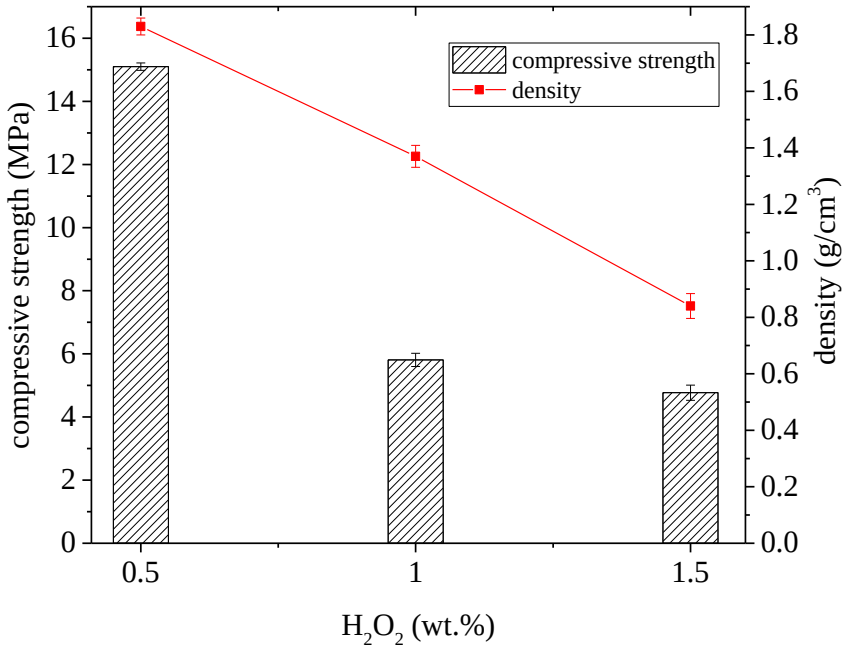

Fig. 6-9 effect of hydrogen peroxide on compressive strength and density of hydrogen peroxide FAAB

3. Effect of manganese dioxide content in hydrogen peroxide FAAB

Fig. 6-10 shows the effect of manganese dioxide content of hydrogen peroxide FAAB. With the increase of manganese dioxide from 0.2 to 0.4 wt.%, both the density and strength dramatically increase due to the catalytic effect of manganese dioxide on the hydrogen peroxide foam. With a content of 0.40%, the foaming action became too severe and unstable, resulting in excessive bubble size and their subsequent rupture. With the increase of manganese dioxide content from 0.40 to 0.60 wt.%, both the density and compressive strength are reduced. Therefore, the appropriate amount of manganese dioxide should be 0.6 wt.%.

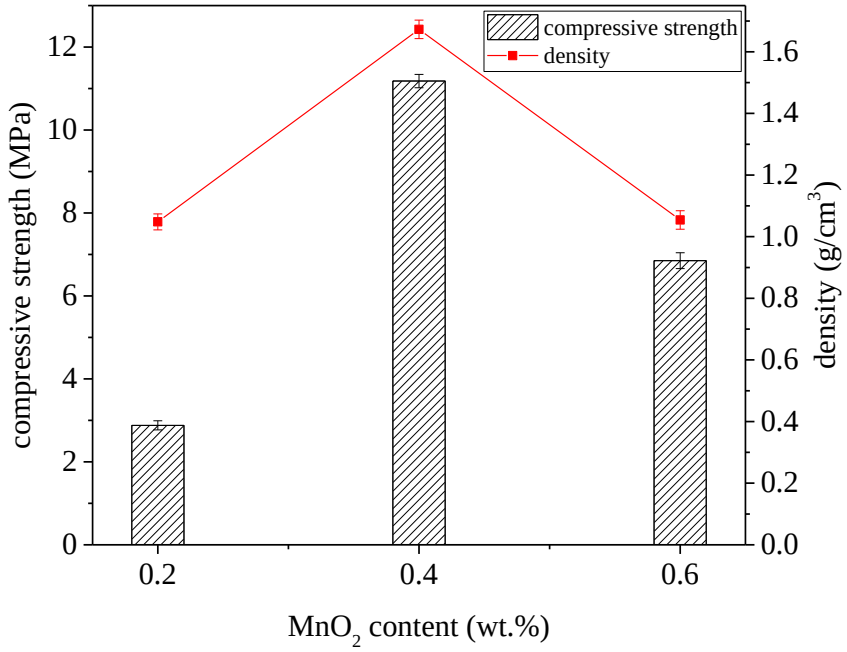

Fig. 6-10 effect of manganese dioxide on compressive strength and density of hydrogen peroxide FAAB

4. Effect of HPC content in hydrogen peroxide FAAB

As shown in Fig. 6-11, with the increase of HPC from 3 to 9 wt.%, both the density and compressive strength increase significantly from 0.85 g/cm^3 to 1.38 g/cm^3 and 1.8 MPa to 6.58 MPa, respectively. The HPC hydrophilic groups adhered to the water molecules present in the activator solution by hydrogen bonding, modifying the water retention properties of the hydrogen peroxide FAAB and thus its rheology. The HPC was responsible for the thickening of the hydrogen peroxide FAAB and subsequent increase in setting time by delaying the formation of reaction products. The extended period of time that the hydrogen peroxide FAAB spent in the fresh state resulted in the foam volume reducing thus increasing the density. Further tests of HPC interaction with the alkaline activator showed that the pH of the chemical activator was reduced from 14.3 to 12.1, contributing to the slowdown of precursor dissolution. With respect to the reference sample H3, no significant reduction in the density or compressive strength is achieved with the addition of HPC.

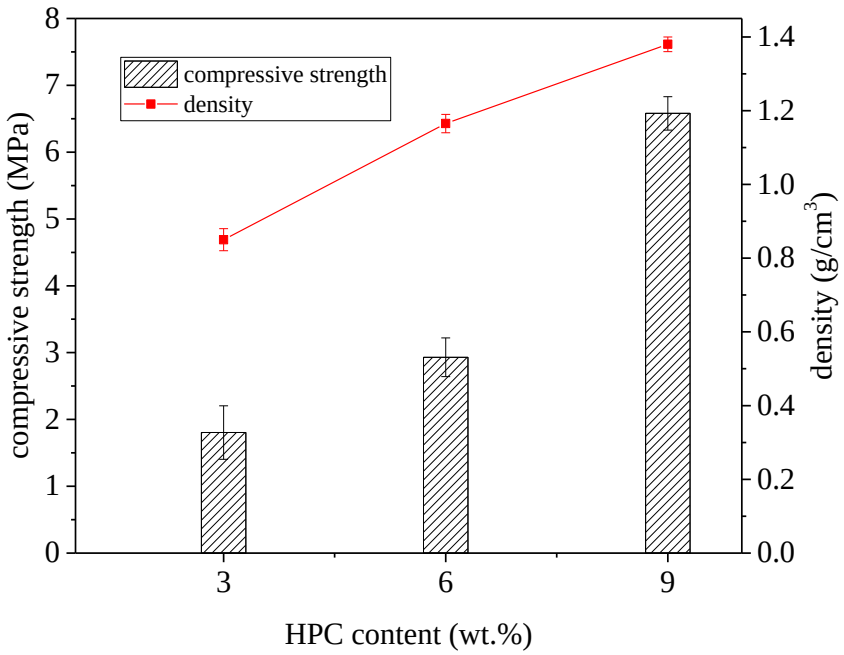

Fig. 6-11 effect of HPC on compressive strength and density of hydrogen peroxide FAAB

6.3.3 Surfactant as a Foaming Agent

Table 6-2 shows the three mixes of FAAB made with varying quantities of anionic surfactant foaming agent used to prepare the foam. Since the preparation of the surfactant, FAAB was more involved than that aluminium powder FAAB or hydrogen peroxide FAAB, Fig. 6-12 shows the steps in its preparation. Fig. 6-12a shows the combined alkali activator and surfactant, Fig. 6-12b shows the "foamed alkali-activator" after 5 minutes of mixing at 1200 rpm, Fig. 6-12c shows the combination of the TMW/WB precursor and "foamed alkali-activator" and finally Fig. 6-12d shows the fresh surfactant FAAB immediately after mixing. In all cases, the precursor-to-foam ratio was maintained at a constant of 0.6.

Table 6-2 compositions of TMW-WG AAB samples foamed with surfactant

	Surfactant (wt.%)	SS/SH ratio (wt.%)	Mixing water content (wt.%)
S1	2	2.0	8
S2	4	2.0	8
S3	6	2.0	8

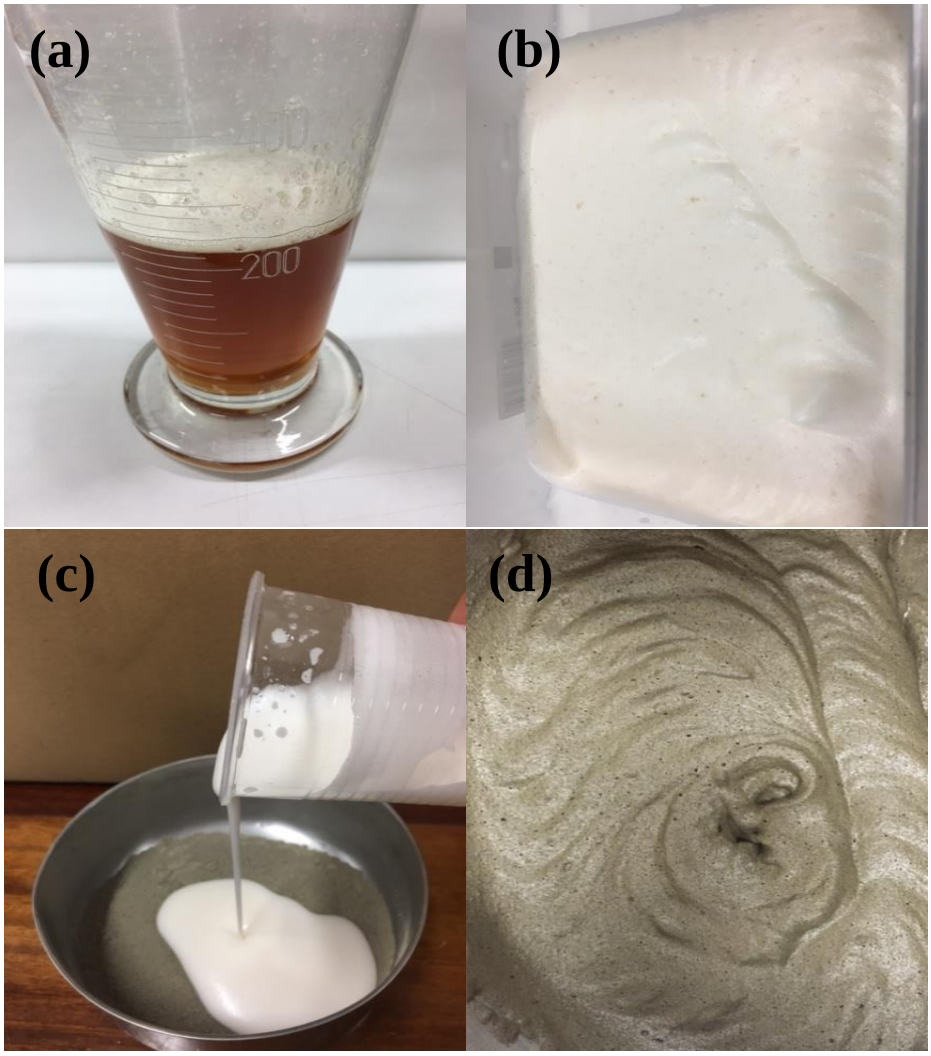

Fig. 6-12 preparation of surfactant FAAB showing (a) the alkali activator/surfactant mixture (b) foamed alkali-activator (c)combination of the precursors and foamed alkali activator (d) foamed AAB using surfactant

1. Effect of Surfactant content on FAAB

Fig. 6-13 shows the effect of the amount of anionic surfactant on the compressive strength and density of the samples i.e. S1-S3. The compressive strength of the samples increased with the increase of the surfactant, and so did the density, reaching a peak with the addition of 4 wt.% of surfactant. Upon the addition of 6 wt.% surfactant, the density of the sample reduced while the compressive strength continued to increase. When the amount of surfactant is initially increased from 2 to 4 wt.%, the bubbles decrease, and the total pore volume decreases, so the compressive strength increases and the density increases. When the surfactant is increased to 6 wt.%, more gas is introduced into the system, so that the sample density decreased whilst maintaining an increase in the sample compressive strength. Generally, however, the pre-foaming method using the anionic surfactant produced an FAAB with a higher density and thermal conductivity, than the chemically foamed samples using aluminium powder.

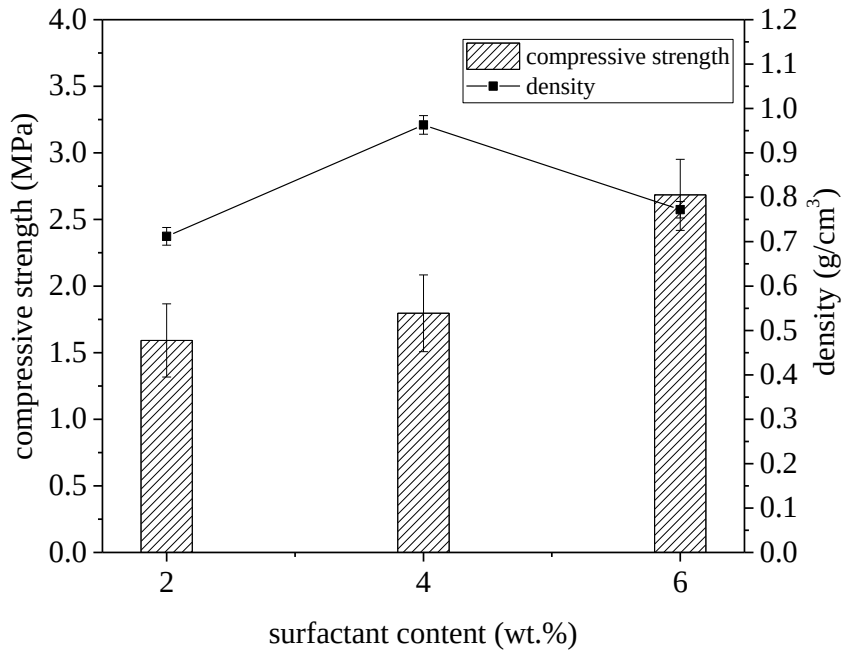

Fig. 6-13 effect of surfactant on compressive strength and density of surfactant FAAB

6.3.4 Thermal Conductivity

Table 6-3 summarises the primary FAAB properties i.e. density, 28-day compressive strength and thermal conductivity for samples produced with the three different foaming agents, namely aluminium powder, hydrogen peroxide and surfactant. The sample ID is shown in brackets. Compared to the un-foamed AAB, all FAABs regardless of the foaming agent used were at least 60% lower in density. The aluminium powder FAAB achieved the lowest density (0.68 g/cm^3) and thermal conductivity (0.11 W/m K) and the second highest compressive strength (3.3 MPa). The hydrogen peroxide FAAB may have achieved the highest compressive strength (4.77 MPa), however also attained the highest thermal conductivity (0.2 W/m K). The surfactant FAAB achieved the lowest compressive strength (1.79 MPa) and an intermediate density and thermal conductivity of 0.77 g/cm^3 and 0.16 W/m K, respectively. The TMW-WG FAABs outperformed the other cement-based thermal insulation materials currently under development (shown in Table 6-4), particularly in terms of density and thermal conductivity. Images of the FAAB pore structure made with aluminium powder, hydrogen peroxide and surfactant respectively, are shown in Fig. 6-14. The pore structure of the aluminium powder FAAB consists of a closed network of pores, regular in shape and distribution. In comparison, the hydrogen peroxide FAAB pore structure appears more randomly distributed and interconnected, allowing for greater conduction of heat and thus higher thermal conductivity. The surfactant FAAB pores, although regularly distributed, were very small, apart from a few large voids because of uneven compaction. Although the pore sizes of the surfactant FAAB were observed to be the smallest, it is assumed that they were more interconnected those of the aluminium or hydrogen peroxide FAAB, thus leading to the lowest compressive strength.

Table 6-3 properties of FAAB made using the three different foaming agents

Sample	Density (g/cm^3)	Compressive strength (MPa)	Thermal conductivity (W/m K)
AAB	2.10	61.0	0.28
Aluminium powder FAAB (A3)	0.68	3.30	0.11
Hydrogen peroxide FAAB (H3)	0.84	4.77	0.20
Surfactant FAAB (S3)	0.77	2.68	0.16

Table 6-4 properties of latest cement based insulation materials

Sample	Density (g/cm^3)	Compressive strength (MPa)	Thermal conductivity (W/m K)
PC cement mortar	1.8	21	0.388
Cement-vermiculite (Shoukry *et al.*, 2016)	1.24	10.5	0.38
Cement-gypsum (Samson, Phelipot-Mardelé and Lanos, 2016)	0.6	2.0	0.20

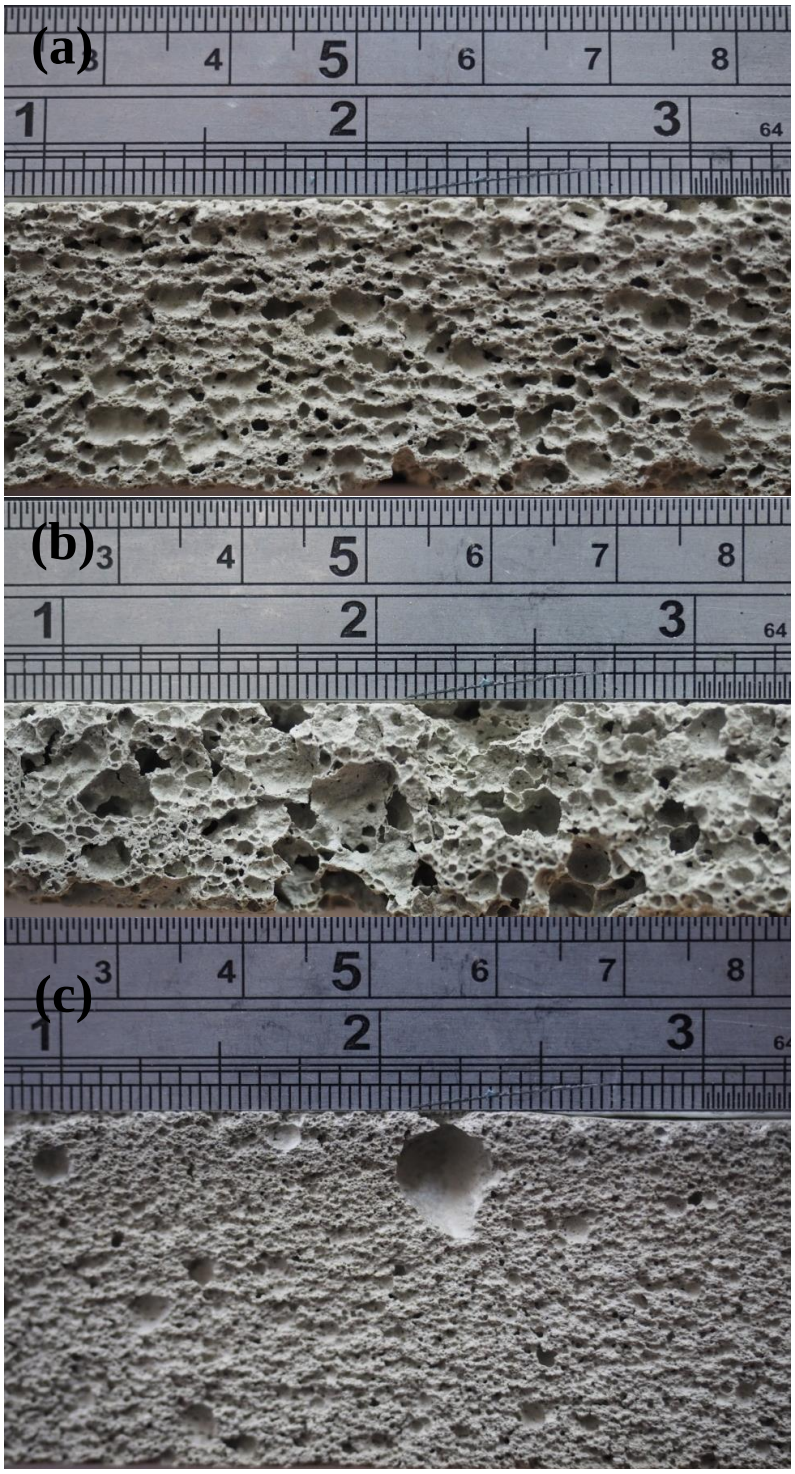

6-14 images of (a) aluminium powder (b) hydrogen peroxide and (c) surfactant FAAB (units are in centimetres and inches)

6.4 Summary

This study revealed that foamed alkali-activated binders (FAAB) based on tungsten mining waste and waste glass could be successfully prepared by a chemical foaming method using aluminium powder and hydrogen peroxide and a pre-foaming method using a surfactant. The following conclusions can be drawn from the results of this work:

- The curing temperature of FAAB influenced the mechanical strength but did not affect the sample porosity, and pore size ranged from 120 μm pores to large voids 1.46 mm in size across all curing temperatures. The final pore structure of FAAB is formed during the initial foaming process and thus curing temperature was chosen based on compressive strength development, which in this case was chosen to be 80°C since it was only marginally lower than for the FAAB cured at 100°C.
- The chemical foaming method, particularly with aluminium powder resulted in the best performing sample in all properties studied i.e. density; compressive strength and thermal conductivity and would be recommended over the pre-foaming method for alkali-activated materials.
- The density of FAAB is sharply reduced when an SS/SH ratio of 2.0-2.45 is used, with the lower end i.e. 2.0 providing the lowest density for both aluminium powder and hydrogen peroxide FAABs. The effect of additional mixing water was determined to be in line with the findings for non-foamed TMW-WG AAB.
- Manganese dioxide catalyst agent, even when present at relatively low levels (0.2 wt.%), was capable of significantly reducing the density, without compromising the compressive strength. On the other hand, the combination of manganese dioxide with the hydrogen peroxide proved to be too intense leading to the rapid formation of unstable foam with reduced half-life.
- The addition of starch to the aluminium powder FAAB can provide a discernible reduction in density by 10% when the content of starch is not more than 2 wt.%. Incorporation of HPC to hydrogen peroxide FAAB did not provide the expected stabilising properties and would therefore not be recommended as a suitable gelling agent for [i]norganic foamed materials.
- Depending on the density and compressive strength requirements, TMW-WG FAAB can be designed to suit a wide variety of applications; from a lightweight material with sufficient strength for structural use and good thermal conductivity to a super-lightweight insulation material with a low thermal conductivity.
- TMW-WG FAAB insulation performance reported in this study displayed superior performance compared to other cement based thermal insulation materials under development such as cement-vermiculite and cement-perlite composites.

7 APPLICATIONS OF ALKALI-ACTIVATED BINDERS FOR ROAD REPAIR

Much of the research concerning alkali-activated binders generally remains confined to the laboratory scale, and only rarely are the research outputs applied to a meaningful application. To evaluate the preliminary performance of the TMW-WG AAB developed in this study, permission was granted by the Covilhã municipality, Portugal, to conduct a pilot test for the repair of a pothole 50cm in width and a maximum of 7cm in depth at a residential road intersection.

7.1 Introduction

As discussed in the Chapter 2.*7 Applications of Alkali-Activated Materials*, AABs are a class of materials proving as materials with a high potential to be employed in the construction industry, essentially as an alternative to Portland Cement (PC). All AABs are based on the number of beneficial features that these binders can develop during and after the alkali-activation. There have been some niche applications to which AABs have been applied to, some of which are listed below.

Fire resistant High-Temperature Materials

During the 1994 and 1995 World Formula One contents, the Renault team first used “geopolymer”/carbon composites as the heat shield for Formula 1 vehicles and won the world championships in both seasons, leading the way for most other Formula 1 teams to implement the technology. Also in 2004, Porsche AG successfully developed a patented system for the manufacture of automotive exhaust pipe systems using “geopolymer” composites (Davidovits, 2002).

In 1986, Air France fitted fighter aircrafts with molds made from "geopolymers", but also developed self-heating carbon/SiC/geopolymer composites for the preparation of tools that were used to prepare a new type of bomb designed for the US Air Force. The United States Federal Aviation Administration, Rutgers State University and other research institutions have been researching "geopolymer" composites in the aviation industry with the potential to achieve first-class fire safety standards in aircraft applications (Air Force Office of Scientific Research, 2010). In 1994, in New Jersey, United States, the Federal Aviation Administration introduced in conjunction with international aviation fire and in-house safety seminar, a "geocomposite" material fabricated to be a fire-resistant fibre laminate for the assembly of in-flight cabin material (Davidovits, 2002). Pechiney also developed and patented high-melting, non-corrosive geopolymers for smelting Al/Li alloys. Since 1985, the French and British nuclear power plants have had their factories equipped with air filters with the filter interface and anti-dust sealant prepared from "geopolymers" with a capacity to resist temperatures of 5000°C (Davidovits, 2002).

Metal and Ceramic Adhesive

Researchers (Kriven, Bell and Gordon, 2012) at the University of Illinois at Urbana-Champaign, USA, applied geopolymer materials made with basalt fibres to achieve promising results. Using fibre reinforcement, the bending strength and work of fracture of geopolymer materials were increased from an average of 2.8 MPa to 10.3 MPa and 0.05 kJ/m2 to 21.8 kJ/m^2, respectively. These composites also proved to remain microstructurally stable to above 1000°C.

Art and Decorative Materials

Recent studies made by researchers at the University of Granada have also shown the artistically inspired applications of alkali-activated materials by successfully demonstrating the technical process of reduction (RAKU) to produce ceramic artwork using tungsten mining waste 'geopolymer' (REMINE, 2015).

Many concrete infrastructures, such as concrete pavements, bridge decks, parking structures, highways and airport runways, have high repair costs when damaged. This is due to the specially formulated materials that are used to for the repairs, commonly based on polyurethane polymers, epoxy polymers, thermosetting vinyl polymers, and magnesium phosphate cement. Rapid concrete repair methods are of economic significance and have been studied for modified Portland cement (Won *et al.*, 2011) and magnesium phosphate cement (Yang and Wu, 1999). However, research into alkali-activated cementitious binders rarely goes beyond the laboratory scale, and efforts of it being put into engineering practice are limited. A typical example of this would be a study conducted by Hawa et al. (2013), who developed a high early strength "geopolymer" for rapid road repair but only on an experimental level. Hence to enrich this study and prevent it from being strictly laboratory scale research, it was decided to conduct a pilot-scale test.

7.2 Materials and Procedure

The raw materials used to produce the TMW-WG mortar i.e. sodium hydroxide and sodium silicate alkali solutions, TMW and WG precursors were of the same quality and composition as previously used in all previous experiments and defined in *3.2.1 Materials*. The alkaline activator was prepared by mixing the sodium hydroxide and sodium silicate

solutions in a separate container at the optimum ratio determined in Chapter *4.3.3 Influence of Alkali-Activator Composition*, i.e. 2.88. Locally available fine aggregate (river sand) in saturated surface dry condition was used. The TMW, WG and fine aggregate were mixed together in a standard 140L capacity cement mixer for 2 minutes to ensure homogeneity of the mixture at a precursor/sand ratio of 0.75 based on trial laboratory tests. The mixer was stopped, and the activator solution containing the sodium hydroxide and sodium silicate was added according to the optimum activator/precursor ratio determined in Chapter *4.3.3 Influence of Alkali-Activator Composition* i.e. 0.22 and mixed for a further 10 minutes. The 8 wt.% of mixing water required to achieve suitable workability previously determined in Chapter *4.3.3 Influence of Alkali-Activator Composition* was increased to 10 wt.% due to the addition of fine aggregates. The total mass of the material produced for the pothole repair was 15 kg. All mixing was conducted on site during which the air temperature was 35°C. The road was made from asphalt, and the pothole was 50cm in width and a maximum of 7cm in depth, situated at an intersection of a residential road. To improve the adhesion with the repair mortar, the pothole was made free of debris (shown in Fig.7-1a). The preparation and application of the TMW-WG repair mortar can be seen in Fig.7-1b. All the tools and equipment used to produce the TMW-WG repair mortar were identical to what would be typically used to prepare a Portland cement based mix. Immediately after mixing, the TMW-AAB mortar was transported using a wheelbarrow to the pothole where it was poured, tampered with a rod approximately 25 times and finally levelled. The repaired pothole can be seen in Fig. 7-1c.

7.3 Evaluation of Pilot Test Repair

The pilot test was conducted on the 8th of August 2016, in Covilhã, Portugal. The equipment and tools used to prepare the AAB mortar were no different from what is normally used in the production of an ordinary PC mix. This is a very encouraging aspect for prospects of AAB implementation in the industry since the closer the production of the AABs resembles that of a PC binder, the more likely it will be for an operator to feel comfortable preparing it. The advantage of conducting the road repair during the hot climate conditions meant that the TMW-WG repair mortar could obtain the necessary heat energy for hardening from the sun, demonstrating the AABs potential as a road repair material in hot weather climates. From qualitative observation, the repair mortar appeared to have reached the final set approximately 45 minutes after casting and was judged to be open to traffic 1 hour after that. Rapid hardening is essential for reducing downtime and supervision costs. The final setting time of the repair on-site closely matches the final setting time of 66 minutes under laboratory conditions, as explained in Chapter 4.3.3 *Influence of Alkali-Activator Composition*. The mortar also had the added benefit of naturally matching the road surface colour, allowing for a more discrete repair. The average daily temperatures during the four months after the repair were 31C, 26°C, 19°C and 13°C and as shown in Fig. 7-1d, 4 months after casting, the repair mortar was assessed to be in satisfactory condition without any observable cracks, spalling or deterioration. Visual monitoring of the repair will continue to check for the appearance of any damage. Future pilot tests will be conducted using different formulations and varying weather temperatures to gather more information about the curing speed, particularly during cold weather.

Fig. 7-1(a) pothole before repair (b) mixing of the TMW-WG mortar (c) pothole immediately after casting (d) appearance of repair after 4 months

7.4 Summary

The pilot test demonstrated the feasibility of re-using both tungsten mining waste and waste glass to produce an AAB in the application of road repair from which the following conclusions can be drawn:

- TMW-WG alkali-activated mortar did not require any special equipment or specialised technique for its production, allowing work personnel accustomed to using PC to adapt to produce this material easily.
- The TMW-WG AAB could be successfully applied to applications particularly when high compressive strength is required such as in the road repair successfully demonstrated in this study.
- The fast setting time of the binder optimised in this study makes it particularly suitable for applications where demolding at an early age is a priority, such as precast applications. Also, this repair mortar would also be useful for the repair of bridge decks, parking structures, highways, and airport runways, all of which have high repair costs when damaged.

8 CONCLUSIONS AND FUTURE RESEARCH

8.1 Conclusions

This study aimed to explore the capacity of tungsten mining waste (TMW) as a precursor for alkali-activated binders (AABs) with supplementary waste materials. From the research outputs, the following conclusions can be made:

- Control of the alkali activator mixing is a crucial task. From the results, it is deduced that prolonged mixing of the alkali metal species from the activating solution will reduce the dissolution and subsequent mobility of Na^{+}, SiO^{4-} and OH^{-} ions. The lower availability of the latter ions would result in limited gel reorganisation and thus reduced strength.

- The results demonstrated that a key reactivity parameter that led to an AAB with optimal binding properties is a WG content of 40%. Reactive silica from the WG can be used to yield an optimum Si/Al ratio for increased dissolution of TMW particles, replacing the soluble silica from the Na_2SiO_3 in the alkali activator and produce calcium containing N-A-S-H gel products. WG is also observed to provide nucleation sites for reaction products, improving gel formation and hence strength.

- This study clearly demonstrates that the properties of an AAB systems can be drastically affected by minor changes in the alkali modulus (Ms). In this case, the Ms which provided the most satisfactory strength for TMW-WG AAB was in the 1.48-1.85 range. Also revealed is the strong influence of the activator/precursor ratio on AAB mechanical performance. When it is useful to have the lowest activator/binder ratio, the employment of SS/SH ratio in the range of 2.8-3.5, an activator/precursor ratio in the range of 0.22-0.25 and 6-8 wt.% mixing water is recommended, thanks to the high compressive strength that can be achieved and favourable compressive workability.

- The sealing performance of the resin-granite powder coating was evaluated leak proof and ensuring the ME-LWAs remained thermally stable after many melting/solidifying cycles. The ME-LWAs durability also proved satisfactory with 60% remaining completely undamaged after exposure to a severe wet and abrasive durability test. The addition of ME-LWA leads to a slight decrease of the compressive strength of the TMW-WG AAB. However, the SEM images revealed good bonding between the ME-LWA and AAB matrix the compressive strength of the AAB with 20% of ME-LWA by volume incorporation in the TMW-WG AAB is still sufficiently high for building applications. The specific heat capacity of the TMW-WG AAB increases significantly after ME-LWAs are incorporated, meaning that the incorporated ME-LWAs can effectively reduce the transport of heat through the geopolymer mortar and save energy consumptions for cooling and heating.

- Using aluminium powder, hydrogen peroxide or surfactant as the foaming agents, blended TMW-WG AABs can be prepared as lightweight foam materials with satisfactory compressive strength and low thermal conductivity. For aluminium foamed samples, the compressive strength of 0.69-11.36 MPa and density of 0.51-1.34 g/cm^3 was achieved. Using hydrogen peroxide as the foaming agent, an FAAB with a compressive strength of 4.77-8.26 MPa and density of 0.84-1.38 g/cm^3 was achieved. For surfactant foamed samples, the compressive strength of 1.59-2.69 MPa and density of 0.71-0.96 g/cm^3 was achieved. The latter results proved the feasibility and high potential of TMW-WG lightweight foam material as building insulation materials. The TMW-WG FAAB achieved better performance in terms of mechanical strength, density and thermal conductivity compared with the latest building insulation materials under research such as cement-vermiculite and cement-perlite composites.

- TMW-WG AAB was successfully applied as a road repair material. Materials based on AABs can be produced on site without requiring any specialised equipment or techniques, meaning that work personnel should not require any special training or skill to produce AABs. The rapid setting and hardening features of the TMW-WG mortar make it particularly suitable for applications where demolding at an early age is a priority, such as precast applications, and for the repair of bridge decks, parking structures, highways, and airport runways, all of which have high repair costs when damaged.

8.2 Innovation

The innovation of this study is mainly reflected in the following four aspects:

- Low reactivity tungsten mining waste can serve as a favourable waste aluminosilicate source material for synthesising AABs to realise the goal of converting zero value waste materials into valuable construction materials.
- Waste glass can successfully supplement the AAB to reduce the sodium silicate component of the alkali activator, reducing the high costs and health risks associated with the production of AABs.

- The energy storing lightweight aggregates were successfully developed for inclusion in an AAB for implementation in both indoor and outdoor building applications.
- The alkali-activated lightweight thermal insulation material was developed based on TMW/WG precursors. By evaluating the preparation conditions, foaming agent type and effectiveness of additives, the strength, density and thermal conductivity of the foamed materials were optimised, displaying material performance superior to that of existing cement-based insulation materials.

8.3 Outlook

Combined with the outputs of the above research work, the focus of future research may be based on the following three areas:

- As demonstrated in this thesis, the addition of waste glass can effectively reduce the quantity of silicate for chemical activation of aluminosilicate materials. Nevertheless, the presence of the sodium hydroxide is inevitably preventing any further reduction in production costs and health risks. Therefore, it is necessary to conduct further research on reducing the dosage of sodium hydroxide by exploring the use of alkali from the chemical waste stream.
- Further investigations on the porosity and the distribution of products are required to elucidate the microstructure-property relationship of the system substituted by WG.
- Compared to the history of Portland cement which boasts a history of more than a century, in-depth durability orientated research on AABs has only been done in the last few decades. Thus, for AABs to have a chance of acceptance in the engineering practice, its long-term performance must be documented and verified.
- Alkali-activated concrete, like Portland cement concrete, requires a variety of additives to make its performance suitable for a variety of applications, while the existing Portland cement concrete is suitable for various additives, an important research direction would also be to develop a series of additives suitable for alkali-activated systems.
- The physical interaction between the ME-LWA and TMW-WG AAB should be further studied. The technique of macro-encapsulation explored in this study should be investigated with other relevant host materials such as construction and demolition waste.

8. REFERENCES

(CEN) European Committee for Standardization (2005a) *Methods of testing cement - Part 3: Determination of setting times and soundness*.
(CEN) European Committee for Standardization (2005b) *Methods of testing cement - Part 3: Determination of setting times and soundness. EN 196-3:2005+A1*.
(CEN) European Committee for Standardization (2006) *Methods of test for mortar for masonry — Part 3: Determination of consistence of fresh mortar (by flow table). EN 1015-3:1999, BS EN 1015-3:1999 +A2*.
Abhat, A. (1983) 'Low temperature latent heat thermal energy storage: Heat storage materials', *Solar Energy*, 30(4), pp. 313–332. doi: 10.1016/0038-092X(83)90186-X.
ACM (2009) *Case Study Swan Street Bridge Retaining Walls*. Victoria. Available at: goo.gl/UzuxSa.
Ahmari, S. and Zhang, L. (2012) 'Production of eco-friendly bricks from copper mine tailings through geopolymerization', *Constr. Build. Mater.* Elsevier Ltd, 29, pp. 323–331. doi: 10.1016/j.conbuildmat.2011.10.048.
Air Force Office of Scientific Research (2010) *Fire Resistance of Geopolymer Concretes*. Available at: goo.gl/EQBcpN (Accessed: 21 November 2016).
Akbulut, H. and Gürer, C. (2007) 'Use of aggregates produced from marble quarry waste in asphalt pavements', *Building and Environment*, 42(5), pp. 1921–1930. doi: http://dx.doi.org/10.1016/j.buildenv.2006.03.012.
Akeiber, H. J. *et al.* (2016) 'Profduction application of paraffin waxes refining process in Iraq and used as phase change materials', 4(2320), pp. 96–100.
Alahrache, S. *et al.* (2016) 'Chemical activation of hybrid binders based on siliceous fly ash and Portland cement', *Cement and Concrete Composites*. Elsevier Ltd, 66, pp. 10–23. doi: 10.1016/j.cemconcomp.2015.11.003.
Allwood, J. M., Cullen, J. M. and Milford, R. L. (2010) 'Options for achieving a 50% cut in industrial carbon emissions by 2050', *Environmental Science and Technology*, 44(6), pp. 1888–1894. doi: 10.1021/es902909k.
Arellano-Aguilar, R. *et al.* (2014) 'Geopolymer mortars based on a low grade metakaolin: Effects of the chemical composition, temperature and aggregate:binder ratio', *Construction and Building Materials*. Elsevier, 50, pp. 642–648. doi: 10.1016/j.conbuildmat.2013.10.023.
Ariffin, M. A. M. *et al.* (2013) 'Sulfuric acid resistance of blended ash geopolymer

concrete', *Construction and Building Materials*, 43, pp. 80–86. doi: 10.1016/j.conbuildmat.2013.01.018.
ASCEM B.V. (2015) 'Cement compound and a method for the production thereof. Patent WO/2015/187022'. Google Patents. Available at: goo.gl/hnsxMW.
Assaedi, H., Shaikh, F. U. A. and Low, I. M. (2015) 'Effect of nano-clay on mechanical and thermal properties of geopolymer'. Taibah University.
Bădănoiu, A. I., Abood Al-Saadi, T. H. and Voicu, G. (2015) 'Synthesis and properties of new materials produced by alkaline activation of glass cullet and red mud', *Int. J. Miner. Process.*, 135, pp. 1–10. doi: 10.1016/j.minpro.2014.12.002.
Bakharev, T. (2005) 'Geopolymeric materials prepared using Class F fly ash and elevated temperature curing', *Cem. Concr. Res.*, 35(6), pp. 1224–1232. doi: 10.1016/j.cemconres.2004.06.031.
Barbosa, V. F. F. and MacKenzie, K. J. D. (2003) 'Synthesis and Thermal Behaviour of Potassium Silate Geopolymers', *Materials Letters*, 57, pp. 1477–1482. doi: 10.1016/S0167-577X(02)01009-1.
Barbosa, V. F. F., Mackenzie, K. J. D. and Thaumaturgo, C. (1999) 'Synthesis and Characterization of Sodium Polysialate Inorganic Polymer Based on Alumina and Silica', *Geopolymer international conference*, 2, pp. 65–78. doi: 10.1016/S1466-6049(00)00041-6.
BASF (2009) *Intelligent Temperature Management for Buildings*. Available at: http://www.micronal.de/portal/basf/ien/dt.jsp?setCursor=1_290798 (Accessed: 15 September 2015).
Bernal, S. A. and Provis, J. L. (2014) 'Durability of alkali-activated materials: Progress and perspectives', *Journal of the American Ceramic Society*, 97(4), pp. 997–1008. doi: 10.1111/jace.12831.
Blackford, M. G. *et al.* (2007) 'Transmission Electron Microscopy and Nuclear Magnetic Resonance Studies of Geopolymers for Radioactive Waste Immobilization', *Journal of the American Ceramic Society*, 90(4), pp. 1193–1199. doi: 10.1111/j.1551-2916.2007.01532.x.
Blissett, R. S. and Rowson, N. A. (2012) 'A review of the multi-component utilisation of coal fly ash', *Fuel*. Elsevier Ltd, 97, pp. 1–23. doi: 10.1016/j.fuel.2012.03.024.
Blockstein, D. and Wiegman, L. (2009) *The Climate Solutions Consensus: What We Know and What To Do About It*. Island Press. Available at: https://books.google.co.uk/books?id=Uc4IQwAACAAJ.
British Standards Institution (2016) *Alkali-activated cementitious material and concrete – PAS 8820:2016*.
Brough, A. R. and Atkinson, A. (2002) 'Sodium silicate-based, alkali-activated slag mortars - Part I. Strength, hydration and microstructure', *Cement and Concrete Research*, 32(6), pp. 865–879. doi: 10.1016/S0008-8846(02)00717-2.
BSI Standards Publication (2011) *BSI Standards Publication Cement Part 1 : Composition , specifications and*.
Buchwald, A. *et al.* (2015) 'Purdocement: application of alkali-activated slag cement in Belgium in the 1950s', *Materials and Structures*, 48(1), pp. 501–511. doi: 10.1617/s11527-013-0200-8.
Buchwald, A., Hilbig, H. and Kaps, C. (2007) 'Alkali-activated metakaolin-slag blends - Performance and structure in dependence of their composition', *Journal of Materials Science*, 42(9), pp. 3024–3032. doi: 10.1007/s10853-006-0525-6.
Cabeza, L. F. *et al.* (2007) 'Use of microencapsulated PCM in concrete walls for energy savings', *Energy and Buildings*, 39(2), pp. 113–119. doi: 10.1016/j.enbuild.2006.03.030.
Cabeza, L. F. *et al.* (2011) 'Materials used as PCM in thermal energy storage in buildings: A review', *Renewable and Sustainable Energy Reviews*. Elsevier, 15(3), pp. 1675–1695. doi: 10.1016/j.rser.2010.11.018.

Cao, Z. *et al.* (2016) 'Effect of calcination condition on the microstructure and pozzolanic activity of calcined coal gangue', *International Journal of Mineral Processing*. Elsevier B.V., 146, pp. 23–28. doi: 10.1016/j.minpro.2015.11.008.
Carroll, R. A. (2015) 'Coal Combustion Products in the United Kingdom and the Potential of Stockpile Ash', in *2015 World of Coal Ash (WOCA) Conference*. Nashville, p. 7.
Castellón, C. *et al.* (2010) 'Effect of microencapsulated phase change material in sandwich panels', *Renewable Energy*, 35(10), pp. 2370–2374. doi: https://doi.org/10.1016/j.renene.2010.03.030.
CEN (European Commitee for Standardization) (2005) *Admixtures for concrete, mortar and grout-Part 4: Determination of bleeding of concrete. BS EN 480-4:2005*.
CEN (European Commitee for Standardization) (2011) *Tests for mechanical and physical properties of aggregates Part 1 : Determination of the resistance*.
Chen, X., Meawad, A. and Struble, L. J. (2014) 'Method to stop geopolymer reaction', *J. Am. Ceram. Soc.*, 97(10), pp. 3270–3275. doi: 10.1111/jace.13071.
Cheng, H. *et al.* (2015) 'The effects of SiO2/Na2O molar ratio on the characteristics of alkali-activated waste catalyst–metakaolin based geopolymers', *Construction and Building Materials*, 95, pp. 710–720. doi: 10.1016/j.conbuildmat.2015.07.028.
Chindaprasirt, P., Chareerat, T. and Sirivivatnanon, V. (2007) 'Workability and strength of coarse high calcium fly ash geopolymer', *Cement and Concrete Composites*, 29(3), pp. 224–229. doi: 10.1016/j.cemconcomp.2006.11.002.
Chindaprasirt, P., Homwuttiwong, S. and Jaturapitakkul, C. (2007) 'Strength and water permeability of concrete containing palm oil fuel ash and rice husk–bark ash', *Construction and Building Materials*, 21(7), pp. 1492–1499. doi: 10.1016/j.conbuildmat.2006.06.015.
Choi, Y. W. *et al.* (2009) 'Utilization of tailings from tungsten mine waste as a substitution material for cement', *Constr. Build. Mater.*, 23(7), pp. 2481–2486. doi: 10.1016/j.conbuildmat.2009.02.006.
Christiansen, M. U. and Sutter, L. L. (2013) 'ACI SP 294 - Advances in green binder systems', in Neithalath, N. and Hicks, J. (eds) *Waste glass for use in geopolymers*. ACI, pp. 31–48.
Criado, M., Palomo, A. and Fernández-Jiménez, A. (2005) 'Alkali activation of fly ashes. Part 1: Effect of curing conditions on the carbonation of the reaction products', *Fuel*, 84(16), pp. 2048–2054. doi: 10.1016/j.fuel.2005.03.030.
Cui, Y. *et al.* (2011) 'The experimental exploration of carbon nanofiber and carbon nanotube additives on thermal behavior of phase change materials', *Solar Energy Materials and Solar Cells*. Elsevier, 95(4), pp. 1208–1212. doi: 10.1016/j.solmat.2011.01.021.
Dai, Y. S. *et al.* (2013) 'A Study on Application of Geopolymeric Green Cement', (I), pp. 15–22.
Das, S. K., Mohapatra, A. K. and Rath, a K. (2014) 'Geo-polymer Concrete – Green Concrete for the Future — A Review', *International Journal of Civil Engineering Research*, 5(1), pp. 21–28.
Davidovits, J. (1991) 'Geopolymers - Inorganic polymeric new materials', *Journal of Thermal Analysis*, 37(8), pp. 1633–1656. doi: 10.1007/BF01912193.
Davidovits, J. (2011) 'Application of Ca-based geopolymer with blast furnace slag , a review', *Proceeding of the Second International Slag Valorisation Symposium*, pp. 33–49.
Davidovits, J. (2015) *Geopolymer Chemistry and Applications*. 3rd edn. Saint-Quentin: Institut Geopolymere.
Davidovits, P. J. (2002) '30 Years of Successes and Failures in Geopolymer Applications . Market Trends and Potential Breakthroughs .', *Geopolymer 2002 Conference*, pp. 1–16.

doi: 10.1017/CBO9781107415324.004.
Van Deventer, J. S. J., Provis, J. L. and Duxson, P. (2012) 'Technical and commercial progress in the adoption of geopolymer cement', *Minerals Engineering*, 29, pp. 89–104. doi: 10.1016/j.mineng.2011.09.009.
Dimas, D. D., Giannopoulou, I. P. and Panias, D. (2009) 'Utilization of Alumina Red Mud for Synthesis of Inorganic Polymeric Materials', *Mineral Processing and Extractive Metallurgy Review*. Taylor & Francis, 30(3), pp. 211–239. doi: 10.1080/08827500802498199.
Dincer, I. and Rosen, M. (2010) *Thermal energy storage: systems and applications*. 2nd Editio. Wiley.
Dixit, M. K. *et al.* (2010) 'Identification of parameters for embodied energy measurement: A literature review', *Energy and Buildings*, 42(8), pp. 1238–1247. doi: 10.1016/j.enbuild.2010.02.016.
Donatello, S., Fernández-Jimenez, A. and Palomo, A. (2013) 'Very high volume fly ash cements. Early age hydration study using Na 2SO4 as an activator', *Journal of the American Ceramic Society*, 96(3), pp. 900–906. doi: 10.1111/jace.12178.
Dong, J., Wang, L. and Zhang, T. (2014) 'Study on the strength development, hydration process and carbonation process of NaOH-activated Pisha Sandstone', *Construction and Building Materials*. Elsevier, 66, pp. 154–162. doi: 10.1016/j.conbuildmat.2014.05.075.
Dong, Z. *et al.* (2016) 'Development of Hollow Steel Ball Macro-Encapsulated PCM for Thermal Energy Storage Concrete', *Materials*, 9(1), p. 59.
Doroudiani, S. and Omidian, H. (2010) 'Environmental, health and safety concerns of decorative mouldings made of expanded polystyrene in buildings', *Building and Environment*, 45(3), pp. 647–654. doi: http://dx.doi.org/10.1016/j.buildenv.2009.08.004.
Duxson, P. *et al.* (2005) 'Understanding the relationship between geopolymer composition, microstructure and mechanical properties', *Colloids and Surfaces A: Physicochemical and Engineering Aspects*, 269(1–3), pp. 47–58. doi: 10.1016/j.colsurfa.2005.06.060.
Duxson, P. *et al.* (2006) '39K NMR of Free Potassium in Geopolymers', *Industrial & Engineering Chemistry Research*, 45(26), pp. 9208–9210.
Duxson, P. *et al.* (2007) 'Geopolymer technology: the current state of the art', *Journal of Materials Science*, 42(9), pp. 2917–2933. doi: 10.1007/s10853-006-0637-z.
Duxson, P., Lukey, G. C. and van Deventer, J. S. J. (2006) '1.Thermal Conductivity of Metakaolin Geopolymers Used as a First Approximation for Determining Gel Interconnectivity', *Industrial & Engineering Chemistry Research*, 45(23), pp. 7781–7788.
Duxson, P. and Provis, J. L. (2008) 'Designing precursors for geopolymer cements', *Journal of the American Ceramic Society*, 91(12), pp. 3864–3869. doi: 10.1111/j.1551-2916.2008.02787.x.
Economist (2014) *Why the oil price is falling*. Available at: https://goo.gl/pVIjNL (Accessed: 23 April 2016).
Eddhahak-Ouni, A. *et al.* (2014) 'Experimental and multi-scale analysis of the thermal properties of Portland cement concretes embedded with microencapsulated Phase Change Materials (PCMs)', *Applied Thermal Engineering*. Elsevier Ltd, 64(1–2), pp. 32–39. doi: 10.1016/j.applthermaleng.2013.11.050.
EFNARC (2002) *Specification and Guidelines for Self-Compacting Concrete*, *Report from EFNARC*. doi: 0 9539733 4 4.
EU Commission (2014) *Construction Products - (EU) 305/2011*. Available at: https://goo.gl/bWFivT.
EuropaProperty (2015) *Construction industry in Russia to resume growth in 2016*. Available at: https://goo.gl/qFt4G2 (Accessed: 17 April 2016).
European Cement Association (2014) *The role of cement in the 2050 low carbon economy*.

Available at: https://goo.gl/GFkrGc (Accessed: 5 July 2016).
European Commission (2012) 'Roadmap 2050', *Policy*, (April), pp. 1–9. doi: 10.2833/10759.
Eurostat (2016a) *Europe 2020 indicators - climate change and energy*. Available at: https://goo.gl/X2LBkW (Accessed: 10 September 2016).
Eurostat (2016b) *Waste Statistics*. Available at: https://goo.gl/nf67ci (Accessed: 28 April 2016).
F. Pacheco-Torgal, J. A. L., C. Leonelli, A. P. and and Chindaprasirt, P. (2013) *Handbook of Alkaliactivated Cements, Mortars and Concretes*, *Woodhead Publishing*. doi: 10.1017/CBO9781107415324.004.
Feldman, D., Banu, D. and Hawes, D. W. (1995) 'Development and application of organic phase change mixtures in thermal storage gypsum wallboard', *Solar Energy Materials and Solar Cells*, 36(2), pp. 147–157. doi: 10.1016/0927-0248(94)00168-R.
Feng, D. *et al.* (2005) 'Preparation of Geopolymeric Materials from Fly Ash Filler by Steam Curing with Special Reference to Binder Products', *Journal of the Ceramic Society of Japan*, 113(1313), pp. 82–86. doi: 10.2109/jcersj.113.82.
Fernandez-Jimenez, A. *et al.* (2005) 'Immobilization of cesium in alkaline activated fly ash matrix', *Journal of Nuclear Materials*, 346(2–3), pp. 185–193. doi: 10.1016/j.jnucmat.2005.06.006.
Fernández-Jiménez, A. *et al.* (2006) 'The role played by the reactive alumina content in the alkaline activation of fly ashes', *Microporous and Mesoporous Materials*, 91(1–3), pp. 111–119. doi: 10.1016/j.micromeso.2005.11.015.
Fernández-Jiménez, A. M., Palomo, A. and López-Hombrados, C. (2006) 'Engineering properties of alkali-activated fly ash concrete', *ACI Materials Journal*, 103(2), pp. 106–112.
Fernández-Jiménez, A. and Palomo, A. (2003) 'Characterisation of fly ashes. Potential reactivity as alkaline cements', *Fuel*, 82(18), pp. 2259–2265. doi: 10.1016/S0016-2361(03)00194-7.
Fernández-Jiménez, A. and Palomo, A. (2005) 'Composition and microstructure of alkali activated fly ash binder: Effect of the activator', *Cement and Concrete Research*, 35(10), pp. 1984–1992. doi: 10.1016/j.cemconres.2005.03.003.
Fernández-Jiménez, A., Palomo, A. and Criado, M. (2006) 'Alkali activated fly ash binders. A comparative study between sodium and potassium activators', *Materiales de Construcción*, 56(281), pp. 51–65. doi: 10.3989/mc.2006.v56.i281.92.
Fernández-Jiménez, A., Palomo, J. G. and Puertas, F. (1999) 'Alkali-activated slag mortars: Mechanical strength behaviour', *Cement and Concrete Research*, 29(8), pp. 1313–1321. doi: http://dx.doi.org/10.1016/S0008-8846(99)00154-4.
Franco, A., Vieira, R. and Bunting, R. (2014) 'The Panasqueira Mine at a Glance', *Tungsten*, pp. 1–12.
Frias, M. *et al.* (2006) 'Recycling of silicomanganese slag as pozzolanic material in Portland cements: Basic and engineering properties', *Cement and Concrete Research*, 36(3), pp. 487–491. doi: 10.1016/j.cemconres.2005.06.014.
Frusteri, F. *et al.* (2005) 'Thermal conductivity measurement of a PCM based storage system containing carbon fibers', *Applied Thermal Engineering*, 25(11–12), pp. 1623–1633. doi: 10.1016/j.applthermaleng.2004.10.007.
Fu, Y. X. *et al.* (2014) 'Thermal conductivity enhancement with different fillers for epoxy resin adhesives', *Applied Thermal Engineering*. Elsevier Ltd, 66(1–2), pp. 493–498. doi: 10.1016/j.applthermaleng.2014.02.044.
Galán, E., González, I. and Fernández-Caliani, J. C. (2002) 'Residual pollution load of soils impacted by the Aznalcóllar (Spain) mining spill after clean-up operations', *Science*

of The Total Environment, 286(1–3), pp. 167–179. doi: http://dx.doi.org/10.1016/S0048-9697(01)00974-3.
Garcia-Lodeiro, I., Fernandez-Jimenez, A. and Palomo, A. (2013a) 'Hydration kinetics in hybrid binders: Early reaction stages', *Cement and Concrete Composites*. Elsevier Ltd, 39, pp. 82–92. doi: 10.1016/j.cemconcomp.2013.03.025.
Garcia-Lodeiro, I., Fernandez-Jimenez, A. and Palomo, A. (2013b) 'Variation in hybrid cements over time. Alkaline activation of fly ash-portland cement blends', *Cement and Concrete Research*. Elsevier Ltd, 52, pp. 112–122. doi: 10.1016/j.cemconres.2013.03.022.
Gelencsér, A. *et al.* (2011) 'The red mud accident in Ajka (Hungary): characterization and potential health effects of fugitive dust.', *Environmental science & technology*. American Chemical Society, 45(4), pp. 1608–15. doi: 10.1021/es104005r.
Geopolymer Institute (2011) *Selected list of laboratories and institutions involved in R&D projects on geopolymer science and technology*. Available at: https://goo.gl/3c3r1n (Accessed: 4 April 2016).
Geopolymer Institute (2013) *World's first public building with structural Geopolymer Concrete*. Available at: https://goo.gl/GupnsF (Accessed: 4 April 2016).
Geopolymer Institute (2014) *70,000 tonnes Geopolymer Concrete for airport*. Available at: https://goo.gl/meRNKe (Accessed: 4 April 2016).
Georgopoulos, C. and Minson, A. (2014) 'Material Specification', in *Sustainable Concrete Solutions*. Wiley-Blackwell, pp. 118–129.
Glass for Europe (2013) *Recycling of end-of-life building glass*. Available at: goo.gl/CzmEvs (Accessed: 8 January 2017).
Görhan, G. and Kürklü, G. (2014) 'The influence of the NaOH solution on the properties of the fly ash-based geopolymer mortar cured at different temperatures', *Composites Part B: Engineering*, 58, pp. 371–377. doi: 10.1016/j.compositesb.2013.10.082.
Gräfe, M., Power, G. and Klauber, C. (2011) 'Bauxite residue issues: III. Alkalinity and associated chemistry', *Hydrometallurgy*, 108(1–2), pp. 60–79. doi: 10.1016/j.hydromet.2011.02.004.
Granizo, M. L. *et al.* (2002) 'Alkaline Activation of Metakaolin : Effect of Calcium Hydroxide in the Products of Reaction', *J. Am. Ceram. Soc.*, 85, pp. 225–231. doi: doi:10.1111/j.1151-2916.2002.tb00070.x.
Granizo, M. L., Blanco-Varela, M. T. and Martínez-Ramírez, S. (2007) 'Alkali activation of metakaolins: parameters affecting mechanical, structural and microstructural properties', *Journal of Materials Science*, 42(9), pp. 2934–2943. doi: 10.1007/s10853-006-0565-y.
Granizo, M. L. and Blanco, M. T. (1998) 'Alkaline Activation of Metakaolin An Isothermal Conduction Calorimetry Study', *Journal of Thermal Analysis and Calorimetry*, 52(3), pp. 957–965. doi: 10.1023/A:1010176321136.
Habert, G., d'Espinose de Lacaillerie, J. B. and Roussel, N. (2011) 'An environmental evaluation of geopolymer based concrete production: reviewing current research trends', *Journal of Cleaner Production*, 19(11), pp. 1229–1238. doi: 10.1016/j.jclepro.2011.03.012.
Hajjaji, W. *et al.* (2013) 'Composition and technological properties of geopolymers based on metakaolin and red mud', *Materials and Design*, 52, pp. 648–654. doi: 10.1016/j.matdes.2013.05.058.
Hardjito, D. *et al.* (2009) 'Strength and setting times of low calcium fly ash-based geopolymer mortar', *Modern Applied Science*, 2(4), p. P3. doi: 10.5539/mas.v2n4P3.
Hardjito D., Wallah S. E. Sumajouw D.M.J., R. B. V. (2004) 'On the Development of Fly AshBased Geopolymer Concrete', *ACI Materials Journal/November-December*, (December), pp. 467–472.
Harris, J., Rumack, B. and Aldrich, F. (1981) 'Toxicology of Urea Formaldehyde and

Polyurethane Foam Insulation', *JAMA*, 245(3), pp. 243–246. doi: 10.1001/jama.1981.03310280019020.
Hawa, A. *et al.* (2013) 'Development and Performance Evaluation of Very High Early Strength Geopolymer for Rapid Road Repair', *Advances in Materials Science and Engineering*, 2013, p. 9. doi: 10.1155/2013/764180.
Heah, C. Y. *et al.* (2011) 'Effect of Curing Profile on Kaolin-based Geopolymers', *Physics Procedia*, 22, pp. 305–311. doi: http://dx.doi.org/10.1016/j.phpro.2011.11.048.
Hebhoub, H. *et al.* (2011) 'Use of waste marble aggregates in concrete', *Construction and Building Materials*. Elsevier, 25(3), pp. 1167–1171. doi: 10.1016/j.conbuildmat.2010.09.037.
Van Den Heede, P. and De Belie, N. (2012) 'Environmental impact and life cycle assessment (LCA) of traditional and "green" concretes: Literature review and theoretical calculations', *Cement and Concrete Composites*. Elsevier Ltd, 34(4), pp. 431–442. doi: 10.1016/j.cemconcomp.2012.01.004.
Heiser, J. A. and King, J. A. (2004) 'Thermally Conductive Carbon Filled Nylon 6,6', *polymer composites*, 25(2), pp. 186–193. doi: 10.1002/pc.20015.
Henon, J. *et al.* (2013) 'Potassium geopolymer foams made with silica fume pore forming agent for thermal insulation', *Journal of Porous Materials*, 20(1), pp. 37–46. doi: 10.1007/s10934-012-9572-3.
Hind, A. R., Bhargava, S. K. and Grocott, S. C. (1999) 'The surface chemistry of Bayer process solids: a review', *Colloids and Surfaces A: Physicochemical and Engineering Aspects*, 146(1–3), pp. 359–374. doi: 10.1016/S0927-7757(98)00798-5.
Hlaváček, P. *et al.* (2015) 'Inorganic foams made from alkali-activated fly ash: Mechanical, chemical and physical properties', *Journal of the European Ceramic Society*, 35(2), pp. 703–709. doi: http://dx.doi.org/10.1016/j.jeurceramsoc.2014.08.024.
Hu, Y., Chung, Y. J. and Mackenzie, J. D. (1993) 'Gelation kinetics of an organically modified silicate', *Journal of Materials Science*, 28(24), pp. 6549–6554. doi: 10.1007/BF00356392.
Huang, K. *et al.* (2016) 'Macro-Encapsulated PCM Cylinder Module Based on Paraffin and Float Stones', *Materials*, 9(5), p. 361. doi: 10.3390/ma9050361.
Hunger, M. *et al.* (2009) 'The behavior of self-compacting concrete containing micro-encapsulated Phase Change Materials', *Cement and Concrete Composites*. Elsevier Ltd, 31(10), pp. 731–743. doi: 10.1016/j.cemconcomp.2009.08.002.
Huntzinger, D. N. and Eatmon, T. D. (2009) 'A life-cycle assessment of Portland cement manufacturing: comparing the traditional process with alternative technologies', *Journal of Cleaner Production*. Elsevier Ltd, 17(7), pp. 668–675. doi: 10.1016/j.jclepro.2008.04.007.
IAL Consultants (2015) *The European Market for Thermal Insulation Products*. London. Available at: www.ialconsultants.com.
Ilić, B. R., Mitrović, A. A. and Miličić, L. (2010) 'Thermal treatment of kaolin clay to obtain metakaolin', *Hemijska Industrija*, 64(4), pp. 351–356. doi: 10.2298/HEMIND100322014I.
Investing News (2015a) *Tungsten Uses: Cemeted Carbide, Alloys and More*. Available at: https://goo.gl/eSDvZP (Accessed: 8 April 2016).
Investing News (2015b) *When Will the Tungsten Price Go Up?* Available at: https://goo.gl/MLUfGo (Accessed: 8 April 2016).
Van Jaarsveld, J.G.S., Van Deventer, J. S. J. (1999) 'Effect of the Alkali Metal Activator on the Properties of Fly Ash Based Geopolymers', *Ind. Eng. Chem. Res. 38*, pp. 3932–3941. Available at: http://dx.doi.org/10.1021/ie980804b.
Van Jaarsveld, J. G. ., Van Deventer, J. S. . and Lukey, G. C. (2002) 'The effect of composition and temperature on the properties of fly ash- and kaolinite-based

geopolymers', *Chem. Eng. J.*, 89(1–3), pp. 63–73. doi: 10.1016/S1385-8947(02)00025-6.
Van Jaarsveld, J. G. S. and Van Deventer, J. S. J. (1999) 'Effect of metal contaminants on the formation and properties of waste-based geopolymers', *Cem. Concr. Res.*, 29(8), pp. 1189–1200. doi: 10.1016/S0008-8846(99)00032-0.
Van Jaarsveld, J. G. S., Van Deventer, J. S. J. and Lorenzen, L. (1997) 'The potential use of geopolymeric materials to immobilise toxic metals: Part I. Theory and applications', *Minerals Engineering*, 10(7), pp. 659–669. doi: 10.1016/S0892-6875(97)00046-0.
Van Jaarsveld, J. G. S., Van Deventer, J. S. J. and Lorenzen, L. (1998) 'Factors affecting the immobilization of metals in geopolymerized flyash', *Metallurgical and Materials Transactions B*, 29(1), pp. 283–291. doi: 10.1007/s11663-998-0032-z.
Van Jaarsveld, J. G. S., Van Deventer, J. S. J. and Lukey, G. C. (2002) 'The effect of composition and temperature on the properties of fly ash- and kaolinite-based geopolymers', *Chemical Engineering Journal*, 89(1–3), pp. 63–73. doi: 10.1016/S1385-8947(02)00025-6.
Van Jaarsveld, J. G. S., Van Deventer, J. S. J. and Schwartzman, a. (1999) 'The potential use of geopolymeric materials to immobilise toxic metals: Part II. Material and leaching characteristics', *Minerals Engineering*, 12(1), pp. 75–91. doi: 10.1016/S0892-6875(98)00121-6.
Jacob, R. and Bruno, F. (2015) 'Review on shell materials used in the encapsulation of phase change materials for high temperature thermal energy storage', *Renewable and Sustainable Energy Reviews*, 48, pp. 79–87. doi: https://doi.org/10.1016/j.rser.2015.03.038.
Jayalath, A. *et al.* (2011) 'Applications of Phase Change Materials in Concrete for Sustainable Built Environment : A Review', *International Conference on Structural Engineering, Construction and Management*, pp. 1–13.
Jiao, X., Zhang, Y. and Chen, T. (2013) 'Thermal stability of a silica-rich vanadium tailing based geopolymer', *Construction and Building Materials*. Elsevier Ltd, 38, pp. 43–47. doi: 10.1016/j.conbuildmat.2012.06.076.
Joshi, S. V. and Kadu, M. S. (2012) 'Role of alkaline activator in development of eco-friendly fly Ash based geo polymer concrete', *International Journal of Environmental Science and Development*, 3(5), pp. 417–421. doi: 10.7763/IJESD.2012.V3.258.
Juška, G. *et al.* (2000) 'Charge transport in pi-conjugated polymers from extraction current transients', *Phys. Rev. B*, 62(24), pp. R16235--R16238. doi: 10.1103/PhysRevB.62.R16235.
Kanagaraj, G. and Mahalingam, A. (2011) 'Designing energy efficient commercial buildings - A systems framework', *Energy and Buildings*. Elsevier B.V., 43(9), pp. 2329–2343. doi: 10.1016/j.enbuild.2011.05.023.
Kastiukas, G., Zhou, X. and Castro-Gomes, J. (2016) 'Development and optimisation of phase change material-impregnated lightweight aggregates for geopolymer composites made from aluminosilicate rich mud and milled glass powder', *Constr. Build. Mater.*, 110, pp. 201–210. doi: 10.1016/j.conbuildmat.2016.02.029.
Katz, A. (1998) 'Microscopic Study of Alkali-Activated Fly Ash', *Cement and Concrete Research*, 28(2), pp. 197–208. doi: http://dx.doi.org/10.1016/S0008-8846(97)00271-8.
Kay, E. A. (2003) '5 - Hot and cold weather concreting', in Newman, J. and Choo, B. S. (eds) *Advanced Concrete Technology*. Oxford: Butterworth-Heinemann, pp. 1–18. doi: http://dx.doi.org/10.1016/B978-075065686-3/50252-4.
Ken, P. W., Ramli, M. and Ban, C. C. (2015) 'An overview on the influence of various factors on the properties of geopolymer concrete derived from industrial by-products', *Construction & Building Materials*. Elsevier Ltd, 77, pp. 370–395. doi: 10.1016/j.conbuildmat.2014.12.065.
Khadiran, T. *et al.* (2015) 'Encapsulation techniques for organic phase change materials as

thermal energy storage medium: A review', *Solar Energy Materials and Solar Cells*. Elsevier, 143, pp. 78–98. doi: 10.1016/j.solmat.2015.06.039.
Khale, D. and Chaudhary, R. (2007) 'Mechanism of geopolymerization and factors influencing its development: A review', *Journal of Materials Science*, 42(3), pp. 729–746. doi: 10.1007/s10853-006-0401-4.
Khankhaje, E. *et al.* (2016) 'On blended cement and geopolymer concretes containing palm oil fuel ash', *Materials and Design*, 89, pp. 385–398. doi: 10.1016/j.matdes.2015.09.140.
Khater, H. M. (2012) 'Effect of Calcium on Geopolymerization of Aluminosilicate Wastes', *Journal of Materials in Civil Engineering*, 24(1), pp. 92–101. doi: 10.1061/(ASCE)MT.1943-5533.0000352.
Khater, H. M. (2013) 'Effect of silica fume on the characterization of the geopolymer materials', *International Journal of Advanced Structural Engineering*, 5(1), p. 12. doi: 10.1186/2008-6695-5-12.
Kheradmand, M. *et al.* (2014) 'Thermal behavior of cement based plastering mortar containing hybrid microencapsulated phase change materials', *Energy and Buildings*. Elsevier B.V., 84, pp. 526–536. doi: 10.1016/j.enbuild.2014.08.010.
Kheradmand, M. *et al.* (2015) 'Assessing the feasibility of impregnating phase change materials in lightweight aggregate for development of thermal energy storage systems', *Construction and Building Materials*. Elsevier Ltd, 89, pp. 48–59. doi: 10.1016/j.conbuildmat.2015.04.031.
Khudhair, A. M. and Farid, M. M. (2004) 'A review on energy conservation in building applications with thermal storage by latent heat using phase change materials', *Energy Conversion and Management*, 45(2), pp. 263–275. doi: 10.1016/S0196-8904(03)00131-6.
Kinuthia, J. M. *et al.* (2000) 'Self-compensating autogenous shrinkage in Portland cement—metakaolin—fly ash pastes', *Advances in Cement Research*, 12(1), pp. 35–43. doi: 10.1680/adcr.2000.12.1.35.
Kirkpatrick, T. and Pyrament, N. V (1985) *Potential applications of alkali-activated aluminosilicate binders in military operations*. Vicksburg. MI.
Komljenović, M., Baščarević, Z. and Bradić, V. (2010) 'Mechanical and microstructural properties of alkali-activated fly ash geopolymers', *Journal of Hazardous Materials*, 181(1–3), pp. 35–42. doi: 10.1016/j.jhazmat.2010.04.064.
Komnitsas, K. and Zaharaki, D. (2007) 'Geopolymerisation: A review and prospects for the minerals industry', *Minerals Engineering*, 20(14), pp. 1261–1277. doi: http://dx.doi.org/10.1016/j.mineng.2007.07.011.
Kong, D. L. Y., Sanjayan, J. G. and Sagoe-Crentsil, K. (2007) 'Comparative performance of geopolymers made with metakaolin and fly ash after exposure to elevated temperatures', *Cement and Concrete Research*, 37(12), pp. 1583–1589. doi: http://dx.doi.org/10.1016/j.cemconres.2007.08.021.
Kosny, J., Shukla, N. and Fallahi, A. (2013) *Cost Analysis of Simple Phase Change Material-Enhanced Building Envelopes in Southern U.S climates*. Available at: http://www.nrel.gov/docs/fy13osti/55553.pdf.
Kriven, W. M., Bell, J. L. and Gordon, M. (2012) 'Microstructure and Microchemistry of Fully-Reacted Geopolymers and Geopolymer Matrix Composites', in Bansal, N. P. et al. (eds) *Advances in Ceramic Matrix Composites IX, Volume 153*. Hoboken, NJ: John Wiley & Sons, Inc. doi: 10.1002/9781118406892.ch15.
Krivenko, P. V (1994) 'Alkaline Cements', in *Proceedings of the First International Conference Edited by*. Kiev, Ukraine: VIPOL Stock Company, pp. 11–129.
Kühl, H. (1908) 'Slag cement and process of making the same - US900939 A'. Germany.
Kumar, S. *et al.* (2013) 'Development of alkali activated cement from mechanically

activated silico-manganese (SiMn) slag', *Cement and Concrete Composites*, 40, pp. 7–13. doi: 10.1016/j.cemconcomp.2013.03.026.
Lafarge (2014) *Lafarge Press Publication - 2014 UK Annual Report*. Available at: https://goo.gl/Lcrs4x.
Lee, W. K. W. and Van Deventer, J. S. J. (2002) 'Structural reorganisation of class F fly ash in alkaline silicate solutions', *Colloids and Surfaces A: Physicochemical and Engineering Aspects*, 211(1), pp. 49–66. doi: 10.1016/S0927-7757(02)00237-6.
Li, C., Sun, H. and Li, L. (2010) 'A review: The comparison between alkali-activated slag (Si + Ca) and metakaolin (Si + Al) cements', *Cement and Concrete Research*, 40(9), pp. 1341–1349. doi: http://dx.doi.org/10.1016/j.cemconres.2010.03.020.
Li, X., Wang, Z. and Jiao, Z. (2013) 'Influence of curing on the strength development of calcium-containing geopolymer mortar', *Materials*, 6(11), pp. 5069–5076. doi: 10.3390/ma6115069.
Lin, K.-L. *et al.* (2012) 'Effect of composition on characteristics of thin film transistor liquid crystal display (TFT-LCD) waste glass-metakaolin-based geopolymers', *Construction and Building Materials*, 36, pp. 501–507. doi: http://dx.doi.org/10.1016/j.conbuildmat.2012.05.018.
Liu, L. P. *et al.* (2012) 'The phase evolution of phosphoric acid-based geopolymers at elevated temperatures', *Materials Letters*. Elsevier B.V., 66(1), pp. 10–12. doi: 10.1016/j.matlet.2011.08.043.
Lucas, C. (2001) 'The Baia Mare and Baia Borsa accidents: cases of severe transboundary water pollution', *Environmental Policy and Law*, 31(2), pp. 106–111.
Manso, M. *et al.* (2013) 'Modular system design for vegetated surfaces- A proposal for energy efficient buildings', in *BESS-SB13 CALIFORNIA: Advancing Towards Net Zero*. California, USA.
Manso, M., Castro-Gomes, J. and Silva, P. (2013) 'Modular system design for vegetated surfaces: a proposal for energy-efficient buildings', in *BESS-SB13: Advancing Towards Net Zero. Pomona, California, USA.*, pp. 1–6. Available at: http://repositorio.ipcb.pt/handle/10400.11/2037.
McLellan, B. C. *et al.* (2011) 'Costs and carbon emissions for geopolymer pastes in comparison to ordinary portland cement', *Journal of Cleaner Production*, 19(9–10), pp. 1080–1090. doi: 10.1016/j.jclepro.2011.02.010.
Memon, S. *et al.* (2015) 'Development of Composite PCMs by Incorporation of Paraffin into Various Building Materials', *Materials*, 8(2), pp. 499–518. doi: 10.3390/ma8020499.
Memon, S. A., Lo, T. Y., Barbhuiya, S. a., *et al.* (2013) 'Development of form-stable composite phase change material by incorporation of dodecyl alcohol into ground granulated blast furnace slag', *Energy and Buildings*. Elsevier B.V., 62, pp. 360–367. doi: 10.1016/j.enbuild.2013.03.026.
Memon, S. A., Lo, T. Y., Cui, H., *et al.* (2013) 'Preparation, characterization and thermal properties of dodecanol/cement as novel form-stable composite phase change material', *Energy and Buildings*. Elsevier B.V., 66, pp. 697–705. doi: 10.1016/j.enbuild.2013.07.083.
Memon, S. A., Lo, T. Y. and Cui, H. (2013) 'Utilization of waste glass powder for latent heat storage application in buildings', *Energy and Buildings*. Elsevier B.V., 66, pp. 405–414. doi: 10.1016/j.enbuild.2013.07.056.
Mijarsh, M. J. A., Megat Johari, M. A. and Ahmad, Z. A. (2014) 'Synthesis of geopolymer from large amounts of treated palm oil fuel ash: Application of the Taguchi method in investigating the main parameters affecting compressive strength', *Construction and Building Materials*. Elsevier Ltd, 52, pp. 473–481. doi: 10.1016/j.conbuildmat.2013.11.039.
Mikulčić, H. *et al.* (2012) 'The application of {CFD} modelling to support the reduction of

{CO2} emissions in cement industry', *Energy*, 45(1), pp. 464–473. doi: http://dx.doi.org/10.1016/j.energy.2012.04.030.
Minerals Council of Australia (2014) *Brown Coal – Lignite*. Victoria. Available at: https://goo.gl/zJuU8R.
Mo, B. *et al.* (2014) 'Effect of curing temperature on geopolymerization of metakaolin-based geopolymers', *Appl. Clay Sci.*, 99, pp. 144–148. doi: http://dx.doi.org/10.1016/j.clay.2014.06.024.
Mo, B. H. *et al.* (2014) 'Effect of curing temperature on geopolymerization of metakaolin-based geopolymers', *Applied Clay Science*. Elsevier B.V., 99, pp. 144–148. doi: 10.1016/j.clay.2014.06.024.
Mun, K. J. *et al.* (2007) 'Influence of fine tailings on polyester mortar properties', *Construction and Building Materials*, 21(6), pp. 1335–1341. doi: http://dx.doi.org/10.1016/j.conbuildmat.2005.12.021.
Murray, H. (2002) 'Industrial clays case study', *Mining, Minerals and Sustainable Development*, 1(64), pp. 1–9. Available at: http://whitemudresources.com/public/Hayn Murray Clays Case Study.pdf.
Najafi Kani, E., Allahverdi, A. and Provis, J. L. (2012) 'Efflorescence control in geopolymer binders based on natural pozzolan', *Cement and Concrete Composites*. Elsevier Ltd, 34(1), pp. 25–33. doi: 10.1016/j.cemconcomp.2011.07.007.
Napp, T. A. *et al.* (2014) 'A review of the technologies, economics and policy instruments for decarbonising energy-intensive manufacturing industries', *Renewable and Sustainable Energy Reviews*, 30, pp. 616–640. doi: http://dx.doi.org/10.1016/j.rser.2013.10.036.
Narayanan, N. and Ramamurthy, K. (2000) 'Structure and properties of aerated concrete: a review', *Cement and Concrete Composites*, 22(5), pp. 321–329. doi: http://dx.doi.org/10.1016/S0958-9465(00)00016-0.
Nature Materials (2007) 'The Asian Opportunity', *Nature Publishing Group*, p. 539. doi: 10.1038/nmat1975.
Nazari, A. *et al.* (2017) *Chapter 11 – An Overview on the Influence of Various Factors on the Properties of Geopolymer Concrete Derived From Industrial Byproducts, Handbook of Low Carbon Concrete*. Elsevier. doi: 10.1016/B978-0-12-804524-4.00011-7.
Nazari, A., Bagheri, A. and Riahi, S. (2011) 'Properties of geopolymer with seeded fly ash and rice husk bark ash', *Materials Science and Engineering A*. Elsevier B.V., 528(24), pp. 7395–7401. doi: 10.1016/j.msea.2011.06.027.
Nepomuceno, M. C. S. and Silva, P. D. (2014) 'Experimental evaluation of cement mortars with phase change material incorporated via lightweight expanded clay aggregate', *Construction and Building Materials*. Elsevier, 63, pp. 89–96. doi: 10.1016/j.conbuildmat.2014.04.027.
O'Brien, K. R., Ménaché, J. and O'Moore, L. M. (2009) 'Impact of fly ash content and fly ash transportation distance on embodied greenhouse gas emissions and water consumption in concrete', *International Journal of Life Cycle Assessment*, 14(7), pp. 621–629. doi: 10.1007/s11367-009-0105-5.
Oosterveer, P. (2015) 'Promoting sustainable palm oil: viewed from a global networks and flows perspective', *Journal of Cleaner Production*, 107, pp. 146–153. doi: 10.1016/j.jclepro.2014.01.019.
Pacheco-Torgal, F., Castro-Gomes, J. and Jalali, S. (2007) 'Investigations about the effect of aggregates on strength and microstructure of geopolymeric mine waste mud binders', *Cem. Concr. Res.*, 37(6), pp. 933–941. doi: 10.1016/j.cemconres.2007.02.006.
Pacheco-Torgal, F., Castro-Gomes, J. and Jalali, S. (2008a) 'Alkali-activated binders: A review. Part 1. Historical background, terminology, reaction mechanisms and hydration products', *Construction and Building Materials*, 22(7), pp. 1305–1314. doi:

10.1016/j.conbuildmat.2007.10.015.
Pacheco-Torgal, F., Castro-Gomes, J. and Jalali, S. (2008b) 'Properties of tungsten mine waste geopolymeric binder', *Construction and Building Materials*, 22(6), pp. 1201–1211. doi: 10.1016/j.conbuildmat.2007.01.022.
Pacheco-Torgal, F., Castro-Gomes, J. and Jalali, S. (2009) 'Tungsten mine waste geopolymeric binder: Preliminary hydration products investigations', *Constr. Build. Mater.*, 23(1), pp. 31–48. doi: 10.1016/j.conbuildmat.2008.01.003.
Pacheco-Torgal, F., Castro-Gomes, J. P. and Jalali, S. (2008) 'Adhesion characterization of tungsten mine waste geopolymeric binder. Influence of {OPC} concrete substrate surface treatment', *Construction and Building Materials*, 22(3), pp. 154–161. doi: http://dx.doi.org/10.1016/j.conbuildmat.2006.10.005.
Pacheco-Torgal, F., Castro-Gomes, J. P. and Jalali, S. (2008) 'Investigations on mix design of tungsten mine waste geopolymeric binder', *Constr. Build. Mater.*, 22(9), pp. 1939–1949. doi: 10.1016/j.conbuildmat.2007.07.015.
Pacheco-Torgal, F., Castro-Gomes, J. P. and Jalali, S. (2009a) 'Utilization of_mining wastes to produce geopolymer binders', in Provis, J. and Van Jaarsveld, J.G.S., Van Deventer, J. S. J. (eds) *Geopolymers: Structures, Processing, Properties and Industrial Applications*. Woodhead Publishing Limited, pp. 267–293.
Pacheco-Torgal, F., Castro-Gomes, J. P. and Jalali, S. (2009b) 'Utilization of mining wastes to produce geopolymer binders', in Provis, J. and Van Jaarsveld, J.G.S., Van Deventer, J. S. J. (eds) *Geopolymers: Structures, Processing, Properties and Industrial Applications*. Woodhead Publishing Limited, pp. 267–293.
Palomo, A., Grutzeck, M. W. and Blanco, M. T. (1999) 'Alkali-activated fly ashes: A cement for the future', *Cement and Concrete Research*, 29(8), pp. 1323–1329. doi: 10.1016/S0008-8846(98)00243-9.
Palomo, a *et al.* (2014) 'A review on alkaline activation : new analytical perspectives', *Materiales de Construcción*, 64(31), pp. 1–23. doi: e022 http:// dx.doi.org/10.3989/mc.2014.00314.
Panagiotopoulou, C., Tsivilis, S. and Kakali, G. (2015) 'Application of the Taguchi approach for the composition optimization of alkali activated fly ash binders', *Construction and Building Materials*. Elsevier Ltd, 91, pp. 17–22. doi: 10.1016/j.conbuildmat.2015.05.005.
Panias, D., Giannopoulou, I. P. and Perraki, T. (2007) 'Effect of synthesis parameters on the mechanical properties of fly ash-based geopolymers', *Colloids and Surfaces A: Physicochemical and Engineering Aspects*, 301(1–3), pp. 246–254. doi: 10.1016/j.colsurfa.2006.12.064.
Pappalardo, A., Jalali, S. and Silva, F. J. (2014) 'Characterization of parameters to predict the structural behaviour of geopolymeric mortar plates strengthened with carbon fiber reinforced polymer', *Key Engineering Materials*, 634, pp. 485–497. doi: 10.4028/www.scientific.net/KEM.634.485.
Part, W. K., Ramli, M. and Cheah, C. B. (2015) 'An overview on the influence of various factors on the properties of geopolymer concrete derived from industrial by-products', *Construction and Building Materials*, 77, pp. 370–395. doi: http://dx.doi.org/10.1016/j.conbuildmat.2014.12.065.
Payá, J., Monzó, J. and Borrachero, M. . (1999) 'Fluid catalytic cracking catalyst residue (FC3R)', *Cement and Concrete Research*, 29(11), pp. 1773–1779. doi: 10.1016/S0008-8846(99)00164-7.
Pendyala, S. (2012) 'Review of Phase Change Materials For Thermal Energy Storage Applications', 2(3), pp. 871–875.
Pereira da Cunha, J. and Eames, P. (2016) 'Thermal energy storage for low and medium

temperature applications using phase change materials - A review', *Applied Energy*. Elsevier Ltd, 177, pp. 227–238. doi: 10.1016/j.apenergy.2016.05.097.
Perera, D. S. *et al.* (2007) 'Influence of curing schedule on the integrity of geopolymers', *Journal of Materials Science*, 42(9), pp. 3099–3106. doi: 10.1007/s10853-006-0533-6.
Pielichowska, K. and Pielichowski, K. (2014) 'Phase change materials for thermal energy storage', *Progress in Materials Science*. Elsevier Ltd, 65, pp. 67–123. doi: 10.1016/j.pmatsci.2014.03.005.
Pomianowski, M. *et al.* (2014) 'A new experimental method to determine specific heat capacity of inhomogeneous concrete material with incorporated microencapsulated-PCM', *Cement and Concrete Research*. Elsevier B.V., 55, pp. 22–34. doi: 10.1016/j.cemconres.2013.09.012.
Potgieter, J. H. (2012) 'An Overview of Cement production: How "green" and sustainable is the industry?', *Environmental Management and Sustainable Development*, 1(2), pp. 14–37. doi: 10.5296/emsd.v1i2.1872.
Praprotnik, M., Janezic, D. and Mavri, J. (2004) 'Temperature Dependence of Water Vibrational Spectrum: A Molecular Dynamics Simulation Study', *J. Phys. Chem. A*, 108(50), pp. 11056–11062. doi: 10.1021/jp046158d.
PRNewswire (2015) *Global Geopolymer Industry Report 2015-2020*.
Programme, T. W. and Portal, P. (2015) 'EN H ORIZON 2020 W ORK P ROGRAMME 2014 – 2015 10 . Secure , clean and efficient energy Revised (European Commission Decision C (2015) 2453 of 17 April 2015)', 2015(April).
Provis, J. L. (2009) *19 - Immobilisation of toxic wastes in geopolymers*, *Geopolymers*. Elsevier. doi: 10.1533/9781845696382.3.421.
Provis, J. L. (2009) '4 - Activating solution chemistry for geopolymers', in Provis, J. L. and Deventer, J. S. J. van (eds) *Geopolymers*. Woodhead Publishing (Woodhead Publishing Series in Civil and Structural Engineering), pp. 50–71. doi: http://dx.doi.org/10.1533/9781845696382.1.50.
Provis, J. L. (2014) 'Geopolymers and other alkali activated materials: why, how, and what?', *Materials and Structures*, 47(1), pp. 11–25. doi: 10.1617/s11527-013-0211-5.
Provis, J. L. and Bernal, S. A. (2014) 'Geopolymers and Related Alkali-Activated Materials', *Annual Review of Materials Research*, 44(1), pp. 299–327. doi: 10.1146/annurev-matsci-070813-113515.
Provis, J. L. and Van Deventer, J. S. . (2014) *Alkali Activated Materials State-of-the-Art Report, RILEM TC 224-AAM*, *RILEM State-of-the-Art Reports*. New York London Library. doi: 10.1007/978-94-007-7672-2.
Provis, J. L. and van Deventer, J. S. J. (2009) 'Geopolymers. Structures, Processing, Properties and Industrial Applications', *CRC Press, Woodhead Publishing, Great Abington, Cambridge, UK*. doi: 10.1533/9781845696382.
Provis, J. L. and Van Deventer, J. S. J. (2009) '1 – Introduction to geopolymers', in *Geopolymers*, pp. 1–11. doi: 10.1533/9781845696382.1.
Provis, J. L., Lukey, G. C. and Van Deventer, J. S. J. (2005a) 'Do geopolymers actually contain nanocrystalline zeolites? a reexamination of existing results', *Chemistry of Materials*, 17(12), pp. 3075–3085. doi: 10.1021/cm050230i.
Provis, J. L., Lukey, G. C. and Van Deventer, J. S. J. (2005b) 'Do geopolymers actually contain nanocrystalline zeolites? a reexamination of existing results', *Chem. Mater.*, 17(12), pp. 3075–3085. doi: 10.1021/cm050230i.
Provis, J. L., Palomo, A. and Shi, C. (2015) 'Cement and Concrete Research Advances in understanding alkali-activated materials', *Cement and Concrete Research*, 78, pp. 110–125. doi: 10.1016/j.cemconres.2015.04.013.
Prusinski, J., Marceau, M. and VanGeem, M. (2004) 'Life cycle inventory of slag cement

concrete', *... Pozzolans in Concrete– ...*, (Lci), pp. 1–26.
Purdon, A. O. (1940) 'The action of alkalis on blast-furnace slag', *J. Soc. Chem. Ind.-Trans.*, 59, pp. 191–202.
Rahier, H. *et al.* (1997) 'Low-temperature synthesized aluminosilicate glasses Part III influence of the composition of the silicate solution on production, structure and properties', *Journal of Materials Science*, 32(9), pp. 2237–2247. doi: doi:10.1023/A:1018563914630.
Rahier, H., Van Mele, B. and Wastiels, J. (1996) 'Low-temperature synthesized aluminosilicate glasses Part II rheological transformations during low-temperature cure and high-temperature properties of a model compound', *Journal of Materials Science*, 31(1), pp. 80–85. doi: doi:10.1007/BF00355129.
Rahier, H., Mele, B. and Wastiels, J. (1996) 'Low-temperature synthesized aluminosilicate glasses', *Journal of Materials Science*, 31(1), pp. 80–85. doi: 10.1007/BF00355129.
Rahman, A. *et al.* (2016) 'Chapter 9 - Cement Kiln Process Modeling to Achieve Energy Efficiency by Utilizing Agricultural Biomass as Alternative Fuels', in Khan, M. M. K. and Hassan, N. M. S. (eds) *Thermofluid Modeling for Energy Efficiency Applications*. Academic Press, pp. 197–225. doi: http://dx.doi.org/10.1016/B978-0-12-802397-6.00009-9.
Rao, A., Jha, K. N. and Misra, S. (2007) 'Use of aggregates from recycled construction and demolition waste in concrete', *Resources, Conservation and Recycling*, 50(1), pp. 71–81. doi: 10.1016/j.resconrec.2006.05.010.
Rashad, A. M. (2013) 'Alkali-activated metakaolin: A short guide for civil Engineer-An overview', *Construction and Building Materials*, 41, pp. 751–765. doi: 10.1016/j.conbuildmat.2012.12.030.
Raupp-Pereira, F. *et al.* (2008) 'New waste based clinkers: Belite and lime formulations', *Cement and Concrete Research*, 38(4), pp. 511–521. doi: http://dx.doi.org/10.1016/j.cemconres.2007.11.008.
Rees, C. A. *et al.* (2007) 'Attenuated Total Reflectance Fourier Transform Infrared Analysis of Fly Ash Geopolymer Gel Aging', *Langmuir*, 23(15), pp. 8170–8179. doi: 10.1021/la700713g.
Reig, L. *et al.* (2013) 'Alkaline activation of ceramic waste materials', *Waste and Biomass Valorization*, 4(4), pp. 729–736. doi: 10.1007/s12649-013-9197-z.
Remberger, M. *et al.* (2004) 'The environmental occurrence of hexabromocyclododecane in Sweden', *Chemosphere*, 54(1), pp. 9–21. doi: http://dx.doi.org/10.1016/S0045-6535(03)00758-6.
REMINE (2015) *RAKU Training Seminar*. Available at: https://goo.gl/5RkDsw (Accessed: 18 October 2016).
Richard, J. A. and Scarlett, J. R. (1997) *A Review and Evaluation of the Micro-Deval Test*. Ottawa. Available at: https://goo.gl/MRu3GV.
Ridtirud, C., Chindaprasirt, P. and Pimraksa, K. (2011) 'Factors affecting the shrinkage of fly ash geopolymers', *International Journal of Minerals, Metallurgy, and Materials*, 18(1), pp. 100–104. doi: 10.1007/s12613-011-0407-z.
Rodriguez, E. D. *et al.* (2013) 'Geopolymers based on spent catalyst residue from a fluid catalytic cracking (FCC) process', *Fuel*. Elsevier Ltd, 109, pp. 493–502. doi: 10.1016/j.fuel.2013.02.053.
Ronc, M. and Bollon, F. (1982) *Heat Storage Using Latent Heat of Fusion of a Substance Adsorbed on a Porous Supporting Material - EUR 7703 EN*. Paris. Available at: https://goo.gl/6m9ze1.
Rovnaník, P. (2010) 'Effect of curing temperature on the development of hard structure of metakaolin-based geopolymer', *Construction and Building Materials*. Elsevier Ltd, 24(7),

pp. 1176–1183. doi: 10.1016/j.conbuildmat.2009.12.023.
Rubenstone, J. (2016) *PCA Forecasts Growth in Cement Consumption at World of Concrete 2016*. Available at: https://goo.gl/kxQ8pe (Accessed: 19 April 2016).
Ryu, G. S. *et al.* (2013) 'The mechanical properties of fly ash-based geopolymer concrete with alkaline activators', *Construction and Building Materials*, 47, pp. 409–418. doi: http://dx.doi.org/10.1016/j.conbuildmat.2013.05.069.
Sakulich, a. R. and Bentz, D. P. (2012) 'Incorporation of phase change materials in cementitious systems via fine lightweight aggregate', *Construction and Building Materials*. Elsevier Ltd, 35, pp. 483–490. doi: 10.1016/j.conbuildmat.2012.04.042.
Samson, G., Phelipot-Mardelé, A. and Lanos, C. (2016) 'Thermal and mechanical properties of gypsum–cement foam concrete: effects of surfactant', *European Journal of Environmental and Civil Engineering*. Taylor & Francis, 8189(April), pp. 1–20. doi: 10.1080/19648189.2016.1177601.
Sarkar, M., Dana, K. and Das, S. (2015) 'Microstructural and phase evolution in metakaolin geopolymers with different activators and added aluminosilicate fillers', *Journal of Molecular Structure*. Elsevier B.V, 1098, pp. e147–e153. doi: 10.1016/j.molstruc.2015.05.046.
Sata, V., Jaturapitakkul, C. and Kiattikomol, K. (2007) 'Influence of pozzolan from various by-product materials on mechanical properties of high-strength concrete', *Construction and Building Materials*, 21(7), pp. 1589–1598. doi: 10.1016/j.conbuildmat.2005.09.011.
Schorcht, F. *et al.* (2013) *Best Available Techniques (BAT) Reference Document for the Production of Cement, Lime and Magnesium Oxide, Joint Research Centre of the European Commission*. Seville.
Shadnia, R., Zhang, L. and Li, P. (2015) 'Experimental study of geopolymer mortar with incorporated PCM', *Construction and Building Materials*. Elsevier Ltd, 84, pp. 95–102. doi: 10.1016/j.conbuildmat.2015.03.066.
Shao, Y. *et al.* (2000a) 'Studies on concrete containing ground waste glass', *Cem. Concr. Res.*, 30(1), pp. 91–100. doi: http://dx.doi.org/10.1016/S0008-8846(99)00213-6.
Shao, Y. *et al.* (2000b) 'Studies on concrete containing ground waste glass', *Cement and Concrete Research*, 30(1), pp. 91–100. doi: http://dx.doi.org/10.1016/S0008-8846(99)00213-6.
Sharma, A. *et al.* (2009) 'Review on thermal energy storage with phase change materials and applications', *Renewable and Sustainable Energy Reviews*, 13(2), pp. 318–345. doi: 10.1016/j.rser.2007.10.005.
Shi, C. and Day, R. L. (1995) 'Acceleration of the reactivity of fly ash by chemical activation', *Cement and Concrete Composites*, 25(1), pp. 15–21.
Shi, C., Krivenko, P. V. and Roy, D. M. (2006) *Alkali-Activated Cements and Concretes*. Abingdon: Taylor & Francis.
Shoukry, H. *et al.* (2016) 'Enhanced physical, mechanical and microstructural properties of lightweight vermiculite cement composites modified with nano metakaolin', *Construction and Building Materials*, 112, pp. 276–283. doi: http://dx.doi.org/10.1016/j.conbuildmat.2016.02.209.
Shvarzman, A. *et al.* (2003) 'The effect of dehydroxylation/amorphization degree on pozzolanic activity of kaolinite', *Cement and Concrete Research*, 33(3), pp. 405–416. doi: 10.1016/S0008-8846(02)00975-4.
Silva, I., Castro-Gomes, J. and Albuquerque, A. (2012) 'Mineral Waste Geopolymeric Artificial Aggregates as Alternative Materials for Wastewater-Treatment Processes: Study of Structural Stability and pH Variation in Water', *Journal of Materials in Civil Engineering*, 24(6), pp. 623–628. doi: 10.1061/(ASCE)MT.1943-5533.0000429.

Silva, I., Castro-Gomes, J. P. and Albuquerque, A. (2012a) 'Effect of immersion in water partially alkali-activated materials obtained of tungsten mine waste mud', *Construction and Building Materials*, 35, pp. 117–124. doi: http://dx.doi.org/10.1016/j.conbuildmat.2012.02.069.

Silva, I., Castro-Gomes, J. P. and Albuquerque, A. (2012b) 'Effect of immersion in water partially alkali-activated materials obtained of tungsten mine waste mud', *Constr. Build. Mater.*, 35, pp. 117–124. doi: http://dx.doi.org/10.1016/j.conbuildmat.2012.02.069.

Sindhunata *et al.* (2006) 'Effect of Curing Temperature and Silicate Concentration on Fly-Ash-Based Geopolymerization', *Industrial & Engineering Chemistry Research*, 45(10), pp. 3559–3568. doi: 10.1021/ie051251p.

Singh, B. *et al.* (2016) 'Effect of activator concentration on the strength, ITZ and drying shrinkage of fly ash/slag geopolymer concrete', *Construction and Building Materials*. Elsevier Ltd, 118, pp. 171–179. doi: 10.1016/j.conbuildmat.2016.05.008.

Singh, P. S., Bastow, T. and Trigg, M. (2005) 'Structural studies of geopolymers by 29Si and 27Al MAS-NMR', *Journal of Materials Science*, 40(15), pp. 3951–3961. doi: 10.1007/s10853-005-1915-x.

Snellings, R., Mertens, G. and Elsen, J. (2012) 'Supplementary Cementitious Materials', *Reviews in Mineralogy and Geochemistry*, 74(1), pp. 211–278. doi: 10.2138/rmg.2012.74.6.

Somna, K. *et al.* (2011) 'NaOH-activated ground fly ash geopolymer cured at ambient temperature', *Fuel*, 90(6), pp. 2118–2124. doi: http://dx.doi.org/10.1016/j.fuel.2011.01.018.

Sonebi, M. and Cevik, A. (2009) 'Genetic programming based formulation for fresh and hardened properties of self-compacting concrete containing pulverised fuel ash', *Construction and Building Materials*, 23(7), pp. 2614–2622. doi: 10.1016/j.conbuildmat.2009.02.012.

Srinivasan, K. and Sivakumar, a. (2013) 'Geopolymer Binders: A Need for Future Concrete Construction', *ISRN Polymer Science*, 2013, pp. 1–8. doi: 10.1155/2013/509185.

Statistia (2016) *Eastern Europe: cement consumption growth 2004-2019*.

Sukmak, P. *et al.* (2013) 'Factors influencing strength development in clay–fly ash geopolymer', *Construction and Building Materials*, 47, pp. 1125–1136. doi: http://dx.doi.org/10.1016/j.conbuildmat.2013.05.104.

Sukmak, P., Horpibulsuk, S. and Shen, S.-L. (2013) 'Strength development in clay–fly ash geopolymer', *Construction and Building Materials*, 40, pp. 566–574. doi: http://dx.doi.org/10.1016/j.conbuildmat.2012.11.015.

Swanepoel, J. C. and Strydom, C. A. (2002) '" Utilisation of Fly Ash in a Geopolymeric Material ,"' 17(8), pp. 1143–1148. doi: 10.1016/S0883-2927(02)00005-7.

Szczepańska, J. (2004) *Solid Waste: Assessment, Monitoring and Remediation, Waste Management Series*. Elsevier (Waste Management Series). doi: 10.1016/S0713-2743(04)80015-1.

Szklorzová, H. and Bílek, V. (2008) 'Influence of alkali ions in the activator on the performance of alkali-activated mortars', in Bílek, V. and Keršner, Z. (eds) *3rd International symposium on non-traditional cement and concrete*. Brno, pp. 777–784.

Tashima, M. M. *et al.* (2012) 'New geopolymeric binder based on fluid catalytic cracking catalyst residue (FCC)', *Materials Letters*. Elsevier B.V., 80, pp. 50–52. doi: 10.1016/j.matlet.2012.04.051.

Tashima, M. M. *et al.* (2013) 'Alkali activated materials based on fluid catalytic cracking catalyst residue (FCC): Influence of SiO2/Na2O and H 2O/FCC ratio on mechanical strength and microstructure', *Fuel*. Elsevier Ltd, 108, pp. 833–839. doi: 10.1016/j.fuel.2013.02.052.

Telesca, A. *et al.* (2017) 'Use of oxyfuel combustion ash for the production of blended cements: A synergetic solution toward reduction of {CO2} emissions', *Fuel Processing Technology*, 156, pp. 211–220. doi: http://dx.doi.org/10.1016/j.fuproc.2016.10.026.
Temuujin, J., van Riessen, A. and Williams, R. (2009) 'Influence of calcium compounds on the mechanical properties of fly ash geopolymer pastes', *Journal of Hazardous Materials*, 167(1–3), pp. 82–88. doi: 10.1016/j.jhazmat.2008.12.121.
Temuujin, J., Williams, R. P. and van Riessen, A. (2009) 'Effect of mechanical activation of fly ash on the properties of geopolymer cured at ambient temperature', *Journal of Materials Processing Technology*, 209(12–13), pp. 5276–5280. doi: http://dx.doi.org/10.1016/j.jmatprotec.2009.03.016.
Tenn, N. *et al.* (2015) 'Formulation of new materials based on geopolymer binders and different road aggregates', *Ceramics International*. Elsevier, 41(4), pp. 5812–5820. doi: 10.1016/j.ceramint.2015.01.010.
Thomas, R. J. and Peethamparan, S. (2015) 'Alkali-activated concrete: Engineering properties and stress–strain behavior', *Construction and Building Materials*. Elsevier Ltd, 93, pp. 49–56. doi: 10.1016/j.conbuildmat.2015.04.039.
Torgal, F. P. (2013) 'Introduction', in *Nearly zero energy building refurbishment*, pp. 1–14. doi: 10.1007/978-1-4471-5523-2_1.
Turner, L. K. and Collins, F. G. (2013) 'Carbon dioxide equivalent (CO2-e) emissions: A comparison between geopolymer and OPC cement concrete', *Construction and Building Materials*. Elsevier Ltd, 43, pp. 125–130. doi: 10.1016/j.conbuildmat.2013.01.023.
Tyagi, V. V. and Buddhi, D. (2007) 'PCM thermal storage in buildings: A state of art', *Renewable and Sustainable Energy Reviews*, 11(6), pp. 1146–1166. doi: 10.1016/j.rser.2005.10.002.
UNFCC (2015) *Japan's Intended Nationally Determined Contribution (INDC)*. Available at: https://goo.gl/LkyQo6.
de Vargas, A. S., Masuero, Â. B. and Vilela, A. C. F. (2006) 'Investigations on the use of electric-arc furnace dust (EAFD) in Pozzolan-modified Portland cement I (MP) pastes', *Cement and Concrete Research*, 36(10), pp. 1833–1841. doi: 10.1016/j.cemconres.2006.06.003.
Vickers, L., Riessen, A. V. and Rickard, W. D. A. (2015) 'Precursors and additives for geopolymer synthesis', in *Fire-Resistant Geopolymers*. Springer Singapore, pp. 17–37. doi: 10.1007/978-981-287-311-8.
Wagners (2016) *Wagners Earth Friendly Concrete*. Available at: https://goo.gl/LquYyF (Accessed: 21 June 2016).
Wahid, M. A. *et al.* (2017) 'An overview of phase change materials for construction architecture thermal management in hot and dry climate region', *Applied Thermal Engineering*. Elsevier, 112, pp. 1240–1259. doi: 10.1016/j.applthermaleng.2016.07.032.
Wang, H., Li, H. and Yan, F. (2005) 'Synthesis and mechanical properties of metakaolinite-based geopolymer', *Colloids and Surfaces A: Physicochemical and Engineering Aspects*, 268(1–3), pp. 1–6. doi: http://dx.doi.org/10.1016/j.colsurfa.2005.01.016.
Wang, J. *et al.* (2015) 'A concrete material with waste coal gangue and fly ash used for farmland drainage in high groundwater level areas', *Journal of Cleaner Production*. Elsevier Ltd, 112, pp. 631–638. doi: 10.1016/j.jclepro.2015.07.138.
WBCSD/CSI (2015) *Low Carbon Technology Partnerships initiative (LCTPi)*. Available at: http://www.lctpi.wbcsdservers.org/ (Accessed: 21 May 2016).
WBCSD Cement Sustainability Initiative (2013) *Getting the Numbers Right (GNR) Project - Emissions Report 2013*. Available at: https://goo.gl/joh5Wb (Accessed: 19 May 2016).
Weng, L. and Sagoe-Crentsil, K. (2007) 'Dissolution processes, hydrolysis and

condensation reactions during geopolymer synthesis: Part I-Low Si/Al ratio systems', *Journal of Materials Science*, 42(9), pp. 2997–3006. doi: 10.1007/s10853-006-0820-2.
Won, J.-P. *et al.* (2011) 'Mix proportion of high-strength, roller-compacted, latex-modified rapid-set concrete for rapid road repair', *Construction and Building Materials*, 25(4), pp. 1796–1800. doi: http://dx.doi.org/10.1016/j.conbuildmat.2010.11.085.
World Cement (2013) *Cement: the Southeast Asia view*. Available at: https://goo.gl/FJvHgi (Accessed: 16 May 2016).
World Health Organization (2014) *Global Health Observatory (GHO) data*. Available at: https://goo.gl/Pi5MDi (Accessed: 11 May 2016).
Xiao, H. and Liu, K. (2010) 'Co-combustion kinetics of sewage sludge with coal and coal gangue under different atmospheres', *Energy Conversion and Management*. Elsevier, 51(10), pp. 1976–1980. doi: 10.1016/j.enconman.2010.02.030.
Xu, H. and van Deventer, J. S. J. (2003) 'Effect of Source Materials on Geopolymerization', *Industrial & Engineering Chemistry Research*, 42(8), pp. 1698–1706. doi: 10.1021/ie0206958.
Xu, H. and Van Deventer, J. S. J. (2000) 'The geopolymerisation of alumino-silicate minerals', *International Journal of Mineral Processing*, 59(3), pp. 247–266. doi: 10.1016/S0301-7516(99)00074-5.
Yamaguchi, N. *et al.* (2013) 'Preparation of monolithic geopolymer materials from urban waste incineration slags', *Journal of the Ceramic Society of Japan*, 121(9), pp. 847–854. doi: 10.2109/jcersj2.121.847.
Yamaguchi, N. and Ikeda, K. (2010) 'Preparation of geopolymeric materials from sewage sludge slag with special emphasis to the matrix compositions', *Journal of the Ceramic Society of Japan*, 118(1374), pp. 107–112. doi: 10.2109/jcersj2.118.107.
Yang, Q. and Wu, X. (1999) 'Factors influencing properties of phosphate cement-based binder for rapid repair of concrete1', *Cement and Concrete Research*, 29(3), pp. 389–396. doi: http://dx.doi.org/10.1016/S0008-8846(98)00230-0.
Ye, J., Zhang, W. and Shi, D. (2014) 'Effect of elevated temperature on the properties of geopolymer synthesized from calcined ore-dressing tailing of bauxite and ground-granulated blast furnace slag', *Construction and Building Materials*, 69, pp. 41–48. doi: http://dx.doi.org/10.1016/j.conbuildmat.2014.07.002.
Ye, N. *et al.* (2016) 'Synthesis and strength optimization of one-part geopolymer based on red mud', *Construction and Building Materials*, 111, pp. 317–325. doi: 10.1016/j.conbuildmat.2016.02.099.
Yellishetty, M. *et al.* (2008) 'Reuse of iron ore mineral wastes in civil engineering constructions: A case study', *Resources, Conservation and Recycling*, 52(11), pp. 1283–1289. doi: 10.1016/j.resconrec.2008.07.007.
Zalba, B. *et al.* (2003) *Review on thermal energy storage with phase change: Materials, heat transfer analysis and applications*, *Applied Thermal Engineering*. doi: 10.1016/S1359-4311(02)00192-8.
Zhang, D. *et al.* (2004) 'Development of thermal energy storage concrete', *Cement and Concrete Research*, 34(6), pp. 927–934. doi: 10.1016/j.cemconres.2003.10.022.
Zhang, D. *et al.* (2005) 'Granular phase changing composites for thermal energy storage', *Solar Energy*, 78(3), pp. 471–480. doi: 10.1016/j.solener.2004.04.022.
Zhang, L., Ahmari, S. and Zhang, J. (2011a) 'Synthesis and characterization of fly ash modified mine tailings-based geopolymers', *Construction and Building Materials*. Elsevier Ltd, 25(9), pp. 3773–3781. doi: 10.1016/j.conbuildmat.2011.04.005.
Zhang, L., Ahmari, S. and Zhang, J. (2011b) 'Synthesis and characterization of fly ash modified mine tailings-based geopolymers', *Constr. Build. Mater.*, 25(9), pp. 3773–3781. doi: 10.1016/j.conbuildmat.2011.04.005.

Zhang, S. A. K. P. L. (2014) 'Alkali Activation of Copper Mine Tailings and Low-Calcium Flash-Furnace Copper Smelter Slag', *Journal of Materials in Civil Engi- neering*, 27(6), pp. 1–11. doi: 10.1061/(ASCE)MT.1943-5533.0001159.
Zhang, Z. *et al.* (2014) 'Geopolymer foam concrete: An emerging material for sustainable construction', *Construction and Building Materials*. Elsevier Ltd, 56, pp. 113–127. doi: 10.1016/j.conbuildmat.2014.01.081.
Zhang, Z., Yao, X. and Zhu, H. (2010) 'Potential application of geopolymers as protection coatings for marine concrete: I. Basic properties', *Applied Clay Science*, 49(1–2), pp. 1–6. doi: http://dx.doi.org/10.1016/j.clay.2010.01.014.
Zhou, T. *et al.* (2013) 'Improving the thermal conductivity of epoxy resin by the addition of a mixture of graphite nanoplatelets and silicon carbide microparticles', *Express Polymer Letters*, 7(7), pp. 585–594. doi: 10.3144/expresspolymlett.2013.56.

Summary of Publications and Conferences

Gediminas KASTIUKAS
Kingston Lane, Uxbridge, London, UB8 3PH, UNITED KINGDOM
e-mail: gediminas.kastiukas@brunel.ac.uk
tel: +44 7979 982926

Published Articles in International Refereed Journals

Kastiukas, G., & Zhou, X. (2017). Effects of Waste Glass on Alkali-Activated Tungsten Mining Waste: Composition and Mechanical Properties. *Journal of Materials and Structures*. doi**:**10.1617/s11527-017-1062-2 MAAS-D-17-00178.1

Kastiukas, G., Zhou, X., & Castro Gomes, J. (2017) Varying Preparation Conditions for The Synthesis of Alkali-Activated Binders Using Tungsten Mining Waste. *Journal of Materials in Civil Engineering (ASCE).* doi: 10.1061/(ASCE)MT.1943-5533.0002029

Zhou, X., Saini, H. and Kastiukas, G. (2017) 'Engineering Properties of Treated Natural Hemp Fiber-Reinforced Concrete', *Frontiers in Built Environment*, 3, 33. doi:10.3389/fbuil.2017.00033.

Sedira, N., Castro Gomes, J., Kastiukas, G., Zhou, X. and Vargas, A. (2017) 'A Review on Mineral Waste for Chemical-activated Binders: Mineralogical and Chemical Characteristics'. *Mining science*, 24 pp. 29 - 58. doi: 10.5277/msc172402

Dong, W., Wu, Z., Zhou, X., Dong, L., & Kastiukas, G. (2017) FPZ evolution of mixed mode fracture in concrete: *Experimental and numerical, Engineering Failure Analysis*, 75, 54-70. doi: https://doi.org/10.1016/j.engfailanal.2017.01.017

Dong, W., Yang, D., Zhou, X., Kastiukas, G., & Zhang, B. (2016). Experimental and numerical investigations on fracture process zone of rock-concrete interface: FPZ Evolution of Rock-Concrete Interface. *Fatigue & Fracture of Engineering Materials & Structures*, doi: 10.1111/ffe.12558.

Kastiukas, G., Zhou, X., & Castro Gomes, J. (2016). Development and optimisation of phase change material-impregnated lightweight aggregates for geopolymer composites made from aluminosilicate rich mud and milled glass powder. *Construction and Building Materials, 110,* 201–210.

Dong, W., Zhou, X., Wu, Z., & Kastiukas, G. (2016). Effects of specimen size on assessment of shrinkage cracking of concrete via elliptical rings: Thin vs. thick. *Computers and Structures, 174*, 66–78.
Kastiukas, G., Zhou, X., Castro-Gomes, J., Huang, S., & Saafi, M. (2015). Effects of lactic and citric acid on early-age engineering properties of Portland/calcium aluminate blended cements. *Construction and Building Materials, 101*, 389–395.

Presentations at International Conferences

Kastiukas, G. (2016). *Effects of Waste Glass and Activating Solution on Tungsten Mining Waste Alkali-Activated Binders.* Paper presented at the International RILEM Conference on Materials, Systems and Structures in Civil Engineering, August 2016, Technical University of Denmark, Lyngby, Denmark.
Kastiukas, G. (2016). Investigating synthesis conditions and activator ratios on the properties of geopolymers based on mining and glass waste: Paper presented at the 7th BaltSilica Conference, May 2016, Kaunas, Lithuania.

Presentations at National (UK) Conferences/Workshops

Kastiukas, G. (2016). *Tungsten mining waste in the presence of chemical activators*. Paper presented at International Workshop on Innovation in Low-carbon Cement & Concrete Technology, September 2016, University College London, United Kingdom
Kastiukas, G. (2016). *Effects of activator synthesis conditions on alkali-activated binders from tungsten mining waste.* Paper presented at the 3rd Young Researchers' Forum, April 2016, Imperial College London, London, United Kingdom.